UNIVERSITÀ DEGLI STUDI DI TORINO

DIPARTIMENTO DI PSICOLOGIA

DOTTORATO DI RICERCA IN NEUROSCIENZE

CICLO XXXII

TITOLO DELLA TESI

Connectomics and pathoconnectomics:
Analysis of gray matter networks in the healthy and pathological brain

TESI PRESENTATA DA: Jordi Manuello

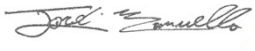

TUTOR: Prof. Franco Cauda

COORDINATORE DEL DOTTORATO: Prof. Marco Sassoè

ANNI ACCADEMICI: 2016-2020

SETTORE SCIENTIFICO-DISCIPLINARE DI AFFERENZA:

M-PSI/02

To my beloved wife and son,

who walked by my side

1 – **Introduction**

1.1 A brief historical perspective on connectomics

The omic perspective is nowadays widespread and consolidated in many fields of biological sciences. In general terms, this refers to the attempt to comprehensively map and analyze the interactions happening between the fundamental elements of a system (Bedia, 2018). Despite the etymology of the suffix "–ome" being far from certainty (Lederberg & McCray, 2001), with one of the most fascinating hypothesis pointing to the Sanskrit intonation "Aum" (a mantra with the meaning of fullness) (Yadav, 2007), it is part of the terms used to define a multitude of scientific concepts. Among the most common: genome, proteome, microbiome. But one term from this family represents a central concept for contemporary neuroscience: connectome. This word was first used 15 years ago by Olaf Sporns to define the "comprehensive structural description of the network of elements and connections forming the human brain" (Sporns, Tononi, & Kötter, 2005). As per many other ideas in science, this intuition can be traced back to the ancient centuries. In fact, representations of proto-connectomes can already be found in fourteenth century books (Figure 1), following the so called "ventricular theory" (Catani, Thiebaut de Schotten, Slater, & Dell'Acqua, 2013).

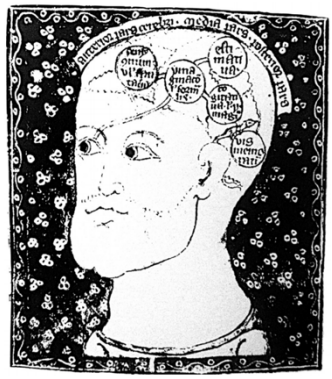

Figure 1: A representation of the ventricular theory in an illustration dating from about 1310 (from Clarke and Dewhurst, 1972)

In more recent times, the idea of tracing neural connections was initiated by Cajal (Swanson & Lichtman, 2016), and the first complete mapping of a brain connectome, that of Caenorhabditis elegans, was completed in 1986 (White,

Southgate, Thomson, & Brenner, 1986) after more than ten years of efforts. Even though the current technical resources could significantly simplify what was a gargantuan endeavour at that time (Lichtman & Sanes, 2008), mapping the whole human connectome is still dramatically challenging at this time. Nonetheless, multiple projects had been founded in this field. Among others, the 10-years "Human Brain Project" was funded by European Commission in 2013, and has among its main objectives the simulation of a real human brain. It brings together around 500 researchers from more than 100 European research institutions. On the other side of the ocean, the "Human Connectome Project" was originally awarded by NIH in 2011 with the aim of studying in depth the connectome of 1200 healthy young adult participants. Over the years, it had evolved to include now tens of satellite projects focused on both healthy and pathological brains, across the almost whole lifespan. There is no lack of criticism in the neuroscientific community toward this kind of approaches. However, as pointed out by Lichtman and Sanes, similar objections had been risen in the first days of the race to the mapping of the human genome, but the meaningfulness of its results is currently widely acknowledged (Lichtman & Sanes, 2008). The presence of more than 3500 connectomics studies indexed in PubMed from 2005 to now suggests the fecundity of this research field.

1.2 One brain, many connectomes

If mapping the whole human connectome still represents a complex challenge, it is also true that bringing the task to a different level of resolution allows to solve technical and computational issue, yet providing meaningful information. Based on a very coarse classification, it is possible to distinguish between micro-connectomics, that observes neural networks at cellular scale (Schröter, Paulsen, & Bullmore, 2017), and macro-connectomics, tracing instead interregional pathways between brain regions (Sporns, 2016). These main modalities rely on different technical solutions as well: while the former benefits from invasive techniques like tracers injection and post-portem histological staining, the latter takes advantages of non-invasive imaging based approaches (Behrens & Sporns, 2012). Leveraging the recent and ongoing multiplication of neuroimaging sequences allowing to detect different kinds of signal, macro-connectomes can now describe more than one connectivity modality, focusing on structural or functional properties.

Structural connectivity aims to reconstruct anatomical connections between brain regions (Huang & Ding, 2016), and is technically based on diffusion tractography. The principle behind this type of MRI acquisition is the isotropic/anisotropic

diffusion of water in brain tissues (Moseley et al., 1990). The voxel-wise observation of the peak diffusion orientations allows to estimate the tracks of bundles of axons across white matter (Tuch, Reese, Wiegell, & Wedeen, 2003).

Functional connectivity implies instead a statistical relationship between voxels. Brain regions are, in fact, considered functionally connected when the time series of their activity are statistically correlated one to each other (van den Heuvel & Hulshoff Pol, 2010). This estimation is based on the detection of the so-called BOLD (Blood Oxygention Level Dependent) effect, described by Seiji Ogawa in early 90s (Ogawa et al., 1993). This signal originates from the change of concentration of hemoglobin and deoxyhemoglobin in the blood, that is related with oxygen consumption and, in turn, with local brain activity (Logothetis & Wandell, 2004). Functional connectivity is thus based on an indirect measurement of the underlying phenomenon.

As mentioned before, functional connectivity is based on statistical correlation. For this reason, it does not provide any information about the direction of the interaction, and does not allow causal interpretations (Schiefer et al., 2018). Several techniques had been proposed to try to overcome this issue (Havlicek et al., 2017; J. F. Smith, Pillai, Chen, & Horwitz, 2010; Ting, Seghouane, Salleh, & Noor, 2015), leading to what is referred as effective connectivity (Friston, 2011). The effort of improving our knowledge about the actual connectivity of the brain can benefit from the combined observation of structural and functional profiles (Schiefer et al., 2018). In some sense, this can be situated in the never solved psychological and philosophical debate on the relationship between structure and function in general. Neuroimaging studies that reconstructed the two kinds of connectomes on a same sample of subjects (Honey et al., 2009; Skudlarski et al., 2008) highlighted a good coherence between them, although without coming out in favour of an hard reductionism. Increasing evidences of multiscale functional connectivity (Liu, Song, Liang, Knöpfel, & Zhou, 2019; Song, Tin, & Poon, 2015), together with plasticity phenomena involving the structural pathways, challenge the clear identification of a unique and stable connectome (Behrens & Sporns, 2012).

1.3 The analysis of abnormal brain networking: Pathoconnectomics

The main lesson of these first fifteen years of connectomics is probably the meaningfulness of looking at the brain-networks to improve our understanding of cognitive and perceptual brain functions. As the classic neuropsychological perspective attempted to assign functions to each brain region, connectomics puts

functions into relationship with complex brain networks instead (Seung, 2013). During last years, more and more evidences have been suggesting that the analysis of brain networks could provide insight to the comprehension of neuropsychiatric disorders (Mohan et al., 2016; van den Heuvel & Fornito, 2014), leading to the birth of pathoconnectomics (Rubinov & Bullmore, 2013). Inside this framework, a disruptive hypothesis reached, proposing that the alteration associated with brain diseases does not spread randomly, but it "follows disease-specific patterns that resemble the architecture of brain connectivity networks" (Raj, Kuceyeski, & Weiner, 2012; Yates, 2012; Zhou, Gennatas, Kramer, Miller, & Seeley, 2012). Thus, the aim of pathoconnectomics is not only to investigate changes occurring to canonical brain networks in concomitance with disease progression, but trying to understand if the detected patterns of alteration exhibit network-like properties. This approach benefits from network analysis methods (Bullmore & Sporns, 2009; Rubinov & Sporns, 2010), in many cases preexisting this specific field. Some of them will be briefly discussed in the published papers included in this thesis. Hence pathoconnectomics has the premises for significantly contribute to a better comprehension of the nature and development of brain disorders, both neurodegenerative and psychiatric (Rubinov & Bullmore, 2013).

1.4 Possible mechanisms behind alteration patterns

Besides detecting networks of alteration and analyzing their properties, pathoconnectomics is enhanced by the production of hypotheses concerning possible mechanisms behind their formation. This is supported by the integration of neuroimaging and network analysis with evidences from biology, physiology and genetics, making this framework highly multidisciplinary. Thus far, three main mechanisms have been hypothesized: transneuronal spread, nodal stress, and shared vulnerability.

Transneuronal spread mechanism is based on the propagation of toxic agents along neuronal connections (Clavaguera, Grueninger, & Tolnay, 2014; Clavaguera et al., 2013; Goedert, Clavaguera, & Tolnay, 2010; Goedert, Masuda-Suzukake, & Falcon, 2017; Jucker & Walker, 2013; Korth, 2012; Kraus, Groveman, & Caughey, 2013; Soto & Estrada, 2008; Walker, Diamond, Duff, & Hyman, 2013). This phenomenon is often referred as "prion-like diffusion" and is particularly fitting for misfolded proteins capable to move along brain axonal fibers (Chevalier-Larsen & Holzbaur, 2006; Clavaguera et al., 2009) inducing a cascade phenomenon of corruptive templating (J. Hardy & Revesz, 2012; Jucker & Walker, 2011). Although prion infections actually cause lethal damages to the brain (Aguzzi, Nuvolone, & Zhu,

2013) this mechanism has been mainly associated with tauopathies (Bourdenx et al., 2017).
Nodal stress hypothesizes that the so-called hubs of functional connectomes may be prone to excessive stress in virtue of their interaction with an high number of brain regions (Crossley et al., 2014; Zhou et al., 2012). Mechanisms of excitotoxicity could in turn induce neuronal damage (Olloquequi et al., 2018), and in recent years excitotoxic-related mechanisms have been targeted to develop treatment strategies against neurodegeneration (Binvignat & Olloquequi, 2020).
Shared vulnerability relies on the hypothesis that common vulnerability to neuropathology of a set of brain regions mainly depends on shared gene expressions (French & Pavlidis, 2011; French, Tan, & Pavlidis, 2011). Supporting evidence was found for schizophrenia (Romme, de Reus, Ophoff, Kahn, & van den Heuvel, 2017), and coherent proteomic changes had been recently analyzed in Alzheimer's disease progression (Mendonça et al., 2019). It should be noted that in addition to disease specific effects, genetics could in turn influence the development of functional and structural healthy connectome (Barabási & Barabási, 2020; Cioli, Abdi, Beaton, Burnod, & Mesmoudi, 2014; Thompson, Hibar, Stein, Prasad, & Jahanshad, 2016). These proposed mechanisms are not to be thought as mutually exclusive. Rather, they likely act with different weights depending on the pathology analyzed.

1.5 The need for a meta-analytic approach

Gray matter alterations have been reported in association with a variety of both psychiatric and neurodegenerative disorders (Lee et al., 2018; Matsuda, 2016; Muñoz-Ruiz et al., 2012; Niu et al., 2017; Pereira et al., 2018; van Haren et al., 2011), and generally considered as a valid marker of atrophy (Frisoni, Fox, Jack, Scheltens, & Thompson, 2010). Among other techniques to analyze structural MRI data, Voxel Based Morphometry (VBM) allows to implement "a voxel-wise comparison of the local concentration of gray matter between two groups of subjects" (Ashburner & Friston, 2000). In clinical studies, this involves a group of patients and the matched healthy controls group, or two groups of patients with different disorders to be compared, or groups of subjects with the same disorder but at different timepoints. Briefly, VBM consists of three main steps: first, images are registered to a common stereotactic space; then segmentation is used to separate brain tissues; lastly, voxel-wise statistic between the groups is performed (Good et al., 2001). One main advantage of this technique is that it does not require a priori hypotheses concerning the expected localization of the possible effect (Ashburner & Friston, 2001). However, discrepancies between results of different investigations

on a same disorder may emerge, probably due to different age of disease, or different criteria used to define the experimental samples. As per many other scientific domains, a meta-analytic approach can help to overcome the issue, estimating an overall effect (Wager, Lindquist, & Kaplan, 2007; Wager, Lindquist, Nichols, Kober, & Van Snellenberg, 2009). In the field of neuroimaging, it is possible to distinguish two main categories: image-based meta-analyses (IBMA) and coordinate-based meta-analyses (CBMA) (Müller et al., 2018). The main difference between the two is the level of detail used for the experiment in the pool. While IBMA methods directly analyze the final results maps of each experiment (Salimi-Khorshidi, Smith, Keltner, Wager, & Nichols, 2009), CBMA take as input the peaks of effect, as they are usually reported in literature through their stereotactic coordinates (Caspers, Zilles, Beierle, Rottschy, & Eickhoff, 2014). Of note, differently from standard meta-analyses that aim to estimate the effect size, CBMA are focused on effect location (Fox, Parsons, & Lancaster, 1998). Among the methodologies that have been developed in this framework, the most used are multilevel kernel density analysis (MKDA) (Wager et al., 2009), signed differential mapping (SDM) (Radua & Mataix-Cols, 2009), parametric voxel-based meta-analysis (PVM) (Costafreda, David, & Brammer, 2009), gaussian-process regression (GPR) (Salimi-Khorshidi, Nichols, Smith, & Woolrich, 2011), and activation likelihood estimation (ALE) (Turkeltaub, Eden, Jones, & Zeffiro, 2002). If IBMA allow to take advantage of the full information provided in the original experiments (Salimi-Khorshidi et al., 2009), it should be considered that the final whole-brain maps of the results are rarely available for other researchers (Müller et al., 2018). By contrast, peaks coordinates can be easily obtained for the majority of published papers by means of established resources as PubMed, Web of Science, Scopus (Tahmasian et al., 2019). In addition to these multidisciplinary databases, a neuroimaging dedicated tool called BrainMap was originally conceived in 1988 and constantly developed through the years (Fox & Lancaster, 1994; Fox & Lancaster, 2002). Its characteristic feature is the combined availability of peaks coordinates and metadata, following an articulate taxonomy of cognitive domains and research design details (Fox et al., 2005). More than 16900 experiments of functional neuroimaging are currently retrievable (November 2020). Together with the database, the BrainMap project also developed a specific freeware tool for data search called Sleuth (Laird, Lancaster, & Fox, 2005), and a second one implementing the ALE method named GingerALE (Eickhoff et al., 2009). Of note, among the various CBMA techniques, ALE was found to be the one to produce the most similar results to IBMA, thus suggesting a limited loss of information when

shifting from whole-brain maps to peaks coordinates (Salimi-Khorshidi et al., 2009). Moreover, based on a literature overview, it also resulted to be the most used (Acar, Seurinck, Eickhoff, & Moerkerke, 2018). In light of all these elements, BrainMap can be considered a leading resource in the framework of CMBA.

1.6 Detecting co-occurrence patterns

The ALE methodology had been originally devised to analyze functional neuroimaging data. However, in recent years it was proved to be equally applicable to structural data, in particular when processed through VBM (Vanasse et al., 2018). A technical description of the ALE algorithm is provided in the published papers included in this thesis. Briefly, it aims to assess whether the spatial coherence of the peaks of effect across the experiments in the pool is larger than what could be expected by chance (Eickhoff et al., 2016). To do so, for every experiment a 0/1 binary map is built reflecting the stereotactic coordinates of the reported peaks. Subsequently, Gaussian spatial smoothing is applied to each active voxel. Of note, the kernel size depends on the sample size of the experiment thus modelling the spatial uncertainty (the smaller the N the larger the kernel). These maps (technically called MA maps) are combined into the final ALE map, computing the union of probabilities (Acar et al., 2018). Voxel-wise thresholding based on Family Wise Error (FEW) rate is recommended, possibly complemented by cluster-level correction (Eickhoff et al., 2016).

The ALE method hence depicts the overall spatial distribution of the investigated effect. When the dataset consists of task-based fMRI experiments the final ALE map can be interpreted in terms of co-activations (Robinson, Laird, Glahn, Lovallo, & Fox, 2010). When performing a meta-analysis on structural data instead, originally processed through VBM, ALE results describe patterns of co-alteration (Vanasse et al., 2018) (with ALE more correctly meaning anatomical likelihood estimation). In this latter case, the effect of interest can follow two opposite directions, reflected in the contrasts design of VBM technique: decrease or increase. Decrease is found when the VBM analysis shows lower values of GM volume/density in pathological subjects compared against healthy controls. This is often considered a marker of brain atrophy, both in neurological and psychiatric disorders (Du et al., 2012; Fornito, Yücel, Patti, Wood, & Pantelis, 2009; Frisoni et al., 2010; Hallahan et al., 2011; Lin, Lee, & Weng, 2016; Stoodley, 2014). On the contrary, the identification of greater GM volume/density in pathological subjects (vs healthy controls) is termed increase. The clinical meaning of this phenomenon is much less clear, with hypothesis concerning synaptogenesis (Sarrazin et al., 2019), modifications of the

glia (Rocha, Achaval, Santos, & Rodnight, 1998), hypertrophic effect of medications (Torres, Portela-Oliveira, Borgwardt, & Busatto, 2013), or compensatory mechanisms in brain disorder (Mancuso et al., 2020). It should be noted that although the ALE method detects patterns of co-activation (or co-alteration), nothing is known about the actual concomitant involvement of specific brain regions at the level of each single experiment (Caspers et al., 2014). In other words, an ALE map showing blobs A, B, and C could originate from a set of experiments reporting co-occurrence of the effect between A and B, and a second set describing the interaction between A and C. In this case, the apparent relationship between B and C would not be backed by experiments actually showing that. In order to solve this issue, a method called PaMiNi (Pattern Mining in NeuroImaging) had been proposed, based on the combination of Gaussian mixture modeling and association analysis (Caspers, Zilles, Eickhoff, & Beierle, 2012). Its rationale was to identify underlying patterns of co-activation actually observed in multiple experiments. This approach indeed allows to detect at least some macro-level spurious apparent co-occurrences between brain regions (i.e. none of the identified patterns includes both blobs B and C). However, the existing relationships between brain regions composing a same pattern are still undescribed. It follows that potential non-direct co-occurrences previously appearing in the final ALE results are still possible in each pattern. In addition to allowing their detection, knowing the existing interactions between each element of a map is particularly meaningful when dealing with brain disorders. In fact, this could open the way to the understanding of the development of patterns of structural alteration across the brain during the progression (and worsening) of the pathology.

1.7 The analysis of structural co-alteration networks

The main aim of my PhD project was thus to develop and apply a method to detect and analyze networks of GM structural co-alteration associated with brain disorders, capable to describe the interaction between each couple of brain regions (or even their parcels) involved. The technical details of this new approach are provided in the published papers included in this thesis. However, a brief outline of the main aspects follows below.

The proposed technique consists of four main steps:

1. Data selection
2. Effect estimation
3. Nodes definition

4. Edges computation

Although originally intended and optimized to analyze GM structural data at a meta-analytic level, our methodology is flexible enough to be adapted to different scenarios. This is mainly due to the adoption of a network analysis perspective, and obtainable by means of different decisions at each step.

1.7.1 Data selection

In its standard use, data selection considers previously published VBM experiments investigating differences between pathological subjects and healthy controls. A first element of arbitrariness concerns the number of disorders to be included. If the detection of the co-alteration network associated with a single disease could allow to consolidate clinical evidence, or discover previously hidden interactions between brain regions, a transdiagnostic approach could highlight pathological processes in common among different disorders. A second decision concerns the direction of the effect, namely increase or decrease. When focusing on the latter, it is possible to specifically define a co-atrophy network (rather than a more general co-alteration one). The decision on the effect can be influenced by the disorder investigated, making sensible or not expecting either atrophy or growth. Due to the issues described in section 1.6 it is generally recommended to avoid mixing the two effects. A better option is to obtain separate networks for increase and decrease, and then compare them. Interestingly, Mancuso et al. (2020) recently adapted our approach to analyze the relationship between co-occurrent increase and decrease on a same set of studies. A third relevant criterion is the imposition of a specific brain region of interest (or more generally a ROI). This way allows to limit the selection to experiments reporting at least one focus of alteration in that brain region. Of note, this doesn't turn the investigation into a ROI study. The final ALE map will be whole-brain, as whole-brain results are still searched in step 1, but they must include the selected region.

Data search can be performed on any database (PubMed, Scopus or similar), provided that it allows to obtain the list of peaks as reported in each paper. As mentioned before, Sleuth (searching on BrainMap) is the optimal solution, allowing to easily manage all the here mentioned options and more.

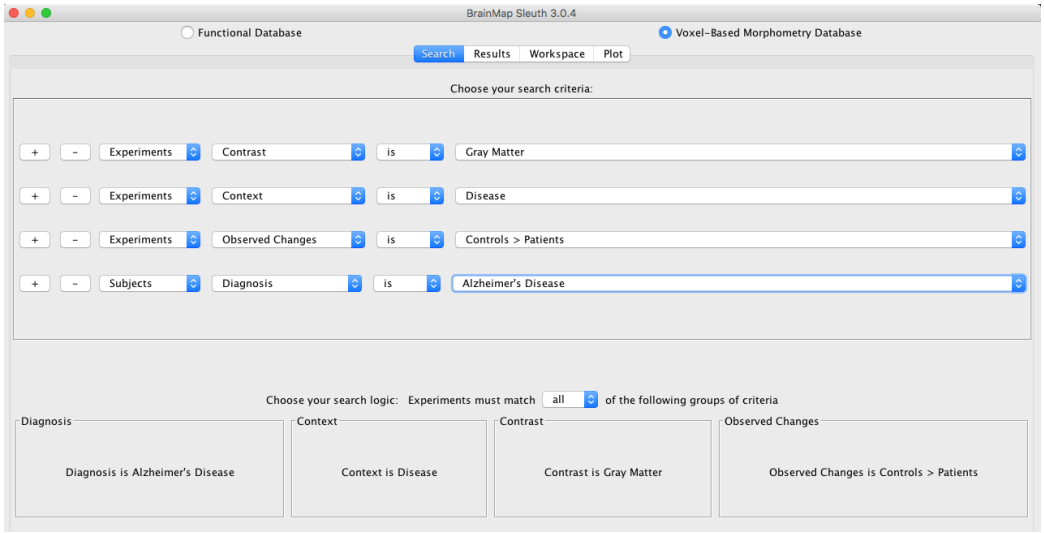

Figure 2: The GUI of Sleuth 3.0.4 showing search criteria for the VBM section of the BrainMap database.

As an example, criteria to perform in Sleuth data selection needed to build the co-atrophy network of Alzheimer's disease are shown in figure 2. The key "Observed Changes is Control > Patients" is set to limit the inclusion to decrease effect.

At the end of the search, irrespective of the tool used, the list of the stereotactic coordinates of the peaks arranged in a way that allows the identification of the different experiments has to be generated (Figure 3).

```
// Baxter L C, 2006: Normals > AD Patients, Gray Matter Density
// Subjects=15
-20.08  -3.45   -26.12
-5.77   28.45   22.19
19.59   -35.68  -24.9
44.35   -20.11  -2.28
-18.9   37.29   38.12
-4.3    -20.99  37.35

// Bernasconi N, 2004: Healthy Controls > Left-Sided TLE Patients, Gray Matter
// Concentration (Unmodulated)
// Subjects=45
-31.84  -14.91  -14.04
18.75   -11.06  -18.56
-22.55  -18.37  -6.99
-22.68  -37.89  .48
19.43   -36.37  1.99
-58.17  -7      7.05
-57.1   8.03    -3.47
-3.02   24.85   30.09
2.67    34.64   25.53
4.32    -16.77  29.56
-35.72  1.01    11.56
-15.53  5.11    64.47
-15.39  25.64   56.19
19.08   1.12    64.55
21.89   -2.52   62.49
-6.06   2.45    49.93
-4.25   -16.35  48.45
-3.03   35.69   36.38
-5.48   62.03   3.25
-50.72  24.53   25.91
-11.1   22.9    -15.29
11.33   17.03   -14.59
2.25    -31.43  47.31
4.28    -68.15  10.1
-40.45  -9.88   13.34
8.23    -4.14   13.46
```

Figure 3: The list of peaks, as generated through Sleuth.

1.7.2 Effect estimation

The second step performs a CBMA based on the peaks list previously obtained. Our approach was developed using the ALE algorithm at this stage. This implies that in step 1 the number of subjects in each experiment has to be recorded, together with the peaks, as this is fundamental for the ALE implementation. However, other CBMA techniques could be used as long as they produce a whole brain map for each experiment in addition to the final map describing the overall effect. All of them will be needed in the following steps. In light of this, our approach can manage IBMA too, since original maps for each experiment could be entered at this step in place of the corresponding MA maps.

1.7.3 Nodes definition

What described so far allowed to identify a pattern of co-alteration. However, in order to be able to analyze the relationships between the involved brain regions (or parcels of them) it is necessary to transform the pattern into a network. To do so, it is first needed to define a set of nodes. As a default in the present methodology, this is obtained by means of a peaks detection algorithm, so that nodes are placed in correspondence with the local maxima of the ALE map. Hence, each node represents a brain site where the effect had been coherently reported by the experiments in the data set. More than one node can be placed in a same brain region, allowing the identification of different involvement of its parcels. Of note, it is more advisable to impose a minimum interpeak distance of 10 mm, to avoid excessive overlap between the nodes (Eickhoff et al., 2009). This data-driven approach is particularly adequate in absence of a priori information, or hypothesis. Nonetheless, many other strategies can be easily implemented in our framework at this stage. A possible one is to impose a pre-determined set of nodes derived on a different dataset. This could be useful to compare different disorders (e.g. observe how nodes describing the co-alteration pattern of MCI are "wired" in Alzheimer's disease), or different stages along the disease progression. Nodes could also represent the functional profile of a cognitive domain, to be matched with the alteration caused by brain pathology. An opposite approach would be using a grid of equidistant nodes, in order to make this step less dependent on the identified ALE map, and completely unbiased by a priori knowledge.

1.7.4 Edges computation

Finally, the network is completed with the edges, expressing the frequency (or likelihood) of co-alteration between the nodes. In a really simplistic way this could simply reflect the raw count of the number of experiments (i.e. the MA maps) in which the two nodes are both altered. A more sophisticated solution is the Jaccard index, then thresholded as in Toro et al., (2008). Alternatively, the Patels' k Bayesian index allows to compute the probability of co-alteration of nodes a and b against the probability of their independent alteration (Patel, Bowman, & Rilling, 2006; S. M. Smith et al., 2011). All the three methods mentioned are based on the observation of the states of the nodes in each MA map, and this is the reason why the CBMA algorithm selected in step 2 has to provide a map for each experiment. Interestingly, the Patel's tau could be easily introduced in our framework allowing to estimate the directed edges, however the soundness of this index to analyze neuroimaging data is still debated (Wang, David, Hu, & Deshpande, 2017).

Of note, the identification of a set of nodes in step 3 does not imply the subsequent detection of a dense network. In fact, some nodes could remain without any edge. When the same set of experiments had been used in step 2, 3, and 4, an isolated node could spot a region often found altered (otherwise discarded by ALE), but not coherently in a pattern, so that no other nodes are co-altered with it often enough to determine an edge. If nodes are based on an external source, the lack of edges between two of them could also mean that no co-alteration was found at all based on the experiments selected in step 1 and used in steps 3 and 4.

1.7.5 Post-hoc analyses

The method developed combines the advantages of meta-analysis, allowing to consider the contribution of thousands of subjects without the need for new data acquisition, and network analysis, with its wide range of techniques now usable after the transition from patterns to networks. Among many indexes, node degree and edge betweenness are particularly useful to characterize the co-alteration networks. The former, simply defined as the number of edges linked to a node, allows to identify potential hubs of the co-alteration networks. When one (or more) of these high degree nodes are affected it is highly probable that many other regions are also found to be altered, maybe describing a later stage of the disease progression. A strong hub could also be considered as the element in common between existing sub-networks (i.e. different patterns of alteration consistently associated with a same disorder, all involving the node with high-degree). The edge betweenness offers a similar insight for the connections, being defined as the number of shortest paths going through an edge (Girvan & Newman, 2002). Using a road metaphor, this index identifies the avenue that if closed imposes an unusually long way to go from home to work. When the data set consists of tens of experiments, the obtained co-alteration network is often really dense (with more than one hundred edges). In these cases, it can be of help the identification of a core sub-network. This is achievable by means of a sparsity criterion, or directly setting an arbitrary Patel's k cut-off value to threshold the edges matrix. Values close to +1 characterize couple of nodes for which co-alteration is considerably more likely than independent alteration. Alternatively, node degree can be used, as in the case of the k-core algorithm (Alvarez-Hamelin, Dall'asta, Barrat, & Vespignani, 2005; Bader & Hogue, 2003) allowing to identify a sub-network of nodes with degree equal or greater than k (not to be confused with the Patel's k). As mentioned before, the creation of networks allows the comparison between multiple conditions. Interestingly, these can even represent different imaging modalities. Provided that a common set of nodes is used, the edges can express whatever kind of relationship among them (e.g. co-alteration,

co-activation, structural connectivity, similarity of genes expression, synchrony of maturation during development, comparable vascularization).

The code behind the method described was developed in Matlab. For the implementation of the ALE the java version of the algorithm was used, freely distributed by the BrainMap project. Results of step 2 are thus fully comparable with those of a CBMA performed using GingerALE tool. Specific elements of the output were designed to allow visualization and post-hoc analyses in Cytoscape (Shannon et al., 2003) and BrainNet Viewer (Xia, Wang, & He, 2013).

1.8 Phenotyping of gray matter networks

The method developed and here described allows to detect networks of GM regions showing structural differences between pathological subjects and healthy controls. However, no other features of the subjects included can be used to better characterize the network, as their age, sex, score on clinical scales, or further medical and demographic variables. This is mainly due to the meta-analytic nature of the approach, not allowing to model the effect deeper than the experiment level. Other strategies exist to analyze the relationship between imaging (i.e. a GM network) and non-imaging properties (i.e. a phenotype) (Congdon, Poldrack, & Freimer, 2010). In general terms, two main scenarios can be distinguished, depending on the direction of the research hypothesis. In one case, one (or more) non-imaging feature of interest has been selected, and the aim is to identify where in the brain the presence of structural (or functional) differences between subjects could be related to difference on that phenotype. As an example, trying to locate brain differences related with smoke habits. This approach could be summarized as going from features to network. In the opposite scenario, starting from an already known GM network you want to identify external factors the variation of which is related with differences in the network. This could be the case of an investigation on the relationship between variability of the default mode network and different lifestyles. This second approach could be summarized as going from network to features. Since in many cases it is not possible (or ethical) to setup an experimental design to actively modify the feature of interest, this kind of studies are mainly correlational (Aggarwal & Ranganathan, 2016). For this reason, a great sample size can improve the interpretability, and reliability, of the results. In some sense, the co-alteration detection method developed could be seen as a “from features to network” case, since it describes where in the brain differences related with the presence/absence of a given disorder exist. However, the diagnostic label is the only feature used, so treat our approach as a real phenotyping would result circular to some extent. For

this reason, part of my PhD project was dedicated to the learning and application of other phenotyping strategies to characterize GM networks in healthy subjects, and to identify brain structural differences associated with medical features.

2 – **Scientific works**

The present section includes a selection of papers I co-authored during my PhD career. They were chosen because the most effective to describe the path followed, and the rationale behind the research hypothesis addressed.

The first three papers concern the analysis of GM networks in the pathological brain, and specifically depict the development and application of the co-alteration network analysis. The first one is dedicated to the co-atrophy network of Alzheimer's disease, and it also was the first work in which our methodology has been described. The clear neurodegenerative nature made this disorder a perfect candidate. Moreover, the wide literature on the topic would have been of help to interpret and validate the results, besides ensuring a considerable data availability. The second study adopted instead a transdiagnostic approach, to investigate possible pathological processes shared by different disorders, both neurological and psychiatric. Moreover, it aimed to understand the relationship between the development of the co-alteration networks and the functional, structural and genetic connectivity of the healthy brain. Finally, the third work changed the focus toward a specific brain region, the insula. This structure was selected in virtue of previous literature showing its alteration in a wide variety of disorders. The aim was to analyze and compare the co-alteration networks associated with different sub-regions of the insula. This group of studies illustrates the above-mentioned flexibility of the method developed across three scenarios: whole brain and one disorder (study 1), whole brain and many disorders (study 2), one brain region and many disorders (study 3).

The fourth study is related with the analysis of GM networks in healthy subjects. It was realized in collaboration with the University of Granada and began during my internship under the supervision of Dr. Juan Verdejo-Roman (PNinsula research group, CTS-581). It is based on the PREOBE trial, a prospective observational cohort study designed to investigate early programming with a specific focus on maternal metabolic pathologies. Along four years of recruitment, a cohort of 331 mother-child pairs was built, to analyze both short-term and long-term effects of maternal overweight, obesity and gestational diabetes in the mother and her offspring (Berglund et al., 2016). The PREOBE trial was included in the DynaHEALTH project (Sebert et al., 2019), funded by Horizon2020. The specific aim of the here included study was to assess possible relationship between structural brain differences in 6 years old children and the presence of gestational diabetes and

excess-weight in their mothers. Hence, the research followed a transgenerational design, and fall under the "from features to network" case.

A further study followed instead the "from network to features" logic, and began during my internship at the University of Oxford under the supervision of Prof. Gwenaëlle Douaud (Translational Image Analysis Group). It is based on a sample of 39,676 subjects from the UK Biobank cohort, and analyzed possible relationship between a set of modifiable risk factors (accounting for smoking habits, alcohol consumption, sleep, hearing, inflammation, diabetes, cholesterol, blood pressure, exposure to pollution, depression, body size measurements, diet, exercise and socialization) and structural differences in a GM transmodal network originally described in Douaud et al. (2014). UK Biobank is probably the largest ongoing prospective epidemiological study, with 500,000 participants recruited between 2006 and 2010 in the age range 40-69. In addition to thousands of medical and demographic variables, genotyping has been undertaken on each of them, and imaging of brain, heart, abdomen, bones, and carotid artery is planned for 100,000 subjects. The final goal of UK Biobank is the improvement of prevention, diagnosis and treatment of a variety of diseases. In addition to the MRFs analysis, the project I was involved in included a genome-wide association study (GWAS) performed for the same mentioned GM network. The subjects' allele counts for two specific significant variants of the sex chromosomes were further associated with 16,924 non-imaging variables of UK Biobank, in a sample of 374,230 participants (not including those who were previously considered for the GWAS analysis). This last project is still in its final stage, and it was therefore not possible to include a detailed description in this thesis.

2.1 The Pathoconnectivity Profile of Alzheimer's Disease: A Morphometric Coalteration Network Analysis

This study was published in Frontiers in Neurology in 2018, as part of the special issue "Network Spread Models of Neurodegenerative Diseases" (doi:10.3389/fneur.2017.00739).

Authors: Manuello J., Nani A., Premi E., Borroni B., Costa T., Tatu K., Liloia D., Duca S., Cauda F.

Abstract

Gray matter alterations are typical features of brain disorders. However, they do not impact on the brain randomly. Indeed, it has been suggested that neuropathological processes can selectively affect certain assemblies of neurons, which typically are at the center of crucial functional networks. Because of their topological centrality, these areas form a core set that is more likely to be affected by neuropathological processes. In order to identify and study the pattern formed by brain alterations in patients' with Alzheimer's disease (AD), we devised an innovative meta-analytic method for analyzing voxel-based morphometry data. This methodology enabled us to discover that in AD gray matter alterations do not occur randomly across the brain but, on the contrary, follow identifiable patterns of distribution. This alteration pattern exhibits a network-like structure composed of co-altered areas that can be defined as co-atrophy network. Within the co-atrophy network of AD, we were able to further identify a core subnetwork of co-altered areas that includes the left hippocampus, left and right amygdalae, right parahippocampal gyrus and right temporal inferior gyrus. In virtue of their network centrality, these brain areas can be thought of as pathoconnectivity hubs.

Introduction

Widespread alterations of gray matter commonly characterize brain disorders. It has been suggested that neuropathological processes can selectively affect certain assemblies of neurons (Saxena and Caroni, 2011), which typically are at the center of crucial functional networks (Saxena and Caroni, 2011; Cauda et al., 2012; Raj et al., 2012; Zhou et al., 2012; Fornito et al., 2015; Iturria-Medina and Evans, 2015; Cauda et al., 2017). Because of their topological centrality, these areas or network hubs form a core set that is more likely to be affected by neuropathological processes (Etkin and Wager, 2007; Ellison-Wright and Bullmore, 2010; Saxena and Caroni, 2011; Hamilton et al., 2012; Jagust, 2013; Menon, 2013; Baker et al., 2014; Crossley et al., 2014; Douaud et al., 2014; Goodkind et al., 2015). In particular,

neurodegenerative diseases exhibit structural alterations that seem to distribute across the brain in network-like patterns (Yates, 2012; Warren et al., 2013). These patterns, which we propose to call morphometric co-alteration networks or, in the case of gray matter decreases, co-atrophy networks, can be thought of as a form of pathological anatomical covariance (Mechelli et al., 2005; Evans, 2013) and appear to develop according to the organization of brain connectivity (Raj et al., 2012; Zhou et al., 2012; Cauda et al., 2017). Studies aiming to investigate the networks formed by co-altered cerebral areas in the pathological brain are providing new insight for a better transdiagnostic and neurobiological understanding of the mechanisms at the root of brain disorders (Buckholtz and Meyer-Lindenberg, 2012; McTeague et al., 2016; Sprooten et al., 2017).

This is particularly true in the case of AD. So far great efforts have been made in order to identify a prototypical pattern of gray matter atrophy due to AD, and to put it into correlation with clinical symptoms (Du et al., 2007). It is now known that cortical thinning of specific brain sites can be already detected even before the appearance of the symptomatology and that the atrophy tends to increase when the condition worsens (Dickerson et al., 2009). Although the cortical reduction is commonly found in normal ageing (Fjell et al., 2014; Minkova et al., 2017), the pathological fingerprints of AD are mainly observed in a temporo-parietal set of brain areas, including hippocampus, entorhinal cortex, precuneus and posterior cingulate cortex (Head et al., 2005; Chapleau et al., 2016). The involvement of these regions has been repeatedly confirmed by meta-analytical studies, which have additionally found the alteration of the right superior frontal gyrus (Wang et al., 2015a). According to Ferreira et al. (2011) the left medial temporal lobe is the most impaired area in AD, even in the preclinical phases of the disease, so much so that the impairment of this area can be a good predictor of the clinical worsening of AD. A study of the relationship between the cortical thinning in AD and large-scale structural organization of the brain has revealed that AD reduces both the nodal centrality of temporal and parietal heteromodal association cortices and the positive correlation of thickness values normally found bilaterally between the parietal regions. In contrast, authors reported an increase of positive correlation among brain areas that are part of the default mode network (He et al., 2008).

Recently, investigations into the cognitive deficits caused by AD have taken advantage of the methodology of network analysis (Tijms et al., 2013; Matsuda, 2016). According to this approach, altered brain areas can be represented by means of a set of nodes, linked together by means of edges representing different statistical

values. Studies in this line of research have found that AD increases the correlation between the values of cortical thickness of the fusiform gyrus, temporal pole, parahippocampal gyrus and cingulum, which are all in proximity to each other. Conversely, a decrease of the correlation has been observed between distant areas (Yao et al., 2010). Of note, it has been suggested that, by combining different sources of information: i) large-scale structural networks data, ii) values of cortical thickness and iii) the pace of cortical thinning along time, it could be possible to distinguish patients with AD from healthy controls with an accuracy of 96.1%, as well as predict the conversion of MCI into AD 6 months before its clinical onset (Li et al., 2012). These studies raise the issue of moving from group analysis to single-subject results, which is an essential aspect when dealing with potential biomarkers for diagnostic purposes and surrogate endpoints for disease-modifying clinical trials. Recent methods of single-subject graph measurements have allowed to link network alterations and cognitive decline. For instance, it has been showed that the more the network becomes disorganized, the worse the clinical condition is (Tijms et al., 2014). Moreover, even in healthy subjects, it has been found an association between Aβ42 CSF low levels and alteration of network properties, which might be interpreted as a very early indication of an underlying pathological process (Tijms et al., 2016). All these results provide evidence that the approach based on network analysis can bring valuable insight to clinical practice (Tijms et al., 2013).

So far, at least four important mechanisms have been proposed to account for the distribution of brain alterations: transneuronal spread, nodal stress, shared vulnerability, and trophic failure (Zhou et al., 2012; Fornito et al., 2015).

The first mechanism suggests that misfolded proteins (native peptides with an incomplete or incorrect folding, as well as de novo polypeptides that become prone to self-aggregation) can diffuse along neuronal pathways (Goedert et al., 2010; Warren et al., 2013; Iturria-Medina et al., 2014; Brettschneider et al., 2015). Increasing evidence indicate that the spread of misfolded proteins presents several similarities to the plasma membrane prion protein intercellular transfer, along axonal fibers, potentially contributing to disease progression (Chevalier-Larsen and Holzbaur, 2006). This mechanism has been demonstrated in neurodegenerative diseases, such as Alzheimer's, Parkinson's, Huntington's, amyotrophic lateral sclerosis and tauopathies (Clavaguera et al., 2013; Bourdenx et al., 2017); more recently it has been also generalized to other brain disorders (Guest et al., 2011).

The second mechanism hypothesizes that the functional stress of the network hubs may result in a greater vulnerability of these areas (Buckner et al., 2005; Saxena and Caroni, 2011; Zhou et al., 2012; Crossley et al., 2014). This susceptibility has been supported in human beings with in vivo neuroimaging techniques and voxel-based meta-analyses (Crossley et al., 2014).

The third mechanism suggests that certain brain regions sharing gene or protein expressions may be more vulnerable to neuropathology (Lichtman and Sanes, 2008; Prieto et al., 2008; French et al., 2011; Wolf et al., 2011; Zhou et al., 2012; Cioli et al., 2014), with a potential relationship between gene expressions and connectivity patterns (French and Pavlidis, 2011; Cioli et al., 2014).

Finally, the fourth mechanism hypothesizes a disruption in the production of trophic factors, which could bring about the deterioration of neural wiring (Appel, 1981; Salehi et al., 2006; Zhou et al., 2012; Fornito et al., 2015).

If we consider the case of Alzheimer's disease (AD), neuropathological signatures, namely amyloid-β (Aβ) plaques and neurofibrillary tangles, are already present in the preclinical phase of the disease, with further spreading during progression. In fact several years before the clinical onset of AD, Aβ and tau progressively accumulate in the brain with a certain degree of spatial specificity as well as a partial overlap among the two deposits (Goedert, 2015). The relationship between tau and amyloid deposits in the cerebral cortex seems to have a hierarchical organization, with tau and Aβ clusters exhibiting distinctive intramodal and intermodal characterizations (Sepulcre et al., 2017). These findings would support the view of AD as an amyloid-facilitated tauopathy (Braak et al., 2000). Furthermore, Aβ and tau propagation and the subsequent deposition and cytotoxicity effects appear to occur mainly between anatomically interconnected areas, thus affecting the functional communication among them (Weiler et al., 2017).

The concept of a gradual spread of pathological signs is a crucial aspect put forward by recent theoretical models. Raj et al. (2012) have proposed a network diffusion model of disease progression in dementia, according to which the propagation of pathogenic proteins follows the regional concentration gradients under the spatial constraints defined by brain connectivity. Other authors have proposed a stochastic epidemic spreading model to describe intra-brain Aβ propagation and deposition processes, according to which regions with a higher connectivity degree are the main target of Aβ, thus suggesting that brain hubs are the more exposed to the negative effects of these aberrant proteins (Iturria-Medina et al., 2014). Finally, in addition

to focusing on misfolded proteins and propagation pathways, a further interesting approach suggests the need to investigate the relationship between these two factors (Warren et al., 2013). This model considers molecular nexopathies as conjunctions of pathogenic protein and brain networks. Key factors are therefore supposed to be structural/functional developmental factors and differential vulnerability of neural connections. Accordingly, long-range axonal connections may be more vulnerable to Aβ, so that functional and structural alterations could occur within the large-scale distributed fronto-temporo-parietal network, such as the one that supports the default mode network (DMN) processing.

In order to identify and study the co-atrophy network of AD, we devised an innovative meta-analytic method for analyzing voxel-based morphometry (VBM) data. This methodology enabled us to address the following issues:

a. How do gray matter alterations distribute across the brain affected by AD?

b. Is it possible to recognize a network-like structure in the pattern formed by these co-altered areas?

c. Can specific clusters of co-altered areas be identified within the co-atrophy network of AD?

Material and methods

Selection of studies

On March 2017 we performed with the software Sleuth an extensive meta-analytic search in the BrainMap VBM database (www.brainmap.org) (Fox and Lancaster, 2002; Laird et al., 2005; Laird et al., 2009). All the studies that fulfilled the following criteria were retrieved: "Contrast is Gray Matter"; "Context is Disease Effect"; "Observed Changes is Controls > Patients" and "Diagnosis is Alzheimer's Disease". Results were controlled so as to keep only experiments comparing subjects diagnosed with AD against healthy controls. Our search focused on gray matter decreased values only, as the development of AD is strongly characterized by axonal deterioration and neuronal loss that result in brain atrophy (Teipel et al., 2013). Furthermore, thus far just a few VBM studies have investigated gray matter increase in AD, so that these data were not sufficient for obtaining reliable results with our meta-analytical methods.

To ensure a transparent description of the selection process, we followed the "PRISMA Statement" international guidelines (Liberati et al., 2009; Moher et al., 2009) (Fig. S1). The characteristics of the sample can be viewed in Table 1.

ID	Reference	Journal	AD patients			Age			Scanner field (T)	Slice thick (mm)	Smoothing (mm)	Software
			Men	Women	Total	Min	Max	Mean ± SD				
1	Agosta et al. (65)	Radiology	14	9	23	–	–	74.6 ± 8.6	1.5	0.9 × 0.5 × 0.5	8	SPM5
2	Baron et al. (66)	NeuroImage	8	11	19	63	85	73 ± 5	1.5	1.5 × 1 × 1	12	SPM2
3	Baxter et al. (67)	Journal of Alzheimer's Disease	11	4	15	64	91	75.5 ± 7.8	1.5	1.5 × 0.9 × 0.9	12	SPM2
4	Berlingeri et al. (68)	Behavioral Neuroscience	8	13	21	–	–	76.5	1.5	1 × 1 × 1	–	SPM2
5	Boxer et al. (69)	Archives of Neurology	8	3	11	–	–	69.6 ± 8.2	1.5	–	12	SPM99
6	Bozzali et al. (70)	Neurology	11	11	22	–	–	67.9 ± 7.6	1.5	1	12	SPM2
7	Brenneis et al. (71)	NeuroReport	3	7	10	–	–	73.1 ± 7.6	1.5	1 × 1 × 1	–	SPM99
8	Canu et al. (72)	Neurobiology of Aging	13	29	42	–	–	77.8 ± 4.8 62.5 ± 4.5	1	1.3	8	SPM8
9	Chetelat et al. (73)	NeuroReport	7	9	16	63	85	72.1 ± 5.8	1.5	2 × 2 × 2	12	SPM99
10	Farrow et al. (74)	Psychiatry Research NeuroImaging	–	–	14	68	87	77 ± 7 78 ± 7	1.5	1 × 1 × 1	8	SPM2
11	Feldmann et al. (75)	Psychiatry Research	4	2	6	–	–	61.1 ± 7.7	1	0.8	8	SPM2
12	Frisoni et al. (76)	Journal of Neurology, Neurosurgery, and Psychiatry	6	23	29	53	86	74 ± 9	1.5	1.3	8	SPM99
13	Guo et al. (77)	Neuroscience Letters	6	7	13	58	81	72.1 ± 6.5	3	0.5 × 0.5 × 1	8	SPM2
14	Hall et al. (78)	Alzheimers Dementia	16	31	47	–	–	83.2 ± 5 79.4	1.5	1 × 1 × 1	10	SPM2
15	Hamalainen et al. (79)	Neurobiology of Aging	5	10	15	62	83	73.1 ± 6.7	1.5	2 × 2 × 2	–	SPM2
16	Hirao et al. (80)	Nuclear Medicine Communications	32	29	61	48	87	70.6 ± 8.4	1.5	1.23	12	SPM2
17	Honea et al. (81)	Alzheimer's Disease and Related Disorders	23	37	60	–	–	74.3 ± 6.3	3	1 × 1 × 1	10	SPM5
18	Ishii et al. (82)	European Journal of Nuclear Medicine and Molecular Imaging	8	22	30	–	–	66.8 ± 7.0	1.5	1.5	12	SPM99
19	Kanda et al. (83)	European Journal of Nuclear Medicine and Molecular Imaging	–	–	20	–	–	65	1.5	1.5	–	SPM2
20	Kawachi et al. (84)	European Journal of Nuclear Medicine and Molecular Imaging	9	23	32	–	–	67 ± 4.5	1.5	–	12	SPM99
21	Kim et al. (85)	Journal of Clinical Neuroscience	–	–	61	–	–	70.1 ± 5.0 71.1 ± 6.1 73.9 ± 5.5	3	1	12	SPM2
22	Matsuda et al. (86)	Journal of Nuclear Medicine	11	4	15	59	81	71.1 ± 7.1	1	1.23	12	SPM99
23	Matsunari et al. (87)	Journal of Nuclear Medicine	12	15	27	–	–	68.6 ± 6.8	1.5	0.78 x 1.04 x 1.4	12	SPM2
24	Mazere et al. (88)	NeuroImage	3	5	8	–	–	80 ± 6.8	1.5	1	8	SPM2
25	Miettinen et al. (89)	European Journal of Neuroscience	5	11	16	63	83	74.8 ± 5.4	1.5	2 × 2 × 2	12	SPM2
26	Ohnishi et al. (90)	American Journal of Neuroradiology	11	15	26	59	79	72.1 ± 1.1	1.5	–	12	–
27	Rabinovici et al. (91)	American Journal of Alzheimer's Disease and Other Dementias	5	6	11	–	–	64.5 ± 9.7	1.5	–	12	SPM2
28	Rami et al. (92)	International Journal of Geriatric Psychiatry	9	22	31	–	–	76.4 ± 6.8	1.5	1.5	10	SPM2
29	Remy et al. (93)	NeuroImage	1	7	8	–	–	72.2 ± 10.8	1.5	1 × 1 × 1	8	SPM2
30	Shiino et al. (94)	NeuroImage	19	21	40	55	82	71.1 + 9.7	1.5	–	12	SPM99
31	Takahashi et al. (95)	American Journal of Neuroradiology	20	31	51	–	–	72.6 ± 2.9	1.5	1.5	6	SPM8
32	Testa et al. (96)	Journal of Magnetic Resonance Imaging	2	5	7	–	–	73 ± 11	1.5	2 × 2 × 2	8	SPM99
33	Waragai et al. (97)	Journal of the Neurological Sciences	7	8	15	–	–	71 ± 5.1	1.5	2	12	SPM5
34	Whitwell et al. (98)	Neurobiology of Aging	16	22	38	–	–	65.3 ± 6.9	1.5	1.6	8	SPM2
35	Xie et al. (99)	Neurology	8	5	13	62	82	71.7	1.5	1.6	8	SPM2
36	Zahn et al. (100)	Psychiatry Research NeuroImaging	4	6	10	–	–	66.5 ± 8.9	1.5	1.5 × 1.5 × 1.5	8	SPM2

Where no information about slice thickness was provided, the voxel-size was expressed. The items are the result of the entire selection process as shown in PRISMA (Figure S1 in Supplementary Material) flow chart.

Table 1: Selected studies for the meta-analysis.

Anatomical likelihood estimation and the creation of modeled activation maps

VBM data were statistically elaborated with the procedure of the anatomical likelihood estimation (ALE). ALE is a voxel-based meta-analytical technique that models the spatial coherence of different results (Eickhoff et al., 2009; Eickhoff et al., 2012; Turkeltaub et al., 2012). A 3-dimensional Gaussian probability distribution is then centered on each focus of every experiment, using the following formula:

$$p(d) = \frac{1}{\sigma^3\sqrt{(2\pi)^3}}\, e^{-\frac{d^2}{2\sigma^2}}$$

in which d refers to the Euclidean distance between voxels and the considered focus, while e refers to the spatial uncertainty. The standard deviation can be obtained by means of the full-width half-maximum (FWHM), such as:

$$\sigma = \frac{FWHM}{\sqrt{8 \ln 2}}$$

The combination of these Gaussian distributions constructs a modeled activation (MA) map for each experiment. The definite ALE map is finally generated by uniting the MA maps. ALE maps were thresholded at a voxel-level FWD $p<0.05$, in line with Eickhoff et al. (2012; 2016; 2017). Given a specific threshold for cluster forming, a null distribution of cluster sizes was derived by simulating a long series of experiments with the same characteristics of real data and then by generating an ALE map. The score histogram so obtained was eventually employed to assign a threshold P values.

Construction of the morphometric co-atrophy network

To identify the distribution of gray matter alterations we have developed a novel methodology capable of constructing the morphometric co-alteration networks associated with brain disorders. Our analysis can in fact discover whether an altered brain area, say A, is statistically related to the alteration of one or more other brain areas (B, C, etc.). Thus, our analysis can construct the morphometric co-atrophy network composed of the areas occurring to be altered together and, subsequently, investigate within the co-atrophy network i) how an altered region is statistically associated with other altered regions and ii) which regions are likely to be involved in a more widespread net of alterations.

Node creation and labeling

We superimposed the ALE map on the Talairach atlas so as to distinguish automatically the anatomical regions identified by the ALE algorithm. If (at least) 20 voxels of the ALE map were found to be inside a certain area of the atlas, then this area was considered to be altered. We chose this cluster threshold so that less relevant regions could be excluded. We employed a peak detection algorithm to identify the local maxima of the ALE map, and we subsequently selected only those peaks that were greater than the 90 percentile of the value distribution. This set was further reduced by applying a minimum inter-peak distance of 10 mm. Finally, we positioned a node, labeled on the basis of the Talairach atlas, in correspondence of every survived peak.

Thresholding values applied during nodes creation and their rationale

As described in the previous paragraph, three thresholds were applied during the nodes creation procedure.

The first threshold regulates the minimum number of voxel (i.e. 20 voxels) necessary to consider a brain area as altered. The rationale behind this threshold is to exclude from the co-atrophy network nodes representing minimally (or, from a meta-analytical point of view, rarely) altered brain areas, thus improving and simplifying the interpretability of the results without losing highly relevant information. However, even considering brain areas in which only one voxel is altered, the results would have not been spurious, since ALE maps were voxel-level thresholded, which implies that each single voxel contains statistically significant information (Eickhoff et al., 2016) (see Fig. S2 for the visualization of the network obtained with different threshold values). This choice, however, would have unnecessarily increased the complexity of the co-atrophy network.

The second threshold, applied to the peaks-value distribution, allowed us to include in the network only nodes representing those areas for which there is a very high consensus between different experiments (i.e. high ALE value) (Eickhoff et al., 2016). Even in this case, this threshold could have been removed; all the nodes that can be created with the present methodology represent statistically significant effects, since they can only lie inside the anatomical regions identified by the ALE algorithm, which already has its own statistical thresholding step (see Fig. S3 for the visualization of the network obtained with different threshold values).

Finally, the inter-peaks distance was chosen considering the mean value (10.2 mm; SD = 0.4 mm) of uncertainty in spatial location associated with the reported coordinate discussed in Eickhoff, et al. (2009).

Therefore, the only effect of those thresholds on our data is to decrease the redundancy of the network, so as to obtain clearer results to be visualized and further analyzed, minimizing the information loss.

Co-atrophy distribution

From the set of the nodes as defined in the previous paragraph, we constructed a NxM matrix or a co-alteration matrix, in which each row referred to an experiment, whereas each column referred to a network node. On the basis of a Bernoulli generation data model, we constructed a probability distribution of joint alteration values for each pair of nodes. In other words, for any couple of nodes (a and b), we

were able to describe their four conjoint states of alteration by means of two binary variables: 1) a and b both altered; 2) a and b both unaltered; 3) a altered and b unaltered; 4) a unaltered and b altered. Consequently, the following four probabilities were obtained by the frequencies of the different combinations of all experiments:

$$\theta_1 = P(a = 1, b = 1)$$

$$\theta_2 = P(a = 1, b = 0)$$

$$\theta_3 = P(a = 0, b = 1)$$

$$\theta_4 = P(a = 0, b = 0)$$

These formulas refer to the conjoint frequencies of a couple of nodes (a and b) in all their four possible combinations. Table 2 shows the marginal probabilities for each couple of nodes.

	Node *a*		
Node *b*	**Altered**	**Unaltered**	
Altered	θ_1	θ_3	$\theta_1 + \theta_3$
Unaltered	θ_2	θ_4	$\theta_2 + \theta_4$
	$\theta_1 + \theta_2$	$\theta_3 + \theta_4$	1

Table 2: Marginal probabilities between altered and unaltered nodes.

On the grounds of these four probabilities, we have applied the Patel's k index (Patel et al., 2006) – which has been validated with simulated data by Smith et al. (2011) – in order to calculate the degree of co-alteration between nodes. This index can measure the probability that two nodes (a and b) are actually co-altered against the probability that node a and node b are altered independently of each other. Patel's k is calculated as follows:

$$\kappa = (\vartheta_1 - E)/(D(\max(\vartheta_1) - E) + (1 - D)(E - \min(\vartheta_1)))$$

where

$$E = (\vartheta_1 + \vartheta_2)(\vartheta_1 + \vartheta_3)$$

$$\max(\vartheta_1) = \min(\vartheta_1 + \vartheta_2, \vartheta_1 + \vartheta_3)$$

$$\min(\vartheta_1) = \max(0, 2\vartheta_1 + \vartheta_2 + \vartheta_3 - 1)$$

The numerator refers to the difference between the probability that a and b are altered together and the expected probability that a and b are altered independently of each other. The denominator refers to a weighted normalizing constant. Min(ϑ_1) refers to the maximum value of the conjoint probability P(a,b), given P(a) and P(b), whereas max(ϑ_1) refers to the minimum value of P(a,b), given P(a) and P(b). Patel's k index has values that range from –1 to 1. A value of |k| that is close to 1 indicates a high degree of connectivity between nodes. The statistical significance of this index was assessed with a Monte Carlo algorithm that simulated a multinomial, generative model, which took into consideration the alteration of all nodes. This statistical procedure obtained an estimation of p(k | z) by sampling a Dirichlet distribution and by calculating the samples' amount for which k>e, where e was the threshold of statistical significance set at p<0.01.

Topological analysis

We defined our system of interconnected nodes as a network of co-atrophy areas and examined it with the network analyzer included in Cytoscape 3.5.1 (Shannon et al., 2003; Smoot et al., 2011). We were therefore able to achieve a good and reliable description of the net formed by the co-atrophy areas under both the aspects of brain structure and functional organization.

Node degree and edge betweenness

The node degree was defined as the number of edges linked to a node. We employed this parameter in order to detect the nodes that were more connected within the network, which are commonly considered as brain hubs. In turn, the parameter of edge betweenness was defined as the number of the shortest routes that go through an edge in a graph or a network (Girvan and Newman, 2002). Thus, edges exhibiting high values of betweenness are supposed to be involved in a large number of shortest routes, so that their elimination is likely to have an impact on communication between many couples of nodes.

Network clustering

Given the great number of nodes as well as the high density of edges within the co-atrophy network, we used the k-core decomposition algorithm (Bader and Hogue,

2003; Alvarez-Hamelin et al., 2005) – as it is implemented in the clusterMaker plugin for Cytoscape – to detect a central sub-network of highly interconnected nodes. This algorithm eliminates all the nodes showing a degree that is lesser than a user-defined k, thus deriving from the original network the highest connected subgraph.

Results

Common patterns of morphometric alterations

The ALE performed on all the data retrieved by our search (57 experiments, 883 subjects, and 691 foci) showed that gray matter alterations caused by AD are mainly located in the right medial frontal gyrus, the right inferior frontal gyrus, the left inferior parietal lobule, the right midcingulate gyrus, the left supramarginal gyrus, the right angular gyrus, the bilateral fusiform gyrus, the right precuneus, the bilateral insula, the right thalamus, the bilateral superior temporal gyrus, the bilateral superior temporal pole, the bilateral hippocampus, the bilateral parahippocampal gyrus, the bilateral amygdala and the left caudate nucleus (Fig. 1).

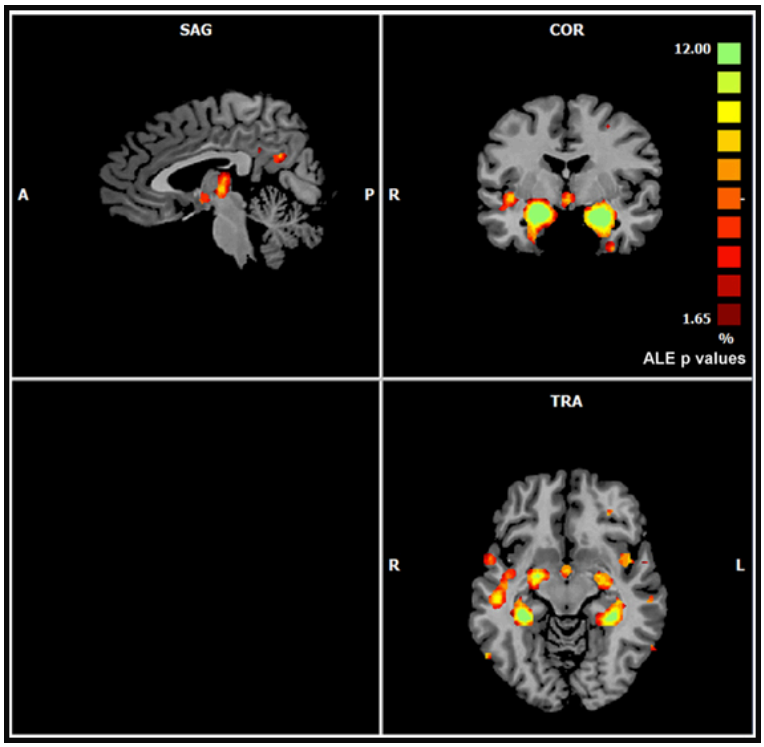

Figure 1: Gray matter anatomical likelihood estimation (ALE) results. The image summarizes the results of all the experiments considered in this meta-analysis. Colors from red to green show gray matter decreases [ALE maps were thresholded using voxel-level FWD $p < 0.05$ and visualized using Brainvoyager QX].

Morphometric co-atrophy network

The left panel of Figure 2 illustrates the 40 nodes used to build the co-atrophy network, while the heat map in Figure 2 shows the relationship between the elements of each possible couple of nodes measured by Patel's k index. Figure 3 illustrates the whole co-atrophy network: the colors' scale ranges from blue to red for the 146 edges and indicates an increase in k values. Edges are to be assumed as undirected.

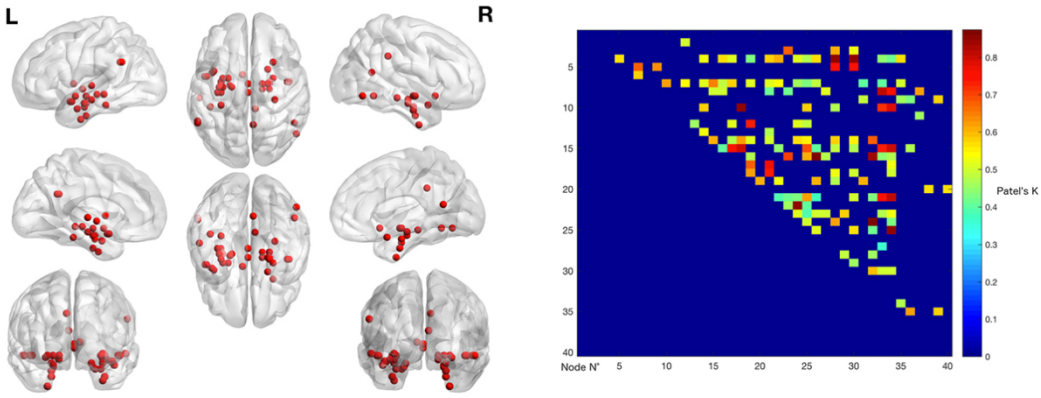

Figure 2: The left panels shows the nodes that entered the coatrophy calculation. The right panel shows the coatrophy matrix. Colors from blue to red indicate increasing Patel's k values (i.e., increasing coalteration probabilities).

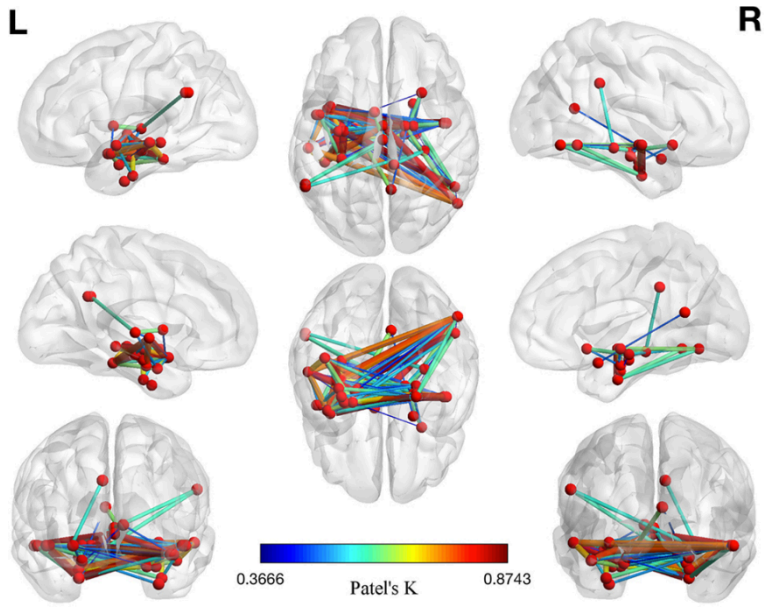

Figure 3: Morphometric coatrophy network results. Colors from blue to red indicate increasing Patel's k values (i.e., increasing coalteration probabilities).

Many nodes densely interconnected characterize the temporal lobe, especially the hippocampus and the parahippocampal gyrus. In contrast, only one node characterizes other brain areas, such as the cingulate cortex and precuneus. Although all the edges that are shown are statistically significant, the ones with the highest k value are those involving the left hippocampus, bilateral amygdala, right parahippocampal gyrus and right inferior temporal lobe (Tab. S1 and Tab. S2).

Figure 4 reports the organic option of the yFiles Layouts available in Cytoscape 3.5.1 (based on a spring-embedded algorithm) attributed to the co-atrophy network. Thick links connect the nodes located in the temporal cortex, parahippocampal gyrus, amygdala, and thalamus. The right precuneus is connected to the rest of the network just through one edge projecting to the left hippocampus, whereas the right cingulate cortex is connected to the network core through the right hippocampus and the right parahippocampal gyrus. In figure 4 colors and dimensions of nodes are proportional to their network degree values. In particular, Amyg_L_1 shows the highest degree value (17), followed by Temp_Inf_R (16). In turn, Fusiform_L, Amyg_L, Temp_Pole_Sup_R, SupraMarginal_L and Cingulum_Mid_R exhibit the lowest degree value (1). The edges' thickness is proportional to their degree of edge betweenness. The edge linking the nodes Hipp_R_2 and ParaHipp_R_2 shows the highest value, while the edge between Amyg_R and ParaHipp_L_1 shows the lowest one.

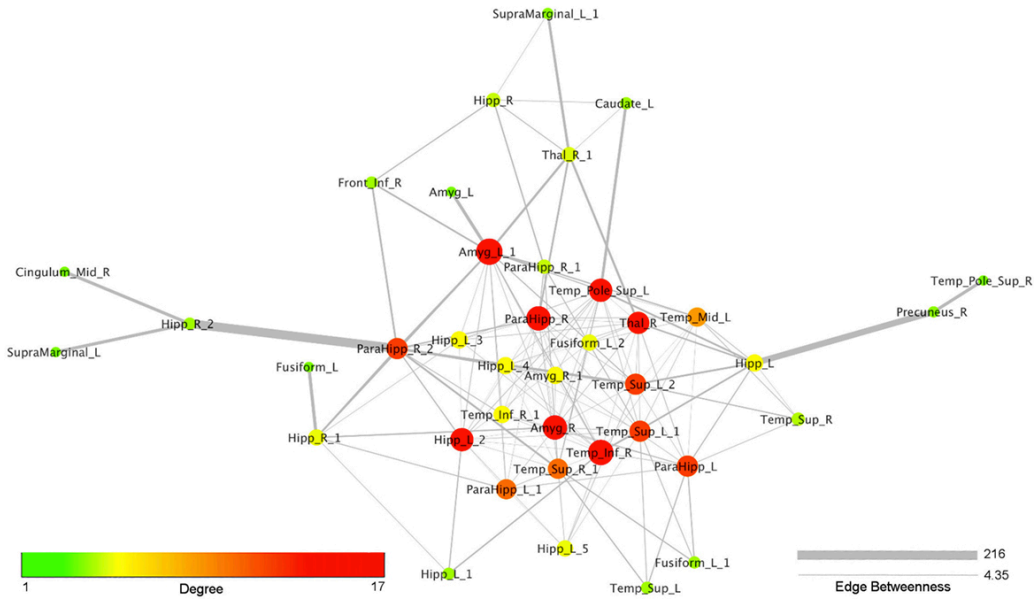

Figure 4: Topological analysis of the coatrophy network of Alzheimer's disease (organic yFiles Layout). Colors and dimensions of nodes indicate their topological degree (smaller node = lower degree; from green to red = from lower to higher values). Thickness of edges indicate the degree of edge betweenness (smaller edge = lower degree).

Figure 5 shows the nodes according to their anatomical position. In order to simplify the visual interpretation, we have merged two or more nodes referring to the same brain area; however, we have kept the edges unchanged. It is worth noting that the co-atrophy network of AD is composed of more inter-hemispheric (75) than intra-hemispheric edges (71). Apart from the hippocampus, most of the inter-hemispheric connections link structures in the medial temporal lobes. Furthermore, unilateral nodes in the right inferior temporal gyrus and right precuneus are linked to areas of both hemispheres.

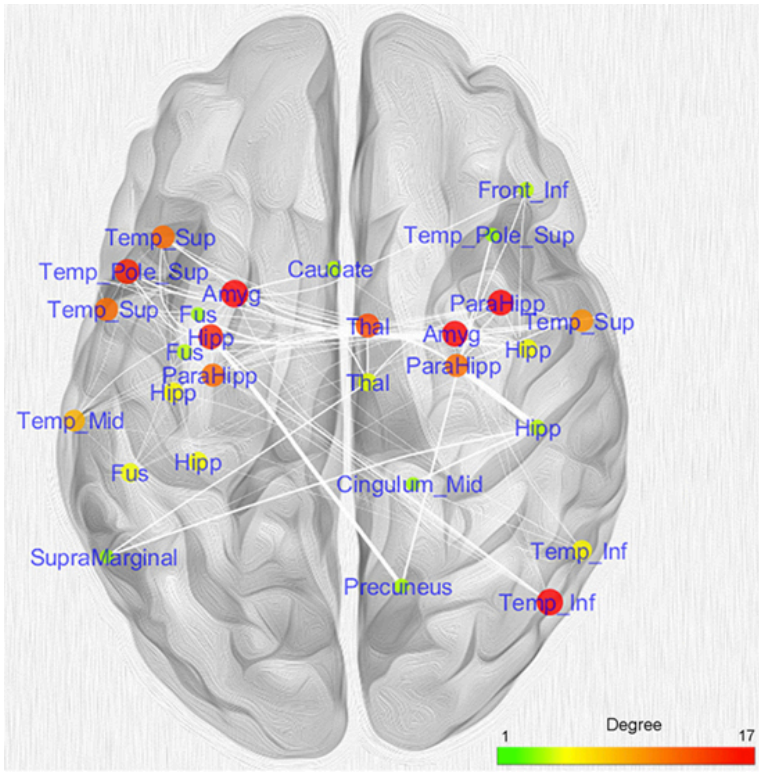

Figure 5: Topological analysis of the coatrophy network of Alzheimer's disease. Nodes referring to the same brain areas or strictly close one to the other have been collapsed in a single node.

As many nodes populate the hippocampi, we projected them on a 2D template in order to better clarify their spatial localization (Fig. 6). Five out of the 6 nodes in the left hippocampus were found to be located in the anterior part, while the remaining one was found to be located in the posterior section. In contrast, the right hippocampus exhibits a more uniform pattern, with 2 anterior nodes and 1 posterior.

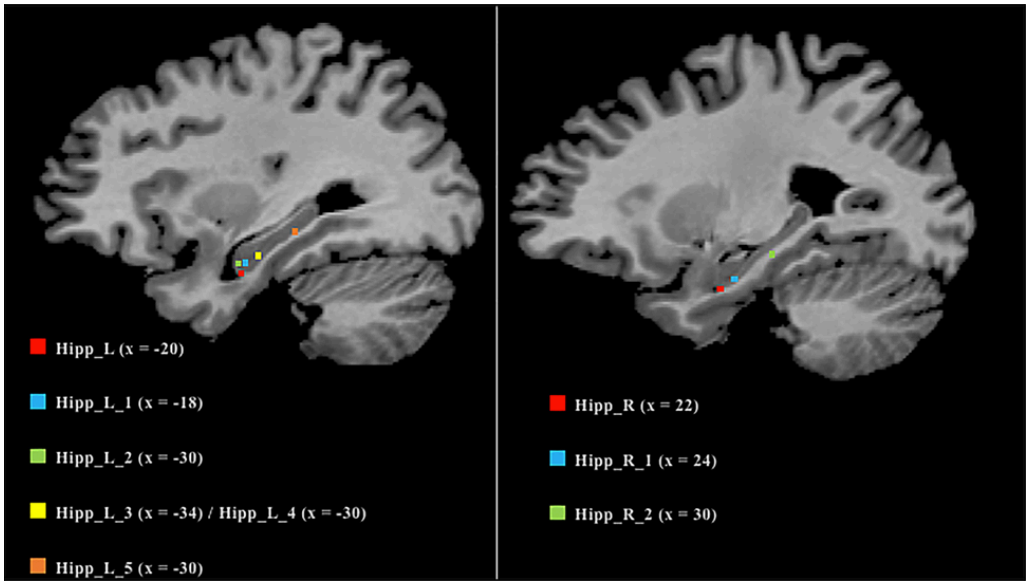

Figure 6: Anatomical localization of the nodes in the hippocampi. Coordinates refers to Talairach space (right sagittal slice x = 25, left x = 30). Nodes are numerically labeled according to a rostrocaudal criterion.

We also analyzed the connectivity profile of the hippocampi within the co-atrophy network so as to better understand their relationship with the other nodes of the network (Fig. 7). Even though hippocampi have a lot of connections, they are scarcely interconnected (red edges) and, in particular, between the nodes of the right hippocampus there are no direct paths linking them to each other. What is more, the left hippocampus presents a greater number of edges (45) than the right hippocampus (15); however, these edges are generally characterized by a low degree of edge betweenness. In contrast, the 15 edges linking the right hippocampus to the other nodes of the co-atrophy network are characterized by a high degree of edge betweenness. Overall, considering the anatomical topology of nodes (Fig. 6), the left anterior hippocampus appears to be the most densely connected.

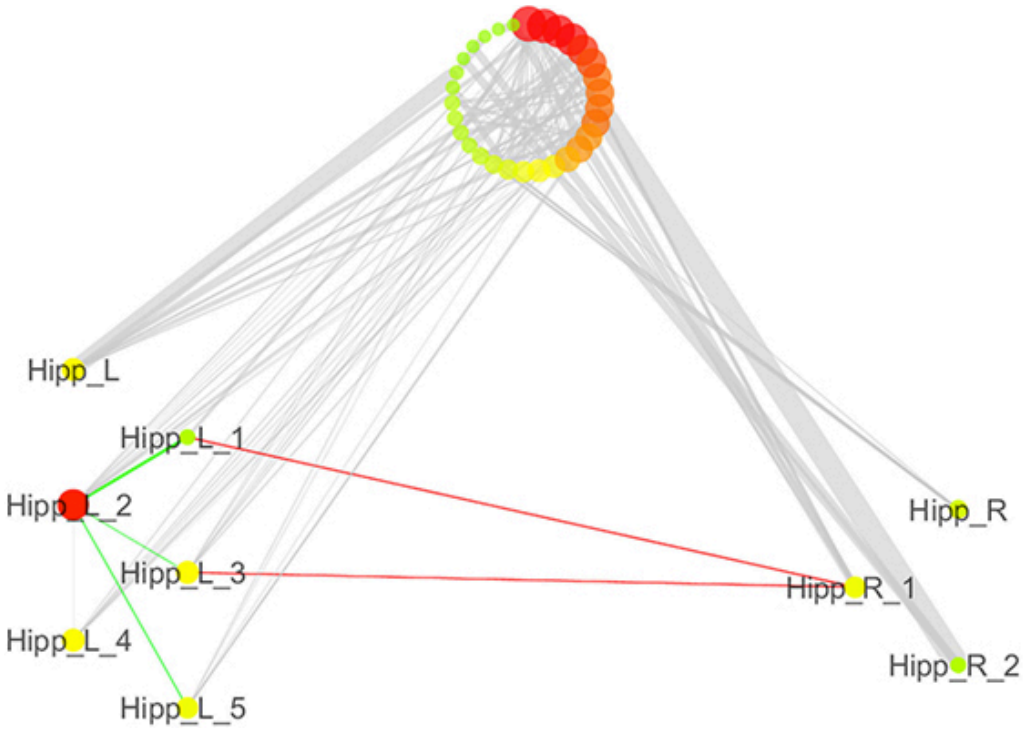

Figure 7: Detailed illustration of the role of the hippocampi in the coatrophy network of Alzheimer's disease. Green edges are intrahemispheric, while red edges are interhemispheric.

Given the great number of nodes and the high density of edges of the co-atrophy network, we used the k-core algorithm to identify the most connected components of the network. The analysis reported a core subnetwork formed by 8 inter-hemispheric nodes (Fig. 8), including the left and right amygdalae, left hippocampus, right parahippocampal gyrus, and right temporal inferior gyrus. The bilateral presence of nodes within this core subnetwork is consistent with the finding that the co-atrophy network is characterized by a large number of inter-hemispheric edges.

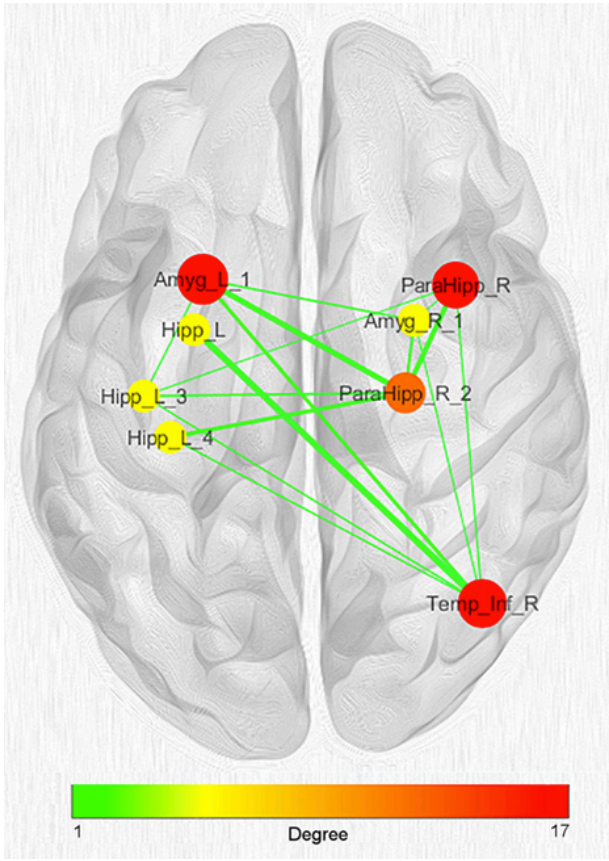

Figure 8: Network clustering with k-core decomposition algorithm. Colors and dimensions of nodes indicate their topological degree (smaller node = lower degree; from green to red = from lower to higher values). Thickness of edges indicate the degree of edge betweenness (smaller edge = lower degree). Both node degree and edge betweenness values refer to the original coatrophy network.

Discussion

With an innovative voxel-based meta-analytic method, this study aimed to find out whether gray matter decreases caused by AD distribute throughout specific and identifiable areas rather than affect randomly the whole brain. After constructing a morphometric co-atrophy network, we intended to identify which brain areas are more likely to be altered in conjunction with other ones rather than alone. Finally, we examined the potential existence of relevant subcomponents within the co-atrophy network.

The gray matter decreases evaluated by ALE involve limbic and temporal areas, in particular the hippocampus and parahippocampal gyrus. This finding is in accordance with most of previous research (Yang et al., 2012; Wang et al., 2015a). Nine out of 40 nodes of the co-atrophy network are localized within the hippocampus. Specifically, 6 nodes are in the left hippocampus (5 in its anterior part, 1 in its posterior part) and 3 in the right one (2 anterior, 1 posterior). This is consistent with the neuropathological studies suggesting that AD is characterized by an earlier and greater involvement of anatomical structures (including hippocampus) in the left hemisphere (Thompson et al., 2007; Woolard and Heckers, 2012; Long et al., 2013). Although there is still debate about the exact functional organization of the hippocampus (Strange et al., 2014), the neuroscientific community has achieved a substantial consensus on its role in learning and memory (Zeidman and Maguire, 2016), which are both deteriorated cognitive functions in AD. According to Thal et al. (2014) the hippocampus (in particular the subfields CA1 and subiculum), along with the amygdala, are pretty soon affected by Aβ plaques during AD evolution (Pievani et al., 2011). In line with AD diagnostic criteria (McKhann et al., 2011) hippocampal and mesial temporal lobe atrophy have been considered as biomarkers of neuronal degeneration, potentially increasing the probability of an underlying AD pathophysiological process. Currently, however, the routinely utilization of hippocampal atrophy in clinical practice is not fully standardized, but preferentially applied in investigational studies and clinical trials. Furthermore, hippocampal atrophy rate could be better accounted for as a sensitive marker of disease progression (Apostolova et al., 2010; Sabuncu et al., 2011), being able to trace AD natural development and potentially representing an interesting surrogate marker for disease-modifying clinical trials (Schuff et al., 2009; Whitwell, 2016). Interestingly, an increased hippocampus and an asymmetry in the shape of the amygdala during the development of AD have been recently demonstrated, with significant correlation to cognitive impairment (Wachinger et al., 2016).

According to our analysis, the gray matter co-atrophy network of AD appears to be densely interconnected, as suggested by the presence of 146 edges and 40 nodes, 39 of which have at least one connection. The existence of a set of nodes (altered areas) is not a proof per se that the disease is spreading. In fact, generally speaking, Patel's k is not always able to identify edges between nodes, which means that, even though some areas are altered, there is no apparent temporal coherence in their capitulation to the disease. The fact, though, that our analysis was able to discover a significant number of edges between nodes is proof of the good reliability of our results

pointing out that the alteration co-occurrence really happens, as well as of the consistency of our sample.

Our analysis suggests that AD tends to target a somewhat limited set of brain regions, rather than randomly affecting distinct sites. Furthermore, the left hippocampus, bilateral amygdala, right parahippocampal gyrus and right inferior temporal lobe seem to follow a very similar pace of degeneration (Fig. S4).

In order to evaluate the likelihood of each node of the co-atrophy network to be co-altered with other ones rather than as an individual spot we calculated their node degree. The highest value pertains to the node of the left amygdala, which is reached by 17 edges, but we found other 13 nodes with at least 10 edges. These nodes are localized in the temporal lobes, right amygdala, parahippocampal gyrus, left hippocampus and right thalamus. The high degree of pathoconnectivity of these nodes suggests that, when gray matter alteration affects one of them, it is highly probable that many other regions are also found to be altered. It is also true the other way round, that is, when nodes characterized by low degree show atrophy, it is very likely that this process co-occurs in one of the high-degree nodes, rather than in another low-degree node. These results, as well as the k-core decomposition, provide evidence that in the co-atrophy network of AD certain nodes have the characteristic of being pathoconnectivity hubs. Furthermore, the values of the edge betweenness distribution indicate the existence of a dense subnetwork, which is composed of the nodes with the higher degree of pathoconnectivity.

The paucity of connections linking the two hippocampi suggests a limited co-occurrence of alterations between them. The hippocampus is known to be greatly affected by AD, and the MRI volume estimation of this structure is currently considered one of the most reliable in vivo biomarker of this disease (Teipel et al., 2013). Our results suggest that both the hippocampi are substantially altered, albeit somewhat independently. According to previous studies, certain molecular alterations typical of AD are more evident in the left hippocampus compared to the right one (Hovorkova et al., 2008; Kristofikova et al., 2008). This discovery might explain the abundance of edges connecting the nodes in the left hippocampus, as well as support the transneuronal spread mechanism in AD. The nodal stress hypothesis could also play a role in virtue of the intense functional activity of this region. Finally, our finding that the anterior part of the hippocampus exhibits a greater number of edges than the posterior part seems consistent with the suggestion that the deterioration of CA1 and subiculum appears to be more correlated with the

development of AD than the deterioration of CA3, which appears to be more correlated with healthy aging (Pievani et al., 2011; Jagust, 2013). Recently, the presubicular-subicular complex has been described as one of the earliest site of atrophy in AD, with a significant correlation with memory performances (even in MCI phase), potentially reflecting the ongoing degenerative process through the subiculum passing from entorhinal cortex to dentate gyrus (Carlesimo et al., 2015; Hirjak et al., 2017).

In addition to the interpretation of the co-atrophy network as a whole, some specific aspects deserve a detailed consideration. The first is the relationship between hippocampus and precuneus. In the co-atrophy network of AD these regions are linked through an edge exhibiting a very high degree of edge betweenness, which reveals a direct interaction. According to the "hippocampus disconnection hypothesis" proposed by Tahmasian et al. (2015), the disruption of functional connectivity between hippocampus and precuneus could induce the characteristic alterations in the hippocampus that we find in AD. Tahmasian et al. (2015) have in fact demonstrated that in AD the hippocampus is much less inhibited, and this disinhibition may result in its hyper-metabolism. A similar situation could induce neurotoxicity, which might be one of the causes behind gray matter decrease measured with VBM, thus explaining the identification of a significant number of nodes in the hippocampus.

A second interesting aspect is the relationship between the left hippocampus and right inferior temporal gyrus, which was highlighted by k-core decomposition. This result is in agreement with the study of Wang et al. (2013), which found that the interaction between these two areas is typical of AD. Of note, Wang et al. (2013) examined 80 pathological subjects using Bayesian network analysis and prior-defined regions of interest, while the present study has applied a meta-analytical approach on a substantially bigger VBM database of 883 patients diagnosed with AD. This agreement supports the sensitivity of our novel methodology. Furthermore, the slight prevalence of inter-hemispheric connections in the co-atrophy network of AD (see Fig. S5) is consistent with the deterioration of white matter bundles in AD, in particular concerning the corpus callosum (Teipel et al., 2002; Ardekani et al., 2014; Bachman et al., 2014; Walterfang et al., 2014; Fischer et al., 2015). Callosal atrophy has been associated with cognitive decline rate as well as to disease progression (Wang et al., 2014; Wang et al., 2015b).

Gray matter alterations found in the hippocampus, precuneus, and inferior parietal cortex can be ascribed to the general disruption of the DMN in patients with AD (Greicius et al., 2004; Weiler et al., 2017). Recently, a study has showed that the DMN dysfunction, as well as the disruption of the interaction between different resting state functional networks, can be attributed to amyloid burden (Weiler et al., 2017). What is more, Chang et al. (2015) have found that amyloid burden in the cingulate cortex might promote gray matter atrophy in the other areas constituting the DMN.

Overall, the crucial role played by pathological proteins in AD supports the transneuronal spread hypothesis at the basis of gray matter alterations' distribution (Chevalier-Larsen and Holzbaur, 2006; Goedert et al., 2010; Guest et al., 2011; Zhou et al., 2012; Iturria-Medina et al., 2014; Fornito et al., 2015). However, the complex relationship among different factors (such as amyloid burden, Tau deposition, gray matter atrophy, and disrupted functional connectivity) and the presence of several hub nodes within the co-atrophy network of AD suggest that the nodal stress mechanism could as well be involved in the development of the disease (Jack et al., 2013). Therefore, it is extremely likely that different spreading mechanisms, which are not mutually exclusive, may be involved in the etiology of AD.

Limitations and future directions

The present investigation and the methodology on which it is based aim to better understand the nature of AD by examining its pathological fingerprints over the brain. To do so, we were able to get access to a very large sample size of patients. If this is an advantage on the one hand, it can also be a limitation on the other, as within this sample it was not possible to determine the average duration of disease, due to unavailability of information in the original studies. This aspect makes it difficult to associate the co-atrophy network with a specific stage of AD progression. However, the methodological procedure for defining the areas to be included in the co-atrophy network considers primarily the frequency of every single area to be found altered. In case of a neurodegenerative condition such as Alzheimer's we could imagine, generally speaking, a group of patients with a recent diagnosis exhibiting alterations in area A, another group with an intermediate development of the disease exhibiting alterations in areas A-B, and another group with an advanced development of the disease exhibiting alterations in areas A-B-C. Since our methodology privileges the frequency of each area to be found altered, in the final network area A will be more likely to be represented, while area C may be even excluded. Moreover, even if the

group of patients exhibiting alterations in A-B-C were greater than the other groups, the pattern A-B-C would be less likely to be represented than the sole area A. For this reason, even if our input data could contain an overrepresented sample of patients in a specific stage of the disease, the resulting co-alteration network would not represent the pattern of altered areas which is typical of that stage.

Future studies on longitudinal data analyzed by different methods are needed in order to investigate the sequential formation of the co-atrophy network identified in this study, so as to achieve a more detailed picture of the temporal evolution of AD.

Conclusion

This meta-analysis was able to address the following important issues.

a. In AD, gray matter alterations do not occur randomly across the brain but, on the contrary, follow identifiable patterns of distribution.

b. This alteration pattern exhibits a network-like structure composed of co-altered areas that can be defined as co-atrophy network.

c. Within the co-atrophy network of AD, certain brain areas, in virtue of their node degree and values of edge betweenness, can be considered as pathoconnectivity hubs. The alteration of these areas is supposed to imply a wider distribution of gray matter abnormalities across the brain.

d. Within the co-atrophy network we can identify a core subnetwork of co-altered areas that includes the left hippocampus, left and right amygdalae, right parahippocampal gyrus and right temporal inferior gyrus.

The innovative methodological analysis developed in this study for constructing the morphometric co-atrophy network of an important neurodegenerative disease such as AD opens a new window into the comprehension of the pathological brain. Increasing evidence is supporting the idea that brain alterations distribute according to a network-like structure. The analysis carried out in this study not only provides support for this hypothesis but also puts forward the significant finding that certain nodes of the co-atrophy network may play the role of pathoconnectivity hubs. What is more, our methodology can be equally applicable to study the morphometric co-alteration network of any other neuropathological condition. Future investigations into this line of research on databases of different diseases promise to provide valuable insight to the study of the dynamics of brain disorders, so as to achieve a better predictive diagnostic power as well as to improve medical care and treatment.

Supplementary material

Selection of studies

The BrainMap database was employed for the retrieval of relevant brain imaging experiments carried out with the voxel-based morphometry (VBM) technique. As reported in the User Manual, BrainMap uses a structured standardized coding scheme that describes published human neuroimaging experimental results. This taxonomy has been used to describe over 3600 publications and 15000 experiments, drawing upon over 110000 subjects and reporting over 120000 coordinates. The main division of the coding scheme is between structural (VBM) and functional data. For this meta-analysis only papers labeled as "Structural" have been used. So, considering only the studies in this category, the database consists of 980 papers, 3093 experiments, 73938 subjects and 21481 locations.

The software application "Sleuth" has been used to search the database for experiments of interest and view the relevant search results in a standard brain space. This procedure allowed us to identify 42 studies about Alzheimer's disease (AD) for a total of 72 experiments.

Two expert researchers have reviewed all the experiments, so as to ensure: (1) both the presence of the healthy control group and the pathological sample; (2) that results describe differences between subjects diagnosed with AD and healthy controls, and not between AD and other pathologies or between subcategories of AD; (3) that results concern VBM parameters (See Fig. S1 [PRISMA flow chart] and Table 1).

All the selected experiments that did not meet the inclusion criteria were excluded.

Relevant descriptive information was extracted from each article. After this searching procedure, 36 papers were included in the meta-analysis, for a total of 57 experiments and 883 subjects. Table S1 provides a detailed description of the sample of the selected studies.

Supplementary figures

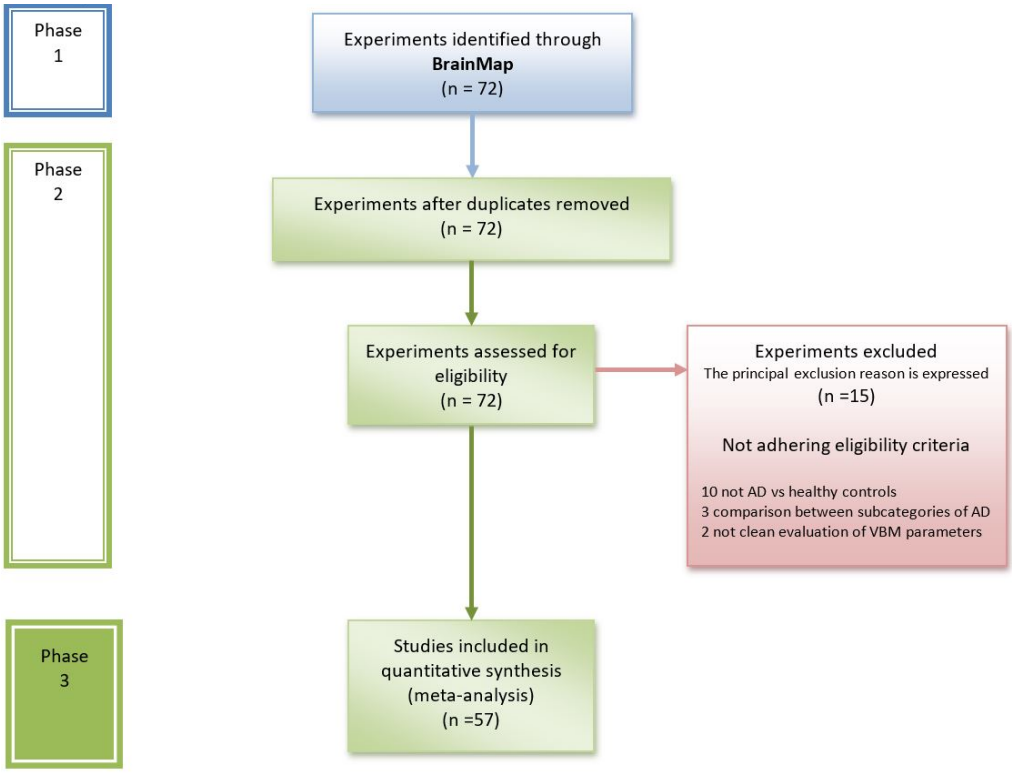

Figure S1: Overview of the selection strategy. Numbers refer to experiments.

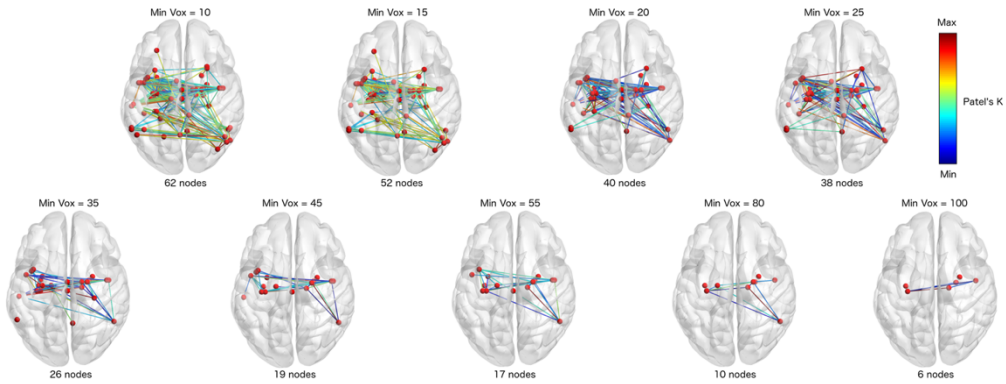

Figure S2: The co-alteration network obtained with different values for the minimum number of voxels threshold. Colors from blue to red indicate increasing Patel's k values (i.e., increasing co-alteration probabilities).

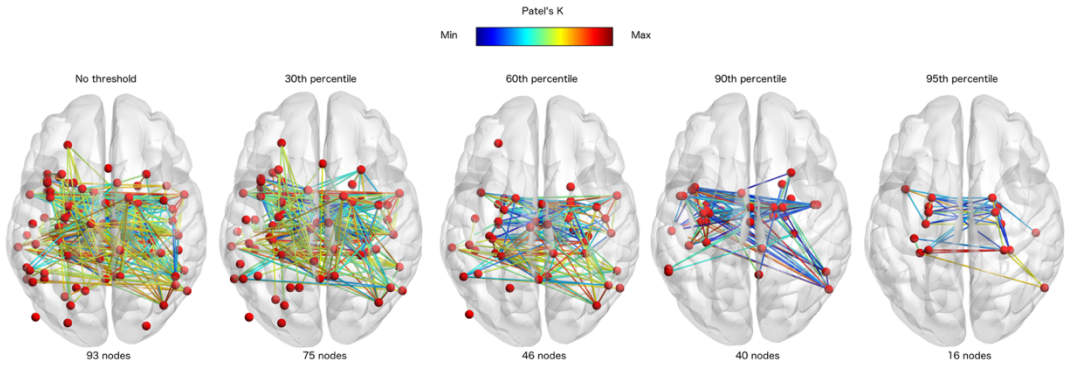

Figure S3: The co-alteration network obtained with different values for the peaks' values percentile threshold. Colors from blue to red indicate increasing Patel's k values (i.e., increasing co-alteration probabilities).

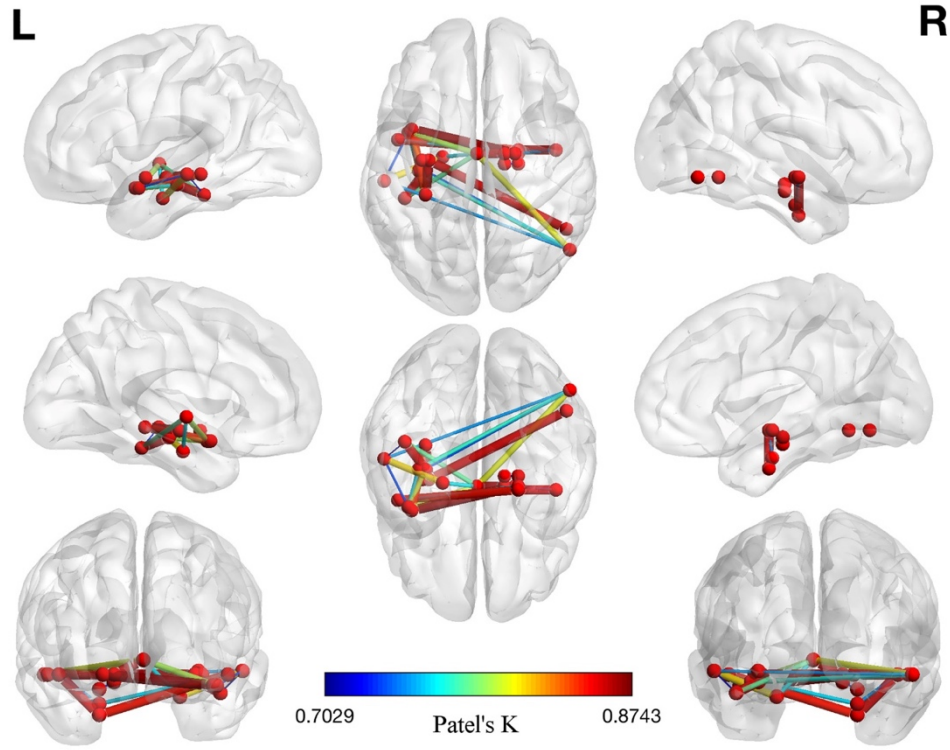

Figure S4: Results of the morphometric co-atrophy network of AD. Colors from blue to red indicate increasing Patel's k values (i.e., increasing co-alteration probabilities). Only edges with k > 0.7 are shown.

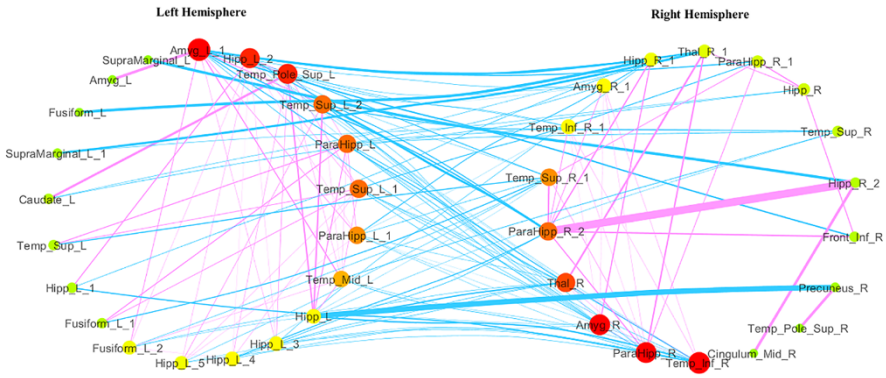

Figure S5: Distribution across hemispheres of the co-atrophy network of AD. Violet edges are intra-hemispheric, while blue edges are inter-hemispheric.

Supplementary tables

Node Name	Corresponding brain area	Node Talairach coordinates			Node Degree
		X	Y	Z	
Amyg_L_1	Left Amygdala	-22	-2	-24	17
Temp_Inf_R	Right Inferior Temporal Gyrus	54	-64	-10	16
Amyg_R	Right Amygdala	16	-8	-10	15
ParaHipp_R	Right Parahippocampal Gyrus	24	-6	-32	15
Hipp_L_2	Left Hippocampus	-30	-10	-18	14
Temp_Pole_Sup_L	Left Superior Temporal Pole	-40	4	-16	14
Thal_R	Right Thalamus	0	-8	-2	13

ParaHipp_L	Left Parahippocampal Gyrus	-32	-12	-10	12
ParaHipp_R_2	Right Parahippocampal Gyrus	16	-14	-14	12
Temp_Sup_L_1	Left Superior Temporal Gyrus	-46	0	-10	12
Temp_Sup_L_2	Left Superior Temporal Gyrus	-38	6	-16	12
ParaHipp_L_1	Left Parahippocampal Gyrus	-28	-12	-10	11
Temp_Sup_R_1	Right Superior Temporal Gyrus	46	-6	-10	11
Temp_Mid_L	Left Middle Temporal Gyrus	-54	-24	-8	10
Amyg_R_1	Right Amygdala	22	-8	-10	8
Hipp_L	Left Hippocampus	-20	-10	-22	8
Hipp_L_3	Left Hippocampus	-34	-18	-14	8
Hipp_L_4	Left Hippocampus	-30	-18	-14	8
Temp_Inf_R_1	Right Inferior Temporal Gyrus	52	-52	-10	8
Fusiform_L_2	Left Fusiform Gyrus	-42	-34	-20	7
Hipp_L_5	Left Hippocampus	-30	-32	-8	7
Hipp_R_1	Right Hippocampus	24	-14	-18	7
Thal_R_1	Right Thalamus	0	-18	2	6
Hipp_R	Right Hippocampus	22	-8	-22	5
ParaHipp_R_1	Right Parahippocampal Gyrus	24	-8	-26	5

Temp_Sup_R	Right Superior Temporal Gyrus	44	-6	-10	4
Caudate_L	Left Caudate Nucleus	-6	2	4	3
Front_Inf_R	Right Inferior Frontal Gyrus	28	16	-10	3
Fusiform_L_1	Left Fusiform Gyrus	-32	-12	-32	3
Hipp_L_1	Left Hippocampus	-18	-12	-18	3
Hipp_R_2	Right Hippocampus	30	-26	-12	3
Temp_Sup_L	Left Superior Temporal Gyrus	-48	0	-10	3
Precuneus_R	Right Precuneus	6	-54	16	2
SupraMarginal_L_1	Left Supramarginal Gyrus	-56	-50	28	2
Amyg_L	Left Amygdala	-28	-2	-24	1
Cingulum_Mid_R	Right Midcingulate cortex	8	-36	34	1
Fusiform_L	Left Fusiform Gyrus	-30	-6	-36	1
SupraMarginal_L	Left Supramarginal Gyrus	-56	-52	28	1
Temp_Pole_Sup_R	Right Superior Temporal Pole	22	8	-20	1
Fusiform_R	Right Fusiform Gyrus	28	-2	-42	0

Table S1: Names, Talairach coordinates and node degree of nodes.

	Node	Node	Patel's K
1	ParaHipp_L_1	Hipp_L_5	0.8743
2	Temp_Sup_L_2	Amyg_R_1	0.8727
3	Temp_Inf_R_1	ParaHipp_L_1	0.8606
4	Amyg_R	Thal_R	0.8602
5	ParaHipp_R	Temp_Sup_R_1	0.8592
6	Fusiform_L_2	Hipp_L_4	0.8574
7	ParaHipp_R	Temp_Sup_L_1	0.8499
8	Temp_Sup_L_2	Hipp_L_5	0.8435
9	Hipp_L	Temp_Mid_L	0.8142
10	Temp_Inf_R	Thal_R	0.8065
11	Temp_Pole_Sup_L	Hipp_L_4	0.7943
12	Temp_Pole_Sup_L	Thal_R	0.7943
13	Fusiform_L_2	Thal_R	0.7804
14	Hipp_L_3	Temp_Inf_R	0.7747
15	Hipp_L	Thal_R	0.7630
16	Temp_Pole_Sup_L	Hipp_L_3	0.7606
17	ParaHipp_R_1	Temp_Sup_L_1	0.7598
18	Temp_Inf_R	Temp_Mid_L	0.7493
19	ParaHipp_R_1	Temp_Sup_R_1	0.7483
20	Hipp_L_4	Temp_Inf_R	0.7359
21	Temp_Pole_Sup_L	Temp_Mid_L	0.7338
22	Hipp_R_1	ParaHipp_R_2	0.7267
23	Fusiform_L_2	Temp_Mid_L	0.7164

24	Temp_Sup_L_2	ParaHipp_L	0.7029
25	Temp_Pole_Sup_L	Amyg_R	0.6901
26	ParaHipp_R_1	Amyg_L_1	0.6778
27	Fusiform_L_1	ParaHipp_L	0.6771
28	Hipp_L_3	ParaHipp_R_2	0.6763
29	Hipp_L_2	Hipp_L_5	0.6763
30	Amyg_L_1	Temp_Pole_Sup_L	0.6476
31	ParaHipp_R_1	Hipp_R	0.6366
32	Temp_Inf_R	Amyg_R	0.6282
33	Amyg_L_1	Fusiform_L_2	0.6274
34	Hipp_L_2	Hipp_L_4	0.6238
35	Hipp_L_4	ParaHipp_R_2	0.6238
36	Hipp_L	Precuneus_R	0.6221
37	ParaHipp_L_1	Temp_Sup_R_1	0.6213
38	Thal_R_1	Caudate_L	0.6202
39	Temp_Sup_L_2	Amyg_R	0.6039
40	Fusiform_L_1	Temp_Sup_R_1	0.6027
41	Hipp_L_2	Temp_Pole_Sup_L	0.6023
42	ParaHipp_R_2	Amyg_R_1	0.6023
43	ParaHipp_R_2	Hipp_R_2	0.6018
44	ParaHipp_R_2	Front_Inf_R	0.6018
45	ParaHipp_R	Temp_Inf_R_1	0.6014
46	Temp_Sup_L_1	Hipp_L_5	0.6000
47	Hipp_R	SupraMarginal_L_1	0.5824

48	Thal_R_1	SupraMarginal_L_1	0.5824
49	ParaHipp_R	Temp_Inf_R	0.5822
50	Amyg_L_1	Hipp_L_3	0.5790
51	Fusiform_L_2	Hipp_L_2	0.5782
52	Hipp_L_2	Temp_Sup_R_1	0.5777
53	Amyg_L	Amyg_L_1	0.5774
54	ParaHipp_L	Temp_Sup_L	0.5773
55	Fusiform_L_2	Amyg_R	0.5761
56	Hipp_L_2	ParaHipp_L_1	0.5717
57	Amyg_R	Temp_Sup_L_1	0.5702
58	Hipp_R_2	SupraMarginal_L	0.5650
59	Hipp_R_2	Cingulum_Mid_R	0.5650
60	ParaHipp_R	ParaHipp_R_1	0.5648
61	ParaHipp_R	Thal_R_1	0.5648
62	ParaHipp_R	Temp_Sup_L_2	0.5611
63	ParaHipp_R	Amyg_R_1	0.5611
64	Hipp_L_2	Amyg_R	0.5510
65	Hipp_L_2	Temp_Sup_L_1	0.5505
66	Amyg_L_1	Hipp_R_1	0.5417
67	Amyg_L_1	Temp_Inf_R_1	0.5390
68	Fusiform_L_1	Temp_Sup_L_1	0.5289
69	ParaHipp_R_2	Temp_Inf_R_1	0.5281
70	Hipp_L_4	Temp_Sup_R_1	0.5269
71	ParaHipp_R	Hipp_L_2	0.5260

72	ParaHipp_L	Thal_R	0.5236
73	Hipp_L_3	Thal_R	0.5224
74	Hipp_L_1	Hipp_L_2	0.5195
75	Hipp_R_1	Hipp_L_3	0.5188
76	Hipp_R_1	ParaHipp_L_1	0.5188
77	Amyg_L_1	Temp_Inf_R	0.5161
78	Hipp_L_2	ParaHipp_R_2	0.5147
79	Amyg_R	Amyg_R_1	0.5137
80	Hipp_L	Temp_Sup_R	0.5123
81	ParaHipp_L	ParaHipp_L_1	0.5093
82	Amyg_L_1	Hipp_L_2	0.5082
83	Amyg_L_1	ParaHipp_R_2	0.5082
84	ParaHipp_R	Hipp_L_3	0.5077
85	ParaHipp_R	ParaHipp_L_1	0.5077
86	Fusiform_L	Hipp_R_1	0.5048
87	Hipp_L	Temp_Pole_Sup_L	0.5029
88	Hipp_L	Temp_Sup_L_2	0.5029
89	Hipp_L_2	Temp_Inf_R	0.5029
90	Hipp_L_4	Thal_R	0.5027
91	Hipp_L_4	Temp_Sup_L_1	0.5025
92	Temp_Inf_R	Temp_Sup_L_1	0.5025
93	Temp_Sup_L_1	Thal_R	0.5025
94	Amyg_L_1	Thal_R_1	0.4994
95	ParaHipp_L_1	Amyg_R	0.4955

96	ParaHipp_L	Temp_Sup_R	0.4946
97	Temp_Sup_L_1	Temp_Mid_L	0.4944
98	ParaHipp_L	Amyg_R_1	0.4941
99	Amyg_L_1	Temp_Sup_L_2	0.4907
100	Amyg_L_1	Amyg_R_1	0.4907
101	Temp_Sup_R_1	Temp_Sup_L	0.4906
102	Temp_Pole_Sup_L	Temp_Sup_R_1	0.4897
103	Hipp_R	Front_Inf_R	0.4859
104	Hipp_R_1	Amyg_R	0.4856
105	Hipp_L_1	Temp_Inf_R	0.4756
106	Thal_R	Thal_R_1	0.4756
107	ParaHipp_L	Temp_Mid_L	0.4755
108	Temp_Sup_L_2	ParaHipp_R_2	0.4747
109	ParaHipp_R	Amyg_R	0.4741
110	Hipp_L_2	Hipp_L_3	0.4687
111	Temp_Sup_L_2	Temp_Sup_R	0.4681
112	ParaHipp_R_2	Temp_Sup_R_1	0.4681
113	Temp_Sup_L_2	Thal_R	0.4679
114	Fusiform_L_2	Temp_Sup_R_1	0.4645
115	Temp_Pole_Sup_L	Temp_Sup_L_1	0.4645
116	Temp_Pole_Sup_L	Caudate_L	0.4645
117	Hipp_R_1	Hipp_L_1	0.4619
118	Temp_Pole_Sup_R	Precuneus_R	0.4619
119	Temp_Sup_R_1	Hipp_L_5	0.4576

120	Amyg_L_1	ParaHipp_L_1	0.4550
121	Temp_Inf_R_1	ParaHipp_L	0.4546
122	Hipp_R	Thal_R_1	0.4545
123	Temp_Sup_L	Temp_Sup_L_1	0.4519
124	Temp_Pole_Sup_L	Temp_Inf_R_1	0.4441
125	Temp_Sup_L_2	Temp_Mid_L	0.4411
126	ParaHipp_R	Temp_Mid_L	0.4386
127	Temp_Inf_R	ParaHipp_L_1	0.4315
128	Temp_Inf_R	Hipp_L_5	0.4315
129	ParaHipp_L_1	Thal_R	0.4315
130	Hipp_R	Caudate_L	0.4312
131	Amyg_L_1	Amyg_R	0.4311
132	ParaHipp_R	ParaHipp_R_2	0.4273
133	Temp_Inf_R	ParaHipp_L	0.4225
134	Hipp_L	Temp_Inf_R	0.4150
135	Amyg_R	Hipp_L_5	0.4128
136	ParaHipp_R	Thal_R	0.4127
137	Hipp_L	ParaHipp_L	0.4104
138	Amyg_L_1	Front_Inf_R	0.4053
139	Temp_Inf_R_1	Amyg_R	0.4038
140	Temp_Pole_Sup_L	Temp_Sup_L_2	0.4006
141	Temp_Pole_Sup_L	Amyg_R_1	0.4006
142	Amyg_L_1	Temp_Mid_L	0.3987
143	ParaHipp_L	Amyg_R	0.3917

144	Temp_Inf_R	Temp_Inf_R_1	0.3914
145	Temp_Inf_R	Amyg_R_1	0.3749
146	Temp_Sup_R	Temp_Mid_L	0.3666

Table S2: Patel's k values of the edges linking each pair of nodes.

References

Alvarez-Hamelin, I., Dall'asta, L., Barrat, A., and Vespignani, A. (2005). K-Core decomposition: A tool for the visualization of large scale networks. Advances in Neural Information Processing Systems 18, 41. arXiv:cs/0504107 [cs.NI].

Apostolova, L.G., Morra, J.H., Green, A.E., Hwang, K.S., Avedissian, C., Woo, E., et al. (2010). Automated 3D mapping of baseline and 12-month associations between three verbal memory measures and hippocampal atrophy in 490 ADNI subjects. Neuroimage 51(1), 488-499. doi: 10.1016/j.neuroimage.2009.12.125.

Appel, S.H. (1981). A unifying hypothesis for the cause of amyotrophic lateral sclerosis, parkinsonism, and Alzheimer disease. Ann Neurol 10(6), 499-505. doi: 10.1002/ana.410100602.

Ardekani, B.A., Bachman, A.H., Figarsky, K., and Sidtis, J.J. (2014). Corpus callosum shape changes in early Alzheimer's disease: an MRI study using the OASIS brain database. Brain Struct Funct 219(1), 343-352. doi: 10.1007/s00429-013-0503-0.

Bachman, A.H., Lee, S.H., Sidtis, J.J., and Ardekani, B.A. (2014). Corpus callosum shape and size changes in early Alzheimer's disease: a longitudinal MRI study using the OASIS brain database. J Alzheimers Dis 39(1), 71-78. doi: 10.3233/jad-131526.

Bader, G.D., and Hogue, C.W. (2003). An automated method for finding molecular complexes in large protein interaction networks. BMC Bioinformatics 4, 2. doi: 10.1186/1471-2105-4-2.

Baker, J.T., Holmes, A.J., Masters, G.A., Yeo, B.T., Krienen, F., Buckner, R.L., et al. (2014). Disruption of cortical association networks in schizophrenia and psychotic bipolar disorder. JAMA Psychiatry 71(2), 109-118. doi: 10.1001/jamapsychiatry.2013.3469.

Bourdenx, M., Koulakiotis, N.S., Sanoudou, D., Bezard, E., Dehay, B., and Tsarbopoulos, A. (2017). Protein aggregation and neurodegeneration in prototypical neurodegenerative diseases: Examples of amyloidopathies, tauopathies and synucleinopathies. Prog Neurobiol 155, 171-193. doi: 10.1016/j.pneurobio.2015.07.003.

Braak, H., Del Tredici, K., Schultz, C., and Braak, E. (2000). Vulnerability of select neuronal types to Alzheimer's disease. Ann N Y Acad Sci 924, 53-61. doi: 10.1111/j.1749-6632.2000.tb05560.x.

Brettschneider, J., Del Tredici, K., Lee, V.M., and Trojanowski, J.Q. (2015). Spreading of pathology in neurodegenerative diseases: a focus on human studies. Nat Rev Neurosci 16(2), 109-120. doi: 10.1038/nrn3887.

Buckholtz, J.W., and Meyer-Lindenberg, A. (2012). Psychopathology and the human connectome: toward a transdiagnostic model of risk for mental illness. Neuron 74(6), 990-1004. doi: 10.1016/j.neuron.2012.06.002.

Buckner, R.L., Snyder, A.Z., Shannon, B.J., LaRossa, G., Sachs, R., Fotenos, A.F., et al. (2005). Molecular, structural, and functional characterization of Alzheimer's disease: evidence for a relationship between default activity, amyloid, and memory. J Neurosci 25(34), 7709-7717. doi: 10.1523/JNEUROSCI.2177-05.2005.

Carlesimo, G.A., Piras, F., Orfei, M.D., Iorio, M., Caltagirone, C., and Spalletta, G. (2015). Atrophy of presubiculum and subiculum is the earliest hippocampal anatomical marker of Alzheimer's disease. Alzheimers Dement (Amst) 1(1), 24-32. doi: 10.1016/j.dadm.2014.12.001.

Cauda, F., Costa, T., Nani, A., Fava, L., Palermo, S., Bianco, F., et al. (2017). Are schizophrenia, autistic, and obsessive spectrum disorders dissociable on the basis of neuroimaging morphological findings?: A voxel-based meta-analysis. Autism Research, n/a-n/a. doi: 10.1002/aur.1759.

Cauda, F., Torta, D.M., Sacco, K., Geda, E., D'Agata, F., Costa, T., et al. (2012). Shared "core" areas between the pain and other task-related networks. PLoS One 7(8), e41929. doi: 10.1371/journal.pone.0041929.

Chang, Y.T., Huang, C.W., Chang, Y.H., Chen, N.C., Lin, K.J., Yan, T.C., et al. (2015). Amyloid burden in the hippocampus and default mode network: relationships with gray matter volume and cognitive performance in mild stage Alzheimer disease. Medicine (Baltimore) 94(16), e763. doi: 10.1097/md.0000000000000763.

Chapleau, M., Aldebert, J., Montembeault, M., and Brambati, S.M. (2016). Atrophy in Alzheimer's Disease and Semantic Dementia: An ALE Meta-Analysis of Voxel-Based Morphometry Studies. J Alzheimers Dis 54(3), 941-955. doi: 10.3233/jad-160382.

Chevalier-Larsen, E., and Holzbaur, E.L. (2006). Axonal transport and neurodegenerative disease. Biochim Biophys Acta 1762(11-12), 1094-1108. doi: 10.1016/j.bbadis.2006.04.002.

Cioli, C., Abdi, H., Beaton, D., Burnod, Y., and Mesmoudi, S. (2014). Differences in human cortical gene expression match the temporal properties of large-scale functional networks. PLoS One 9(12), e115913. doi: 10.1371/journal.pone.0115913.

Clavaguera, F., Lavenir, I., Falcon, B., Frank, S., Goedert, M., and Tolnay, M. (2013). "Prion-like" templated misfolding in tauopathies. Brain Pathol 23(3), 342-349. doi: 10.1111/bpa.12044.

Crossley, N.A., Mechelli, A., Scott, J., Carletti, F., Fox, P.T., McGuire, P., et al. (2014). The hubs of the human connectome are generally implicated in the anatomy of brain disorders. Brain 137(Pt 8), 2382-2395. doi: 10.1093/brain/awu132.

Dickerson, B.C., Bakkour, A., Salat, D.H., Feczko, E., Pacheco, J., Greve, D.N., et al. (2009). The cortical signature of Alzheimer's disease: regionally specific cortical thinning relates to symptom severity in very mild to mild AD dementia and is detectable in asymptomatic amyloid-positive individuals. Cereb Cortex 19(3), 497-510. doi: 10.1093/cercor/bhn113.

Douaud, G., Groves, A.R., Tamnes, C.K., Westlye, L.T., Duff, E.P., Engvig, A., et al. (2014). A common brain network links development, aging, and vulnerability to disease. Proc Natl Acad Sci U S A 111(49), 17648-17653. doi: 10.1073/pnas.1410378111.

Du, A.T., Schuff, N., Kramer, J.H., Rosen, H.J., Gorno-Tempini, M.L., Rankin, K., et al. (2007). Different regional patterns of cortical thinning in Alzheimer's disease and frontotemporal dementia. Brain 130(Pt 4), 1159-1166. doi: 10.1093/brain/awm016.

Eickhoff, S.B., Bzdok, D., Laird, A.R., Kurth, F., and Fox, P.T. (2012). Activation likelihood estimation meta-analysis revisited. Neuroimage 59(3), 2349-2361. doi: 10.1016/j.neuroimage.2011.09.017.

Eickhoff, S.B., Laird, A.R., Fox, P.M., Lancaster, J.L., and Fox, P.T. (2017). Implementation errors in the GingerALE Software: Description and recommendations. Hum Brain Mapp 38(1), 7-11. doi: 10.1002/hbm.23342.

Eickhoff, S.B., Laird, A.R., Grefkes, C., Wang, L.E., Zilles, K., and Fox, P.T. (2009). Coordinate-based activation likelihood estimation meta-analysis of neuroimaging data: a random-effects approach based on empirical estimates of spatial uncertainty. Hum Brain Mapp 30(9), 2907-2926. doi: 10.1002/hbm.20718.

Eickhoff, S.B., Nichols, T.E., Laird, A.R., Hoffstaedter, F., Amunts, K., Fox, P.T., et al. (2016). Behavior, sensitivity, and power of activation likelihood estimation characterized by massive empirical simulation. Neuroimage 137, 70-85. doi: 10.1016/j.neuroimage.2016.04.072.

Ellison-Wright, I., and Bullmore, E. (2010). Anatomy of bipolar disorder and schizophrenia: a meta-analysis. Schizophr Res 117(1), 1-12. doi: 10.1016/j.schres.2009.12.022.

Etkin, A., and Wager, T.D. (2007). Functional neuroimaging of anxiety: a meta-analysis of emotional processing in PTSD, social anxiety disorder, and specific phobia. Am J Psychiatry 164(10), 1476-1488. doi: 10.1176/appi.ajp.2007.07030504.

Evans, A.C. (2013). Networks of anatomical covariance. Neuroimage 80, 489-504. doi: 10.1016/j.neuroimage.2013.05.054.

Ferreira, L.K., Diniz, B.S., Forlenza, O.V., Busatto, G.F., and Zanetti, M.V. (2011). Neurostructural predictors of Alzheimer's disease: a meta-analysis of VBM studies. Neurobiol Aging 32(10), 1733-1741. doi: 10.1016/j.neurobiolaging.2009.11.008.

Fischer, F.U., Wolf, D., Scheurich, A., and Fellgiebel, A. (2015). Altered whole-brain white matter networks in preclinical Alzheimer's disease. Neuroimage Clin 8, 660-666. doi: 10.1016/j.nicl.2015.06.007.

Fjell, A.M., McEvoy, L., Holland, D., Dale, A.M., and Walhovd, K.B. (2014). What is normal in normal aging? Effects of aging, amyloid and Alzheimer's disease on the cerebral cortex and the hippocampus. Prog Neurobiol 117, 20-40. doi: 10.1016/j.pneurobio.2014.02.004.

Fornito, A., Zalesky, A., and Breakspear, M. (2015). The connectomics of brain disorders. Nat Rev Neurosci 16(3), 159-172. doi: 10.1038/nrn3901.

Fox, P.T., and Lancaster, J.L. (2002). Opinion: Mapping context and content: the BrainMap model. Nat Rev Neurosci 3(4), 319-321. doi: 10.1038/nrn789.

French, L., and Pavlidis, P. (2011). Relationships between gene expression and brain wiring in the adult rodent brain. PLoS Comput Biol 7(1), e1001049. doi: 10.1371/journal.pcbi.1001049.

French, L., Tan, P.P., and Pavlidis, P. (2011). Large-Scale Analysis of Gene Expression and Connectivity in the Rodent Brain: Insights through Data Integration. Front Neuroinform 5, 12. doi: 10.3389/fninf.2011.00012.

Girvan, M., and Newman, M.E. (2002). Community structure in social and biological networks. Proc Natl Acad Sci U S A 99(12), 7821-7826. doi: 10.1073/pnas.122653799.

Goedert, M., Clavaguera, F., and Tolnay, M. (2010). The propagation of prion-like protein inclusions in neurodegenerative diseases. Trends Neurosci 33(7), 317-325. doi: 10.1016/j.tins.2010.04.003.

Goedert, M. (2015). NEURODEGENERATION. Alzheimer's and Parkinson's diseases: The prion concept in relation to assembled Abeta, tau, and alpha-synuclein. Science 349(6248), 1255555. doi: 10.1126/science.1255555.

Goodkind, M., Eickhoff, S.B., Oathes, D.J., Jiang, Y., Chang, A., Jones-Hagata, L.B., et al. (2015). Identification of a common neurobiological substrate for mental illness. JAMA Psychiatry 72(4), 305-315. doi: 10.1001/jamapsychiatry.2014.2206.

Greicius, M.D., Srivastava, G., Reiss, A.L., and Menon, V. (2004). Default-mode network activity distinguishes Alzheimer's disease from healthy aging: evidence from functional MRI. Proc Natl Acad Sci U S A 101(13), 4637-4642. doi: 10.1073/pnas.0308627101.

Guest, W.C., Silverman, J.M., Pokrishevsky, E., O'Neill, M.A., Grad, L.I., and Cashman, N.R. (2011). Generalization of the prion hypothesis to other neurodegenerative diseases: an imperfect fit. J Toxicol Environ Health A 74(22-24), 1433-1459. doi: 10.1080/15287394.2011.618967.

Hamilton, J.P., Etkin, A., Furman, D.J., Lemus, M.G., Johnson, R.F., and Gotlib, I.H. (2012). Functional neuroimaging of major depressive disorder: a meta-analysis and new integration of base line activation and neural response data. Am J Psychiatry 169(7), 693-703. doi: 10.1176/appi.ajp.2012.11071105.

He, Y., Chen, Z., and Evans, A. (2008). Structural insights into aberrant topological patterns of large-scale cortical networks in Alzheimer's disease. J Neurosci 28(18), 4756-4766. doi: 10.1523/jneurosci.0141-08.2008.

Head, D., Snyder, A.Z., Girton, L.E., Morris, J.C., and Buckner, R.L. (2005). Frontal-hippocampal double dissociation between normal aging and Alzheimer's disease. Cereb Cortex 15(6), 732-739. doi: 10.1093/cercor/bhh174.

Hirjak, D., Wolf, R.C., Remmele, B., Seidl, U., Thomann, A.K., Kubera, K.M., et al. (2017). Hippocampal formation alterations differently contribute to autobiographic memory deficits in mild cognitive impairment and Alzheimer's disease. Hippocampus 27(6), 702-715. doi: 10.1002/hipo.22726.

Hovorkova, P., Kristofikova, Z., Horinek, A., Ripova, D., Majer, E., Zach, P., et al. (2008). Lateralization of 17beta-hydroxysteroid dehydrogenase type 10 in hippocampi of demented and psychotic people. Dement Geriatr Cogn Disord 26(3), 193-198. doi: 10.1159/000151778.

Iturria-Medina, Y., and Evans, A.C. (2015). On the central role of brain connectivity in neurodegenerative disease progression. Front Aging Neurosci 7, 90. doi: 10.3389/fnagi.2015.00090.

Iturria-Medina, Y., Sotero, R.C., Toussaint, P.J., and Evans, A.C. (2014). Epidemic spreading model to characterize misfolded proteins propagation in aging and associated neurodegenerative disorders. PLoS Comput Biol 10(11), e1003956. doi: 10.1371/journal.pcbi.1003956.

Jack, C.R., Jr., Knopman, D.S., Jagust, W.J., Petersen, R.C., Weiner, M.W., Aisen, P.S., et al. (2013). Tracking pathophysiological processes in Alzheimer's disease: an updated hypothetical model of dynamic biomarkers. Lancet Neurol 12(2), 207-216. doi: 10.1016/s1474-4422(12)70291-0.

Jagust, W. (2013). Vulnerable neural systems and the borderland of brain aging and neurodegeneration. Neuron 77(2), 219-234. doi: 10.1016/j.neuron.2013.01.002.

Kristofikova, Z., Kozmikova, I., Hovorkova, P., Ricny, J., Zach, P., Majer, E., et al. (2008). Lateralization of hippocampal nitric oxide mediator system in people with Alzheimer disease, multi-infarct dementia and schizophrenia. Neurochem Int 53(5), 118-125. doi: 10.1016/j.neuint.2008.06.009.

Laird, A.R., Eickhoff, S.B., Kurth, F., Fox, P.M., Uecker, A.M., Turner, J.A., et al. (2009). ALE Meta-Analysis Workflows Via the Brainmap Database: Progress Towards A Probabilistic Functional Brain Atlas. Front Neuroinform 3, 23. doi: 10.3389/neuro.11.023.2009.

Laird, A.R., Fox, P.M., Price, C.J., Glahn, D.C., Uecker, A.M., Lancaster, J.L., et al. (2005). ALE meta-analysis: controlling the false discovery rate and performing statistical contrasts. Hum Brain Mapp 25(1), 155-164. doi: 10.1002/hbm.20136.

Li, Y., Wang, Y., Wu, G., Shi, F., Zhou, L., Lin, W., et al. (2012). Discriminant analysis of longitudinal cortical thickness changes in Alzheimer's disease using dynamic and network features. Neurobiol Aging 33(2), 427.e415-430. doi: 10.1016/j.neurobiolaging.2010.11.008.

Liberati, A., Altman, D.G., Tetzlaff, J., Mulrow, C., Gotzsche, P.C., Ioannidis, J.P., et al. (2009). The PRISMA statement for reporting systematic reviews and meta-analyses of studies that evaluate healthcare interventions: explanation and elaboration. BMJ 339, b2700. doi: 10.1136/bmj.b2700.

Lichtman, J.W., and Sanes, J.R. (2008). Ome sweet ome: what can the genome tell us about the connectome? Curr Opin Neurobiol 18(3), 346-353. doi: 10.1016/j.conb.2008.08.010.

Long, X., Zhang, L., Liao, W., Jiang, C., and Qiu, B. (2013). Distinct laterality alterations distinguish mild cognitive impairment and Alzheimer's disease from healthy aging: statistical parametric mapping with high resolution MRI. Hum Brain Mapp 34(12), 3400-3410. doi: 10.1002/hbm.22157.

Matsuda, H. (2016). MRI morphometry in Alzheimer's disease. Ageing Res Rev 30, 17-24. doi: 10.1016/j.arr.2016.01.003.

McKhann, G.M., Knopman, D.S., Chertkow, H., Hyman, B.T., Jack, C.R., Jr., Kawas, C.H., et al. (2011). The diagnosis of dementia due to Alzheimer's disease: recommendations from the National Institute on Aging-Alzheimer's Association workgroups on diagnostic guidelines for Alzheimer's disease. Alzheimers Dement 7(3), 263-269. doi: 10.1016/j.jalz.2011.03.005.

McTeague, L.M., Goodkind, M.S., and Etkin, A. (2016). Transdiagnostic impairment of cognitive control in mental illness. J Psychiatr Res 83, 37-46. doi: 10.1016/j.jpsychires.2016.08.001.

Mechelli, A., Friston, K.J., Frackowiak, R.S., and Price, C.J. (2005). Structural covariance in the human cortex. J Neurosci 25(36), 8303-8310. doi: 10.1523/jneurosci.0357-05.2005.

Menon, V. (2013). Developmental pathways to functional brain networks: emerging principles. Trends Cogn Sci 17(12), 627-640. doi: 10.1016/j.tics.2013.09.015.

Minkova, L., Habich, A., Peter, J., Kaller, C.P., Eickhoff, S.B., and Kloppel, S. (2017). Gray matter asymmetries in aging and neurodegeneration: A review and meta-analysis. Hum Brain Mapp. doi: 10.1002/hbm.23772.

Moher, D., Liberati, A., Tetzlaff, J., and Altman, D.G. (2009). Preferred reporting items for systematic reviews and meta-analyses: the PRISMA statement. J Clin Epidemiol 62(10), 1006-1012. doi: 10.1016/j.jclinepi.2009.06.005.

Patel, R.S., Bowman, F.D., and Rilling, J.K. (2006). A Bayesian approach to determining connectivity of the human brain. Hum Brain Mapp 27(3), 267-276. doi: 10.1002/hbm.20182.

Pievani, M., Galluzzi, S., Thompson, P.M., Rasser, P.E., Bonetti, M., and Frisoni, G.B. (2011). APOE4 is associated with greater atrophy of the hippocampal formation in Alzheimer's disease. Neuroimage 55(3), 909-919. doi: 10.1016/j.neuroimage.2010.12.081.

Prieto, C., Risueno, A., Fontanillo, C., and De las Rivas, J. (2008). Human gene coexpression landscape: confident network derived from tissue transcriptomic profiles. PLoS One 3(12), e3911. doi: 10.1371/journal.pone.0003911.

Raj, A., Kuceyeski, A., and Weiner, M. (2012). A network diffusion model of disease progression in dementia. Neuron 73(6), 1204-1215. doi: 10.1016/j.neuron.2011.12.040.

Sabuncu, M.R., Desikan, R.S., Sepulcre, J., Yeo, B.T., Liu, H., Schmansky, N.J., et al. (2011). The dynamics of cortical and hippocampal atrophy in Alzheimer disease. Arch Neurol 68(8), 1040-1048. doi: 10.1001/archneurol.2011.167.

Salehi, A., Delcroix, J.D., Belichenko, P.V., Zhan, K., Wu, C., Valletta, J.S., et al. (2006). Increased App expression in a mouse model of Down's syndrome disrupts NGF transport and causes cholinergic neuron degeneration. Neuron 51(1), 29-42. doi: 10.1016/j.neuron.2006.05.022.

Saxena, S., and Caroni, P. (2011). Selective neuronal vulnerability in neurodegenerative diseases: from stressor thresholds to degeneration. Neuron 71(1), 35-48. doi: 10.1016/j.neuron.2011.06.031.

Schuff, N., Woerner, N., Boreta, L., Kornfield, T., Shaw, L.M., Trojanowski, J.Q., et al. (2009). MRI of hippocampal volume loss in early Alzheimer's disease in relation to ApoE genotype and biomarkers. Brain 132(Pt 4), 1067-1077. doi: 10.1093/brain/awp007.

Sepulcre, J., Grothe, M.J., Sabuncu, M., Chhatwal, J., Schultz, A.P., Hanseeuw, B., et al. (2017). Hierarchical Organization of Tau and Amyloid Deposits in the Cerebral Cortex. JAMA Neurol. doi: 10.1001/jamaneurol.2017.0263.

Shannon, P., Markiel, A., Ozier, O., Baliga, N.S., Wang, J.T., Ramage, D., et al. (2003). Cytoscape: a software environment for integrated models of biomolecular interaction networks. Genome Res 13(11), 2498-2504. doi: 10.1101/gr.1239303.

Smith, S.M., Miller, K.L., Salimi-Khorshidi, G., Webster, M., Beckmann, C.F., Nichols, T.E., et al. (2011). Network modelling methods for FMRI. Neuroimage 54(2), 875-891. doi: 10.1016/j.neuroimage.2010.08.063.

Smoot, M.E., Ono, K., Ruscheinski, J., Wang, P.L., and Ideker, T. (2011). Cytoscape 2.8: new features for data integration and network visualization. Bioinformatics 27(3), 431-432. doi: 10.1093/bioinformatics/btq675.

Sprooten, E., Rasgon, A., Goodman, M., Carlin, A., Leibu, E., Lee, W.H., et al. (2017). Addressing reverse inference in psychiatric neuroimaging: Meta-analyses of task-related brain activation in common mental disorders. Hum Brain Mapp 38(4), 1846-1864. doi: 10.1002/hbm.23486.

Strange, B.A., Witter, M.P., Lein, E.S., and Moser, E.I. (2014). Functional organization of the hippocampal longitudinal axis. Nat Rev Neurosci 15(10), 655-669. doi: 10.1038/nrn3785.

Tahmasian, M., Pasquini, L., Scherr, M., Meng, C., Forster, S., Mulej Bratec, S., et al. (2015). The lower hippocampus global connectivity, the higher its local metabolism in Alzheimer disease. Neurology 84(19), 1956-1963. doi: 10.1212/wnl.0000000000001575.

Teipel, S.J., Bayer, W., Alexander, G.E., Zebuhr, Y., Teichberg, D., Kulic, L., et al. (2002). Progression of corpus callosum atrophy in Alzheimer disease. Arch Neurol 59(2), 243-248. doi: 10.1001/archneur.59.2.243.

Teipel, S.J., Grothe, M., Lista, S., Toschi, N., Garaci, F.G., and Hampel, H. (2013). Relevance of magnetic resonance imaging for early detection and diagnosis of Alzheimer disease. Med Clin North Am 97(3), 399-424. doi: 10.1016/j.mcna.2012.12.013.

Thal, D.R., Attems, J., and Ewers, M. (2014). Spreading of amyloid, tau, and microvascular pathology in Alzheimer's disease: findings from neuropathological and neuroimaging studies. J Alzheimers Dis 42 Suppl 4, S421-429. doi: 10.3233/jad-141461.

Thompson, P.M., Hayashi, K.M., Dutton, R.A., Chiang, M.C., Leow, A.D., Sowell, E.R., et al. (2007). Tracking Alzheimer's disease. Ann N Y Acad Sci 1097, 183-214. doi: 10.1196/annals.1379.017.

Tijms, B.M., Kate, M.T., Wink, A.M., Visser, P.J., Ecay, M., Clerigue, M., et al. (2016). Gray matter network disruptions and amyloid beta in cognitively normal adults. Neurobiol Aging 37, 154-160. doi: 10.1016/j.neurobiolaging.2015.10.015.

Tijms, B.M., Wink, A.M., de Haan, W., van der Flier, W.M., Stam, C.J., Scheltens, P., et al. (2013). Alzheimer's disease: connecting findings from graph theoretical studies of brain networks. Neurobiol Aging 34(8), 2023-2036. doi: 10.1016/j.neurobiolaging.2013.02.020.

Tijms, B.M., Yeung, H.M., Sikkes, S.A., Moller, C., Smits, L.L., Stam, C.J., et al. (2014). Single-subject gray matter graph properties and their relationship with cognitive impairment in early- and late-onset Alzheimer's disease. Brain Connect 4(5), 337-346. doi: 10.1089/brain.2013.0209.

Turkeltaub, P.E., Eickhoff, S.B., Laird, A.R., Fox, M., Wiener, M., and Fox, P. (2012). Minimizing within-experiment and within-group effects in Activation Likelihood Estimation meta-analyses. Hum Brain Mapp 33(1), 1-13. doi: 10.1002/hbm.21186.

Wachinger, C., Salat, D.H., Weiner, M., and Reuter, M. (2016). Whole-brain analysis reveals increased neuroanatomical asymmetries in dementia for hippocampus and amygdala. Brain 139(Pt 12), 3253-3266. doi: 10.1093/brain/aww243.

Walterfang, M., Luders, E., Looi, J.C., Rajagopalan, P., Velakoulis, D., Thompson, P.M., et al. (2014). Shape analysis of the corpus callosum in Alzheimer's disease and frontotemporal lobar degeneration subtypes. J Alzheimers Dis 40(4), 897-906. doi: 10.3233/jad-131853.

Wang, P.N., Chou, K.H., Chang, N.J., Lin, K.N., Chen, W.T., Lan, G.Y., et al. (2014). Callosal degeneration topographically correlated with cognitive function in amnestic mild cognitive impairment and Alzheimer's disease dementia. Hum Brain Mapp 35(4), 1529-1543. doi: 10.1002/hbm.22271.

Wang, W.Y., Yu, J.T., Liu, Y., Yin, R.H., Wang, H.F., Wang, J., et al. (2015a). Voxel-based meta-analysis of grey matter changes in Alzheimer's disease. Transl Neurodegener 4, 6. doi: 10.1186/s40035-015-0027-z.

Wang, X.D., Ren, M., Zhu, M.W., Gao, W.P., Zhang, J., Shen, H., et al. (2015b). Corpus callosum atrophy associated with the degree of cognitive decline in patients with Alzheimer's dementia or mild cognitive impairment: a meta-analysis of the region of interest structural imaging studies. J Psychiatr Res 63, 10-19. doi: 10.1016/j.jpsychires.2015.02.005.

Wang, Y., Chen, K., Yao, L., Jin, Z., and Guo, X. (2013). Structural interactions within the default mode network identified by Bayesian network analysis in Alzheimer's disease. PLoS One 8(8), e74070. doi: 10.1371/journal.pone.0074070.

Warren, J.D., Rohrer, J.D., Schott, J.M., Fox, N.C., Hardy, J., and Rossor, M.N. (2013). Molecular nexopathies: a new paradigm of neurodegenerative disease. Trends Neurosci 36(10), 561-569. doi: 10.1016/j.tins.2013.06.007.

Weiler, M., de Campos, B.M., Teixeira, C.V., Casseb, R.F., Carletti-Cassani, A.F., Vicentini, J.E., et al. (2017). Intranetwork and internetwork connectivity in patients with Alzheimer disease and the association with cerebrospinal fluid biomarker levels. J Psychiatry Neurosci 42(3), 160190. doi: 10.1503/jpn.160190.

Whitwell, J.L. (2016). Biomarkers in Randomized Clinical Trials: Magnetic Resonance Imaging. Front Neurol Neurosci 39, 101-108. doi: 10.1159/000445419.

Wolf, L., Goldberg, C., Manor, N., Sharan, R., and Ruppin, E. (2011). Gene expression in the rodent brain is associated with its regional connectivity. PLoS Comput Biol 7(5), e1002040. doi: 10.1371/journal.pcbi.1002040.

Woolard, A.A., and Heckers, S. (2012). Anatomical and functional correlates of human hippocampal volume asymmetry. Psychiatry Res 201(1), 48-53. doi: 10.1016/j.pscychresns.2011.07.016.

Yang, J., Pan, P., Song, W., Huang, R., Li, J., Chen, K., et al. (2012). Voxelwise meta-analysis of gray matter anomalies in Alzheimer's disease and mild cognitive impairment using anatomic likelihood estimation. J Neurol Sci 316(1-2), 21-29. doi: 10.1016/j.jns.2012.02.010.

Yao, Z., Zhang, Y., Lin, L., Zhou, Y., Xu, C., and Jiang, T. (2010). Abnormal cortical networks in mild cognitive impairment and Alzheimer's disease. PLoS Comput Biol 6(11), e1001006. doi: 10.1371/journal.pcbi.1001006.

Yates, D. (2012). Neurodegenerative networking. Nat Rev Neurosci 13(5), 288. doi: 10.1038/nrn3248.

Zeidman, P., and Maguire, E.A. (2016). Anterior hippocampus: the anatomy of perception, imagination and episodic memory. Nat Rev Neurosci 17(3), 173-182. doi: 10.1038/nrn.2015.24.

Zhou, J., Gennatas, E.D., Kramer, J.H., Miller, B.L., and Seeley, W.W. (2012). Predicting regional neurodegeneration from the healthy brain functional connectome. Neuron 73(6), 1216-1227. doi: 10.1016/j.neuron.2012.03.004

2.2 Brain structural alterations are distributed following functional, anatomic and genetic connectivity

This study was published in Brain in 2018, and was selected as editor's choice (doi.org/10.1093/brain/awy252).

Authors: Cauda F., Nani A., Manuello J., Premi E., Palermo S., Tatu K., Duca S., Fox. P.T., Costa T.

Abstract

The pathological brain is characterized by distributed morphological or structural alterations in the grey matter, which tend to follow identifiable network-like patterns. We analysed the patterns formed by these alterations (increased and decreased grey matter values detected with the voxel-based morphometry technique) conducting an extensive transdiagnostic search of voxel-based morphometry studies in a large variety of brain disorders. We devised an innovative method to construct the networks formed by the structurally co-altered brain areas, which can be considered as pathological structural co-alteration patterns, and to compare these patterns with three associated types of connectivity profiles (functional, anatomical, and genetic). Our study provides transdiagnostical evidence that structural co-alterations are influenced by connectivity constraints rather than being randomly distributed. Analyses show that although all the three types of connectivity taken together can account for and predict with good statistical accuracy, the shape and temporal development of the co-alteration patterns, functional connectivity offers the better account of the structural co-alteration, followed by anatomic and genetic connectivity. These results shed new light on the possible mechanisms at the root of neuropathological processes and open exciting prospects in the quest for a better understanding of brain disorders.

Introduction

Brain disorders are characterized by diffuse alterations of grey matter. Especially in neurodegenerative diseases, neuroanatomical abnormalities have been found to spread from one brain area to another according to distinctive network-like patterns (Yates, 2012; Pandya et al., 2017). These patterns of pathological structural co-alterations seem to develop along pathways that are influenced by the organization of brain connectivity (Raj et al., 2012; Zhou et al., 2012; Iturria-Medina and Evans, 2015; Oxtoby et al., 2017; Yuan et al., 2017; Cauda et al., 2018; Manuello et al., 2018; Tatu et al., 2018). Indeed, patterns of brain atrophy caused by neurodegenerative diseases appear to somewhat resemble the patterns of neuronal

connections (Warren et al., 2013). Furthermore, brain disorders selectively target certain subpopulations of neurons that often lie at the centre of important functional networks (Saxena and Caroni, 2011). Arguably, their high topological centrality makes those areas brain hubs and, as a consequence, more likely to be affected by pathological processes (Crossley et al., 2014; Cope et al., 2018).

Thus far, at least four important mechanisms (not necessarily mutually exclusive) have been invoked to explain the spread of brain alterations: transneuronal spread, nodal stress, shared vulnerability, and trophic failure (Zhou et al., 2012; Fornito et al., 2015). The first mechanism is based on the involvement of certain toxic agents that propagate along neuronal connections (Soto and Estrada, 2008; Goedert et al., 2010; Korth, 2012; Jucker and Walker, 2013; Kraus et al., 2013; Walker et al., 2013; Clavaguera et al., 2014). A growing body of evidence indicates that misfolded proteins may spread in a prion-like way along brain axonal fibres (Chevalier-Larsen and Holzbaur, 2006) throughout a corruptive templating as a cascade phenomenon of misfolded protein propagation (Jucker and Walker, 2011; Hardy and Revesz, 2012; Warren et al., 2013). Borrowed from prion diseases (Aguzzi et al., 2007), this mechanism has been subsequently explored in neurodegenerative diseases such as Alzheimer's disease, Parkinson's disease, Huntington's disease, amyotrophic lateral sclerosis and tauopathies (Clavaguera et al., 2013; Bourdenx et al., 2017), and more recently has been tentatively generalized to other brain disorders (Guest et al., 2011). However, the application of the prion-like mechanism to neurodegenerative diseases is still an open field of research.

The second mechanism (Zhou et al., 2012) is based on the hypothesis that the most active brain regions (i.e. network hubs) may also be the most functionally stressed (Crossley et al., 2014) and, as a result, susceptible to be structurally altered (Buckner et al., 2005; Saxena and Caroni, 2011). This phenomenon has been confirmed in humans by using in vivo neuroimaging techniques and voxel-based meta-analyses (Crossley et al., 2014). The third mechanism relies on the hypothesis that certain areas with shared gene or protein expressions may exhibit common vulnerability to neuropathology (Zhou et al., 2012). This phenomenon could be partially mediated by the relationship between expression of genes and patterns of brain connectivity (French and Pavlidis, 2011; Cioli et al., 2014). The fourth mechanism invokes a failure in the process of trophic factors production, which can lead to the pathological deterioration of neural wiring (Zhou et al., 2012; Fornito et al., 2015).

Studies analysing the networks formed by cerebral regions that appear to be co-altered in the pathological brain are guiding research to a new perspective, which claims a neurobiological and transdiagnostic approach for a better understanding of how the brain responds in a variety of both neurological and psychiatric conditions (Buckholtz and Meyer-Lindenberg, 2012; Raj et al., 2012; Zhou et al., 2012; Fornito et al., 2015; Goodkind et al., 2015; Iturria-Medina and Evans, 2015; McTeague et al., 2016; Sprooten et al., 2017; Cauda et al., 2018). This view may be counter-intuitive, as we are inclined to think that brain disorders have specific aetiological and pathogenetic mechanisms, which, in turn, produce peculiar patterns of neuronal alterations. However, a growing body of evidence points out that, apart from some pathology-specific alterations, a 'core set' of co-altered cerebral areas is frequently involved in the majority of brain diseases (Etkin and Wager, 2007; Ellison-Wright and Bullmore, 2010; Saxena and Caroni, 2011; Hamilton et al., 2012; Jagust, 2013; Menon, 2013; Baker et al., 2014; Douaud et al., 2014; Goodkind et al., 2015; Cauda et al., 2018).

This 'core set' is generally composed of areas that are related to important associative and cognitive functions, among which the insular and anterior cingulate cortices are the most prominent. These regions are essential parts of the cognitive control system, which is supposed to monitor a host of higher brain functions (Cauda et al., 2012b). Thus, for both its topological and functional features, the activity of the cognitive control system may be affected by a wide variety of brain disorders (McTeague et al., 2016). This would make it more difficult to differentiate neuropathological conditions solely based on structural or functional alterations exhibited by the areas constituting this system (Sprooten et al., 2017).

The contamination between neurodegenerative and psychiatric disorders may be highlighted by a number of studies. Genetic studies in neurodegenerative dementias show how brain abnormalities antedate the onset of symptoms by many years (Quiroz et al., 2015; Rohrer et al., 2015; Chhatwal et al., 2018), suggesting a less defined border between neurodegenerative and neurodevelopmental disorders (Zawia and Basha, 2005; Lahiri and Maloney, 2010; Warren et al., 2013). Moreover, a growing body of literature, demonstrating structural and functional brain changes in psychiatric illnesses, is bringing psychiatry and the study of neurological conditions together (Douaud et al., 2014; Gupta et al., 2015; Du et al., 2017).

The lack of direct correspondence between the development of neuropathological processes and the manifestation of brain alterations implies an overlap of symptoms

that strictly depends on the disruption of large-scale networks. What is more, transdiagnostic symptoms are often produced by genetic and environmental risk factors that affect system-level circuits for many dimensions of cognitive functions. The impairment of these circuits brings about vulnerability to vast domains of psychopathology rather than distinct diseases (Buckholtz and Meyer-Lindenberg, 2012).

Given that the spread of brain alterations is likely to be non-random in both neurological and psychiatric diseases (Cauda et al., 2018; Tatu et al., 2018), an important and as yet unresolved issue is the prevalence of one or more mechanisms at the root of the propagation in different brain disorders. To our knowledge, thus far only one study (Cope et al., 2018) has tried to estimate, with the help of in vivo techniques, which mechanism is mostly associated with the distribution patterns of two neurodegenerative diseases (i.e. Alzheimer's disease and progressive supranuclear palsy). Indeed, if neuronal alterations follow the patterns of brain connectivity, it should be possible to predict their spread based on brain connectivity profiles (Raj et al., 2012; Robinson, 2012; Zhou et al., 2012; Iturria-Medina et al., 2014). It should also be possible to simulate the temporal evolution of these alterations and to infer which of the different connectivity profiles (i.e. functional, anatomic, and genetic) can better explain the development of a certain structural co-alteration pattern. In light of this, it is reasonable to hypothesize that the different contributions of the aforementioned propagation mechanisms might lead to typical patterns of structural co-alterations (Cope et al., 2018). For instance, the prevalence of a pattern composed of anatomically connected areas may be better explained by the mechanism of the transneuronal spread, which implies a propagation across more contiguously and directly connected areas. By contrast, the prevalence of a pattern composed of functionally connected regions suggests that the mechanism of the nodal stress may be more effective in generating this network of co-alterations (Biswal, 2011, 2012; Buckner et al., 2013). In turn, the shared vulnerability hypothesis implies that structurally co-altered areas may be characterized by similar gene co-expression patterns (Stuart et al., 2003).

To address these important questions, we recently developed a methodology to estimate how each type of brain connectivity can predict the pattern formed by neuropathological co-alterations (Cauda et al., 2018). Herein, this methodology has been applied transdiagnostically so as to have a great deal of meta-analytical data to work on and, at the same time, to provide proof of concept. We would like to show

that this method is applicable to every brain disorder and, in the future, we plan to use it for the analysis of specific neurological or psychiatric conditions.

To this aim, we began by examining the whole BrainMap (Fox and Lancaster, 2002; Fox et al., 2005; Laird et al., 2005b) voxel-based morphometry (VBM) database of brain MRI studies to construct the most comprehensive transdiagnostic map of pathological structural co-alterations. To do so we used the grey matter alterations detected by VBM as a proxy for the morphological brain abnormalities. Given a brain area (say, 'A') that is altered, our method was able to detect if other areas appeared to be altered together with 'A' (i.e. co-altered) (Cauda et al., 2018; Manuello et al., 2018; Tatu et al., 2018).

The result of this analysis was the creation of undirected co-alteration graphs showing the brain areas forming the structural co-alteration patterns. Then, to assess which of the three different connectivity profiles could account better for the structural co-alteration patterns, we calculated the anatomical, resting state functional, and genetic (i.e. the correlated gene expression pattern) connectivity networks using the brain most altered areas as starting points (i.e. nodes). The comparison of the different network matrices to the structural co-alteration patterns allowed us to find out the contribution of each connectivity profile to the co-alteration pattern and, consequently, to better understand its development through the spread of alterations [for the relationship between co-alteration patterns and the concept of propagation or spread, see Cauda et al. (2018)]. On these grounds, we also estimated—with simulation techniques—both the spatial and temporal progression of the distribution of alterations, so as to find out how the patterns of structural co-alterations could be predictable in terms of functional, anatomic, and genetic connectivity.

This method allowed us to address the following issues. How are structural co-alteration patterns distributed across the pathological brain? Since neuronal alterations seem to spread from one cerebral region to another, do these propagation patterns follow the routes of brain connectivity? Which type of connectivity (anatomic, functional, or genetic) is most involved in the generation of structural co-alterations? What is the temporal evolution of these co-alteration patterns?

Materials and methods

Selection of studies

We queried the VBM BrainMap database (Fox and Lancaster, 2002; Fox et al., 2005; Laird et al., 2005b; Vanasse et al., 2018) (December 2017) using the following search criteria: (i) decreases: Experiments Context is Disease AND Experiment Contrast is Gray Matter AND Experiments Observed Changes is Controls>Patients; and (ii) increases: Experiments Context is Disease AND Experiment Contrast is Gray Matter AND Experiments Observed Changes is Patients>Controls.

We retrieved 912 experiments and 350 experiments for the first and the second query, respectively. All the retrieved experiments with a sample size smaller than eight subjects were excluded. The identification of this lower bound is in accordance with the work of Scarpazza et al. (2015), which showed that VBM experiments based on an equivalent sample should not be biased by an increased false positive rate. We further decided to exclude all the experiments not clearly comparing pathological population with healthy controls, as well as considering subjects 'at risk'. The remaining items were then coded according to the ICD-10 system. As a further criterion, all the experiments not coded with F (i.e. mental, behavioural and neurodevelopmental disorders) or G (i.e. diseases of the nervous system) labels were excluded. From the remaining records, we also expunged those related to codes that could not be considered as primary brain disorders (i.e. F10: Alcohol related disorders; F15: Other stimulant related disorders; F28: Other psychotic disorder not due to a substance or known physiological condition; F91: Conduct disorders; G11: Hereditary ataxia; G43: Migraine; G44: Other headache syndromes; G47: Sleep disorders; G50: Disorders of trigeminal nerve; and G71: Primary disorders of muscles). At the end of this procedure the 642 remaining experiments from the first query (for 15 820 subjects, and 7704 foci) and the 204 remaining experiments from the second query (for 4966 subjects, and 2244 foci) were used for the analyses.

For the first query, most studies explored F20: Schizophrenia (17.9%); F32-F33: Major depressive disorder, single episode/recurrent (9.8%); G40: Epilepsy and recurrent seizures (8.7%); G30: Alzheimer's disease (8.3%) and G31: Other degenerative diseases of the nervous system (8.1%). For the second query, most studies explored F20: Schizophrenia (16.2%); G40: Epilepsy and recurrent seizures (12.7%); F84: Pervasive developmental disorders (11.3%); F31: Bipolar disorder (9.8%) and F32-F33: Major depressive disorder, single episode/recurrent (9.3%). The complete overview of the diagnostic spectra distribution is reported in Supplementary Table 1.

The overview of data search strategy and datasets is reported in the Supplementary material. A flow chart of key steps (used to generate the dataset of information, analyse data and obtain several levels of results) is also reported in Supplementary Fig. 1. The full list of the studies designated as suitable for meta-analysis, are reported in Supplementary Tables 2 and 3.

To calculate the pattern of structural co-alterations we used the same methodology previously applied in Cauda et al. (2018), Manuello et al. (2018) and Tatu et al. (2018).

Anatomical likelihood estimation and modelled alteration creation

First, we performed an anatomical likelihood estimation (ALE) (Eickhoff et al., 2009, 2012; Turkeltaub et al., 2012) to summarize the results of the retrieved experiments statistically using an in-house developed MATLABr script following both the algorithms used in Gingerale 2.3.6 (Eickhoff et al., 2009, 2012; Turkeltaub et al., 2012) and the recommendation of Eickhoff et al. (2017). Results are clustered at a level of $P < 0.05$, family-wise error (FWE)-corrected for multiple comparisons, with a cluster-forming threshold of $P < 0.001$ (Eickhoff et al., 2016).

The ALE is a quantitative voxel-based meta-analysis technique able to give information about the anatomical reliability of results through a comparison by using a sample of reference studies from the existing literature (Laird et al., 2005a). An ALE meta-analysis considers each focus of every experiment as a Gaussian probability distribution:

$$p(d) = \frac{1}{\sigma^3\sqrt{(2\pi)^3}}\, e^{-\frac{d^2}{2\sigma^2}} \qquad [1]$$

where d is the Euclidean distance between the voxels and the focus taken into account and σ is the spatial uncertainty.

A modelled alteration (MA) map was calculated for each experiment as the union of the Gaussian probability distribution of each focus present in the experiment itself. Then the ALE map was determined as the union of the MA maps.

The significance of alteration values within the ALE map was calculated by a permutation test, in which we redistributed the same number of foci across the brain and recalculated an ALE map as described before. The histogram of the obtained score was used to assign a threshold P-value.

Creation of nodes

The creation of nodes was obtained from the ALE map using a peak detection algorithm that returns the set of local maxima. A local peak is a voxel whose ALE value is higher than the values of its neighbouring voxels. We selected the voxels with a peak value greater than a given threshold, which was set at the 75th percentiles of the peak values distribution. Then we created a distance matrix calculating the Euclidean distance between peaks. To avoid overlaps between regions of interest, we excluded all the peaks within a distance of 10 mm from the other peaks. Around each of those peaks we designed a 10 mm2 region of interest, which was used for the subsequent analysis (see Fig. 1 for a schema depicting the node detection pipeline; see Supplementary Tables 6 and 7 for the coordinates of nodes). For a detailed discussion of the rationales at the basis of our methodological choices, see Cauda et al. (2018).

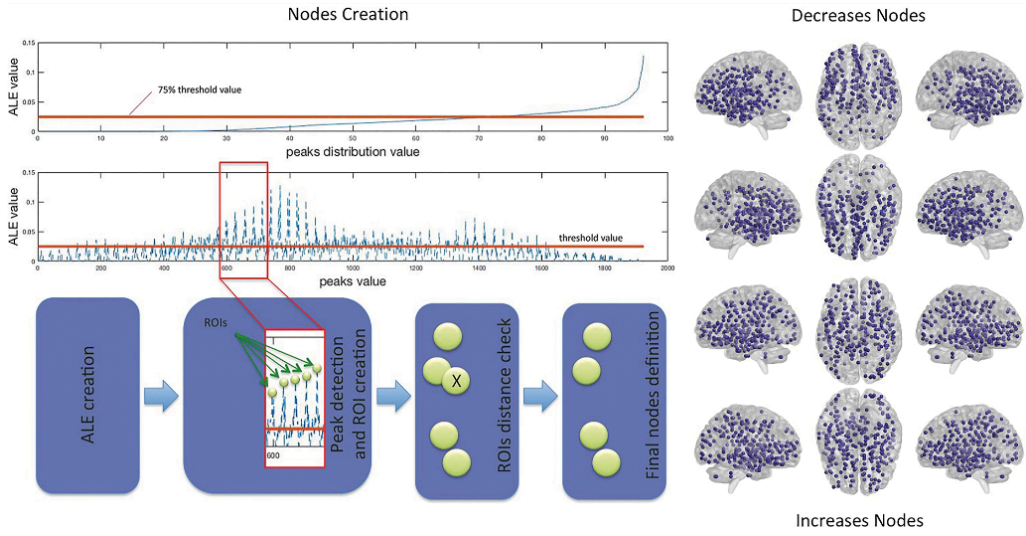

Figure 1: Node detection pipeline. Left: The schema illustrates the pipeline utilized for the detection of the regions of interest (i.e. nodes). Right: The obtained nodes for the decrease (top) and increase (bottom) conditions. See Supplementary Tables 6 and 7 for the node coordinates.

The structural co-alteration network

To trace the distribution of brain alterations we used a methodology aimed to characterize the structural co-alterations in the evolution of brain disorders (Cauda et al., 2015, 2018; Manuello et al., 2018; Tatu et al., 2018). This method can establish whether the alteration of a brain area statistically co-occurs with the alteration of one or more other brain areas. Specifically, we created a co-alteration matrix using the previously defined set of nodes. In the matrix of N × M dimension, the N rows represent experiments and the M columns the network nodes. For each pair of nodes of the co-alteration matrix, it is possible to obtain the strength of their co-alteration using the Jaccard index, which is defined as the number of experiments (rows) activating both the nodes divided by the union of the experiments activating the two nodes independently.

The obtained Jaccard matrix was thresholded at $P < 0.01$ using the method proposed by Toro et al. (2008). Given two nodes A and B, the null hypothesis states that the probability of B being altered does not depend on the value observed for A; by

contrast, the alternative hypothesis states that a relationship of dependence between A and B exists. This can be expressed formally as:

$$p_0=\text{Prob}(B=1|A=0) \quad [2]$$

$$p_1=\text{Prob}(B=1|A=1) \quad [3]$$

$$H_0:p_0=p_1=p \quad [4]$$

$$H_1:p_0\neq p_1 \quad [5]$$

We can obtain from the data an estimate $\hat{p}$ under the null hypothesis as $\hat{p}=m/N$, where m is the number of experiments in which node B is altered and N the total number of experiments. Similarly, we can obtain the estimated probabilities under the alternative hypothesis as:

$$\hat{p}_0=(m-k)/(N-n) \quad [6]$$

and

$$\hat{p}_1=k/n \quad [7]$$

where n is the number of experiments in which the node A is altered and k is the number of experiments in which both nodes A and B are altered. The likelihood-ratio test is calculated with the following formula:

$$\lambda=L(H_1)/L(H_0) \quad [8]$$

This formula is used to evaluate the alternative hypothesis H1 with respect to the null hypothesis H0.

The likelihood of the null hypothesis is defined as follows:

$$L(H_0)=B(k;n,p)B(m-k;N-n,p)$$

[9]

where B is the binomial distribution in which n is the number of contrasts that alters the second node, m is the number of contrasts that alters the first node, N is the total number of contrasts, and p=m/N and k are the numbers of contrasts that alter both nodes.

The likelihood of the alternative hypothesis is defined as follows:

$$L(H_1)=B(k;n,p_1)B(m-k;N-n,p_0)$$

[10]

The λ distribution is shaped by a $\chi 2$ function with one degree of freedom. Connection at $P < 0.01$ corrected for false discovery rate (FDR) was maintained, otherwise discarded.

Functional connectivity matrix

For the same set of nodes considered in the previous analysis we calculated the functional connectivity matrix using resting state data (minimally preprocessed and ICA-FIX de-noised) from 200 healthy adult subjects in the 22–35 age range, obtained from the Human Connectome Project (2015 Q4, 900-subject release). For further details on the preprocessing of these data see Glasser et al. (2013) and Van Essen et al. (2012).

The matrix was constructed in the following manner. The previously determined nodes were used to create a spatial map and to generate subject-specific associated time series of the functional data, using the dual regression approach (Beckmann et al., 2009; Filippini et al., 2009). For each subject, the spatial map is regressed (as spatial regressors in a multiple regression) into the subject's 4D space-time dataset. This results in a set of subject-specific time series. The output of the dual regression was a set of 200 matrices, one for each subject, where each column represents the time series of the corresponding node. Starting from these matrices we calculated the partial correlation between the nodes for each subject and then we mediated to obtain a final partial correlation matrix of the subjects' group. This group connectivity matrix was then thresholded ($\alpha < 0.05$) with a one sample permutation

test (5000 permutation) using the FSL randomise program (Smith and Nichols, 2009; Winkler et al., 2014).

Anatomical connectivity matrix

The anatomical connectivity matrix was constructed using diffusion tensor imaging (DTI) data of 842 subjects in the 22–35 age range. These data were retrieved from the Human Connectome Project (2015 Q4, 900-subject release) (Van Essen et al., 2013). The diffusion images were acquired using a multishell diffusion scheme. The b-values were 1000, 2000 and 3000 s/mm2. The numbers of the diffusion sampling directions were 90, 90 and 90. The in-plane resolution was 1.25 mm. The slice thickness was 1.25 mm. The diffusion data were reconstructed in the MNI space using the q-space diffeomorphic reconstruction (Yeh and Tseng, 2011) to obtain the spin distribution function (Yeh et al., 2010). A diffusion sampling length ratio of 1.25 was used, and the output resolution was 1 mm. The atlas was constructed by averaging the spike density functions of the 842 subjects.

A deterministic fibre tracking algorithm (Yeh et al., 2013) was used to reveal the brain anatomical connections. The parameters were the following: whole brain seeding region method; angular threshold of 60°; step size of 0.5 mm; the anisotropy threshold was determined automatically by DSI Studio (Yeh et al., 2016). Tracks with length less than 30 mm were discarded. A total of 5000 seeds were placed in the brain. The nodes, obtained from the meta-analysis, were used to calculate the connectivity matrix by using the numbers of tracts passing between two nodes normalized by the median length of the connecting tracks.

Genetic co-expression matrix

Differently to the gene co-expression networks (Zhang and Horvath, 2005) that can quantify gene-to-gene relationships across different anatomical samples, the correlated ‘gene expression network’ proposed by Richiardi et al. (2015) is a form of genetic connectivity that quantifies anatomical region to anatomical region (i.e. region of interest to region of interest) across genes. This network has been obtained by using the complete microarray datasets of six brains, available for download from the Human Brian Atlas Project (Hawrylycz et al., 2012). The datasets contain values of gene expression that are normalized across all brains with an improved normalization process—for further information about the sample normalization see ALLEN Human Brain Atlas (2013). The downloaded files contain normalized microarray expression values as well as probe and sample metadata necessary for analysis.

It should be noted that the Allen Brain Atlas has some idiosyncrasies. For example, only two of the individuals whose data are stored in the database have bi-hemispheric samples. Moreover, the samples of brain areas were obtained with different stereotactic coordinates so that the variability among them is high. To address these issues, we used a method based on the Voronoi tessellation (Cauda et al., 2012a). Voronoi tessellation (Voronoi, 1907) is a specific decomposition of a metric space based on a finite set of points. In a 3D space, a given set of points S is a partition that associates a volume V(p) with every point $p \in S$ so that all the points of the surface of V(p) are closer to p than to any other point in S. With this method, for each subject, we were able to create a parcellation of the brain based on the position of the samples, which are considered as the barycentres of the Voronoi polygons. We then assigned to all the voxels encompassed in a specific polygon the gene expression pattern of the sample located in the barycentre of that polygon.

Six parcellations were then constructed, one for each individual of the Allen project. In every parcellation, each voxel was characterized by a gene expression vector related to its closer sample. With regard to the four individuals with samples coming from one hemisphere, only one half brain was parcellated. Afterwards, we averaged the gene expressions of the six subjects voxel-wise. Gene expressions that are reported as non-statistically significant in the Allen database were excluded from the averaging process. This method made it possible to reduce the variance among the gene expression patterns of the six individuals, thus minimizing the weaknesses of the Allen database as much as possible.

The result was a tessellation of the brain in which every Voronoi polygon contains the mean gene expression of the six individuals (Cauda et al., 2012a). Subsequently, this information has been used to create the genetic co-expression matrix based on the set of nodes obtained from the meta-analysis. To every node we assigned the gene expression related to the Voronoi polygon associated with that node. We then constructed a matrix in which rows represent the gene expressions and columns represent the nodes. From this matrix we calculated the full and partial correlation of the mean gene expression between the nodes, so as to obtain a partial correlation matrix. This final matrix was probabilistically thresholded ($\alpha < 0.05$) with a permutation test (5000 permutations).

Reliability measures

To assess the consistency of our measures (reliability) we used a Spearman-Brown split half methodology (or Spearman-Brown prediction formula) (Stanley, 1971;

Allen and Yen, 2001). We divided each dataset (meta-analytic, functional, and genetic) into even and odd groups; for each group, we calculated the corresponding connectivity matrices. We then calculated the correlation between these connectivity matrices applying the Spearman-Brown correction (Allen and Yen, 2001) to get a better estimate of the reliability, as follows:

$$\rho=2r/(1+r) \quad [11]$$

where r is the classical Spearman correlation.

Since DTI data were provided by the Human Connectome Project as 'mean connectivity matrices', we used a different approach to calculate the reliability of the anatomical connectivity measures. We used another mean DTI connectivity matrix obtained from a different dataset as a replication dataset. The replication dataset consisted of a different structural connectivity matrix that was constructed using a total of 842 subjects' diffusion MRI data, in the 22–35 age range, obtained from the Human Connectome Project (2015 Q4, 900-subject release) (Van Essen et al., 2013). Finally, we calculated the correlation between the anatomical connectivity matrix derived from the primary dataset and the one derived from the replication dataset.

Comparison between connectivity matrices

The comparison between the different matrices (co-alteration, anatomical, functional, and genetic) was done using the Mantel test (Mantel, 1967; Glerean et al., 2016). In the Mantel test the correlation between two matrices was determined with a permutation test (5000 permutations). We calculated the correlation between the matrices by randomly permutating rows and columns. We subsequently obtained the distribution of the different correlations and calculated the P-value.

Diffusion connectivity matrix: spatial and temporal evolution

To assess the temporal evolution of the different types of connectivity, we developed a simple diffusion model. We considered the spread of neuronal alterations as a diffusion process by using a brain network-based model $G=\{N,E\}$ where nodes $n_i \in N$, which represents the cortical and subcortical structure as obtained from our meta-analysis, while edges $e_{ij} \in E$, which represents the connection strength linking node i and node j. We used three types of connection strength for each model obtained from the anatomical, functional and genetic connectivity matrices.

Following Abdelnour et al. (2014) and Kondor and Lafferty (2002), we modelled the diffusion process using the heat equation, defined as:

$$dx(t)/dt = -\beta \mathcal{L} x(t) \quad [12]$$

where the matrix $\mathcal{L}$ is the following Laplacian graph:

$$\mathcal{L} = I - \Delta^{-1/2} E \Delta^{1/2} \quad [13]$$

in which Δ is the diagonal matrix with $\delta_i = \sum_j e_{ij}$ as the ith diagonal element. The heat Equation 12 can be solved explicitly as follows:

$$x(t) = \exp(-\beta \mathcal{L} t) x_0 \quad [14]$$

This formula defines the evolution of the initial configuration x_0. We hypothesized an initial configuration in which the disease factor was uniform in all the nodes, thus obtaining the following equation:

$$Cov(t) = \exp(-\beta \mathcal{L} t) \quad [15]$$

which, having as free parameters the diffusion factor β and time t, can express the covariance of the system at each time of its evolution.

In our case we had the covariance matrix (the meta-analytic data) and the Laplacian matrices obtained from the resting state data, the anatomical data and genetic data, respectively. We estimated therefore the diffusion factor β and obtained the evolution of the diffusion for the functional, anatomical and genetic data. The best estimate of the parameter β and the time evolution of the diffusion were determined using a grid search on the parameter β, ranging between (0,1) with a step of 0.1. For each β-value, the matrix obtained from this simulation was correlated with the meta-analytic covariance matrix. With a Mantel test we assessed the significance of this correlation. Finally, the β-value that could maximize the correlation was chosen.

Contribution of the different kind of connectivity profiles to the structural co-alteration patterns

To find out the contribution of the different types of connectivity to the structural co-alteration patterns, we developed the following model:

$$D=\alpha M_{F-Conn}+\beta M_{A-Conn}+\gamma M_{G-Conn} \quad [16]$$

where D is the structural co-alteration matrix and M_{F-Conn} is the functional connectivity matrix, M_{A-Conn} is the anatomical connectivity matrix, and M_{G-Conn} is the genetic connectivity matrix, respectively.

Using an unconstrained non-linear optimization, we found the minimum of a scalar function of several variables. The algorithm was the simplex search method of Lagarias et al. (1998):

$$\min_{\alpha,\beta,\gamma} | |(D-\alpha M_{F-Conn}-\beta M_{A-Conn}-\gamma M_{G-Conn})^2| | \quad [17]$$

The final results are the coefficients that minimize the square difference norm between the structural co-alteration matrix and the other matrices. The algorithm was executed 1000 times with different initial conditions, each time to check the stability of the obtained minimum (Fig. 2, bottom).

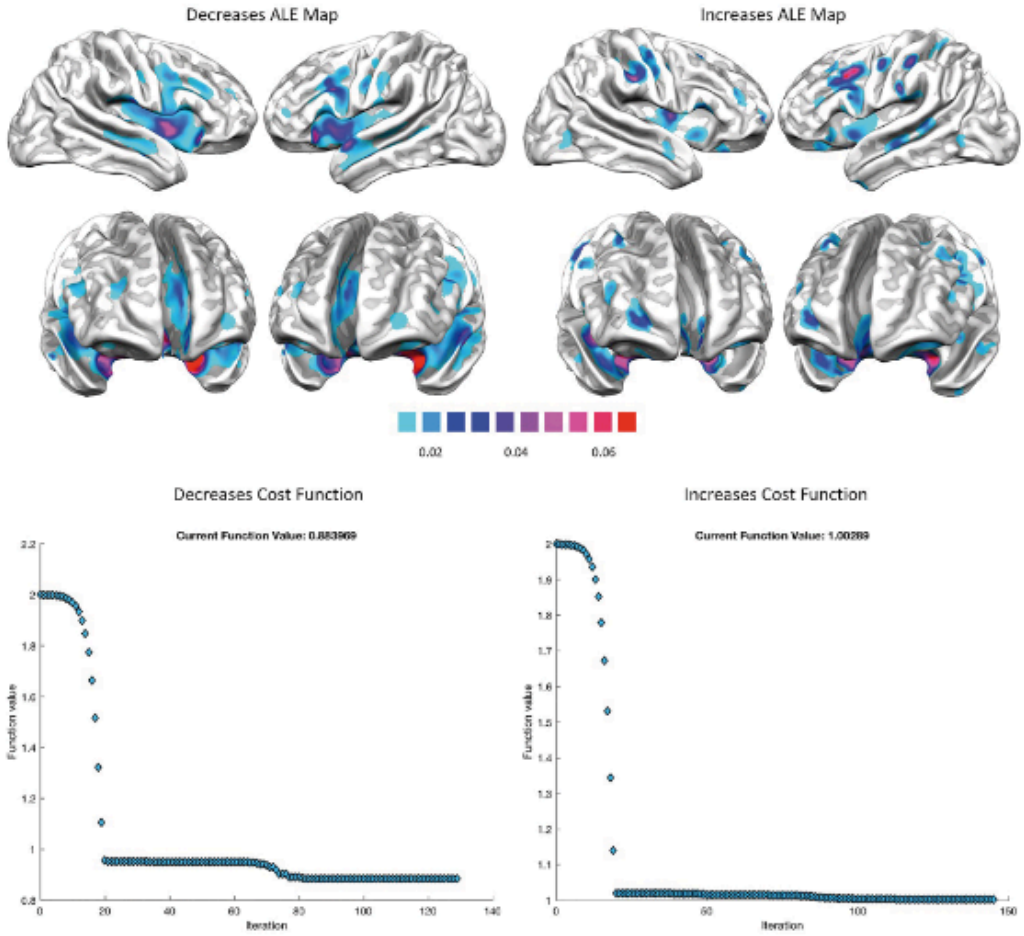

Figure 2: ALE results and cost functions. Top: ALE results for decreased (left) and increased foci (right). ALE results are clustered at the level of $P < 0.05$ and family-wise error-corrected for multiple comparisons, with a cluster-forming threshold of $P < 0.001$. Bottom: The schema illustrates the evolution of the cost function of the minimization algorithm for predicting the distribution of the structural co-alteration patterns.

Network analysis techniques

We analysed the co-alteration patterns further using a network-based analysis technique.

The node degree is the number of connections that the node has with the other nodes. We used the degree distribution to compare the node degree of the nodes of different networks. It was therefore possible to compare the structural co-alteration network with random networks. The degree distribution is the fraction of nodes with degree k, defined as follows:

$$P(k)=n_k/n \quad [18]$$

The average shortest path length is defined as the average number of steps along the shortest paths for all pairs of nodes of the network under consideration. For an unweighted graph G with n vertices, the average path length is defined as follows:

$$l_G=1/(n(n-1))*\sum_{i\neq j}d(v_i,v_j) \quad [19]$$

where d is the shortest distance between node vi and node v_j, with d = 0 if v_j cannot be reached from v_i.

This is one of the most robust measures in network topology and is inversely related to efficiency, which is a measure of how efficiently the network exchanges information. In particular, the local efficiency quantifies the network resistance when a failure occurs within it.

Data availability

The datasets we used in this study are from publicly available sources:

BrainMap (meta-analytic datasets) http://brainmap.org/.

Allen Brain Atlas (gene expression datasets) http://human.brain-map.org/static/download.

Human Connectome Project (resting state connectivity and DTI anatomical connectivity datasets) http://www.humanconnectomeproject.org/data/.

Above, we describe in detail which parts of these datasets were used or how we queried the BrainMap database.

A complete list of the literature involved in the meta-analytic analyses is provided in the Supplementary material.

Results

The 'core set' of altered brain areas

Figure 2 (top) shows the brain areas that appear to be altered in the VBM studies retrieved from our search. These areas form the 'core set' that is likely to be frequently affected by brain diseases. Areas showing significant statistical decreases are the insulae, anterior cingulate cortices, superior and middle temporal gyri, superior, middle and inferior frontal, pre- and postcentral gyri. Areas showing significant statistical increases are the right anterior and posterior insula, left middle insula, right pre- and postcentral gyri, right superior frontal gyrus, right superior temporal gyrus, left inferior temporal and inferior frontal gyri (see also Supplementary Tables 4 and 5).

Node creation and structural co-alteration network

Our automatic node creation procedure derived 277 nodes from the core set of decreased areas and 271 nodes from the core set of increased areas. These nodes are illustrated in the right panel of Fig. 1 (see also Supplementary Tables 6 and 7).

Given the nodes previously designed, we constructed the structural co-alteration networks for both the VBM datasets (decreases and increases). These networks are visualized in Fig. 3.

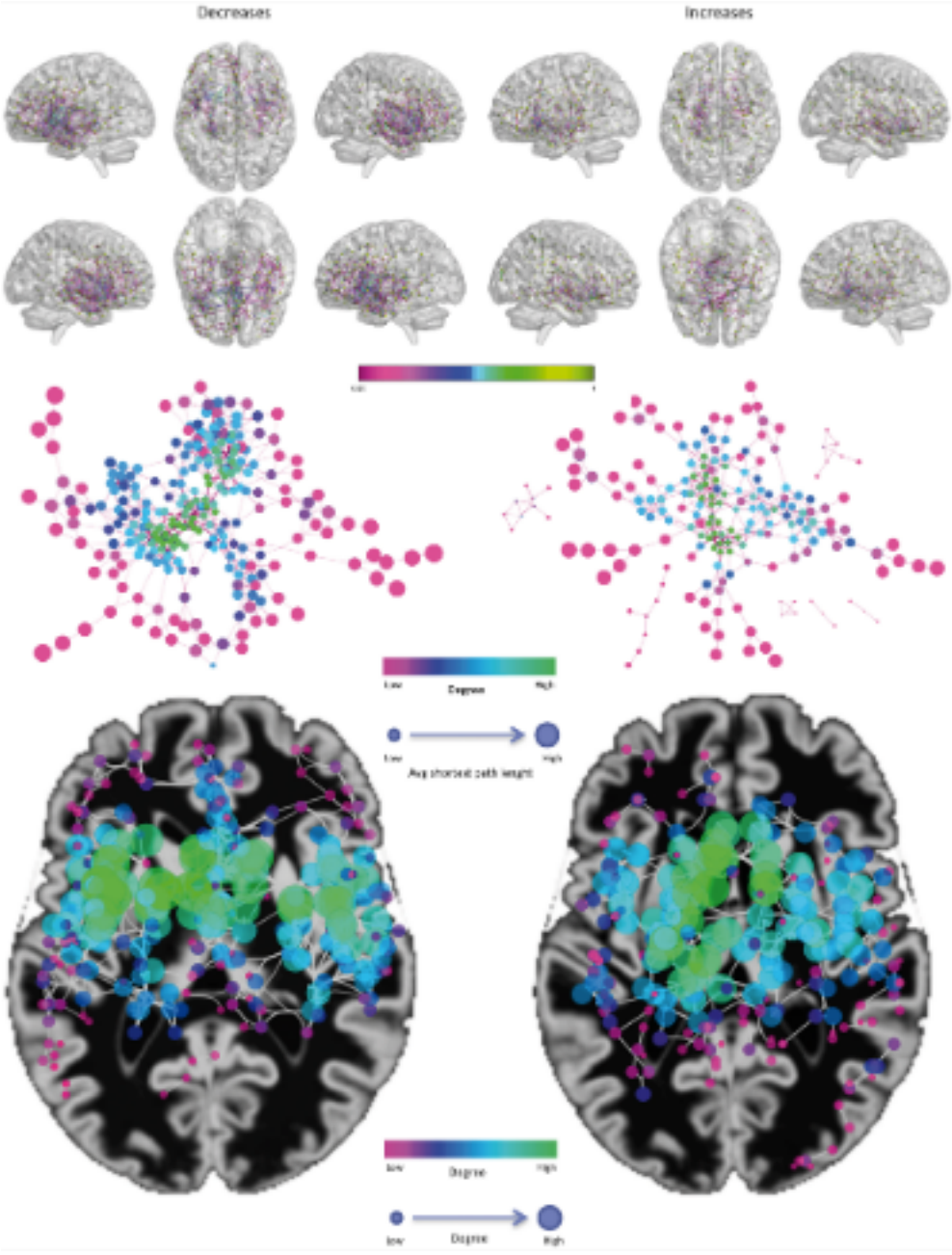
Decreases
Increases
Low
Degree
High
Avg shortest path length
Low
High
Low
Degree
High
low
Degree
high

Figure 3: Co-alteration networks. Top: The decrease-related (left) and increase-related (right) structural co-alterations. Only for visualization purposes, the matrices were thresholded at the 95th percentile. Colours ranging from magenta to green represent lower to higher correlation values. Middle: Topological analysis of the structural co-alteration network, using a force directed spring embedded layout. Smaller nodes show lower average shortest path length. Colour tones from magenta to green indicate lower to greater degree values. Bottom: A geotagged layout of the networks. Node dimension and colour tones from green to red indicate lower to greater degree values.

Interestingly, the two structural co-alteration networks are topologically different (Fig. 3, middle and bottom). The one formed by decreased areas is more restricted and principally involves the insulae and the anterior cingulate cortices. These regions exhibit the nodes with the highest values of degree. In turn, the other network formed by increased areas is more widespread and less anatomically defined, albeit it includes parts of the insulae and is slightly prevalent in subcortical regions.

Anatomical, functional and genetic connectivity

For the same sets of nodes, we calculated the resting state functional, anatomical and genetic networks. These networks are visualized in Figs 4 and 5. In line with the previous literature (Gong et al., 2014; Huang and Ding, 2016), functional and anatomical connectivity appear to be correlated (decreased nodes $r = 0.14$, $P < 2.383 \times 10^{-5}$; increased nodes $r = 0.12$, $P < 2.421 \times 10^{-5}$). Notably, the genetic connectivity also appears to correlate with both anatomical (decreased nodes $r = 0.21$, $P < 2.195 \times 10^{-5}$; increased nodes $r = 0.18$, $P < 3.028 \times 10^{-5}$) and functional connectivity (decreased nodes $r = 0.18$, $P < 3.021 \times 10^{-5}$; increased nodes $r = 0.14$, $P < 2.359 \times 10^{-5}$).

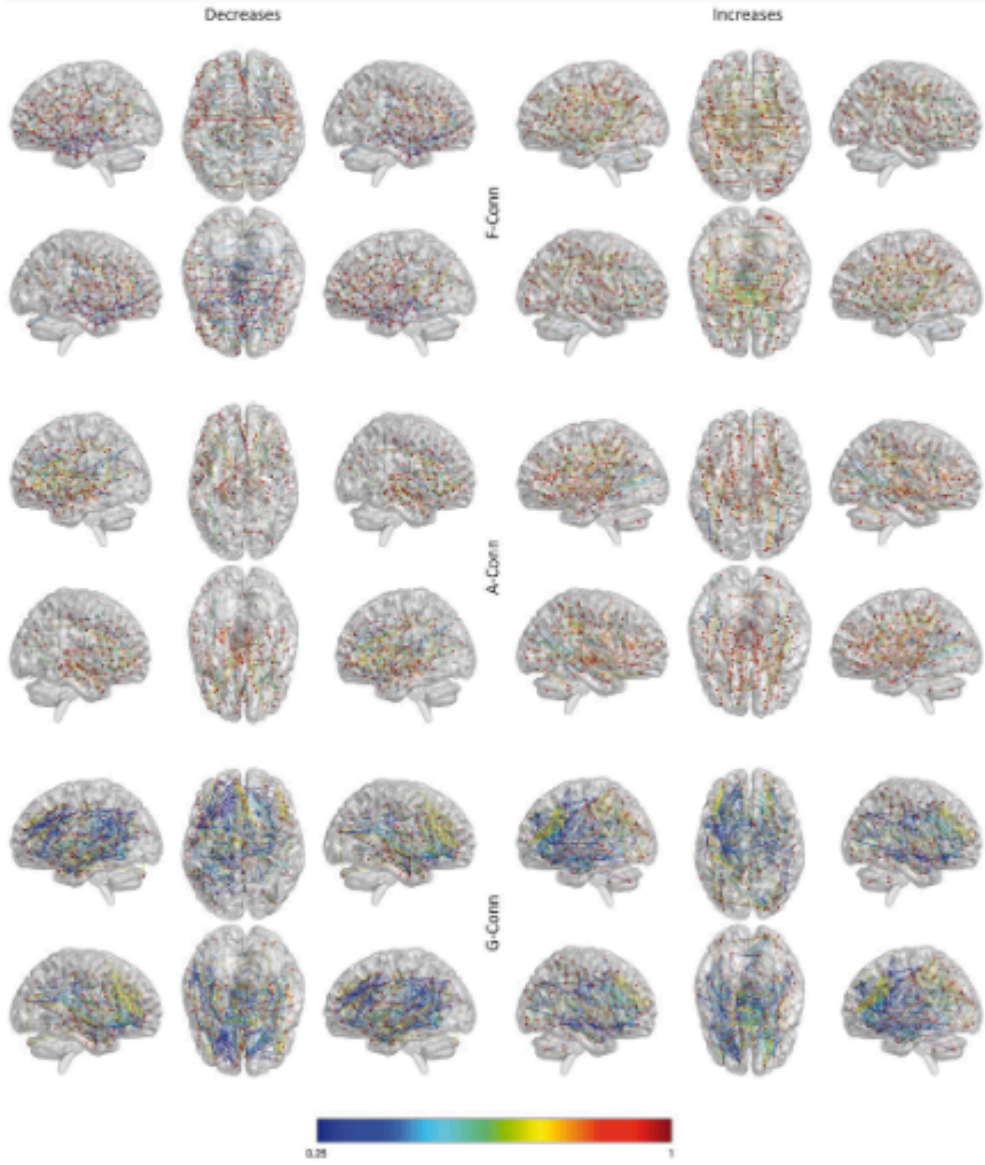

Figure 4: Connectivity networks. The functional connectivity (F-Conn) network (top), the anatomical connectivity (A-Conn) network (middle), and the genetic connectivity (G-Conn) network or genetic co-expression network (bottom). Only for visualization purposes the matrices were thresholded at the 95th percentile. Colours ranging from blue to red represent lower to higher correlation values. For anatomical connectivity, colour ranging from blue to red represent lower to higher fibre density values.

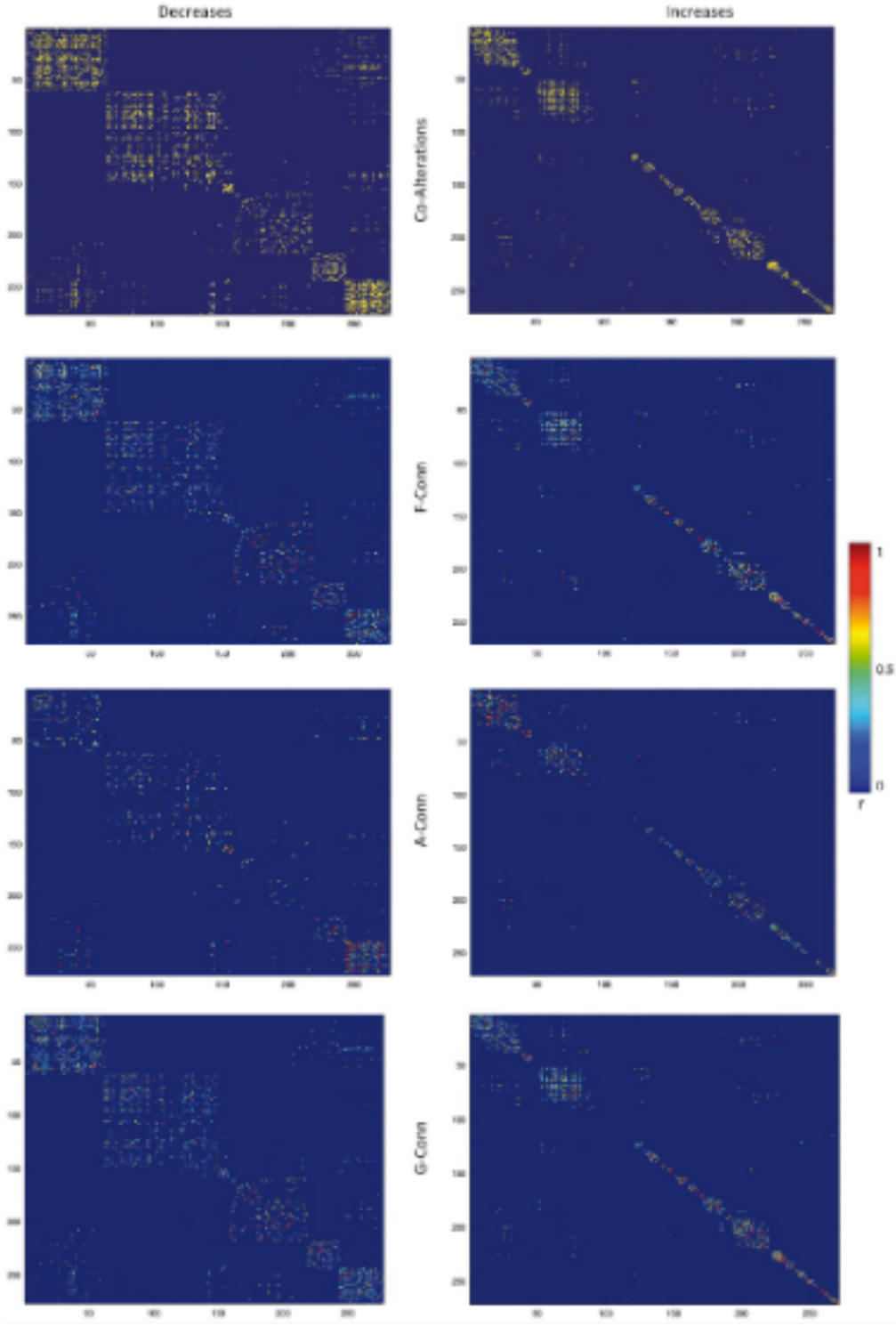
Decreases
Increases
Co-Alterations
F-Conn
A-Conn
G-Conn
1
0.5
0
r

Figure 5: Distance matrices regarding the structural co-alteration, functional, anatomical and genetic connectivity. Colours ranging from blue to red represent lower to higher correlation values.

Reliability

Our connectivity matrices present a good reliability (Spearman-Brown split half test). Indeed, we have obtained mean values of 0.80, 0.72, 0.80, and 0.75 for the structural co-alteration, the functional, the gene co-expression and the anatomical connectivity matrices, respectively. These values indicate a good internal consistency of measures. In particular, the Spearman-Brown formula is related to the Cronbach's alpha (Nunnally and Bernstein, 1994; Carlson et al., 2009); both formulas measure the ratio of the true-score and total-score variances. As suggested by Nunnally and Bernstein (1994), the rule of thumb for that measure usually considers a good internal consistency of data with values of >0.7.

Correlational analyses

As our experimental question is to investigate whether and how neuropathological co-alterations (independently related to both grey matter decreases and grey matter increases) are influenced by different types of normal brain connectivity (i.e. functional, anatomical, and genetic connectivity), we compared neuropathological co-alteration patterns with normal patterns of brain connectivity as they are measured in healthy individuals.

The statistical comparison between the structural co-alteration matrix and the other matrices (functional, anatomical, and genetic) shows that each of the three connectivity profiles is statistically correlated with the structural co-alteration patterns associated with grey matter decreases and grey matter increases, that is, each type of connectivity explains a statistically significant portion of those patterns.

Figure 6 (top left) illustrates the correlation between the structural co-alteration matrix and the other three connectivity matrices. While the decrease-related structural co-alteration is better explained by functional connectivity ($r = 0.28$), followed by anatomical and genetic connectivity ($r = 0.19$ and $r = 0.18$, respectively), the increase-related structural co-alteration is better explained by functional connectivity ($r = 0.26$), followed by genetic and anatomical connectivity ($r = 0.23$ and $r = 0.22$, respectively).

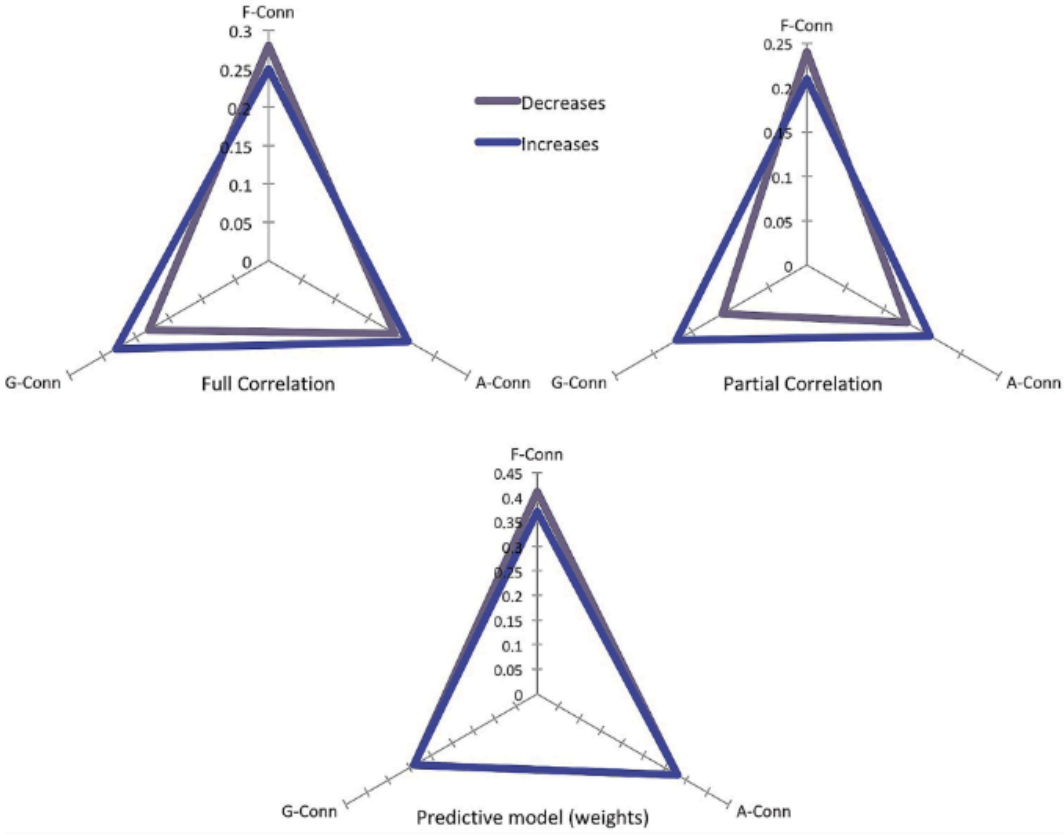

Figure 6: Results of the correlational and predictive tests. The top panel shows the correlational results (the left panel illustrates the full correlation, while the right panel illustrates the partial correlation). The bottom panel shows the predictive results.

However, as these three types of connectivity are known to be correlated with each other and exhibit a shared variance, as we previously mentioned, we decided to calculate the partial correlation between the three connectivity matrices and the structural co-alteration matrix with the aim to report how each type of connectivity correlates with the structural co-alteration pattern with the exclusion of their common shared variance. This analysis is described in Fig. 6 (top right), and provides further evidence that the decrease-related structural co-alteration correlates more with functional connectivity ($r = 0.24$), followed by anatomical ($r = 0.14$) and genetic ($r = 0.11$) connectivity. In turn, the increase-related structural co-alteration appears to correlate in a similar way with the three types of connectivity; it is slightly

better explained by functional connectivity (r = 0.22), followed by genetic and anatomical connectivity (r = 0.17 and r = 0.16, respectively). Of note, all the partial and full correlation results are statistically significant: P-values < 2 × 10−7 for the partial correlation results, and P-values < 3 × 10−4 for the full correlation results. Overall, this indicates that structural co-alterations are in part explained by all these three types of connectivity.

Spatial and temporal progressions

Our model is able to predict the propagation patterns of neuronal alterations with good statistical confidence (all predictions survive the conservative statistic threshold of $P < 10^{-5}$).

Figure 7 illustrates the temporal evolution of the structural co-alteration patterns (expressed in arbitrary units) as it is predicted by every β-value, used in the grid search, of the model. For each β-value we calculated the temporal evolution of the diffusion process and for each time we correlated the diffusion matrix derived from the distribution model of co-alterations and the co-alteration matrix obtained from the meta-analysis. What is clear is that around 30 temporal steps, all the connectivity models predict the complete diffusion of brain alterations. However, within the initial steps, only the genetic model can substantially show a prediction of how structural co-alterations are expected to develop. This result provides evidence that with the help of genetic connectivity, it is possible to predict a substantial portion of the pattern formed by neuropathological alterations in a variety of brain disorders just based on its initial manifestation. The chart in Fig. 7 illustrates how the average temporal evolution of structural co-alterations, calculated by the model based on grey matter increases, is characterized by a faster development compared with that calculated by the model based on grey matter decreases.

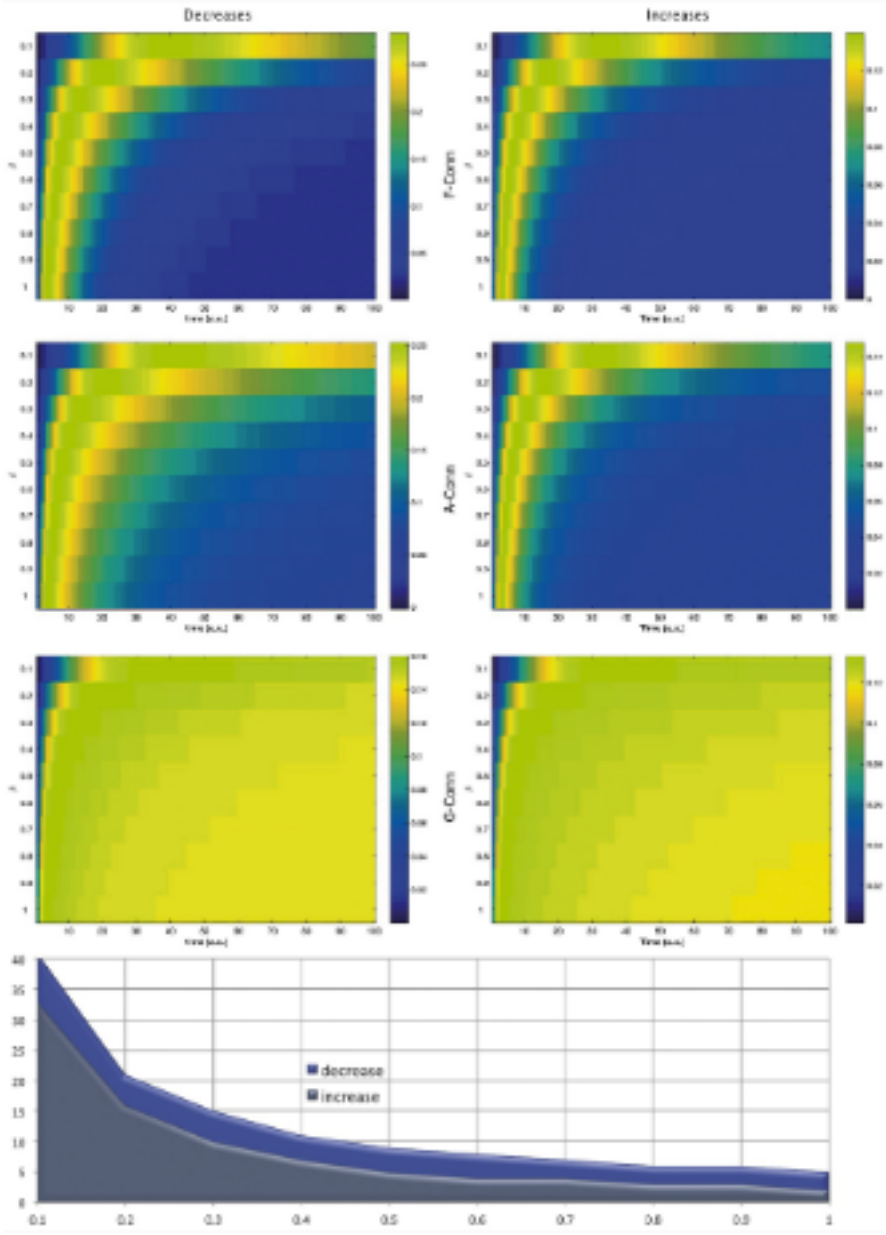
Decreases
Increases
P-Conn
A-Conn
G-Conn
decrease
increase

Figure 7: Model's temporal evolution. Top: This series of maps shows the correlations of the functional, anatomical and genetic matrices with the structural co-alteration matrix for different beta values as a function of time (arbitrary units), as described in Equation 12. Colours ranging from blue to red represent lower to higher correlation values. Bottom: The chart summarizes the time in which the diffusion of brain alterations reaches the steady state as a function of the beta rate for the decrease and increase conditions. Note that the average temporal evolution of structural co-alterations calculated by the model based on grey matter increases is characterized by a faster development compared with that calculated by the model based on grey matter decreases.

The model of the distribution of the structural co-alteration patterns ($D = \alpha M_{F-Conn} + \beta M_{A-Conn} + \gamma M_{G-Conn}$) shows that it is possible to describe the meta-analytic structural co-alteration matrix as a weighted sum of the functional, anatomical and genetic connectivity matrices. After the optimization procedure for the three parameters, we correlated the D matrix of the model with the co-alteration matrix obtained from the meta-analytical data and found a variance explained for the grey matter decreases of $R^2 = 0.77$ ($P < 0.0012$) and for the grey matter increases of $R^2 = 0.72$ ($P < 0.0025$). Furthermore, all the three matrices appear to contribute significantly to the description of the meta-analytic structural co-alteration matrix (Table 1 and Fig. 6, bottom). It is worth noting that, in our model, with regard to both grey matter decreases and increases the major contribution is made by the functional connectivity matrix, followed by anatomic and genetic connectivity.

	F-Conn R^2	A-Conn R^2	G-Conn R^2	Total R^2
Decrease	0.41	0.34	0.25	0.77
Increase	0.38	0.33	0.29	0.72

Table 1: Parametric values of correlation between the three connectivity matrices and the meta-analytic structural co-alteration matrix constructed with either grey matter increase or decrease data. The total R^2 value is the result of the correlation between the diffusion matrix obtained from the model and the co-alteration matrix obtained from the meta-analytic data. In this way we calculated the contribution of each connectivity profile to the variance explained, determining the R^2 of each network profile with the diffusion matrix obtained from the model. A-Conn = anatomical connectivity matrix; F-Conn = functional connectivity matrix; G-Conn = genetic connectivity matrix.

Discussion

The analyses carried out in this study provide support for the following points: (i) brain areas affected by neuropathological processes form typical patterns of structural co-alterations; (ii) the development of these transdiagnostic structural co-alterations is not random but preferentially follows the routes of brain connectivity; (iii) anatomical, functional and genetic connectivity are differently involved in shaping structural co-alterations; and (iv) starting from the brain connectivity matrices, it is possible to create a model that allows us to predict with relatively high accuracy the development of the structural co-alteration patterns and, based on this model, to estimate the evolution of how structural co-alterations are distributed across the brain in terms of the involvement of the type of brain connectivity. To the best of our knowledge, this is the first time that these issues have been addressed in humans using in vivo approaches.

Our results provide evidence that brain morphological alterations are distributed according to a statistically significant pattern: alterations are distributed across brain areas so as to form a network of pathological nodes. This pattern of structural co-alteration exhibits a topological definite structure and includes some regions (the insular and anterior cingulate cortices) that are thought to be important functional hubs of the brain.

We performed a predictive analysis of the structural co-alteration patterns by creating a model that, based on brain connectivity matrices, attempts to estimate the development of the co-alteration patterns; this model was able to explain the 77%

and the 72% of the variance in the decrease and increase structural co-alteration patterns, respectively. This finding supports the idea that the two structural co-alteration patterns, as well as their temporal development (Cauda et al., 2018), are strictly associated with the brain connectivity patterns. Specifically, our model shows that, based on functional and anatomical connectivity, more consecutive steps are needed to completely predict the propagation of structural co-alterations. On the other hand, this is not the case for a model based on genetic connectivity, which is able to predict the propagation of structural co-alterations just at its early stages.

Our analysis proposes to take into consideration the contribution of three (i.e. transneuronal spread, nodal stress, and shared vulnerability) of the four possible mechanisms so far hypothesized for the spread of brain alterations (Saxena and Caroni, 2011; Zhou et al., 2012; Fornito et al., 2015), each of which with its typical temporal evolution. Future studies will be able to apply our model in order to better understand which mechanisms are more specifically involved in particular brain disorders.

With regard to both grey matter decreases and increases, the functional connectivity appears to be the best predictor of the pattern of structural co-alterations. Although a certain type of connectivity seems to play a prevalent role in both grey matter decreases and increases, it is worth noting that the other types of connectivity are also important factors in the generation of structural co-alterations; their contribution, however, is characterized by different timings. This result is consistent with the fact that we worked on a cross-diagnostic dataset (Goodkind et al., 2015), which includes a wide range of brain disorders. As recently demonstrated by Cope et al. (2018), certain brain disorders can be characterized by the prevalence of specific mechanisms.

The distribution of brain alterations

Our analysis of the VBM studies about a great variety of brain disorders, especially regarding grey matter decreases, shows that a core set of cerebral areas appears to be frequently altered in a large number of neuropathological conditions (for a review of this transdiagnostic approach see Buckholtz and Meyer-Lindenberg, 2012; McTeague et al., 2016). This finding confirms a similar result obtained by other meta-analyses, which, however, were only restricted to three (Cauda et al., 2017) or six psychiatric diseases (Goodkind et al., 2015).

The recurrence of this common alteration pattern is well illustrated by the ALE analysis (Fig. 2). Interestingly, this peculiar pattern overlaps to a great extent with

those areas that have been proposed to be part of the cognitive control network (Cauda et al., 2012b, 2017; McTeague et al., 2016). It must be highlighted that the finding of a common alteration pattern in a vast number of brain diseases does not rule out the possibility that each disorder may be characterized by its own typical alterations (Crossley et al., 2015). However, here our aim was to investigate how alterations are generally spread across the pathological brain so as to achieve an overarching analysis supported by the most numerous sample of studies we could retrieve. Future studies will be needed to understand how the structural co-alteration patterns found in this meta-analysis differ with regard to each brain disorder independently considered.

A number of studies (Pearson et al., 1985; Saper et al., 1987; Braak and Braak, 1991; Brooks, 1991; Weintraub and Mesulam, 1996; Braak et al., 2011; Raj et al., 2012; Cauda et al., 2014; Iturria-Medina et al., 2014; Ravits, 2014; Fornito et al., 2015; Iturria-Medina and Evans, 2015) have proposed that the spread of neuronal alterations caused by neuropathological processes is not random but, rather, associated with typical network-like patterns. These data were already supported (Seeley et al., 2006, 2009; Zhou et al., 2012) and now receive further support from our study: brain alterations are distributed according to a statistically significant 'neurodegenerative networking' (Yates, 2012) or, as we have called it, 'morphometric co-alteration network' (Cauda et al., 2018); this broader term has the advantage to refer to all types of disorders capable of producing neuronal alterations, without committing to just the neurodegenerative factors, which consists of cerebral regions with pathologically grey matter increases or decreases.

Grey matter decreased areas are largely parts of the cognitive control network (Goodkind et al., 2015; McTeague et al., 2016) and include the insulae, anterior cingulate cortices, superior and middle temporal gyri, superior, middle and inferior frontal, pre- and postcentral gyri. In turn, grey matter increased areas include the right anterior and posterior insula, left middle insula, right pre- and postcentral gyri, right superior frontal gyrus, right superior temporal gyrus, left inferior temporal and inferior frontal gyri. The minor involvement of the precuneus in the co-alterations patterns may be viewed as counter-intuitive, given that this area is highly connected and is a central hub of the default mode network. Probably, because of the transdiagnostic approach of this study, similarities between brain disorders are likely to be highlighted and, though in some diseases the precuneus appears to be altered, the frequency of this alteration is not sufficient for being statistically relevant. Moreover, it must be considered that a high number of alterations in a certain brain

area does not necessarily imply for this area to be co-altered with other ones. With regard to this point, a recent study by our group (Manuello et al., 2018) has investigated the co-alterations of Alzheimer's disease and found out only a significant node of strong co-alterations within the precuneus. Even in the case of Alzheimer's disease, therefore, the precuneus level of co-alteration appeared to be less significant than theoretically thought.

The structural co-alteration pattern differs significantly for decreased and increased VBM values. With regard to grey matter decreases, it appears to be more concentrated in insular, cingulate and prefrontal cortices (areas of the cognitive control/salience network) (Seeley et al., 2007; Cauda et al., 2011, 2012a, 2013), whereas with regard to grey matter increases it appears to be slightly more uniformly distributed, albeit with a little prevalence in subcortical regions (Fig. 3). This differentiation is likely to be because of the different factors at the root of the development of grey matter increases and decreases in brain density. In fact, grey matter decreased areas are generally associated with neurodegenerative processes, while grey matter increased areas are generally associated with compensatory mechanisms (Lin et al., 2013; Premi et al., 2014, 2016), which are supposed to occur at the initial phases of brain deterioration. This interpretation is consistent with the temporal evolution shown by our predictive model, according to which patterns of grey matter increased values present a faster temporal development than patterns of grey matter decreased values (Fig. 7, bottom).

From the viewpoint of the topological analysis, when altered, the brain areas showing a higher node degree and/or less average shortest path length are likely to play a central role in the spread of neuronal alterations. Their greater number of connections as well as their more intense activity may enhance the mechanisms hypothesized to be the causes of alterations, especially the nodal stress and the transneuronal spread mechanisms. As suggested by our predictive model, these two mechanisms are supposed to be more involved in the formation of the structural co-alterations (both increase-related and decrease-related), which seems to be more influenced by both functional and anatomical connectivity. However, as the hypothesized causal mechanisms are not mutually exclusive, they are all likely involved in the formation of structural co-alterations, each with distinctive temporal patterns.

The relationship between the spread of neuronal alterations and brain connectivity

All three types of connectivity taken into consideration in this meta-analysis (functional, anatomical, and genetic) account well for a substantial part of the variance of the development of structural co-alterations (see Supplementary Fig. 2 for an infographic).

In particular, functional connectivity is able to explain a greater part of the structural co-alteration patterns than the other matrices, followed by anatomic and genetic connectivity. This result has also been achieved by determining the partial correlation between the structural co-alteration matrix and each connectivity matrix excluding the contribution of the other connectivity matrices. This procedure was required because both functional and anatomical connectivity profiles are known to be partially correlated (Skudlarski et al., 2008; Honey et al., 2009; van den Heuvel et al., 2009; Misic et al., 2016) and because both these connectivity profiles have also been found to be associated with patterns of genetic co-expressions (Lichtman and Sanes, 2008; French and Pavlidis, 2011; French et al., 2011; Wolf et al., 2011; Cioli et al., 2014; Goel et al., 2014; Richiardi et al., 2015).

It is worth noting that the temporal evolution of the alterations' spread predicted by our model, based on the functional and anatomical connectivity profiles, needs numerous steps (between 30 and 40, arbitrary units) before reaching completion. On the contrary, the prediction based on the genetic connectivity profile requires a shorter time: between 10 and 20 units. This interesting finding is consistent with the shared vulnerability hypothesis, according to which the spread of alterations caused by dysfunction in the co-expression of certain genes is supposed to need a shorter accretion time than when the other mechanisms are involved. Already at the early phases of neuropathological processes, many brain areas with similar genetic patterns can be altered. What is more, the genetic risk for brain disorders is pleiotropic and, thereby, can affect broad and transdiagnostic dimensions (Buckholtz and Meyer-Lindenberg, 2012) of symptomatically-related diseases (Gejman et al., 2011), thus disrupting brain connectivity patterns of core networks associated with fundamental cognitive functions (Cauda et al., 2012b). Our predictive model could therefore suggest that a chain of pathological factors is likely involved in a variety of neuropathological processes represented or better explained by different kinds of brain connectivity profiles (Supplementary Fig. 2). In other words, pathological patterns of gene co-expressions may lead to a neuronal shared vulnerability, which, in turn, may engender the alteration of important brain

networks, with the subsequent involvement of abnormal functional and anatomical connectivity patterns. As highlighted by Buckholtz and Meyer-Lindenberg (2012), 'genetic factors shape connectivity in networks linked to symptom domains, and imply that connectivity changes observed in mental disorders reflect a cause, rather than a consequence, of being ill'. The same authors remark that 'the latent structure of psychopathology may reflect, in part, a genetically determined latent structure of brain connectivity'.

The result achieved by our predictive model—i.e. that functional and anatomical connectivity seem to better account for the development of structural co-alterations in a longer run than the genetic one—is consistent with the fact that the nodal stress and the transneuronal spread mechanisms need time to make their effects. The nodal stress implies a progressive intensification of excitotoxicity factors, whereas the transneuronal spread implies the transport of pathological substances through axons or the extracellular liquid. All these processes need time to exert disruption and this point is well illustrated by the temporal evolution of the structural co-alteration patterns (Fig. 7).

It is worth suggesting that the three mechanisms taken into consideration in the present work (transneuronal spread, nodal stress and shared vulnerability) may play a synergistic role not only in the pathogenesis of neurodegenerative diseases but also, to some extent, in psychiatric as well as in neurodevelopmental disorders. Although these conditions are not directly related to the presence of a defined brain proteinopathy, structural and functional alterations are not randomly distributed across the brain, following specific connectivity constraints that produce identifiable morphometric co-atrophy patterns, as already shown by our group in neurodevelopmental (autistic spectrum disorder) and psychiatric (schizophrenia spectrum disorder and obsessive-compulsive spectrum disorder) conditions (Cauda et al., 2018). Furthermore, from a speculative perspective, it has been proposed that it would be more appropriate to view schizophrenia as a failure of communication between critical nodes of large neuronal networks rather than a dysfunction of separate areas, thus suggesting the expression of 'spatiotemporal psychopathology' to describe this condition (Kasparek et al., 2010; Northoff and Duncan, 2016). In this sense, different pathogenic mechanisms (i.e. pathogenic proteins propagating preferentially based on intrinsic network vulnerabilities—molecular nexopathies—for neurodegenerative diseases, and genetic/environmental interactions for both psychiatric and autistic spectrum disorders) may be at play. Overall, these pathological mechanisms can 'stress' the brain networks and 'shape' the grey matter

alterations in a network-based fashion, as described by the present work and others already cited. As defined for neurodegenerative proteinopathies (Warren et al., 2013), in other disorders (like psychiatric and autistic) the pathological and complex interaction between neurodevelopmental alterations and environmental/genetic modulators might trigger brain dysfunction (both functional and structural), even without a detectable proteinopathy (as in neurodegenerative diseases) but with a similar impact on brain connectivity and functioning, thus accounting for the good degree of concordance of the present findings.

Thus, given that the transneuronal spread mechanisms (Zhou et al., 2012; Fornito et al., 2015) implies a form of propagation along structural (axonal) pathways, that the nodal stress mechanism implies a form of common activity between altered brain areas, and that the shared vulnerability mechanism implies common gene expressions between cerebral regions, it is possible to advance the hypothesis that, based on our analysis, the decrease-related and increase-related structural co-alterations might be more shaped, in order, by nodal stress, transneuronal spread, and shared vulnerability mechanisms. Especially taking into consideration the transdiagnostic nature of our data, this finding suggests that the prevalence of a particular type of connectivity in the production and development of structural co-alterations leaves open the possibility that the other two types of connectivity could play a significant role as well. Indeed, this phenomenon may also be due to the fact that the data retrieved from BrainMap are about a great variety of brain disorders, which are likely to be originated by different combinations of the hypothesized factors underlying the formation of structural co-alterations.

Brain connectivity can predict the distribution of alterations

Taken together in a conjoint model, the three connectivity matrices are able to account for the development of structural co-alterations with good accuracy. This is a remarkable finding for the comprehension of how the pathological brain responds to diseases, as it allows one to predict the evolution of grey matter alterations from changes of the neurobiological substrate. Our result provides further support for the important role played by brain connectivity in the neuropathological processes and sheds new light on its involvement in their development and progression (Iturria-Medina and Evans, 2015). With the help of analyses based on brain connectivity profiles, we could achieve an in-depth understanding of the mechanisms at the root of brain disorders. Some suggestions along this line of research have already been proposed. For instance, in patients with Alzheimer's disease, functional alterations and grey matter decreases within different brain areas reflect covariance patterns of

part of the default mode network, thus indicating that these atrophic regions are not independently affected; rather, the primary deterioration in one of these areas might lead to a secondary deterioration in other connected areas (Wang et al., 2013, 2015). The cognitive decline would progress via sequential increases in connectivity, bringing about a functional overload. For example, in the case of Alzheimer's disease increased connectivity in frontal areas (especially those associated with the salience network) seems to have a compensatory role, representing the other side of the coin. Interestingly, this pattern of complex functional alterations appears to largely mirror the one that can be highlighted in frontotemporal dementia, which involves primarily frontal regions and the salience network (Zhou et al., 2010).

Two important points need to be clarified. First, although brain connectivity profiles seem to guide the development of structural co-alterations, this does not imply that each brain disorder is expected to produce similar structural co-alterations, for as regards to each brain disorder, as well as to the particular patients involved, different network nodes can be altered. Moreover, given a final set of altered nodes, the foci from which alterations began to spread might have been different and, as a result, different temporal progressions might have occurred.

The second point is a methodological caveat and concerns the relationship between our co-alteration network analysis and the anatomical covariance (Mechelli et al., 2005). Anatomical covariations are defined as 'the covariance of morphological metrics derived from morphological MRI' (Evans, 2013). Apparently, then, the morphological co-alterations studied here may be thought of as a type of anatomical covariance. However, anatomical covariance is always derived from single-subject data, whereas our meta-analytic approach works on data originated from a statistical comparison between pathological and healthy subjects. Therefore, from the methodological point of view, the two approaches, albeit similar, are different and should not be confused (for a more detailed discussion about this similarity see Cauda et al., 2018).

Limitations and future directions

The pathological structural co-alterations have been studied with a method that uses meta-analytic data, which, compared to their original quality, are known to be affected, to some extent, by deterioration. This loss of quality increases the degree of spatial uncertainty and, therefore, can influence the detection of alterations by reducing the likelihood of statistical co-occurrences between the nodes. Therefore,

future investigations with native data, possibly obtained from the same group of individuals, are needed.

VBM studies are at the basis of the methodology proposed here. Although being a widely used and well-validated technique, there are a number of procedural aspects that could influence the results of every single VBM experiment (e.g. field strength of the scanner, software used for the analysis, smoothing amount). However, since different combinations of these parameters had been used in the experiments considered for our research, it is unlikely that some of them can affect the results in a systematic way. Moreover, it has been recently suggested that possible false positive findings in VBM tend to be distributed randomly across the brain rather than accumulate in specific sites (Scarpazza et al., 2015); this aspect should prevent the spurious inclusion of nodes of alteration in the detected co-alteration networks. However, it is not possible to completely rule out this kind of inclusion.

To address the issue of heterogeneity due to studies with low sample sizes we decided to establish a lower bound of eight subjects for sample size and, consequently, all the retrieved experiments with a sample size smaller than eight subjects were excluded. As already mentioned, the identification of this lower bound is in line with the work of Scarpazza et al. (2015), which found that the use of balanced small samples in the VBM studies does not influence the false positive rate, even when considering only eight subjects. Thus, this suggests that our results should not be biased by the presence in our database of heterogeneous sample sizes. Moreover, since our methodology reveals the co-occurrences between alterations across the studies, experiments on small samples reporting different results from the others tend to bring about a sort of 'random noise' that is likely to increase the false negatives rather than the false positives (Acar et al., 2017). This consideration should lead us to think that, even though we cannot completely rule out the bias potentially caused by the inclusion of studies with a limited sample size, it is much more likely that we missed to detect real co-alterations rather than we identified false ones. However, to address this issue properly, future investigations on these data are needed as soon as larger and more controlled samples are available in the literature.

The ALE approach is one of the most used methods in the field of coordinate-based meta-analysis. One of the main concerns with this methodology is the possibility of the results to be driven by one, or a few, experiments, thus reflecting a specific case among the ones pooled for the meta-analysis rather that an overall representative

effect. However, a minimum amount of 20 experiments is usually thought to be sufficient to resolve this issue (Eickhoff et al., 2016), so that analyses based on large databases, as the one used here, should not be so much biased as to produce invalid results.

The genetic matrix, too, is characterized by spatial uncertainty and other idiosyncrasies. First, the sample used for this analysis is made of six human brains only. So, the results obtained with this analysis can hardly be generalized to the whole population. Second, not all of the six brains were sampled completely. Third, the samples are not evenly spaced but have different stereotactic coordinates in each of the six brains. Although our methodology has tried to address these issues, especially the inhomogeneity of the samples, the results of the genetic analysis are to be interpreted cautiously and need to be supported by further evidence. However, to date the complex procedure and costs of the acquisition of gene expressions data do not allow better precision.

Spatial and temporal errors, related to specific aspects of the functional MRI and DTI procedures, may affect both functional and anatomical connectivity patterns. Still, it is worth noting that, with regard to correlation and prediction results, such errors are supposed to increase more the number of false negatives than the number of false positives, thus reducing the correlation values between matrices. Therefore, given the good statistical significance achieved by our model, we are inclined to think that the results are not caused by spatial or temporal errors but describe real phenomena. To support our findings further, the reliability values of the connectivity matrices are very good; this leads us to believe that the difficulties inherent in the neuroimaging procedures are not likely to undermine the conclusions reached in this study. However, we hope that future studies will be carried out with different statistical techniques and on wider and better samples so as to find out whether or not our results can be further supported.

Finally, this study focused on mixed data, coming transdiagnostically from a variety of brain disorders as well as from heterogeneous patients investigated in different time courses of their symptomatology. The aim was (i) to provide a proof of concept of our method; and (ii) to get the broadest retrievable sample to achieve a good statistical significance for the detection of structural co-alterations. We therefore obtained mean alteration patterns, which are not specifically related to one or another brain disorder, so as to study globally how neuronal alterations are distributed across the brain. Future investigations are needed to look into more

specific patterns of structural co-alterations with regard to specific diseases. In particular, it would be interesting to calculate the co-alteration patterns starting from native single subject data stored in publicly available MRI datasets (e.g. ADNI) and to compare the results of this analysis with longitudinal data. It is also of primary importance to understand how each connectivity profile (functional, anatomical, and genetic) contributes in shaping the structural co-alterations of different brain disorders. An intriguing topic in this line of research could be the study of how structural co-alterations differ in patients' population with fast or slow cognitive deterioration. Furthermore, it would be of great interest to understand which gene co-expressions play a major role in the developments of structural co-alterations associated with different brain disorders.

Conclusion

This study has investigated fundamental issues about how the brain is affected by pathological processes that were still unresolved in humans. Our research investigated which one among three types of connectivity profiles (functional, anatomical, and genetic) could shape and explain better the distribution of structural co-alterations. Intriguingly, our prediction model suggests that in our transdiagnostic sample, all three types of connectivity are involved and can statistically account for a very good portion of the pattern variance of structural co-alterations for both grey matter increases and grey matter decreases (72% and 77%, respectively) (Table 1). In addition, it shows that the three patterns of brain connectivity need different timings to play their role in the development of the co-alteration networks.

These results shed new light on the possible mechanisms at the root of neuropathological processes. Our analysis points out that three (i.e. nodal stress, shared vulnerability, and transneuronal spread) of the four mechanisms put forward so far (Saxena and Caroni, 2011; Zhou et al., 2012; Fornito et al., 2015) are likely to play a role with different temporal progressions in the formation and development of structural co-alterations. In particular, we found that functional connectivity offers the better account of the structural co-alteration patterns, followed by anatomic and genetic connectivity. Although one type of connectivity can be prevalent in the co-alteration patterns, it must be noted that all these three types are significantly involved in the progression of brain alterations. This is consistent with the cross-diagnostic nature of data used in this study (Goodkind et al., 2015).

Overall, the three different types of brain connectivity can account extremely well for the distribution and evolution of structural co-alterations across the human brain. This finding presents an exciting prospect for future research in the quest for a better understanding of brain disorders.

Supplementary material

Overview of data analysis strategy and datasets

Figure S1 summarizes the analysis strategy and datasets used in our study. The studies included in the meta-analysis were collected from the BrainMap database (http://www.brainmap.org/). This is an open access database of published functional and structural neuroimaging experiments with coordinate-based results (x,y,z) in Talairach or MNI space. BrainMap uses a structured standardized coding scheme which describes published human neuroimaging experimental results. This taxonomy has been used to describe over 3600 publications and 15000 experiments, drawing upon over 110.000 subjects and reporting over 120.000 coordinates as results. This has been estimated to be 20-30% of the compliant literature in the field. The quality of the coding of each of these papers has been verified by a BrainMap taxonomy expert.

The papers have to respond to the following inclusion criteria:

1) For the decreases: Experiments Context is Disease AND Experiment Contrast is Gray Matter AND Experiments Observed Changes is Controls>Patients;

2) For the increases: Experiments Context is Disease AND Experiment Contrast is Gray Matter AND Experiments Observed Changes is Patients>Controls.

All the retrieved experiments with a sample size smaller than 8 subjects were excluded. The same was done for experiments not clearly comparing pathological population with healthy controls, as well as considering subjects “at risk”. The remaining items were then coded according to the ICD-10 system. As a further criterion, all the experiments not coded with F (i.e. Mental, Behavioral and Neurodevelopmental disorders) or G (i.e. Diseases of the nervous system) labels were excluded. From the remaining records, we also expunged those experiments related to codes that could not be considered as primary brain disorders (i.e. F10: Alcohol related disorders; F15: Other stimulant related disorders; F28: Other psychotic disorder not due to a substance or known physiological condition; F91: Conduct disorders; G11: Hereditary ataxia; G43: Migraine; G44: Other headache

syndromes; G47: Sleep disorders; G50: Disorders of trigeminal nerve; G71: Primary disorders of muscles).

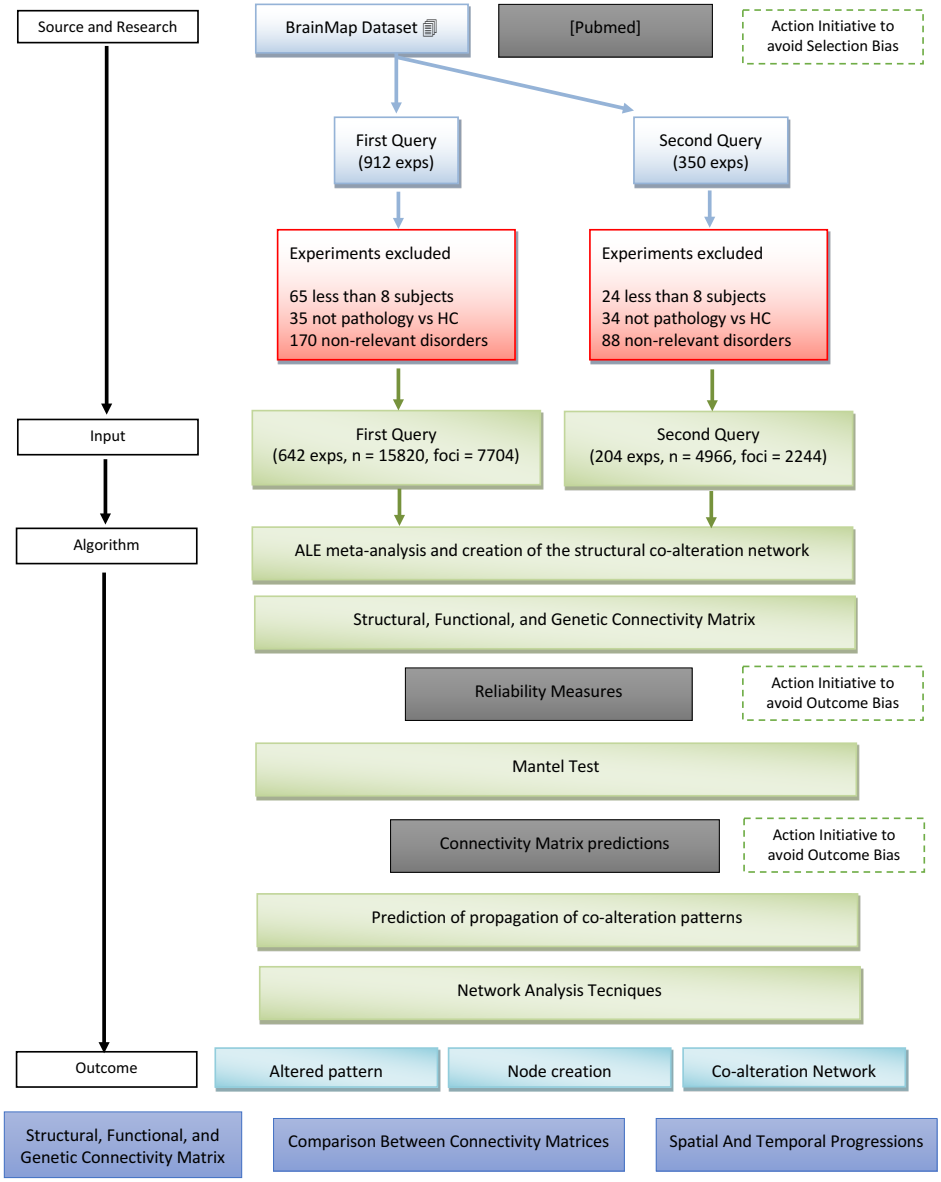

Figure S1: Flow chart of key steps used to generate the dataset of information, analyzed data and obtain several levels of results.

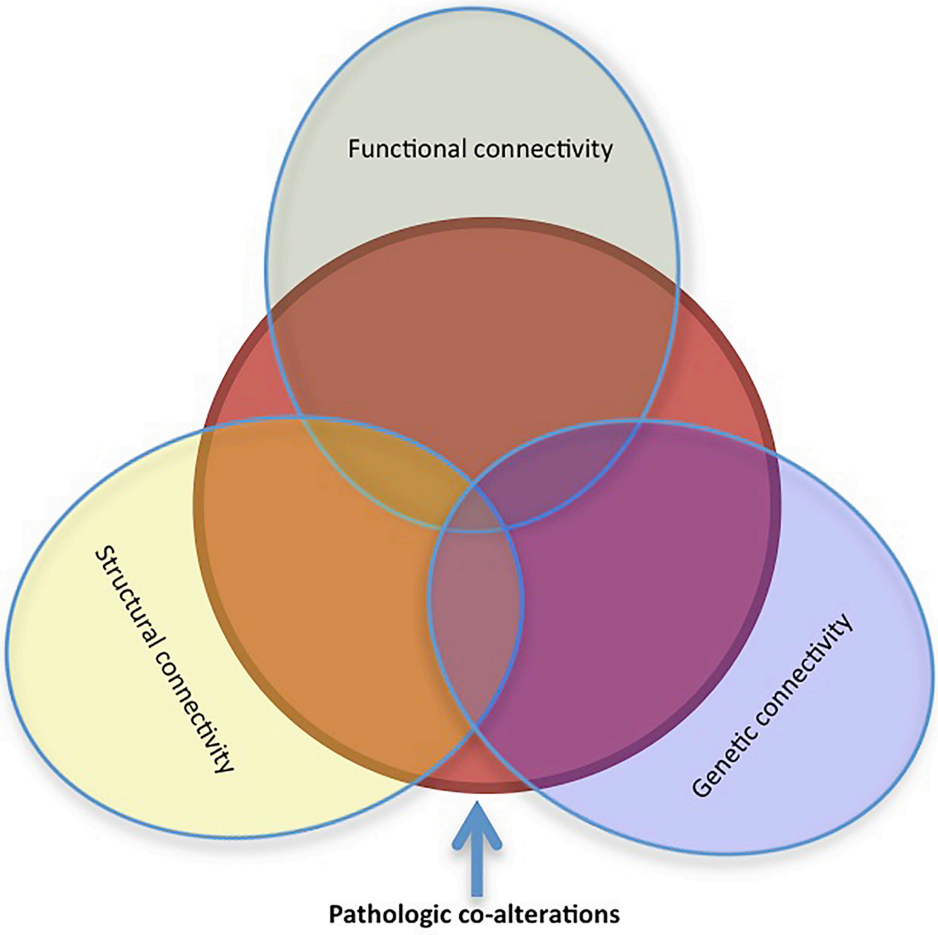

Figure S2: This figure depicts the relationship between the three types of connectivity taken into consideration in this meta-analysis (functional, anatomical, and genetic) and the development of structural co-alterations.

	ICD-10 code	Exp (n)	Exp (%)	Subj (n)
First query	**F20: Schizophrenia**	115	17.9	3807
	F28: Other psychotic disorder not due to a substance or known physiological condition	3	0.5	68
	F31: Bipolar Disorder	45	7.0	1191
	F32-F33: Major depressive disorder, single episode/recurrent	63	9.8	1919
	F41: Other Anxiety Disorders	13	2.0	306
	F42: Obsessive Compulsive Disorder	12	1.9	377
	F43: Reaction to Severe Stress and Adjustment Disorders	24	3.7	367
	F50: Eating Disorders	12	1.9	148
	F60: Specific Personality Disorders	10	1.6	222
	F65: Paraphilias	1	0.2	18
	F80: Specific Developmental Disorders of Speech and Language	2	0.3	22
	F84: Pervasive Developmental Disorders	29	4.5	696
	F90: Attention Deficit/Hyperactivity Disorder	9	1.4	139
	F95: Tic Disorder	2	0.3	33
	G10: Huntington's Disease	12	1.9	258
	G12: Spinal Muscular Atrophy and Related Syndromes	14	2.2	211
	G20: Parkinson's Disease	28	4.4	501
	G23: Other degenerative diseases of basal ganglia	13	2.0	212
	G24: Dystonia	6	0.9	89
	G25: Other extrapyramidal and movement disorders	7	1.1	135
	G30: Alzheimer's Disease	53	8.3	1194
	G31: Other Degenerative Diseases of Nervous System	52	8.1	838
	G35: Multiple Sclerosis	45	7.0	1422
	G40: Epilepsy and Recurrent Seizures	56	8.7	1426
	G90: Disorders Autonomic Nervous System	13	2.0	181
	G93: Other disorders of brain	3	0.5	40
	Total	**642**	**100%**	**15820**

Second query	**F20: Schizophrenia**	33	16.2	1175
	F28: Other psychotic disorder not due to a substance or known physiological condition	3	1.5	75
	F31: Bipolar Disorder	20	9.8	545
	F32-F33: Major depressive disorder, single episode/recurrent	19	9.3	453
	F41: Other Anxiety Disorders	4	2.0	51
	F42: Obsessive Compulsive Disorder	10	4.9	287
	F43: Reaction to Severe Stress and Adjustment Disorders	2	1.0	48
	F50: Eating Disorders	4	2.0	54
	F80: Specific Developmental Disorders of Speech and Language	3	1.5	48
	F84: Pervasive Developmental Disorders	23	11.3	515
	F90: Attention Deficit/Hyperactivity Disorder	2	1.0	27
	F95: Tic Disorder	2	1.0	45
	G10: Huntington's Disease	1	0.5	21
	G12: Spinal Muscular Atrophy and Related Syndromes	1	0.5	22
	G20: Parkinson's Disease	9	4.4	139
	G24: Dystonia	8	3.9	133
	G25: Other extrapyramidal and movement disorders	7	3.4	125
	G30: Alzheimer's Disease	7	3.4	114
	G31: Other Degenerative Diseases of Nervous System	10	4.9	123
	G35: Multiple Sclerosis	10	4.9	253
	G40: Epilepsy and Recurrent Seizures	26	12.7	713
	Total	**204**	**100%**	**4966**

Table S1: Synopsis of the diagnostic spectra in the database used for the analyses. Exp (n) = number of experiments; Exp (%) = percentage of the total of the experiments; Subj (n) = number of subjects.

	Year	1st Author	Medline	ICD-10 Code
1	2010	Abe O	-	F32-F33: Major depressive disorder. single episode/recurrent
2	1999	Abell F	10501551	F84: Pervasive Developmental Disorders
3	2012	Adleman N E	3472043	F31: Bipolar Disorder
4	2005	Adler C M	15922309	F31: Bipolar Disorder
5	2007	Agosta F	17370339	G12: Spinal Muscular Atrophy and Related Syndromes
6	2010	Agosta F	20597976	G23: Other degenerative diseases of basal ganglia
7	2011	Agosta F	21177393	G30: Alzheimer's Disease
8	2011	Agosta F	21177393	G31: Other Degenerative Diseases of Nervous System
9	2012	Ahmed F	22948482	F43: Reaction to Severe Stress and Adjustment Disorders
10	2011	Ahrendts J	20879808	F90: Attention Deficit/Hyperactivity Disorder
11	2013	Alemany S	-	F32-F33: Major depressive disorder. single episode/recurrent
12	2009	Almeida J R C	19101126	F31: Bipolar Disorder
13	2016	Alonso_Lana S	4957815	F31: Bipolar Disorder
14	2013	Ambrosi E	-	F31: Bipolar Disorder
15	2002	Ananth H	12202269	F20: Schizophrenia
16	2005	Antonova E	16039619	F20: Schizophrenia
17	2009	Arnone D	-	F32-F33: Major depressive disorder. single episode/recurrent

18	2013	Arnone D	23128153	F32-F33: Major depressive disorder. single episode/recurrent
19	2009	Asami T	19560907	F41: Other Anxiety Disorders
20	2011	Ash S	21689852	G31: Other Degenerative Diseases of Nervous System
21	2004	Audoin B	15503338	G35: Multiple Sclerosis
22	2006	Audoin B	17093899	G35: Multiple Sclerosis
23	2010	Audoin B	20392976	G35: Multiple Sclerosis
24	2007	Audoin B	17463071	G35: Multiple Sclerosis
25	2008	Barbeau E	18191160	G31: Other Degenerative Diseases of Nervous System
26	2001	Baron J C	11467904	G30: Alzheimer's Disease
27	2007	Bassitt D P	16960651	F20: Schizophrenia
28	2006	Baxter L C	16914835	G30: Alzheimer's Disease
29	2005	Bell-McGinty S	16157746	G31: Other Degenerative Diseases of Nervous System
30	2011	Bergè	21054282	F20: Schizophrenia
31	2009	Bergouignan L	19071222	F32-F33: Major depressive disorder. single episode/recurrent
32	2008	Berlingeri M	18413913	G30: Alzheimer's Disease
33	2004	Bernasconi N	15488421	G40: Epilepsy and Recurrent Seizures
34	2013	Bertsch K	23381548	F60: Specific Personality Disorders
35	2008	Beste C	17497629	G10: Huntington's Disease
36	2007	Beyer M K	17028119	G20: Parkinson's Disease
37	2011	Biundo R	21862438	G20: Parkinson's Disease

38	2005	Boccardi M	15585344	G31: Other Degenerative Diseases of Nervous System
39	2009	Bodini B	19172648	G35: Multiple Sclerosis
40	2011	Boghi A	21546219	F50: Eating Disorders
41	2011	Bonavita S	21239414	G35: Multiple Sclerosis
42	2008	Bonilha L	18164594	F20: Schizophrenia
43	2004	Bonilha L	15364683	G40: Epilepsy and Recurrent Seizures
44	2010	Borgwardt S J	20006324	F20: Schizophrenia
45	2008	Borroni B	18541800	G31: Other Degenerative Diseases of Nervous System
46	2009	Bose S K	19450953	F20: Schizophrenia
47	2008	Bouilleret V	18195263	G40: Epilepsy and Recurrent Seizures
48	2006	Boxer A L	16401739	G23: Other degenerative diseases of basal ganglia
49	2003	Boxer A L	12873851	G30: Alzheimer's Disease
50	2003	Boxer A L	12873851	G31: Other Degenerative Diseases of Nervous System
51	2006	Boxer A L	16401739	G31: Other Degenerative Diseases of Nervous System
52	2006	Bozzali M	16894107	G30: Alzheimer's Disease
53	2006	Bozzali M	16894107	G31: Other Degenerative Diseases of Nervous System
54	2009	Brambati S M	17604879	G31: Other Degenerative Diseases of Nervous System
55	2009	Brazdil M	18609565	G40: Epilepsy and Recurrent Seizures
56	2004	Brenneis C	14742598	G23: Other degenerative diseases of basal ganglia

57	2004	Brenneis C	15257132	G30: Alzheimer's Disease
58	2004	Brenneis C	15257132	G31: Other Degenerative Diseases of Nervous System
59	2003	Brenneis C	14534916	G90: Disorders Autonomic Nervous System
60	2006	Brenneis C	16161039	G90: Disorders Autonomic Nervous System
61	2007	Brieber S	-	F84: Pervasive Developmental Disorders
62	2007	Brieber S	-	F90: Attention Deficit/Hyperactivity Disorder
63	2010	Brunner R	19660555	F60: Specific Personality Disorders
64	2004	Burton E J	14749292	G20: Parkinson's Disease
65	2002	Burton E J	12377138	G31: Other Degenerative Diseases of Nervous System
66	2015	Cai Y	25502401	F31: Bipolar Disorder
67	2015	Cai Y	25502401	F32-F33: Major depressive disorder. single episode/recurrent
68	2009	Camicioli R	18573676	G20: Parkinson's Disease
69	2010	Canu E	21074899	G30: Alzheimer's Disease
70	2005	Carmona S	16129560	F90: Attention Deficit/Hyperactivity Disorder
71	2007	Caroli A	17990057	G30: Alzheimer's Disease
72	2010	Cascella N	20452187	F20: Schizophrenia
73	2009	Castro-Fornieles J	18486147	F50: Eating Disorders
74	2011	Castro-Manglano P D	22017223	F20: Schizophrenia
75	2009	Ceccarelli A	19172642	G35: Multiple Sclerosis
76	2008	Ceccarelli A	18501636	G35: Multiple Sclerosis

77	2010	Celle S	19768657	G25: Other extrapyramidal and movement disorders
78	2013	Ceresa A	23271221	G35: Multiple Sclerosis
79	2006	Chan C H	16499767	G40: Epilepsy and Recurrent Seizures
80	2014	Chaney A	23900024	F32-F33: Major depressive disorder. single episode/recurrent
81	2009	Chang C C	19486137	G90: Disorders Autonomic Nervous System
82	2005	Chang J L	16009889	G12: Spinal Muscular Atrophy and Related Syndromes
83	2012	Chao L L	22453299	F43: Reaction to Severe Stress and Adjustment Disorders
84	2009	Chen S	19538748	F43: Reaction to Severe Stress and Adjustment Disorders
85	2006	Chen S	16371250	F43: Reaction to Severe Stress and Adjustment Disorders
86	2007	Chen X	17464719	F31: Bipolar Disorder
87	2012	Chen Y	23155380	F43: Reaction to Severe Stress and Adjustment Disorders
88	2015	Cheng B	26347628	F43: Reaction to Severe Stress and Adjustment Disorders
89	2010	Cheng Y	20594947	F32-F33: Major depressive disorder. single episode/recurrent
90	2011	Cheng Y	21541322	F84: Pervasive Developmental Disorders
91	2002	Chetelat G	12395096	G30: Alzheimer's Disease
92	2002	Chetelat G	12395096	G31: Other Degenerative Diseases of Nervous System
93	2011	Chow E W	21362743	F20: Schizophrenia

94	2007	Chua S E	17098398	F20: Schizophrenia
95	2012	Compta Y	22595621	G20: Parkinson's Disease
96	2008	Cooke M A	18539438	F20: Schizophrenia
97	2005	Corbo V	16038682	F43: Reaction to Severe Stress and Adjustment Disorders
98	2005	Cordato N J	15843423	G20: Parkinson's Disease
99	2005	Cordato N J	15843423	G23: Other degenerative diseases of basal ganglia
100	2005	Cormack F	16006149	G93: Other disorders of brain
101	2012	Cosottini M	22226599	G12: Spinal Muscular Atrophy and Related Syndromes
102	2007	Craig M C	17766762	F84: Pervasive Developmental Disorders
103	2003	Critchley H D	12725766	G90: Disorders Autonomic Nervous System
104	2011	Cui L	21138758	F20: Schizophrenia
105	2011	Cui L	21138758	F31: Bipolar Disorder
106	2009	de Araujo-Filho G M	19303459	G40: Epilepsy and Recurrent Seizures
107	2008	de Oliveira-Souza R	18289882	F60: Specific Personality Disorders
108	2007	Delmaire C	17646630	G24: Dystonia
109	2009	Deng M Y	19641900	F20: Schizophrenia
110	2007	Di Paola M	17404777	G30: Alzheimer's Disease
111	2005	Dickstein D P	15997014	F31: Bipolar Disorder
112	2004	Doris A	15033185	F31: Bipolar Disorder
113	2007	Douaud G	17698497	F20: Schizophrenia
114	2003	Draganski B	14610125	G24: Dystonia

115	2010	Ebdrup B H	20184807	F20: Schizophrenia
116	2011	Eckart C	21118656	F43: Reaction to Severe Stress and Adjustment Disorders
117	2012	Ecker C	22310506	F84: Pervasive Developmental Disorders
118	2010	Ecker C	19683584	F84: Pervasive Developmental Disorders
119	2008	Egger K	19013058	F32-F33: Major depressive disorder. single episode/recurrent
120	2001	Ellis C M	11706094	G12: Spinal Muscular Atrophy and Related Syndromes
121	2014	Eshaghi A	3898881	G35: Multiple Sclerosis
122	2005	Etgen T	15670702	G25: Other extrapyramidal and movement disorders
123	2009	Euler M	19775870	F20: Schizophrenia
124	2005	Farrow T F D	15993858	F31: Bipolar Disorder
125	2011	Focke N K	21246668	G20: Parkinson's Disease
126	2001	Foong J	11335691	F20: Schizophrenia
127	2012	Friedrich H C	21967727	F50: Eating Disorders
128	2002	Frisoni G B	12438466	G30: Alzheimer's Disease
129	2008	Frodl T	18838632	F32-F33: Major depressive disorder. single episode/recurrent
130	2013	Gao W	-	F31: Bipolar Disorder
131	2008	Garcia-Marti G	17716795	F20: Schizophrenia
132	2011	Gaudio S	21081268	F50: Eating Disorders
133	2007	Gavazzi C	17882035	G10: Huntington's Disease
134	2012	Ghosh B C	22637582	G23: Other degenerative diseases of basal ganglia

135	2008	Gilbert A R	18342953	F42: Obsessive Compulsive Disorder
136	2013	Giordano A	23477861	G23: Other degenerative diseases of basal ganglia
137	2005	Giuliani N R	15721994	F20: Schizophrenia
138	2014	Gobbi C	23812284	G35: Multiple Sclerosis
139	2010	Gold B T	20063353	G31: Other Degenerative Diseases of Nervous System
140	2011	Gong Q	21134472	F32-F33: Major depressive disorder. single episode/recurrent
141	2011	Granert O	21705464	G24: Dystonia
142	2012	Gregory S	22566562	F60: Specific Personality Disorders
143	2013	Grieve S M	24273717	F32-F33: Major depressive disorder. single episode/recurrent
144	2010	Gross RG	20299856	G31: Other Degenerative Diseases of Nervous System
145	2006	Grosskreutz J	16638121	G12: Spinal Muscular Atrophy and Related Syndromes
146	2009	Guedj E	19224210	G31: Other Degenerative Diseases of Nervous System
147	2014	Guo W	24863419	F32-F33: Major depressive disorder. single episode/recurrent
148	2010	Guo X	19879920	G30: Alzheimer's Disease
149	2004	Ha T H	15664796	F20: Schizophrenia
150	2010	Ha T H	19429131	F31: Bipolar Disorder
151	2007	Hakamata Y	17923164	F43: Reaction to Severe Stress and Adjustment Disorders
152	2008	Haldane M	18308812	F31: Bipolar Disorder
153	2008	Hall A M	18631978	G30: Alzheimer's Disease

154	2011	Haller S	21284917	F31: Bipolar Disorder
155	2007	Hamalainen A	16997428	G30: Alzheimer's Disease
156	2007	Hamalainen A	16997428	G31: Other Degenerative Diseases of Nervous System
157	2009	Henley S M	19266143	G10: Huntington's Disease
158	2009	Herold R	19016669	F20: Schizophrenia
159	2012	Herringa R	23021615	F43: Reaction to Severe Stress and Adjustment Disorders
160	2008	Hirao K	18774263	F20: Schizophrenia
161	2006	Hirao K	16404228	G30: Alzheimer's Disease
162	2008	Honea R A	17689500	F20: Schizophrenia
163	2009	Honea R A	19812458	G30: Alzheimer's Disease
164	2009	Horn H	19182174	F20: Schizophrenia
165	2010	Horn H	20418073	F20: Schizophrenia
166	2009	Huey E D	19822784	G31: Other Degenerative Diseases of Nervous System
167	2001	Hulshoff Pol H E	11735840	F20: Schizophrenia
168	2004	Hulshoff Pol H E	14741639	F20: Schizophrenia
169	2006	Hulshoff Pol H E	16497519	F20: Schizophrenia
170	2010	Hwang J	-	F32-F33: Major depressive disorder. single episode/recurrent
171	2010	Hyde K L	19790171	F84: Pervasive Developmental Disorders
172	2011	Ille R	21406159	G10: Huntington's Disease
173	2011	Inkster B	20977527	F32-F33: Major depressive disorder. single episode/recurrent
174	2005	Ishii K	15800784	G30: Alzheimer's Disease

175	2008	Janssen J	18827723	F20: Schizophrenia
176	2008	Janssen J	18827723	F28: Other psychotic disorder not due to a substance or known physiological condition
177	2008	Janssen J	18827723	F31: Bipolar Disorder
178	2005	Jayakumar P N	15866362	F20: Schizophrenia
179	2010	Joos A	20400273	F50: Eating Disorders
180	2008	Kanda T	18661129	G30: Alzheimer's Disease
181	2008	Kanda T	18661129	G31: Other Degenerative Diseases of Nervous System
182	2008	Kasai K	17825801	F43: Reaction to Severe Stress and Adjustment Disorders
183	2010	Kasparek T	19777553	F20: Schizophrenia
184	2007	Kasparek T	17011096	F20: Schizophrenia
185	2009	Kasparek T	19647777	F20: Schizophrenia
186	2005	Kassubek J	15459079	G10: Huntington's Disease
187	2004	Kassubek J	14742591	G10: Huntington's Disease
188	2007	Kassubek J	17332050	G12: Spinal Muscular Atrophy and Related Syndromes
189	2012	Kato S	21850388	G20: Parkinson's Disease
190	2006	Kawachi T	16550383	G30: Alzheimer's Disease
191	2009	Kawada R	19625009	F20: Schizophrenia
192	2004	Kawasaki Y	15538599	F20: Schizophrenia
193	2007	Kawasaki Y	17045492	F20: Schizophrenia
194	2008	Ke X	18520994	F84: Pervasive Developmental Disorders
195	2007	Keller S S	17412561	G40: Epilepsy and Recurrent Seizures

196	2002	Keller S S	12438464	G40: Epilepsy and Recurrent Seizures
197	2007	Khaleeli Z	17566765	G35: Multiple Sclerosis
198	2013	Kim D	23769608	F31: Bipolar Disorder
199	2007	Kim E J	17615169	G31: Other Degenerative Diseases of Nervous System
200	2007	Kim J H	17689105	G40: Epilepsy and Recurrent Seizures
201	2008	Kim M J	18930633	F32-F33: Major depressive disorder. single episode/recurrent
202	2011	Kim S	21570296	G30: Alzheimer's Disease
203	2010	Kobel M	20702071	F90: Attention Deficit/Hyperactivity Disorder
204	2009	Koprivova J	19666084	F42: Obsessive Compulsive Disorder
205	2010	Kosaka H	20123027	F84: Pervasive Developmental Disorders
206	2009	Koskenkorva P	19704079	G40: Epilepsy and Recurrent Seizures
207	2008	Koutsouleris N	18054834	F20: Schizophrenia
208	2002	Kubicki M	12498745	F20: Schizophrenia
209	2002	Kubicki M	12498745	F28: Other psychotic disorder not due to a substance or known physiological condition
210	2011	Kurth F	21531390	F84: Pervasive Developmental Disorders
211	2004	Kwon H	15540637	F84: Pervasive Developmental Disorders
212	2010	Labate A	19780790	G40: Epilepsy and Recurrent Seizures
213	2008	Ladoucer C D	18356765	F31: Bipolar Disorder
214	2013	Lagarde J	24278277	G23: Other degenerative diseases of basal ganglia
215	2013	Lagarde J	24278277	G31: Other Degenerative Diseases of Nervous System

216	2015	Lai C H	-	F32-F33: Major depressive disorder. single episode/recurrent
217	2015	Lai C H	-	F41: Other Anxiety Disorders
218	2012	Lai C H	22386047	F41: Other Anxiety Disorders
219	2011	Lee H Y	21546094	F32-F33: Major depressive disorder. single episode/recurrent
220	2009	Leung K K	18945378	F32-F33: Major depressive disorder. single episode/recurrent
221	2010	Li C T	19931620	F32-F33: Major depressive disorder. single episode/recurrent
222	2006	Li L	16838824	F43: Reaction to Severe Stress and Adjustment Disorders
223	2011	Li M	21236649	F31: Bipolar Disorder
224	2009	Libon D J	19687454	G31: Other Degenerative Diseases of Nervous System
225	2013	Lin A	25206504	G35: Multiple Sclerosis
226	2013	Lin C H	23785322	G20: Parkinson's Disease
227	2013	Lin C H	23785322	G25: Other extrapyramidal and movement disorders
228	2009	Lin K	19570650	G40: Epilepsy and Recurrent Seizures
229	2014	Liu C H	24406440	F32-F33: Major depressive disorder. single episode/recurrent
230	2011	Liu M	22092238	G40: Epilepsy and Recurrent Seizures
231	2010	Lu C	19375076	F80: Specific Developmental Disorders of Speech and Language
232	2006	Ludolph A G	16648537	F95: Tic Disorder
233	2009	Lui S	18981063	F20: Schizophrenia
234	2004	Lyoo I K	15013835	F31: Bipolar Disorder

235	2012	Mainz V	22511729	F50: Eating Disorders
236	2009	Mak A K	19596037	F32-F33: Major depressive disorder. single episode/recurrent
237	2013	Mak E	24133286	G20: Parkinson's Disease
238	2003	Marcelis M	12694890	F28: Other psychotic disorder not due to a substance or known physiological condition
239	2007	Marti-Bonmati L	17641373	F20: Schizophrenia
240	2003	Massana G	12611840	F41: Other Anxiety Disorders
241	2002	Matsuda H	11884488	G30: Alzheimer's Disease
242	2010	Matsumoto R	20923432	F42: Obsessive Compulsive Disorder
243	2007	Matsunari I	18006622	G30: Alzheimer's Disease
244	2008	Mazere J	18191587	G30: Alzheimer's Disease
245	2005	McAlonan G M	15548557	F84: Pervasive Developmental Disorders
246	2002	McAlonan G M	12077008	F84: Pervasive Developmental Disorders
247	2008	McAlonan G M	18673405	F84: Pervasive Developmental Disorders
248	2007	McAlonan G M	17291727	F90: Attention Deficit/Hyperactivity Disorder
249	2004	McIntosh A M	15476683	F20: Schizophrenia
250	2004	McIntosh A M	15476683	F31: Bipolar Disorder
251	2004	McMillan A B	15325363	G40: Epilepsy and Recurrent Seizures
252	2008	Meda S A	18378428	F20: Schizophrenia
253	2008	Meisenzahl E M	18703313	F20: Schizophrenia
254	2011	Mengotti P	21146593	F84: Pervasive Developmental Disorders
255	2011	Meppelink A M	20922809	G20: Parkinson's Disease

256	2008	Mesaros S	18272867	G35: Multiple Sclerosis
257	2007	Mezzapesa D M	17296989	G12: Spinal Muscular Atrophy and Related Syndromes
258	2011	Miettinen P S	21692882	G30: Alzheimer's Disease
259	2011	Miettinen P S	21692882	G31: Other Degenerative Diseases of Nervous System
260	2005	Milham M P	15860335	F41: Other Anxiety Disorders
261	2007	Minnerop M	17512219	G90: Disorders Autonomic Nervous System
262	2011	Molina V	21188405	F20: Schizophrenia
263	2010	Molina V	20153145	F20: Schizophrenia
264	2011	Molina V	21188405	F31: Bipolar Disorder
265	2005	Moorhead T W	16085427	F20: Schizophrenia
266	2006	Morgen K	16360321	G35: Multiple Sclerosis
267	2006	Mueller S G	16686655	G40: Epilepsy and Recurrent Seizures
268	2007	Muhlau M	17024326	G10: Huntington's Disease
269	2013	Muhlau M	23462349	G35: Multiple Sclerosis
270	2009	Muller-Vahl K R	19435502	F95: Tic Disorder
271	2013	Na K S	-	F41: Other Anxiety Disorders
272	2005	Nagano-Saito A	15668417	G20: Parkinson's Disease
273	2013	Nardo D	23113800	F43: Reaction to Severe Stress and Adjustment Disorders
274	2011	Narita K	21115089	F31: Bipolar Disorder
275	2006	Neckelmann G	-	F20: Schizophrenia
276	2003	Nestor P J	12902311	G31: Other Degenerative Diseases of Nervous System

277	2013	Niedtfeldl I	23776553	F60: Specific Personality Disorders
278	2010	Nishio Y	20298422	G20: Parkinson's Disease
279	2006	Nugent A C	16256376	F31: Bipolar Disorder
280	2007	O'Daly O	17720459	F20: Schizophrenia
281	2011	O'Muircheartaigh J	21205693	G40: Epilepsy and Recurrent Seizures
282	2007	Obermann M	17443700	G24: Dystonia
283	2006	Ohnishi T	16330500	F20: Schizophrenia
284	2001	Ohnishi T	11673161	G30: Alzheimer's Disease
285	2011	Ortiz-Gil J	21727234	F20: Schizophrenia
286	2001	Overmeyer S	11722157	F90: Attention Deficit/Hyperactivity Disorder
287	2006	Padovani A	16306152	G23: Other degenerative diseases of basal ganglia
288	2010	Pail M	19817822	G40: Epilepsy and Recurrent Seizures
289	2001	Paillere-Martinot M L	11378311	F20: Schizophrenia
290	2011	Pantano P	20947646	G24: Dystonia
291	2009	Pardini M	19139305	G31: Other Degenerative Diseases of Nervous System
292	2014	Parisi L	24952616	G35: Multiple Sclerosis
293	2005	Peinemann A	16185716	G10: Huntington's Disease
294	2008	Pell G S	18042496	G40: Epilepsy and Recurrent Seizures
295	2010	Peng J	20466498	F32-F33: Major depressive disorder. single episode/recurrent
296	2005	Pennanen C	15607988	G31: Other Degenerative Diseases of Nervous System
297	2009	Pereira J B	19349926	G20: Parkinson's Disease

298	2009	Pereira J M	19433738	G31: Other Degenerative Diseases of Nervous System
299	2010	Pomarol-Clotet E	20065955	F20: Schizophrenia
300	2010	Prakash R S	19560443	G35: Multiple Sclerosis
301	2016	Preziosa P	26833969	G35: Multiple Sclerosis
302	2010	Price G	19632338	F20: Schizophrenia
303	2004	Pujol J	15237084	F42: Obsessive Compulsive Disorder
304	2011	Qiu L	21991357	F20: Schizophrenia
305	2008	Quattrone A	18653686	G25: Other extrapyramidal and movement disorders
306	2007	Rabinovici G D	18166607	G30: Alzheimer's Disease
307	2007	Rabinovici G D	18166607	G31: Other Degenerative Diseases of Nervous System
308	2009	Rami L	19259976	G30: Alzheimer's Disease
309	2009	Rami L	19259976	G31: Other Degenerative Diseases of Nervous System
310	2007	Ramirez-Ruiz B	17594330	G20: Parkinson's Disease
311	2015	Ranjeva J P	15661713	G35: Multiple Sclerosis
312	2014	Redlich R	25188810	F31: Bipolar Disorder
313	2014	Redlich R	25188810	F32-F33: Major depressive disorder. single episode/recurrent
314	2005	Remy F	15734360	G30: Alzheimer's Disease
315	2012	Riccitelli G	22422807	G35: Multiple Sclerosis
316	2008	Riederer F	18678824	G40: Epilepsy and Recurrent Seizures
317	2009	Ries M L	19701486	F32-F33: Major depressive disorder. single episode/recurrent

318	2011	Riva D	21700792	F84: Pervasive Developmental Disorders
319	2014	Rocca M A	24927473	G35: Multiple Sclerosis
320	2012	Rocha-Rego V	22952599	F43: Reaction to Severe Stress and Adjustment Disorders
321	2012	Rossi R	23146251	F31: Bipolar Disorder
322	2012	Rossi R	23146251	F60: Specific Personality Disorders
323	2004	Rusch N	15260365	G40: Epilepsy and Recurrent Seizures
324	2003	Salgado-Pineda P	12814586	F20: Schizophrenia
325	2004	Salgado-Pineda P	15006650	F20: Schizophrenia
326	2011	Salgado-Pineda P	21095105	F20: Schizophrenia
327	2007	Salmond C H	17710821	F84: Pervasive Developmental Disorders
328	2011	Salvadore G	21073959	F32-F33: Major depressive disorder. single episode/recurrent
329	2016	Sanchis-Segura C	27436479	G35: Multiple Sclerosis
330	2010	Santana M	20223639	G40: Epilepsy and Recurrent Seizures
331	2015	Saricicek A	26233321	F31: Bipolar Disorder
332	2010	Sasayama D	20546170	F90: Attention Deficit/Hyperactivity Disorder
333	2006	Saykin A J	16966547	G31: Other Degenerative Diseases of Nervous System
334	2010	Scheuerecker J	20569645	F32-F33: Major depressive disorder. single episode/recurrent
335	2013	Schiffer B	23015687	F20: Schizophrenia
336	2007	Schiffer B	16876824	F65: Paraphilias
337	2009	Schmidt-Wilcke T	19442751	G31: Other Degenerative Diseases of Nervous System

338	2012	Schuster C	21205677	F20: Schizophrenia
339	2008	Seeley W W	18268196	G31: Other Degenerative Diseases of Nervous System
340	2011	Senda J	21271792	G12: Spinal Muscular Atrophy and Related Syndromes
341	2006	Sepulcre J	16908748	G35: Multiple Sclerosis
342	2013	Serra-Blasco M	23620451	F32-F33: Major depressive disorder. single episode/recurrent
343	2012	Shad M U	22537357	F32-F33: Major depressive disorder. single episode/recurrent
344	1998	Shah P J	9828995	F32-F33: Major depressive disorder. single episode/recurrent
345	2002	Shapleske J	12427683	F20: Schizophrenia
346	2006	Shiino A	16904912	G30: Alzheimer's Disease
347	2006	Shiino A	16904912	G31: Other Degenerative Diseases of Nervous System
348	2012	Shin S	22933812	G20: Parkinson's Disease
349	2001	Sigmundsson T	11156806	F20: Schizophrenia
350	2012	Singh M K	3433284	F31: Bipolar Disorder
351	2010	Smesny S	20478385	F20: Schizophrenia
352	2010	Sobanski T	20056020	F41: Other Anxiety Disorders
353	2011	Soriano-Mas C	20875637	F32-F33: Major depressive disorder. single episode/recurrent
354	2010	Spano B	20007429	G35: Multiple Sclerosis
355	2003	Specht K	14568814	G90: Disorders Autonomic Nervous System
356	2005	Specht K	15734363	G90: Disorders Autonomic Nervous System

357	2006	Spencer M D	16996749	F84: Pervasive Developmental Disorders
358	2009	Stanfield A C	19267696	F31: Bipolar Disorder
359	2014	Stratmann M	25051163	F32-F33: Major depressive disorder. single episode/recurrent
360	2010	Suchan B	19729041	F50: Eating Disorders
361	2010	Sui S G	-	F43: Reaction to Severe Stress and Adjustment Disorders
362	2005	Summerfield C	15710857	G20: Parkinson's Disease
363	2002	Suzuki M	11955962	F20: Schizophrenia
364	2008	Szeszko P R	18413702	F42: Obsessive Compulsive Disorder
365	2006	Tae W S	16969045	G40: Epilepsy and Recurrent Seizures
366	2010	Tae W S	20046492	G40: Epilepsy and Recurrent Seizures
367	2011	Takahashi R	22187545	G23: Other degenerative diseases of basal ganglia
368	2010	Takahashi R	20634303	G30: Alzheimer's Disease
369	2010	Takahashi R	20634303	G31: Other Degenerative Diseases of Nervous System
370	2005	Taki Y	16150493	F32-F33: Major depressive disorder. single episode/recurrent
371	2014	Tang L R	25218414	F31: Bipolar Disorder
372	2012	Tavanti M	21710131	F43: Reaction to Severe Stress and Adjustment Disorders
373	2012	Tavazzi E	25228014	G12: Spinal Muscular Atrophy and Related Syndromes
374	2012	Tessitore A	22538070	G20: Parkinson's Disease
375	2007	Theberge J	17906243	F20: Schizophrenia

376	2007	Thivard L	17635981	G12: Spinal Muscular Atrophy and Related Syndromes
377	2010	Thomaes K	20673548	F43: Reaction to Severe Stress and Adjustment Disorders
378	2011	Tian L	22174900	F20: Schizophrenia
379	2008	Tiihonen J	18662866	F60: Specific Personality Disorders
380	2009	Tir M	19194988	G20: Parkinson's Disease
381	2009	Tir M	19194988	G90: Disorders Autonomic Nervous System
382	2010	Toal F	19891805	F84: Pervasive Developmental Disorders
383	2010	Togao O	20833001	F42: Obsessive Compulsive Disorder
384	2009	Tomelleri L	19717283	F20: Schizophrenia
385	2010	Tost H	19419772	F31: Bipolar Disorder
386	2007	Tregallas J R	17890058	F20: Schizophrenia
387	2010	Tzarouchi L C	19187475	G90: Disorders Autonomic Nervous System
388	2008	Uchida R R	18417322	F41: Other Anxiety Disorders
389	2005	Valente A A Jr	15978549	F42: Obsessive Compulsive Disorder
390	2015	van de Pavert S H	25926483	G35: Multiple Sclerosis
391	2009	van den Heuvel O A	18952675	F42: Obsessive Compulsive Disorder
392	2013	van Eijndhoven P	23929204	F32-F33: Major depressive disorder. single episode/recurrent
393	2010	van Tol M J	20921116	F32-F33: Major depressive disorder. single episode/recurrent
394	2013	van Tol M J	24176247	F32-F33: Major depressive disorder. single episode/recurrent
395	2010	van Tol M J	20921116	F41: Other Anxiety Disorders

396	2008	Venkatasubramanian G	19019637	F20: Schizophrenia
397	2008	Voets N L	18793730	F20: Schizophrenia
398	2008	Wagner G	18592043	F32-F33: Major depressive disorder. single episode/recurrent
399	2011	Wagner G	20832482	F32-F33: Major depressive disorder. single episode/recurrent
400	2011	Wang F	21666263	F31: Bipolar Disorder
401	2007	Wang J	1735333	F90: Attention Deficit/Hyperactivity Disorder
402	2009	Waragai M	19552926	G30: Alzheimer's Disease
403	2002	Watkins K E	11872605	F80: Specific Developmental Disorders of Speech and Language
404	2012	Watson D R	22056751	F20: Schizophrenia
405	2012	Watson D R	22056751	F31: Bipolar Disorder
406	2016	Wei W	26962820	G40: Epilepsy and Recurrent Seizures
407	2006	Whitford T J	16677830	F20: Schizophrenia
408	2013	Whitwell J L	23078273	G23: Other degenerative diseases of basal ganglia
409	2007	Whitwell J L	16797786	G30: Alzheimer's Disease
410	2005	Whitwell J L	16157747	G31: Other Degenerative Diseases of Nervous System
411	2007	Whitwell J L	16797786	G31: Other Degenerative Diseases of Nervous System
412	2007	Whitwell J L	17240166	G31: Other Degenerative Diseases of Nervous System
413	2001	Wilke M	11304078	F20: Schizophrenia

414	2010	Wilson S M	20542982	G31: Other Degenerative Diseases of Nervous System
415	2000	Woermann F G	10644781	G40: Epilepsy and Recurrent Seizures
416	2008	Wolf R C	18434103	F20: Schizophrenia
417	2009	Wolf R C	18172852	G10: Huntington's Disease
418	2006	Xie S	16801648	G30: Alzheimer's Disease
419	2009	Xu L	18266214	F20: Schizophrenia
420	2007	Yamada M	17240165	F20: Schizophrenia
421	2010	Yasuda C L	20350980	G40: Epilepsy and Recurrent Seizures
422	2003	Yoneyama E	14531753	F60: Specific Personality Disorders
423	2005	Yoo H K	16262646	F41: Other Anxiety Disorders
424	2008	Yoo S Y	18303194	F42: Obsessive Compulsive Disorder
425	2008	Yoshihara Y	19102744	F20: Schizophrenia
426	2005	Zahn R	16253483	G30: Alzheimer's Disease
427	2008	Zamboni G	18765649	G31: Other Degenerative Diseases of Nervous System
428	2011	Zhang J	21498053	F43: Reaction to Severe Stress and Adjustment Disorders
429	2009	Zhang T	19211150	F32-F33: Major depressive disorder. single episode/recurrent
430	2012	Zhang X	22129771	F32-F33: Major depressive disorder. single episode/recurrent
431	2016	Zhang X	28035997	G35: Multiple Sclerosis
432	2010	Zou K	19897176	F32-F33: Major depressive disorder. single episode/recurrent

Table S2: Selected studies for the meta-analysis of the First Query.

	Year	1st Author	Medline	ICD-10 Code
1	1999	Abell F	10501551	F84: Pervasive Developmental Disorders
2	2005	Adler C M	15922309	F31: Bipolar Disorder
3	2007	Adler C M	17027928	F31: Bipolar Disorder
4	2011	Amico F	20964952	F32-F33: Major depressive disorder. single episode/recurrent
5	2004	Antonini G	15489397	G12: Spinal Muscular Atrophy and Related Syndromes
6	2005	Antonova E	16039619	F20: Schizophrenia
7	2009	Arnone D	-	F32-F33: Major depressive disorder. single episode/recurrent
8	2013	Arnone D	23128153	F32-F33: Major depressive disorder. single episode/recurrent
9	2009	Asami T	19560907	F41: Other Anxiety Disorders
10	2007	Bassitt D P	16960651	F20: Schizophrenia
11	2006	Baxter L C	16914835	G30: Alzheimer's Disease
12	2007	Beal D S	17632278	F80: Specific Developmental Disorders of Speech and Language
13	2006	Betting L E	16702001	G40: Epilepsy and Recurrent Seizures
14	2015	Biederman S V	25809140	F32-F33: Major depressive disorder. single episode/recurrent
15	2004	Bonilha L	15364683	G40: Epilepsy and Recurrent Seizures
16	2008	Bonilha L	18362056	F84: Pervasive Developmental Disorders

17	2007	Bonilha L	17012334	G40: Epilepsy and Recurrent Seizures
18	2007	Brieber S	-	F84: Pervasive Developmental Disorders
19	2007	Brieber S	-	F90: Attention Deficit/Hyperactivity Disorder
20	2011	Brown G G	21924872	F20: Schizophrenia
21	2011	Brown G G	21924872	F31: Bipolar Disorder
22	2009	Butler C R	19073652	G40: Epilepsy and Recurrent Seizures
23	2012	Calderoni S	21896334	F84: Pervasive Developmental Disorders
24	2006	Calhoun V D	16108017	F20: Schizophrenia
25	2009	Carrion V G	19349151	F43: Reaction to Severe Stress and Adjustment Disorders
26	2009	Castro-Fornieles J	18486147	F50: Eating Disorders
27	2010	Celle S	19768657	G25: Other extrapyramidal and movement disorders
28	2006	Chan C H	16499767	G40: Epilepsy and Recurrent Seizures
29	2014	Chaney A	23900024	F32-F33: Major depressive disorder. single episode/recurrent
30	2007	Chen X	17464719	F31: Bipolar Disorder
31	2012	Chen Z	22119745	F31: Bipolar Disorder
32	2011	Cheng Y	21541322	F84: Pervasive Developmental Disorders
33	2008	Christian C J	18938065	F42: Obsessive Compulsive Disorder
34	2011	Cui L	21138758	F20: Schizophrenia
35	2011	Cui L	21138758	F31: Bipolar Disorder

36	2009	de Araujo-Filho G M	19303459	G40: Epilepsy and Recurrent Seizures
37	2011	de Castro-Manglano P	21316203	F28: Other psychotic disorder not due to a substance or known physiological condition
38	2009	Deng M Y	19641900	F20: Schizophrenia
39	2012	Ecker C	22310506	F84: Pervasive Developmental Disorders
40	2010	Ecker C	19683584	F84: Pervasive Developmental Disorders
41	2007	Egger K	17588241	G24: Dystonia
42	2005	Etgen T	15670702	G25: Other extrapyramidal and movement disorders
43	2012	Frangou S	3277296	F31: Bipolar Disorder
44	2006	Garraux G	16437578	F95: Tic Disorder
45	2004	Garraux G	15122716	G24: Dystonia
46	2003	Gee J	14697007	G30: Alzheimer's Disease
47	2008	Gilbert A R	18342953	F42: Obsessive Compulsive Disorder
48	2005	Giuliani N R	15721994	F20: Schizophrenia
49	2011	Gong Q	21134472	F32-F33: Major depressive disorder. single episode/recurrent
50	2011	Granert O	21705464	G24: Dystonia
51	2013	Grieve S M	24273717	F32-F33: Major depressive disorder. single episode/recurrent
52	2004	Grossman M	14761903	G30: Alzheimer's Disease
53	2004	Grossman M	14761903	G31: Other Degenerative Diseases of Nervous System
54	2010	Ha T H	19429131	F31: Bipolar Disorder

55	2004	Ha T H	15664796	F20: Schizophrenia
56	2008	Haldane M	18308812	F31: Bipolar Disorder
57	2007	Hamalainen A	17683950	G31: Other Degenerative Diseases of Nervous System
58	2006	Hendry J	16214373	F84: Pervasive Developmental Disorders
59	2009	Henley S M	19266143	G10: Huntington's Disease
60	2008	Honea R A	17689500	F20: Schizophrenia
61	2007	Hornyak M	17512782	G25: Other extrapyramidal and movement disorders
62	2001	Hulshoff Pol H E	11735840	F20: Schizophrenia
63	2010	Hwang J	-	F32-F33: Major depressive disorder. single episode/recurrent
64	2010	Hyde K L	19790171	F84: Pervasive Developmental Disorders
65	2008	Hyde T M	18669483	F20: Schizophrenia
66	2010	Kasparek T	19777553	F20: Schizophrenia
67	2004	Kawasaki Y	15538599	F20: Schizophrenia
68	2008	Ke X	18520994	F84: Pervasive Developmental Disorders
69	2007	Keller S S	17412561	G40: Epilepsy and Recurrent Seizures
70	2002	Keller S S	12438464	G40: Epilepsy and Recurrent Seizures
71	2009	Kempton M J	19726644	F31: Bipolar Disorder
72	2007	Kim J H	17689105	G40: Epilepsy and Recurrent Seizures
73	2001	Kim J J	11581113	F42: Obsessive Compulsive Disorder
74	2010	Kostic V S	20686125	G20: Parkinson's Disease

75	2013	Kozicky J M	23919287	F31: Bipolar Disorder
76	2008	Ladoucer C D	18356765	F31: Bipolar Disorder
77	2013	Lee S H	23474765	G20: Parkinson's Disease
78	2009	Leung K K	18945378	F32-F33: Major depressive disorder. single episode/recurrent
79	2013	Lin C H	23785322	G20: Parkinson's Disease
80	2013	Lin C H	23785322	G25: Other extrapyramidal and movement disorders
81	2009	Lin K	19570650	G40: Epilepsy and Recurrent Seizures
82	2010	Lu C	19375076	F80: Specific Developmental Disorders of Speech and Language
83	2006	Ludolph A G	16648537	F95: Tic Disorder
84	2015	Mallik S	4390521	G35: Multiple Sclerosis
85	2003	Marcelis M	12694890	F28: Other psychotic disorder not due to a substance or known physiological condition
86	2005	McDonald C	15863740	F20: Schizophrenia
87	2011	Mengotti P	21146593	F84: Pervasive Developmental Disorders
88	2011	Molina V	21188405	F20: Schizophrenia
89	2010	Moriya J	19854618	F20: Schizophrenia
90	2007	O'Daly O	17720459	F20: Schizophrenia
91	2007	Obermann M	17443700	G24: Dystonia
92	2011	Perico C A M	21320250	F31: Bipolar Disorder
93	2011	Perico C A M	21320250	F32-F33: Major depressive disorder. single episode/recurrent
94	2013	Prell T	24131497	G24: Dystonia

95	2010	Price G	19632338	F20: Schizophrenia
96	2004	Pujol J	15237084	F42: Obsessive Compulsive Disorder
97	2014	Qiu L	24713859	F32-F33: Major depressive disorder. single episode/recurrent
98	2009	Raji C A	19846828	G30: Alzheimer's Disease
99	2007	Ramirez-Ruiz B	17594330	G20: Parkinson's Disease
100	2008	Riederer F	18678824	G40: Epilepsy and Recurrent Seizures
101	2015	Rocca M A	26348234	G35: Multiple Sclerosis
102	2002	Rosen H J	11805245	G31: Other Degenerative Diseases of Nervous System
103	2004	Rusch N	15260365	G40: Epilepsy and Recurrent Seizures
104	2003	Salgado-Pineda P	12814586	F20: Schizophrenia
105	2007	Salmond C H	17710821	F84: Pervasive Developmental Disorders
106	2015	Saricicek A	26233321	F31: Bipolar Disorder
107	2010	Schafer A	20035881	F50: Eating Disorders
108	2010	Scheuerecker J	20569645	F32-F33: Major depressive disorder. single episode/recurrent
109	2013	Schiffer B	23015687	F20: Schizophrenia
110	2006	Schmitz N	16140278	F84: Pervasive Developmental Disorders
111	2002	Shapleske J	12427683	F20: Schizophrenia
112	2010	Smesny S	20478385	F20: Schizophrenia
113	2002	Suzuki M	11955962	F20: Schizophrenia
114	2008	Szeszko P R	18413702	F42: Obsessive Compulsive Disorder
115	2014	Tang L R	25218414	F31: Bipolar Disorder

116	2010	Tanskanen P	19015212	F20: Schizophrenia
117	2012	Tavazzi E	25228014	G35: Multiple Sclerosis
118	2007	Theberge J	17906243	F20: Schizophrenia
119	2010	Toal F	19891805	F84: Pervasive Developmental Disorders
120	2013	Truong W	24099630	F32-F33: Major depressive disorder. single episode/recurrent
121	2008	Uchida R R	18417322	F41: Other Anxiety Disorders
122	2005	Valente A A Jr	15978549	F42: Obsessive Compulsive Disorder
123	2013	van Eijndhoven P	23929204	F32-F33: Major depressive disorder. single episode/recurrent
124	2004	Waiter G D	15193590	F84: Pervasive Developmental Disorders
125	2007	Wang J	1735333	F90: Attention Deficit/Hyperactivity Disorder
126	2002	Watkins K E	11872605	F80: Specific Developmental Disorders of Speech and Language
127	2012	Watson D R	22056751	F20: Schizophrenia
128	2012	Watson D R	22056751	F31: Bipolar Disorder
129	2009	Wattendorf E	20007465	G20: Parkinson's Disease
130	2006	Whitford T J	16677830	F20: Schizophrenia
131	2004	Whitwell J L	16908994	G31: Other Degenerative Diseases of Nervous System
132	2001	Wilke M	11304078	F20: Schizophrenia
133	1999	Woermann F G	10545395	G40: Epilepsy and Recurrent Seizures
134	2010	Yasuda C L	20350980	G40: Epilepsy and Recurrent Seizures
135	2008	Yoo S Y	18303194	F42: Obsessive Compulsive Disorder

Table S3: Selected studies for the meta-analysis of the Second Query.

Cluster #	Voxels	x	y	z	Side	Label	BA
1	33473	-1	-19	5	R	Thalamus (Medial Dorsal Nucleus)	
		12	9	12	R	Caudate (Caudate Body)	
		-8	8	6	L	Caudate (Caudate Body)	
		-3	-19	8	L	Thalamus (Medial Dorsal Nucleus)	
		-27	-32	-7	L	Parahippocampal Gyrus. Hippocampus	
2	11924	22	-7	-16	R	Amygdala	
		30	-10	9	R	Putamen	
3	10606	37	17	-1	R	Insula	13
		50	8	6	R	Precentral Gyrus	44
4	10558	-35	20	2	L	Insula	13
		-54	5	-4	L	Superior Temporal Gyrus	22
5	3596	1	35	26	R	Anterior Cingulate	32
6	1606	2	53	-1	R	Medial Frontal Gyrus	10
7	1485	-44	8	32	L	Middle Frontal Gyrus	9
		-50	8	29	L	Inferior Frontal Gyrus	9
8	416	1	38	-16	R	Medial Frontal Gyrus	11
9	362	51	-22	14	R	Insula	
		55	-21	16	R	Postcentral Gyrus	40
10	320	-53	-20	14	L	Transverse Temporal Gyrus	41

Table S4: Clusters of GM Decrease

Cluster #	Voxels	x	y	z	Side	Label	BA
1	88629	-8	2	-1	L	Lentiform Nucleus	
		-4	-2	0	L	Thalamus	
		7	-7	-2	R	Hypothalamus	
		24	-10	-14	R	Amygdala	
		-36	-14	-7	L	Insula	
2	3688	-52	-25	26	L	Inferior Parietal Lobule	40
		49	-25	23	R	Insula	13
3	1834	18	50	23	R	Superior Frontal Gyrus	10
4	1538	-2	-49	53	L	Precuneus	7
5	1512	-35	-61	30	L	Middle Temporal Gyrus	39
6	1276	-53	-28	28	L	Inferior Parietal Lobule	40
7	864	-48	-25	41	L	Postcentral Gyrus	2
8	789	-14	38	-7	L	Medial Frontal Gyrus	10
9	629	34	-63	-13	R	Fusiform Gyrus	
10	615	-18	35	-19	L	Inferior Frontal Gyrus	11
11	489	-53	-17	44	L	Postcentral Gyrus	1
12	445	-48	-10	-27	L	Inferior Temporal Gyrus	20

Table S5: Clusters of GM Increase

Record number	*X*	*Y*	*Z*	*Side*	*Label*	*BA*
1	-4	-4	12	L	Thal	/
2	6	-16	14	R	VLN	/
3	-8	-12	20	L	Thal	/
4	14	-40	-6	R	Culm	/
5	-52	38	-2	L	IFG	BA 10
6	-24	-4	-34	L	Uncus	BA 36
7	-34	-10	-34	L	Uncus	BA 20
8	40	52	0	R	IFG	/
9	46	14	38	R	MFG	BA 9
10	54	-2	12	R	PrecG	BA 6
11	40	4	0	R	Ins	BA 13
12	-46	18	34	L	MFG	BA 9
13	-54	-4	-30	L	ITG	BA 20
14	-50	10	-28	L	MTG	BA 21
15	-60	-32	-2	L	MTG	BA 39
16	26	-82	-34	R	Pyr	/
17	-30	-34	-14	L	PHG	BA 36
18	50	-30	18	R	Ins	BA 13
19	-44	2	-22	L	MTG	BA 21
20	30	-42	-10	R	PHG	BA 37
21	-28	48	28	L	SFG	BA 9
22	-8	54	28	L	SFG	BA 9
23	54	-8	32	R	PrecG	BA 6
24	-40	46	-14	L	MFG	BA 11
25	42	-4	-4	R	Ins	BA 13
26	42	-30	50	R	PostcG	BA 40
27	-52	-8	34	L	PrecG	BA 6
28	46	4	34	R	PrecG	BA 6
29	-42	10	-4	L	Ins	BA 13
30	58	-14	42	R	PrecG	BA 6
31	8	2	6	R	Cau Body	/
32	-52	2	36	L	PrecG	BA 6

33	-38	18	6	L	Ins	BA 13
34	52	-48	24	R	SMG	BA 40
35	54	8	-20	R	MTG	BA 21
36	-58	-50	-10	L	MTG	BA 37
37	-10	8	10	L	Cau Body	/
38	38	16	6	R	Ins	BA 13
39	42	-6	6	R	Ins	BA 13
40	42	-14	12	R	Ins	BA 13
41	-48	-52	28	L	SMG	BA 40
42	50	-24	6	R	STG	BA 41
43	-48	-30	10	L	STG	BA 41
44	44	-12	0	R	Ins	BA 13
45	-42	-10	12	L	Ins	BA 13
46	-12	-58	8	L	PCC	BA 30
47	6	24	20	R	ACC	BA 24
48	0	-34	44	L	PCun	BA 7
49	10	10	12	R	Cau Body	/
50	-4	26	20	L	ACC	BA 24
51	-42	-4	4	L	Ins	BA 13
52	-56	-4	-20	L	MTG	BA 21
53	-38	6	6	L	Ins	BA 13
54	6	24	-24	R	RG	BA 11
55	40	12	-34	R	STG	BA 38
56	-40	16	-28	L	STG	BA 38
57	32	14	-24	R	STG	BA 38
58	-10	0	16	L	Cau Body	/
59	-2	14	26	L	Cing	BA 24
60	38	4	10	R	Ins	BA 13
61	-10	-22	36	L	Cing	BA 31
62	10	-22	40	R	Cing	BA 31
63	0	-18	34	L	Cing	BA 24
64	-8	-12	38	L	Cing	BA 24
65	50	12	6	R	PrecG	BA 44
66	-2	10	50	L	SFG	BA 6
67	16	6	64	R	SFG	BA 6
68	56	-16	12	R	TTG	BA 41

69	40	8	-22	R	STG	BA 38
70	0	40	38	L	MedFG	BA 8
71	-40	0	14	L	Ins	BA 13
72	-12	-28	44	L	Cing	BA 31
73	36	-24	-22	R	PHG	BA 36
74	-34	10	-22	L	STG	BA 38
75	40	16	-16	R	IFG	BA 47
76	-40	8	-14	L	STG	BA 38
77	-46	10	38	L	MFG	BA 8
78	38	22	12	R	Ins	BA 13
79	-38	12	14	L	Ins	BA 13
80	-6	28	-20	L	RG	BA 11
81	14	-72	32	R	Cun	BA 7
82	4	-70	32	R	Cun	BA 7
83	-2	-50	32	L	PCun	BA 31
84	38	-10	16	R	Ins	BA 13
85	-8	-2	36	L	Cing	BA 24
86	-48	-20	14	L	TTG	BA 41
87	-12	-74	38	L	PCun	BA 7
88	42	4	-12	R	STG	BA 38
89	-62	-32	12	L	STG	BA 22
90	46	12	-6	R	STG	BA 38
91	-10	-52	38	L	PCun	BA 7
92	-62	-22	-14	L	MTG	BA 21
93	24	-8	-14	R	PHG	/
94	-58	-54	14	L	STG	BA 22
95	-8	20	-4	L	Cau Head	/
96	-6	66	-4	L	MedFG	BA 10
97	-4	58	2	L	MedFG	BA 10
98	-48	-36	20	L	Ins	BA 13
99	10	-30	46	R	PCL	BA 31
100	-20	-64	14	L	PCC	BA 31
101	18	-60	16	R	PCC	BA 31
102	4	0	46	R	Cing	BA 24
103	-28	28	40	L	MFG	BA 8
104	0	0	-6	L	ACC	BA 25

105	34	-36	-18	R	FFG	BA 20
106	10	20	-6	R	Cau Head	/
107	52	-22	-14	R	MTG	BA 21
108	24	-72	24	R	PCun	BA 31
109	-26	18	46	L	MFG	BA 8
110	-46	-8	-16	L	ITG	BA 20
111	-26	6	-30	L	Uncus	BA 28
112	-52	-14	14	L	PostcG	/
113	-46	-76	10	L	MTG	BA 39
114	62	-6	16	R	PostcG	BA 43
115	-6	10	0	L	Cau Head	/
116	0	40	6	L	ACC	BA 32
117	44	-18	22	R	Ins	BA 13
118	-22	-4	-12	L	PHG	/
119	2	-48	42	R	Cing	BA 31
120	56	-4	-12	R	MTG	BA 21
121	0	-14	8	L	MDN	/
122	-52	0	-12	L	MTG	BA 21
123	-6	50	10	L	MedFG	BA 10
124	-42	0	-8	L	Ins	BA 13
125	-48	14	10	L	IFG	BA 44
126	-48	6	16	L	IFG	BA 44
127	-8	-20	14	L	Thal	/
128	14	-34	10	R	Pulv	/
129	12	-24	10	R	Pulv	/
130	58	-12	-10	R	MTG	BA 21
131	-54	-64	-4	L	MOG	BA 19
132	-30	-86	18	L	MOG	BA 19
133	-22	2	-20	L	Uncus	BA 34
134	38	-84	18	R	MOG	BA 19
135	-30	-42	-8	L	PHG	BA 37
136	0	26	-12	L	MedFG	BA 11
137	-48	-62	28	L	MTG	BA 39
138	-56	-18	42	L	PostcG	BA 4
139	-8	22	6	L	Cau Body	/
140	12	20	4	R	Cau Head	/

141	28	-16	-20	R	PhG	BA 28
142	52	-30	-6	R	MTG	BA 21
143	-60	-18	-6	L	MTG	BA 21
144	-60	-46	-4	L	MTG	BA 21
145	4	48	12	R	MedFG	BA 10
146	-8	60	14	L	MedFG	BA 10
147	0	36	-8	L	ACC	BA 32
148	-60	-10	24	L	PostcG	BA 3
149	-50	-10	44	L	PrecG	BA 4
150	-28	-12	-16	L	PHG	/
151	-62	-52	4	L	MTG	BA 21
152	-22	10	-8	L	LentN	/
153	44	44	-6	R	MFG	BA 10
154	2	32	12	R	ACC	BA 24
155	2	34	46	R	SFG	BA 8
156	-50	30	18	L	MFG	BA 46
157	34	-28	-12	R	Hip	/
158	-24	2	-2	L	Put	/
159	-28	-74	40	L	PCun	BA 19
160	-4	2	4	L	Cau Head	/
161	0	4	-16	L	SubcallG	BA 25
162	-34	-24	48	L	PrecG	BA 4
163	-34	-26	-8	L	Hip	/
164	-20	8	6	L	Put	/
165	-26	26	-20	L	IFG	BA 11
166	52	-34	6	R	MTG	BA 22
167	-30	50	-4	L	MFG	BA 10
168	-30	56	4	L	MFG	BA 10
169	60	-24	44	R	PostcG	BA 2
170	58	-20	-22	R	FFG	BA 20
171	2	16	-12	R	SubcallG	BA 25
172	4	-26	-6	R	RedN	/
173	-24	-20	-8	L	PHG	BA 28
174	32	-34	-4	R	Hip	/
175	4	-16	-6	R	RedN	/
176	-18	-34	-16	L	Culm	/

177	-46	-38	-24	L	Culm	/
178	-60	-38	6	L	MTG	BA 22
179	-40	28	-12	L	IFG	BA 47
180	50	-20	-4	R	STG	BA 22
181	42	-4	-18	R	Fus	BA 20
182	12	-32	0	R	PHG	BA 27
183	-14	-34	0	L	PHG	BA 27
184	48	32	24	R	MFG	BA 46
185	-28	-34	-2	L	Hip	/
186	-16	-42	-8	L	Culm	/
187	-26	-30	-24	L	Culm	/
188	50	6	22	R	IFG	BA 44
189	8	-40	-20	R	Culm	/
190	-58	-4	-4	L	MTG	BA 21
191	8	-6	14	R	Thal	/
192	-6	44	-4	L	ACC	BA 32
193	52	20	24	R	IFG	BA 9
194	-38	22	-20	L	IFG	BA 47
195	-62	-24	6	L	STG	BA 22
196	56	8	14	R	IFG	BA 44
197	-26	56	20	L	MFG	BA 10
198	38	42	22	R	MFG	BA 10
199	38	-6	-38	R	ITG	BA 20
200	28	-4	-32	R	Unc	BA 36
201	-42	54	2	L	IFG	BA 10
202	-2	42	16	L	MedFG	BA 9
203	-52	4	26	L	IFG	BA 9
204	-54	-60	-14	L	Fus	BA 37
205	-46	-20	8	L	STG	BA 13
206	50	20	12	R	IFG	BA 45
207	-48	24	10	L	IFG	BA 45
208	54	-10	6	R	STG	BA 22
209	4	-32	-14	R	Culm	/
210	-52	-20	-32	L	ITG	BA 20
211	6	52	-8	R	MedFG	BA 10
212	-2	34	26	L	Cing	BA 32

213	24	-14	-30	R	Unc	BA 28
214	6	20	30	R	Cing	BA 32
215	52	28	18	R	MFG	BA 46
216	-8	10	36	L	Cing	BA 32
217	58	6	28	R	IFG	BA 9
218	-2	-4	-14	L	HypoThal	/
219	34	28	-12	R	IFG	BA 47
220	42	-16	-32	R	ITG	BA 20
221	-46	46	-4	L	IFG	BA 10
222	-30	60	-6	L	SFG	BA 10
223	-54	-10	-28	L	ITG	BA 20
224	58	-10	-20	R	ITG	BA 20
225	58	-52	-14	R	ITG	BA 20
226	30	58	-4	R	SFG	BA 10
227	-56	-46	36	L	IPL	BA 40
228	4	24	42	R	Cing	BA 32
229	26	58	6	R	SFG	BA 10
230	-24	4	-12	L	SubcallG	BA 34
231	26	6	-30	R	Unc	BA 28
232	-24	-8	-28	L	Unc	BA 28
233	-50	24	26	L	MFG	BA 46
234	-2	52	20	L	MedFG	BA 9
235	26	-16	-8	R	LentN	/
236	28	50	14	R	SFG	BA 10
237	12	16	-22	R	RG	BA 11
238	-50	16	20	L	IFG	BA 9
239	-40	18	-10	L	IFG	BA 47
240	4	30	34	R	MedFG	BA 6
241	-26	46	18	L	SFG	BA 10
242	-48	36	-10	L	IFG	BA 47
243	-34	36	-8	L	MFG	BA 11
244	38	20	-6	R	IFG	BA 47
245	26	4	-20	R	Unc	BA 28
246	-56	-32	-12	L	ITG	BA 20
247	-36	24	-2	L	IFG	BA 47
248	16	30	-24	R	OrbG	BA 47

249	28	38	-20	R	MFG	BA 11
250	-10	-10	48	L	MedFG	BA 6
251	-2	38	-18	L	MedFG	BA 11
252	6	46	-16	R	MedFG	BA 11
253	26	2	-10	R	SubcallG	BA 34
254	22	-6	-24	R	PhG	BA 35
255	56	-20	24	R	IPL	BA 40
256	4	-14	52	R	MedFG	BA 6
257	-4	48	-14	L	MedFG	BA 11
258	48	38	2	R	IFG	BA 46
259	-50	24	0	L	IFG	BA 47
260	-28	-22	-18	L	PhG	BA 35
261	-42	6	48	L	MFG	BA 6
262	-54	-4	8	L	PrecG	BA 6
263	-32	34	-18	L	MFG	BA 11
264	38	24	0	R	IFG	BA 47
265	44	14	28	R	MFG	BA 9
266	-40	-54	44	L	IPL	BA 40
267	-50	36	10	L	IFG	BA 46
268	-58	-16	32	L	PostcG	BA 3
269	44	38	-14	R	MFG	BA 11
270	18	36	28	R	MedFG	BA 9
271	44	32	-6	R	MFG	BA 47
272	-18	-28	-8	L	PHG	BA 28
273	-28	-18	-28	L	PhG	BA 36
274	48	38	12	R	IFG	BA 46
275	-2	44	28	L	MedFG	BA 9
276	-46	42	18	L	MFG	BA 46
277	-44	10	28	L	IFG	BA 9

Table S6: Synopsis of decrement nodes

Record Number	*X*	*Y*	*Z*	*Side*	*Label*	*BA*
1	34	-44	-40	R	CerTons	/
2	-22	-70	-40	L	Inf_Semi-lunar_Lob	/
3	14	-68	-40	R	Inf_Semi-lunar_Lob	/
4	-52	-12	-38	L	ITG	BA 20
5	-34	-16	-38	L	Uncus	BA 20
6	46	-44	-34	R	CerTons	/
7	-42	0	-30	L	MTG	BA 21
8	-24	-2	-30	L	Uncus	BA 36
9	38	2	-30	R	MTG	BA 21
10	-48	-16	-28	L	ITG	BA 20
11	-30	-10	-30	L	Uncus	BA 28
12	28	-22	-26	R	PHG	BA 36
13	24	-8	-26	R	Uncus	BA 28
14	22	2	-26	R	Uncus	BA 28
15	2	-36	-24	R	Culm	/
16	-46	-34	-24	L	FFG	BA 20
17	-30	-30	-24	L	Culm	/
18	-52	-26	-24	L	FFG	BA 20
19	34	-14	-24	R	Uncus	BA 20
20	-24	-12	-22	L	PHG	/
21	-24	4	-22	L	Uncus	BA 28
22	34	-38	-22	R	Culm	/
23	-16	-24	-22	L	Culm	/
24	-30	-18	-20	L	PHG	/
25	38	-4	-22	R	MTG	BA 21
26	24	10	-20	R	IFG	BA 47
27	8	28	-20	R	RG	BA 11
28	8	38	-20	R	RG	BA 11
29	18	40	-20	R	MFG	BA 11
30	-8	20	-18	L	RG	BA 11
31	24	28	-18	R	IFG	BA 11
32	-20	42	-18	L	SFG	BA 11
33	36	-80	-16	R	Declive	/
34	34	-46	-16	R	Culm	/
35	6	-30	-16	R	Culm	/

36	32	-28	-18	R	PHG	BA 36
37	28	-14	-16	R	PHG	/
38	20	-6	-16	R	Amyg	/
39	-16	4	-16	L	PHG	BA 34
40	38	16	-16	R	IFG	BA 47
41	-22	28	-20	L	IFG	BA 11
42	34	32	-18	R	IFG	BA 47
43	36	-70	-14	R	FFG	BA 19
44	-36	-66	-16	L	Declive	/
45	-26	-38	-14	L	Culm	/
46	-34	-28	-14	L	PHG	BA 36
47	-64	-22	-14	L	MTG	BA 21
48	-52	-22	-14	L	MTG	BA 21
49	40	4	-14	R	STG	BA 38
50	10	20	-14	R	MedFG	BA 25
51	-36	-86	-12	L	IOG	BA 18
52	50	-56	-12	R	FFG	BA 37
53	-12	-18	-12	L	SN	/
54	-26	-12	-12	L	PHG	/
55	-48	-4	-14	L	MTG	BA 21
56	20	4	-12	R	SubcallG	BA 34
57	-18	12	-10	L	LentN	/
58	-42	12	-12	L	STG	BA 38
59	-6	30	-14	L	MedFG	BA 11
60	-12	40	-12	L	MedFG	BA 10
61	56	-48	-10	R	ITG	BA 20
62	28	-38	-10	R	PHG	BA 36
63	-6	-28	-6	L	Thal	/
64	-20	-26	-12	L	PHG	BA 35
65	50	-22	-10	R	STG	BA 22
66	-4	-8	-12	L	MammB	/
67	22	16	-12	R	SubcallG	BA 47
68	34	24	-10	R	IFG	BA 47
69	6	30	-10	R	ACC	BA 32
70	-28	34	-10	L	MFG	BA 11
71	26	-92	-10	R	FFG	BA 18

72	-14	-48	-10	L	Culm	/
73	-54	-44	-8	L	MTG	BA 20
74	-28	-46	-6	L	PHG	BA 19
75	26	-8	-8	R	Amyg	/
76	-42	2	-8	L	Ins	BA 13
77	-10	18	-8	L	Cau Head	/
78	-20	22	-6	L	LentN	/
79	-36	40	-8	L	MFG	BA 11
80	34	48	-10	R	MFG	BA 11
81	40	-78	-6	R	IOG	BA 19
82	40	-64	-6	R	FFG	BA 19
83	-44	-62	-10	L	FFG	BA 37
84	12	-38	-6	R	Culm	/
85	28	-26	-8	R	Hip	/
86	40	-12	-6	R	Ins	BA 13
87	-30	-4	-6	L	Put	/
88	-18	-4	-6	L	LGP	/
89	8	-2	-8	R	HypoThal	/
90	36	10	-6	R	Ins	BA 13
91	-36	20	-8	L	IFG	BA 47
92	-10	48	-4	L	MedFG	BA 10
93	30	62	-6	R	SFG	BA 10
94	38	-90	-4	R	IOG	BA 18
95	16	-48	-6	R	Culm	/
96	-26	-32	-6	L	PHG	Hip
97	10	8	-4	R	Cau Head	/
98	48	-56	0	R	ITG	BA 19
99	-14	-40	-4	L	PHG	BA 30
100	12	-24	-2	R	MGB	/
101	-28	-16	0	L	LentN	/
102	52	-14	-4	R	STG	BA 22
103	12	-12	-2	R	SN	/
104	48	-4	-4	R	STG	BA 22
105	-18	6	-2	L	LentN	/
106	22	6	-2	R	Put	/
107	-40	10	-2	L	Ins	BA 13

108	-8	24	0	L	Cau Head	/
109	10	36	0	R	ACC	/
110	-40	58	-4	L	MFG	BA 10
111	20	-92	-2	R	LG	BA 17
112	58	-36	-2	R	MTG	BA 21
113	-40	-24	-2	L	Ins	BA 13
114	40	-24	-2	R	Ins	BA 13
115	-8	-10	0	L	VLN	/
116	-40	-4	0	L	Ins	BA 13
117	-10	8	0	L	Cau Head	/
118	-10	40	4	L	ACC	BA 32
119	6	-56	2	R	Culm	/
120	-48	-36	2	L	STG	BA 22
121	-16	-32	2	L	Pulv	/
122	2	-14	0	R	Thal	/
123	28	-8	2	R	Put	/
124	40	-2	2	R	Ins	BA 13
125	42	18	2	R	Ins	/
126	-44	22	2	L	IFG	BA 47
127	10	46	0	R	ACC	BA 32
128	26	52	2	R	SFG	BA 10
129	14	-36	4	R	PHG	BA 30
130	-18	-18	4	L	VPLN	/
131	-28	-8	4	L	Put	/
132	-20	-2	4	L	Put	/
133	10	12	4	R	Cau Head	/
134	-46	32	4	L	IFG	BA 47
135	-32	56	2	L	MFG	BA 10
136	-8	-56	6	L	PCC	BA 30
137	-64	-30	4	L	MTG	BA 22
138	12	-18	6	R	Pulv	/
139	44	-16	4	R	Ins	BA 13
140	-42	4	6	L	PrecG	BA 44
141	44	8	4	R	Ins	BA 13
142	-24	12	6	L	Put	/
143	-6	18	8	L	Cau Body	/

144	24	0	12	R	LentN	/
145	28	46	10	R	MFG	BA 10
146	20	60	6	R	SFG	BA 10
147	24	-90	8	R	MOG	BA 18
148	10	6	8	R	Cau Body	/
149	32	30	8	R	IFG	BA 45
150	-36	40	10	L	MFG	BA 10
151	32	58	10	R	MFG	BA 10
152	-32	-92	12	L	MOG	BA 18
153	36	-78	12	R	MOG	BA 19
154	-10	-50	12	L	PCC	BA 30
155	-46	-40	12	L	STG	BA 41
156	-16	-30	12	L	Pulv	/
157	16	-22	14	R	LPN	/
158	30	-14	12	R	Put	/
159	6	-10	12	R	MDN	/
160	38	-8	10	R	Ins	BA 13
161	-22	4	12	L	Put	/
162	-48	10	12	L	PrecG	BA 44
163	52	12	10	R	IFG	BA 44
164	-4	28	10	L	ACC	BA 24
165	40	38	10	R	MFG	BA 10
166	-32	50	10	L	MFG	BA 10
167	-26	-10	14	L	Put	/
168	38	2	12	R	Ins	BA 13
169	46	20	12	R	IFG	BA 45
170	12	28	14	R	ACC	BA 24
171	-44	34	14	L	MFG	BA 46
172	20	54	14	R	SFG	BA 10
173	-36	-82	16	L	MOG	BA 19
174	-56	-30	16	L	STG	BA 42
175	-8	48	16	L	MedFG	BA 10
176	34	-86	18	R	MOG	BA 19
177	44	-34	18	R	Ins	BA 13
178	56	-26	18	R	PostcG	BA 40
179	12	-18	18	R	LDN	/

180	18	-6	18	R	Cau Body	/
181	20	64	16	R	SFG	BA 10
182	22	-90	20	R	Cun	BA 18
183	-10	-42	18	L	PCC	BA 29
184	-50	-22	20	L	Ins	BA 13
185	56	-6	18	R	PrecG	BA 4
186	-18	-8	20	L	Cau Body	/
187	-52	4	20	L	IFG	BA 44
188	-46	16	20	L	IFG	BA 9
189	-52	34	16	L	MFG	BA 46
190	-38	-72	18	L	MTG	BA 39
191	-8	24	20	L	ACC	BA 32
192	12	-48	24	R	PCC	BA 31
193	-48	-32	24	L	IPL	BA 40
194	48	-60	26	R	STG	BA 39
195	-12	-56	26	L	Pcun	BA 31
196	48	-40	26	R	IPL	BA 40
197	56	-20	24	R	IPL	BA 40
198	54	14	26	R	IFG	BA 9
199	-44	-78	26	L	SOG	BA 19
200	-38	-58	28	L	STG	BA 39
201	56	-30	28	R	IPL	BA 40
202	-4	-28	28	L	Cing	BA 23
203	-52	-16	28	L	PostcG	BA 4
204	-44	-2	26	L	IFG	BA 9
205	-46	12	28	L	IFG	BA 9
206	-2	14	26	L	ACC	BA 24
207	-48	24	26	L	MFG	BA 46
208	12	-90	28	R	Cun	BA 19
209	8	-56	28	R	PCC	BA 31
210	-60	-56	30	L	SMG	BA 40
211	-8	-38	28	L	PCC	BA 31
212	-56	2	32	L	PrecG	BA 6
213	-12	56	32	L	SFG	BA 9
214	40	-62	34	R	AngG	BA 39
215	-48	-26	32	L	PostcG	BA 2

216	32	-80	34	R	Pcun	BA 19
217	-10	-62	34	L	Pcun	BA 7
218	-36	-50	34	L	IPL	BA 40
219	8	-36	32	R	PCC	BA 31
220	52	-8	34	R	PrecG	BA 6
221	-52	-68	36	L	AngG	BA 39
222	-34	-66	36	L	PCun	BA 19
223	38	-42	36	R	SMG	BA 40
224	58	-26	34	R	IPL	BA 40
225	6	-12	36	R	ACC	BA 24
226	50	4	38	R	MFG	BA 6
227	-44	6	36	L	PrecG	BA 9
228	-46	16	34	L	MFG	BA 9
229	22	46	34	R	SFG	BA 9
230	48	-70	38	R	AG	BA 39
231	-34	-42	40	L	IPL	BA 40
232	-50	-18	38	L	PostcG	BA 3
233	-52	-8	38	L	PrecG	BA 6
234	-8	-54	40	L	Pcun	BA 7
235	-8	48	38	L	SFG	BA 8
236	-32	-58	42	L	IPL	BA 7
237	-48	-30	40	L	IPL	BA 40
238	58	-18	40	R	PrecG	BA 4
239	32	18	42	R	MFG	BA 8
240	12	-46	46	R	PCun	BA 7
241	-44	12	44	L	MFG	BA 8
242	-44	-44	44	L	IPL	BA 40
243	-22	20	46	L	MFG	BA 8
244	-2	-42	46	L	PCun	BA 7
245	44	-40	46	R	IPL	BA 40
246	-32	-36	48	L	PostcG	BA 3
247	-46	-26	50	L	PostcG	BA 2
248	48	-26	46	R	PostcG	BA 2
249	-38	-20	46	L	PostcG	BA 3
250	-52	-16	48	L	PostcG	BA 1
251	-52	-6	48	L	PrecG	BA 4

252	8	6	44	R	ACC	BA 24
253	32	24	50	R	SFG	BA 8
254	22	-26	48	R	PostcG	BA 3
255	16	-4	50	R	ACC	BA 24
256	30	10	50	R	MFG	BA 6
257	-34	-52	52	L	SPL	BA 40
258	20	12	50	R	SFG	BA 6
259	4	-50	52	R	PCun	BA 7
260	46	-18	52	R	PostcG	BA 3
261	0	-68	54	L	PCun	BA 7
262	-30	-30	56	L	PrecG	BA 4
263	-20	-50	56	L	PCun	BA 7
264	-12	-42	56	L	PCun	BA 7
265	2	-40	56	R	ParacLob	BA 5
266	12	-54	58	R	PCun	BA 7
267	10	-32	62	R	PostcG	BA 3
268	-6	-48	66	L	PostcG	BA 7
269	-18	-44	64	L	PostcG	BA 5
270	6	6	66	R	SFG	BA 6
271	16	-48	66	R	PostcG	BA 7

Table S7: Synopsis of increment nodes

References

Abdelnour F, Voss HU, Raj A. Network diffusion accurately models the relationship between structural and functional brain connectivity networks. Neuroimage 2014; 90: 335–47.

Acar F, Seurinck R, Eickhoff SB, Moerkerke B. Assessing robustness against potential publication bias in coordinate based fMRI meta-analyses using the Fail-Safe N bioRxiv 2017, 189001. doi: 10.1101/189001.

Aguzzi A, Heikenwalder M, Polymenidou M. Insights into prion strains and neurotoxicity. Nat Rev Mol Cell Biol 2007; 8: 552–61.

ALLEN Human Brain Atlas. Technical white paper: microarray data normalization, v.1. Seattle, WA: Allen Institute; 2013.

Allen MJ, Yen WM. Introduction to measurement theory Long Grove, IL: Waveland Press; 2001.

Baker JT, Holmes AJ, Masters GA, Yeo BT, Krienen F, Buckner RL,et al. . Disruption of cortical association networks in schizophrenia and psychotic bipolar disorder. JAMA Psychiatry 2014; 71: 109–18.

Beckmann CF, Mackay CE, Filippini N, Smith SM. Group comparison of resting-state FMRI data using multi-subject ICA and dual regression. Neuroimage 2009; S39–41.

Biswal BB. Resting state functional connectivity In: Biological psychiatry New York, NY: Elsevier Science Inc; 2011. p. 200S.

Biswal BB. Resting state fMRI: a personal history. Neuroimage 2012; 62: 938–44.

Bourdenx M, Koulakiotis NS, Sanoudou D, Bezard E, Dehay B, Tsarbopoulos A. Protein aggregation and neurodegeneration in prototypical neurodegenerative diseases: examples of amyloidopathies, tauopathies and synucleinopathies. Prog Neurobiol 2017; 155: 171–93.

Braak H, Braak E. Neuropathological stageing of Alzheimer-related changes. Acta Neuropathol 1991; 82: 239–59.

Braak H, Thal DR, Ghebremedhin E, Del Tredici K. Stages of the pathologic process in Alzheimer disease: age categories from 1 to 100 years. J Neuropathol Exp Neurol 2011; 70: 960–9.

Brooks B. The role of axonal transport in neurodegenerative disease spread: a meta-analysis of experimental and clinical poliomyelitis compares with amyotrophic lateral sclerosis. Can J Neurol Sci 1991; 18 (3 Suppl): 435–8.

Buckholtz JW, Meyer-Lindenberg A. Psychopathology and the human connectome: toward a transdiagnostic model of risk for mental illness. Neuron 2012; 74: 990–1004.

Buckner RL, Krienen FM, Yeo BT. Opportunities and limitations of intrinsic functional connectivity MRI. Nat Neurosci 2013; 16: 832–7.

Buckner RL, Snyder AZ, Shannon BJ, LaRossa G, Sachs R, Fotenos AF,et al. . Molecular, structural, and functional characterization of Alzheimer's disease: evidence for a relationship between default activity, amyloid, and memory. J Neurosci 2005; 25: 7709–17.

Carlson N, Buskist W, Heth CD, Schmaltz R. Psychology: the science of behaviour. 4th Canadian edn. Toronto: Pearson Education Canada; 2009.

Cauda F, Costa T, Fava L, Palermo S, Bianco F, Duca S,et al. . Predictability of autism, schizophrenic and obsessive spectra diagnosis. toward a damage network approach bioRxiv 2015, 014563. doi: 10.1101/014563.

Cauda F, Costa T, Nani A, Fava L, Palermo S, Bianco F,et al. . Are schizophrenia, autistic, and obsessive spectrum disorders dissociable on the basis of neuroimaging morphological findings?. A voxel-based meta-analysis. Autism Res 2017: 10: 1079–95.

Cauda F, Costa T, Palermo S, D'Agata F, Diano M, Bianco F,et al. . Concordance of white matter and gray matter abnormalities in autism spectrum disorders: a voxel-based meta-analysis study. Hum Brain Mapp 2014; 35: 2073–98.

Cauda F, Costa T, Torta DM, Sacco K, D'Agata F, Duca S,et al. . Meta-analytic clustering of the insular cortex: characterizing the meta-analytic connectivity of the insula when involved in active tasks. Neuroimage 2012a; 62: 343–55.

Cauda F, D'Agata F, Sacco K, Duca S, Geminiani G, Vercelli A. Functional connectivity of the insula in the resting brain. Neuroimage 2011; 55: 8–23.

Cauda F, Nani A, Costa T, Palermo S, Tatu K, Manuello J,et al. . The morphometric co-atrophy networking of schizophrenia, autistic and obsessive spectrum disorders. Hum Brain Mapp 2018; 39: 1898–928.

Cauda F, Torta DM, Sacco K, D'Agata F, Geda E, Duca S,et al. . Functional anatomy of cortical areas characterized by Von Economo neurons. Brain Struct Funct 2013; 218: 1–20.

Cauda F, Torta DM, Sacco K, Geda E, D'Agata F, Costa T,et al. . Shared "core" areas between the pain and other task-related networks. PLoS One 2012b; 7: e41929.

Chevalier-Larsen E, Holzbaur EL. Axonal transport and neurodegenerative disease. Biochim Biophys Acta 2006; 1762: 1094–108.

Chhatwal JP, Schultz AP, Johnson KA, Hedden T, Jaimes S, Benzinger TLS,et al. . Preferential degradation of cognitive networks differentiates Alzheimer's disease from ageing. Brain 2018; 141: 1486–500.

Cioli C, Abdi H, Beaton D, Burnod Y, Mesmoudi S. Differences in human cortical gene expression match the temporal properties of large-scale functional networks. PLoS One 2014; 9: e115913.

Clavaguera F, Grueninger F, Tolnay M. Intercellular transfer of tau aggregates and spreading of tau pathology: implications for therapeutic strategies. Neuropharmacology 2014; 76 (Pt A): 9–15.

Clavaguera F, Lavenir I, Falcon B, Frank S, Goedert M, Tolnay M. "Prion-like" templated misfolding in tauopathies. Brain Pathol 2013; 23: 342–9.

Cope TE, Rittman T, Borchert RJ, Jones PS, Vatansever D, Allinson K,et al. . Tau burden and the functional connectome in Alzheimer's disease and progressive supranuclear palsy. Brain 2018; 141: 550–67.

Crossley NA, Mechelli A, Scott J, Carletti F, Fox PT, McGuire P,et al. . The hubs of the human connectome are generally implicated in the anatomy of brain disorders. Brain 2014; 137 (Pt 8): 2382–95.

Crossley NA, Scott J, Ellison-Wright I, Mechelli A. Neuroimaging distinction between neurological and psychiatric disorders. Br J Psychiatry 2015; 207: 429–34.

Douaud G, Groves AR, Tamnes CK, Westlye LT, Duff EP, Engvig A,et al. . A common brain network links development, aging, and vulnerability to disease. Proc Natl Acad Sci USA 2014; 111: 17648–53.

Du Y, Fryer SL, Fu Z, Lin D, Sui J, Chen J,et al. . Dynamic functional connectivity impairments in early schizophrenia and clinical high-risk for psychosis. Neuroimage 2017; 180 (Pt B): 632–45.

Eickhoff SB, Bzdok D, Laird AR, Kurth F, Fox PT. Activation likelihood estimation meta-analysis revisited. Neuroimage 2012; 59: 2349–61.

Eickhoff SB, Laird AR, Fox PM, Lancaster JL, Fox PT. Implementation errors in the GingerALE software: description and recommendations. Hum Brain Mapp 2017; 38: 7–11.

Eickhoff SB, Laird AR, Grefkes C, Wang LE, Zilles K, Fox PT. Coordinate-based activation likelihood estimation meta-analysis of neuroimaging data: a random-effects approach based on empirical estimates of spatial uncertainty. Hum Brain Mapp 2009; 30: 2907–26.

Eickhoff SB, Nichols TE, Laird AR, Hoffstaedter F, Amunts K, Fox PT,et al. . Behavior, sensitivity, and power of activation likelihood estimation characterized by massive empirical simulation. Neuroimage 2016; 137: 70–85.

Ellison-Wright I, Bullmore E. Anatomy of bipolar disorder and schizophrenia: a meta-analysis. Schizophr Res 2010; 117: 1–12.

Etkin A, Wager TD. Functional neuroimaging of anxiety: a meta-analysis of emotional processing in PTSD, social anxiety disorder, and specific phobia. Am J Psychiatry 2007; 164: 1476–88.

Evans AC. Networks of anatomical covariance. Neuroimage 2013; 80: 489–504.

Filippini N, MacIntosh BJ, Hough MG, Goodwin GM, Frisoni GB, Smith SM,et al. . Distinct patterns of brain activity in young carriers of the APOE-epsilon4 allele. Proc Natl Acad Sci USA 2009; 106: 7209–14.

Fornito A, Zalesky A, Breakspear M. The connectomics of brain disorders. Nat Rev Neurosci 2015; 16: 159–72.

Fox PT, Laird AR, Fox SP, Fox PM, Uecker AM, Crank M,et al. . BrainMap taxonomy of experimental design: description and evaluation. Hum Brain Mapp 2005; 25: 185–98.

Fox PT, Lancaster JL. Opinion: mapping context and content: the brainmap model. Nat Rev Neurosci 2002; 3: 319–21.

French L, Pavlidis P. Relationships between gene expression and brain wiring in the adult rodent brain. PLoS Comput Biol 2011; 7: e1001049.

French L, Tan PP, Pavlidis P. Large-scale analysis of gene expression and connectivity in the rodent brain: insights through data integration. Front Neuroinform 2011; 5: 12.

Gejman PV, Sanders AR, Kendler KS. Genetics of schizophrenia: new findings and challenges. Annu Rev Genomics Hum Genet 2011; 12: 121–44.

Glasser MF, Sotiropoulos SN, Wilson JA, Coalson TS, Fischl B, Andersson JL,et al. . The minimal preprocessing pipelines for the Human Connectome Project. Neuroimage 2013; 80: 105–24.

Glerean E, Pan RK, Salmi J, Kujala R, Lahnakoski JM, Roine U,et al. . Reorganization of functionally connected brain subnetworks in high-functioning autism. Hum Brain Mapp 2016; 37: 1066–79.

Goedert M, Clavaguera F, Tolnay M. The propagation of prion-like protein inclusions in neurodegenerative diseases. Trends Neurosci 2010; 33: 317–25.

Goel P, Kuceyeski A, LoCastro E, Raj A. Spatial patterns of genome-wide expression profiles reflect anatomic and fiber connectivity architecture of healthy human brain. Hum Brain Mapp 2014; 35: 4204–18.

Gong X, Lu W, Kendrick KM, Pu W, Wang C, Jin L,et al. . A brain-wide association study of DISC1 genetic variants reveals a relationship with the structure and functional connectivity of the precuneus in schizophrenia. Hum Brain Mapp 2014; 35: 5414–30.

Goodkind M, Eickhoff SB, Oathes DJ, Jiang Y, Chang A, Jones-Hagata LB,et al. . Identification of a common neurobiological substrate for mental illness. JAMA Psychiatry 2015; 72: 305–15.

Guest WC, Silverman JM, Pokrishevsky E, O'Neill MA, Grad LI, Cashman NR. Generalization of the prion hypothesis to other neurodegenerative diseases: an imperfect fit. J Toxicol Environ Health A 2011; 74: 1433–59.

Gupta CN, Calhoun VD, Rachakonda S, Chen J, Patel V, Liu J,et al. . Patterns of gray matter abnormalities in schizophrenia based on an international mega-analysis. Schizophr Bull 2015; 41: 1133–42.

Hamilton JP, Etkin A, Furman DJ, Lemus MG, Johnson RF, Gotlib IH. Functional neuroimaging of major depressive disorder: a meta-analysis and new integration of base line activation and neural response data. Am J Psychiatry 2012; 169: 693–703.

Hardy J, Revesz T. The spread of Neurodegenerative disease. N Engl J Med 2012; 366: 2126–8.

Hawrylycz MJ, Lein ES, Guillozet-Bongaarts AL, Shen EH, Ng L, Miller JA,et al. . An anatomically comprehensive atlas of the adult human brain transcriptome. Nature 2012; 489: 391–9.

Honey CJ, Sporns O, Cammoun L, Gigandet X, Thiran JP, Meuli R,et al. . Predicting human resting-state functional connectivity from structural connectivity. Proc Natl Acad Sci USA 2009; 106: 2035–40.

Huang H, Ding M. Linking functional connectivity and structural connectivity quantitatively: a comparison of methods. Brain Connect 2016; 6: 99–108.

Iturria-Medina Y, Evans AC. On the central role of brain connectivity in neurodegenerative disease progression. Front Aging Neurosci 2015; 7: 90.

Iturria-Medina Y, Sotero RC, Toussaint PJ, Evans AC. Epidemic spreading model to characterize misfolded proteins propagation in aging and associated neurodegenerative disorders. PLoS Comput Biol 2014; 10: e1003956.

Jagust W. Vulnerable neural systems and the borderland of brain aging and neurodegeneration. Neuron 2013; 77: 219–34.

Jucker M, Walker LC. Pathogenic protein seeding in Alzheimer disease and other neurodegenerative disorders. Ann Neurol 2011; 70: 532–40.

Jucker M, Walker LC. Self-propagation of pathogenic protein aggregates in neurodegenerative diseases. Nature 2013; 501: 45–51.

Kasparek T, Marecek R, Schwarz D, Prikryl R, Vanicek J, Mikl M,et al. . Source-based morphometry of gray matter volume in men with first-episode schizophrenia. Hum Brain Mapp 2010; 31: 300–10.

Kondor RI, Lafferty J. Diffusion kernels on graphs and other discrete input spaces. In: Proceedings of the nineteenth international conference on machine learning (ICML). Morgan Kaufmann Publishers Inc.; 2002. p. 315–22.

Korth C. Aggregated proteins in schizophrenia and other chronic mental diseases: DISC1opathies. Prion 2012; 6: 134–41.

Kraus A, Groveman BR, Caughey B. Prions and the potential transmissibility of protein misfolding diseases. Annu Rev Microbiol 2013; 67: 543–64.

Lagarias JC, Reeds JA, Wright MH, Wright PE. Convergence properties of the nelder–mead simplex method in low dimensions. SIAM J. Optim 1998; 9: 112–47.

Lahiri DK, Maloney B. The “LEARn” (Latent Early-life Associated Regulation) model integrates environmental risk factors and the developmental basis of Alzheimer’s disease, and proposes remedial steps. Exp Gerontol 2010; 45: 291–6.

Laird AR, Fox PM, Price CJ, Glahn DC, Uecker AM, Lancaster JL,et al. . ALE meta-analysis: controlling the false discovery rate and performing statistical contrasts. Hum Brain Mapp 2005a; 25: 155–64.

Laird AR, Lancaster JL, Fox PT. BrainMap: the social evolution of a human brain mapping database. Neuroinformatics 2005b; 3: 65–78.

Lichtman JW, Sanes JR. Ome sweet ome: what can the genome tell us about the connectome?. Curr Opin Neurobiol 2008; 18: 346–53.

Lin CH, Chen CM, Lu MK, Tsai CH, Chiou JC, Liao JR,et al. . VBM reveals brain volume differences between Parkinson’s disease and essential tremor patients. Front Hum Neurosci 2013; 7: 247.

Mantel N. The detection of disease clustering and a generalized regression approach. Cancer Res 1967; 27: 209–20.

Manuello J, Nani A, Premi E, Borroni B, Costa T, Tatu K,et al. . The pathoconnectivity profile of alzheimer’s disease: a morphometric coalteration network analysis. Front Neurol 2018; 8: 739.

McTeague LM, Goodkind MS, Etkin A. Transdiagnostic impairment of cognitive control in mental illness. J Psychiatr Res 2016; 83: 37–46.

Mechelli A, Friston KJ, Frackowiak RS, Price CJ. Structural covariance in the human cortex. J Neurosci 2005; 25: 8303–10.

Menon V. Developmental pathways to functional brain networks: emerging principles. Trends Cogn Sci 2013; 17: 627–40.

Misic B, Betzel RF, de Reus MA, van den Heuvel MP, Berman MG, McIntosh AR,et al. . Network-level structure-function relationships in human neocortex. Cereb Cortex 2016; 26: 3285–96.

Northoff G, Duncan NW. How do abnormalities in the brain's spontaneous activity translate into symptoms in schizophrenia? From an overview of resting state activity findings to a proposed spatiotemporal psychopathology. Prog Neurobiol 2016; 145–6: 26–45.

Nunnally JC, Bernstein IH. Psychometric theory. 3rd edn. New York: McGraw-Hill; 1994.

Oxtoby NP, Garbarino S, Firth NC, Warren JD, Schott JM, Alexander DC. Data-driven sequence of changes to anatomical brain connectivity in sporadic Alzheimer's disease. Front Neurol 2017; 8: 580.

Pandya S, Mezias C, Raj A. Predictive model of spread of progressive supranuclear palsy using directional network diffusion. Front Neurol 2017; 8: 692.

Pearson RC, Esiri MM, Hiorns RW, Wilcock GK, Powell TP. Anatomical correlates of the distribution of the pathological changes in the neocortex in Alzheimer disease. Proc Natl Acad Sci USA 1985; 82: 4531–4.

Premi E, Cauda F, Costa T, Diano M, Gazzina S, Gualeni V,et al. . Looking for neuroimaging markers in frontotemporal lobar degeneration clinical trials: a multi-voxel pattern analysis study in granulin disease. J Alzheimers Dis 2016; 51: 249–62.

Premi E, Cauda F, Gasparotti R, Diano M, Archetti S, Padovani A,et al. . Multimodal FMRI resting-state functional connectivity in granulin mutations: the case of fronto-parietal dementia PLoS One 2014; 9: e106500.

Quiroz YT, Schultz AP, Chen K, Protas HD, Brickhouse M, Fleisher AS,et al. . Brain imaging and blood biomarker abnormalities in children with autosomal dominant Alzheimer disease: a cross-sectional study. JAMA Neurol 2015; 72: 912–19.

Raj A, Kuceyeski A, Weiner M. A network diffusion model of disease progression in dementia. Neuron 2012; 73: 1204–15.

Ravits J. Focality, stochasticity and neuroanatomic propagation in ALS pathogenesis. Exp Neurol 2014; 262 (Pt B): 121–6.

Richiardi J, Altmann A, Milazzo AC, Chang C, Chakravarty MM, Banaschewski T,et al. . Brain networks. correlated gene expression supports synchronous activity in brain networks. Science 2015; 348: 1241–4.

Robinson PA. Interrelating anatomical, effective, and functional brain connectivity using propagators and neural field theory. Phys Rev E Stat Nonlin Soft Matter Phys 2012; 85 (1 Pt 1): 011912.

Rohrer JD, Nicholas JM, Cash DM, van Swieten J, Dopper E, Jiskoot L,et al. . Presymptomatic cognitive and neuroanatomical changes in genetic frontotemporal dementia in the genetic frontotemporal dementia initiative (GENFI) study: a cross-sectional analysis. Lancet Neurol 2015; 14: 253–62.

Saper CB, Wainer BH, German DC. Axonal and transneuronal transport in the transmission of neurological disease: potential role in system degenerations, including Alzheimer's disease. Neuroscience 1987; 23: 389–98.

Saxena S, Caroni P. Selective neuronal vulnerability in neurodegenerative diseases: from stressor thresholds to degeneration. Neuron 2011; 71: 35–48.

Scarpazza C, Tognin S, Frisciata S, Sartori G, Mechelli A. False positive rates in voxel-based morphometry studies of the human brain: should we be worried?. Neurosci Biobehav Rev 2015; 52: 49–55.

Seeley WW, Carlin DA, Allman JM, Macedo MN, Bush C, Miller BL,et al. . Early frontotemporal dementia targets neurons unique to apes and humans. Ann Neurol 2006; 60: 660–7.

Seeley WW, Crawford RK, Zhou J, Miller BL, Greicius MD. Neurodegenerative diseases target large-scale human brain networks. Neuron 2009; 62: 42–52.

Seeley WW, Menon V, Schatzberg AF, Keller J, Glover GH, Kenna H,et al. . Dissociable intrinsic connectivity networks for salience processing and executive control. J Neurosci 2007; 27: 2349–56.

Skudlarski P, Jagannathan K, Calhoun VD, Hampson M, Skudlarska BA, Pearlson G. Measuring brain connectivity: diffusion tensor imaging validates resting state temporal correlations. Neuroimage 2008; 43: 554–61.

Smith SM, Nichols TE. Threshold-free cluster enhancement: addressing problems of smoothing, threshold dependence and localisation in cluster inference. Neuroimage 2009; 44: 83–98.

Soto C, Estrada LD. Protein misfolding and neurodegeneration. Arch Neurol 2008; 65: 184–9.

Sprooten E, Rasgon A, Goodman M, Carlin A, Leibu E, Lee WH,et al. . Addressing reverse inference in psychiatric neuroimaging: meta-analyses of task-related brain activation in common mental disorders. Hum Brain Mapp 2017; 38: 1846–64.

Stanley J. Educational measurement Washington, DC: American Council on Education; 1971.

Stuart JM, Segal E, Koller D, Kim SK. A gene-coexpression network for global discovery of conserved genetic modules. Science 2003; 302: 249–55.

Tatu K, Costa T, Nani A, Diano M, Quarta DG, Duca S,et al. . How do morphological alterations caused by chronic pain distribute across the brain? A meta-analytic co-alteration study. Neuroimage 2018; 18: 15–30.

Toro R, Fox PT, Paus T. Functional coactivation map of the human brain. Cereb Cortex 2008; 18: 2553–9.

Turkeltaub PE, Eickhoff SB, Laird AR, Fox M, Wiener M, Fox P. Minimizing within-experiment and within-group effects in activation likelihood estimation meta-analyses. Hum Brain Mapp 2012; 33: 1–13.

van den Heuvel MP, Mandl RC, Kahn RS, Hulshoff Pol HE. Functionally linked resting-state networks reflect the underlying structural connectivity architecture of the human brain. Hum Brain Mapp 2009; 30: 3127–41.

Van Essen DC, Smith SM, Barch DM, Behrens TE, Yacoub E, Ugurbil K. The wu-minn human connectome project: an overview. Neuroimage 2013; 80: 62–79.

Van Essen DC, Ugurbil K, Auerbach E, Barch D, Behrens TE, Bucholz R,et al. . The human connectome project: a data acquisition perspective. Neuroimage 2012; 62: 2222–31.

Vanasse TJ, Fox PM, Barron DS, Robertson M, Eickhoff SB, Lancaster JL,et al. . BrainMap VBM: an environment for structural meta-analysis. Hum Brain Mapp 2018; 39: 3308–25.

Voronoi G. Nouvelles applications des paramètres continus à la théorie des formes quadratiques. J Reine Angew Math 1907: 97–178.

Walker LC, Diamond MI, Duff KE, Hyman BT. Mechanisms of protein seeding in neurodegenerative diseases. JAMA Neurol 2013; 70: 304–10.

Wang WY, Yu JT, Liu Y, Yin RH, Wang HF, Wang J,et al. . Voxel-based meta-analysis of grey matter changes in Alzheimer's disease. Transl Neurodegener 2015; 4: 6.

Wang Y, Chen K, Yao L, Jin Z, Guo X. Structural interactions within the default mode network identified by bayesian network analysis in Alzheimer's disease. PLoS One 2013; 8: e74070.

Warren JD, Rohrer JD, Schott JM, Fox NC, Hardy J, Rossor MN. Molecular nexopathies: a new paradigm of neurodegenerative disease. Trends Neurosci 2013; 36: 561–9.

Weintraub S, Mesulam MM. From neuronal networks to dementia: four clinical profiles In: La Demence: Pourquoi? Paris: Foundation Nationale de Gerontologie; 1996.

Winkler AM, Ridgway GR, Webster MA, Smith SM, Nichols TE. Permutation inference for the general linear model. Neuroimage 2014; 92: 381–97.

Wolf L, Goldberg C, Manor N, Sharan R, Ruppin E. Gene expression in the rodent brain is associated with its regional connectivity. PLoS Comput Biol 2011; 7: e1002040.

Yates D. Neurodegenerative networking. Nat Rev Neurosci 2012; 13: 288.

Yeh FC, Badre D, Verstynen T. Connectometry: a statistical approach harnessing the analytical potential of the local connectome. Neuroimage 2016; 125: 162–71.

Yeh FC, Tseng WY. NTU-90: a high angular resolution brain atlas constructed by q-space diffeomorphic reconstruction. Neuroimage 2011; 58: 91–9.

Yeh FC, Verstynen TD, Wang Y, Fernandez-Miranda JC, Tseng WY. Deterministic diffusion fiber tracking improved by quantitative anisotropy. PLoS One 2013; 8: e80713.

Yeh FC, Wedeen VJ, Tseng WY. Generalized q-sampling imaging. IEEE Trans Med Imaging 2010; 29: 1626–35.

Yuan B, Fang Y, Han Z, Song L, He Y, Bi Y. Brain hubs in lesion models: predicting functional network topology with lesion patterns in patients. Sci Rep 2017; 7: 17908.

Zawia NH, Basha MR. Environmental risk factors and the developmental basis for Alzheimer's disease. Rev Neurosci 2005; 16: 325–37.

Zhang B, Horvath S. A general framework for weighted gene co-expression network analysis. Stat Appl Genet Mol Biol 2005; 4: Article 17.

Zhou J, Gennatas ED, Kramer JH, Miller BL, Seeley WW. Predicting regional neurodegeneration from the healthy brain functional connectome. Neuron 2012; 73: 1216–27.

Zhou J, Greicius MD, Gennatas ED, Growdon ME, Jang JY, Rabinovici GD,et al. . Divergent network connectivity changes in behavioural variant frontotemporal dementia and Alzheimer's disease. Brain 2010; 133 (Pt 5): 1352–67.

2.3 The Pathoconnectivity Network Analysis of the Insular Cortex:

A Morphometric Fingerprinting

This study was published in NeuroImage in 2020 (doi.org/10.1016/j.neuroimage.2020.117481).

Authors: Nani A., Manuello J., Mancuso L., Liloia D., Costa T., Vercelli A., Duca S., Cauda F.

Abstract

Brain disorders tend to impact on many different regions in a typical way: alterations do not spread randomly; rather, they seem to follow specific patterns of propagation that show a strong overlap between different pathologies. The insular cortex is one of the brain areas more involved in this phenomenon, as it seems to be altered by a wide range of brain diseases. On these grounds we thoroughly investigated the impact of brain disorders on the insular cortices analyzing the patterns of their structural co-alteration. We therefore investigated, applying a network analysis approach to meta-analytic data, 1) what pattern of grey matter alteration is associated with each of the insular cortex parcels; 2) whether or not this pattern correlates and overlaps with its functional meta-analytic connectivity; and, 3) the behavioral profile related to each insular co-alteration pattern. All the analyses were repeated considering two solutions: one with two clusters and another with three. Our study confirmed that the insular cortex is one of the most altered cerebral regions among the cortical areas, and exhibits a dense network of co-alteration including a prevalence of cortical rather than sub-cortical brain regions. Regions of the frontal lobe are the most involved, while occipital lobe is the less affected. Furthermore, the co-alteration and co-activation patterns greatly overlap each other. These findings provide significant evidence that alterations caused by brain disorders are likely to be distributed according to the logic of network architecture, in which brain hubs lie at the center of networks composed of co-altered areas. For the first time, we shed light on existing differences between insula sub-regions even in the pathoconnectivity domain.

Introduction

Connectomics is "a comprehensive structural description of the network of elements and connections forming the human brain" (Sporns et al., 2005). This approach has led to a picture of cerebral functioning in terms of networks and has emphasized the

great need for an overarching mapping of the whole structure of connections that shapes the human brain (the so-called connectome).

Recent studies provide evidence that brain disorders cause rarely alterations on a single cerebral site; rather, they tend to impact on many different regions. Moreover, converging findings suggest that pathological alterations of neuronal assemblies do not occur randomly but follow specific patterns of propagation based on anatomical and functional pathways (Cauda et al., 2017; Cauda et al., 2018b; Crossley et al., 2014; Fornito et al., 2015; Manuello et al., 2018b; McTeague et al., 2016; Menon, 2013).

A certain set of co-altered brain areas, which can subserve several cognitive processes, has been suggested to overlap in different diseases (Crossley et al., 2014). With regard to mental illness, for instance, it has been proposed that abnormalities in a certain set of brain areas might be frequently associated with a wide spectrum of psychiatric conditions (Crossley et al., 2016b; Goodkind et al., 2015). Another recent meta-analysis provides further evidence for overlapping patterns of brain alterations in certain neuropsychiatric disorders – i.e., autism spectrum disorder, schizophrenia, and obsessive spectrum disorder (Cauda et al., 2017; Cauda et al., 2012b).

These findings may be counterintuitive, as we are inclined to think that each brain disorder should exhibit a specific pattern of brain alterations, related to both its pathogenesis and development. Indeed, intriguing results from animal models indicate that degenerative pathologies principally impact on the network hubs that are more vulnerable to disruption by virtue of their extensive connections and activity (Crossley et al., 2014; Raj et al., 2012; Seeley et al., 2009). As a result, a small set of brain regions may be more likely to be frequently affected by a large number of brain disorders (Cauda et al., 2019; Ellison-Wright and Bullmore, 2010; Goodkind et al., 2015; Liloia et al., 2018; Menon, 2013; Saxena and Caroni, 2011).

The propagation of neuronal alterations within brain areas might form recognizable networks that depend on the structure of brain connectivity (Cauda et al., 2018b; Manuello et al., 2018b; Raj et al., 2012; Tatu et al., 2018; Yates, 2012; Zhou et al., 2012). This aspect is so important that it could generate a new perspective as to how clinicians are used to consider brain disorders (Buckholtz and Meyer-Lindenberg, 2012; Caspi et al., 2014; Cole et al., 2014). Finding out what kind of patterns are associated to the alteration of different brain sites is the first fundamental step in

order to reach a comprehensive understanding of how brain disorders impact on the connectome.

The co-alteration network analysis, which can be considered as a fascinating new subfield of pathoconnectomics, can be defined as the description of networks formed by co-altered brain areas. This type of analysis can describe the undirected (non-causal) propagation patterns of alterations produced by brain disorders. If certain brain areas – typically those playing a functional central role (brain hubs) – are thought to be frequently affected in brain deterioration (Cole et al., 2014; Crossley et al., 2016a; Crossley et al., 2014), then it can also be hypothesized that each hub may form typical connecting patterns with other altered cerebral areas.

In principle, the method we are proposing could be equally applied to the study of any brain region, whether a hub or not. However, several elements made us identify the insular cortex as a particularly suitable candidate. Among the brain hubs, the insula has vast and extensive connections to many regions of the cortex and limbic system (Cauda et al., 2011; Cauda et al., 2013; Cauda and Vercelli, 2013; Chang et al., 2013; Kelly et al., 2012; Stephani et al., 2011; Uddin, 2015; Vercelli et al., 2016). The insular cortex has been associated with a variety of important functions, ranging from pain perception and speech production to social emotions (Cauda et al., 2012b), including the conscious monitoring of the body's condition via the integration of different unconscious stimuli (both external and internal) with emotional processes, as well as the conscious detection of error (Cauda et al., 2012a; Cauda et al., 2011; Klein et al., 2013; Nieuwenhuys, 2012; Vercelli et al., 2016; Wylie and Tregellas, 2010). The integration of external sensory stimuli with inputs coming from the limbic system has led to suggest that the insula may play a fundamental role in the generation and maintenance of a state of awareness related to the body's condition (Cauda et al., 2011; Manuello et al., 2018a). These relevant roles put the insula at the interface between the inner and the external worlds, thus making it a pivotal center within the brain functional architecture (Ahmed et al., 2016; Douaud et al., 2014; Fjell et al., 2015; Jagust, 2013; Jones et al., 2016; Klein et al., 2013; Voytek and Knight, 2015).

It has been shown by several researches that the insula is among the most anatomically and functionally altered regions of the brain across psychiatric and neurological disorders (Crossley et al., 2014; Crossley et al., 2015; Goodkind et al., 2015; McTeague et al., 2016; McTeague et al., 2017; Namkung et al., 2017; Sprooten et al., 2017). Critically, previous work from our group has highlighted that

the insula is not only one of the areas that are more affected across the literature, but also one of those involved by the majority of brain disorders (Cauda et al., 2019; Liloia et al., 2018). This suggests that the insular cortex may have as yet an unknown role in the development of alterations caused by brain disorders. Moreover, this heterogeneity with respect of disease affection, made the insula the perfect focus for a transdiagnostic approach, allowing in principle to account for different pathological processes behind the development of the co-alteration network. As a further element, and coherently with all this, as pointed out by Behrens and colleagues in 2013, the insula is among the most often investigated brain regions. Based on this, and considering the equal suitability of any brain region to our approach, we therefore decided to direct our attention to a structure of potential interest for a wide part of neuroscience researchers. Finally, given the importance of the insula as a brain hub, we thought it to be ideal in order to also test the hypothesis that, when a crucial brain hub is affected by pathology, the associated co-alteration network may largely reflect its functional connectivity.

It is well known that the insular cortex exhibits a marked heterogeneity both in functional and cytoarchitectonical aspects (Cauda et al., 2012a; Cauda et al., 2011). For this reason, this brain area can be better described adopting some kind of parcellation. However, no consensus has been reached on the number of parcels to be used (Cauda and Vercelli, 2013), nor on the modalities better capturing differences between sub-regions. We decided to follow the solution proposed by Kelly et al. (2012), based on multi-modal convergence criterion and non-hierarchical clustering. Among the various dimensionality options (i.e., from 2 to 15 clusters), we selected those showing the best cross-model agreement for both the hemispheres (i.e., 2, 3 and 9 clusters), as highlighted by Cauda and Vercelli (2013). Since a number of clusters over 3 was not sufficient to guarantee reliable amount of data for statistical results (for an explanation of this aspect see (Cauda et al., 2018a), we focused on the bipartite (labeled as K2 throughout the text) and tripartite (labeled as K3 throughout the text) solutions (Fig. S2). The bipartite option follows the anterior-posterior distinction (Cauda et al., 2011; Cauda and Vercelli, 2013; Tian and Zalesky, 2018). Following the behavioral domain analysis described in the original work by Kelly et al. (2012), the anterior parcel is associated with language and memory functions, while the posterior one is associated with action execution, somesthesis and sexuality. The tripartite option consists, coherently between hemispheres, of an anterior dorsal parcel, a middle parcel covering both ventral and dorsal insula, and a dorsal posterior parcel. According to literature, the dorsal portion of the anterior insula is mainly involved in salience evaluation (Menon and

Uddin, 2010; Xue et al., 2018), while the dorsal posterior region is classically described as the seat of interoceptive representation (Craig, 2003). The ventral insula is described as associated with emotion and empathy processing, especially in its anterior part, while the central insula is mainly involved in interoception and somatosensation (Kurth et al., 2010). The related regions of interest (ROIs) where available on http://fcon_1000.projects.nitrc.org.

The aim of this study was to investigate: 1) what pattern of neuronal alterations' distribution is associated with different portions of the insula; 2) whether or not the insula meta-analytic co-activation patterns can provide meaningful elements to interpret the co-alteration patterns; and 3) the behavioral profile associated with the areas of the insular co-alteration patterns. To do so, we used the voxel-based morphometry (VBM) data of the BrainMap database.

Studies of brain morphometry with the help of the VBM technique have been performed by many researchers as structural magnetic resonance imaging-based measures of decreased values are considered as valid markers of atrophy which can describe disease state and development (Frisoni et al., 2010). Furthermore, the VBM approach is such that it is not biased to one specific brain structure but gives a comprehensive evaluation of anatomical differences throughout the brain (Ashburner and Friston, 2001). A number of studies show that gray matter abnormalities are associated with many psychiatric diseases. For instance, cortical thickness has been found to be variously reduced in patients with major depressive disorder and bipolar disorder (Niu et al., 2017), schizophrenia (Kuperberg et al., 2003; van Haren et al., 2011), borderline personality disorder (Soloff et al., 2008), autism spectrum disorder (Pereira et al., 2018), obsessive-compulsive spectrum disorder (van den Heuvel et al., 2008), and neurodegenerative diseases such as Alzheimer's (Manuello et al., 2018; Matsuda, 2013), frontotemporal dementia (Muñoz-Ruiz et al., 2012), Parkinson's disease (Lee et al., 2018), dementia with Lewy bodies (Burton et al., 2002), Huntington's disease (Mühlau et al., 2009). As VBM can be applied regardless of the type of neuropathological condition in a transdiagnostic approach (Cauda et al., 2019; McTeague et al., 2016), we decided to use the data obtained from all brain disorders that were present in the BrainMap VBM database, with the aim to achieve the most overarching analysis of how pathological processes affect the insular cortex.

Materials and methods

Selection of studies

We conducted an extensive meta-analytic search using the software Sleuth to query the VBM database of BrainMap (Fox et al., 2005; Fox and Lancaster, 2002; Laird et al., 2005b). BrainMap is one of the largest international repositories of neuroimaging data (Vanasse et al., 2018). It comprises a database of thousands of brain imaging studies (functional and structural MRI data), from which data on regional effects can be retrieved (in our case, regions of altered gray matter density, volume or concentration). Data are reported in MNI/Talairach coordinates and are ideal to conduct meta-analyses from a large subject pool, by making meta-analytic morphologic queries. At the moment of the search (February 2018), the BrainMap VBM database contained 994 articles, for a total of 3151 experiments, 75727 subjects, and 21827 locations.

In order to assess the impact of brain disorders on the insular cortex, we performed a first search capable of retrieving all the VBM studies that matched the following query:

Search 1:

[Experiments Contrast is Gray Matter] AND [Experiment Context is Disease Effects] AND [Observed Changes is Controls>Patients] AND [Locations TD Label is Gyrus Insula].

(see section 1 of Supplementary methods for details of the literature search process). We decided to focus on decreased values only. From a theoretical point of view, there is general agreement in the neuroscientific literature that decreased values can be seen as density reduction or atrophy of GM.

Additionally, we performed a second search using the following criteria:

Search 2:

[Experiments Contrast is Gray Matter] AND [Experiment Context is Disease Effects] AND [Observed Changes is Controls>Patients] AND [Locations MNI image is *]

where the MNI images represent each of the parcels selected from the work of Kelly et al. (2012). The two searches were designed to retrieve foci of alteration from both the hemispheres, although every extracted experiment could report an effect either in both hemispheres or in only one of the two. Search 2 was repeated twice to retrieve the data related to the K=2 segmentation (i.e. K2_ant and K2_post) and 3 times for what concerns the K=3 segmentation (i.e. K3_ant, K3_mid, K3_post) (See section 3 in the Supplementary methods for details of the alteration density analysis).

Anatomical likelihood estimation on co-alteration and co-activation data

The VBM data retrieved were statistically elaborated with the method of the anatomical likelihood estimation (ALE) (Eickhoff et al., 2012; Eickhoff et al., 2009; Turkeltaub et al., 2012), so as to obtain modeled anatomical effect maps representing the overall distribution of gray matter co-alterations with the insula. ALE is a quantitative method that can be used for estimating consistent morphological alterations across several neuroimaging studies (Laird et al., 2005a; Laird et al., 2009; Turkeltaub et al., 2002) (See section 4 of the Supplementary methods and Fig.S3 for the estimation of possible selection bias).

ALE maps showed the brain areas in which multiple studies reported statistically significant alteration peaks (i.e., foci of interest) Since we analyzed locations with morphologic alterations, ALE maps revealed the brain regions that were likely to be altered together (Cauda et al., 2018a; Manuello et al., 2018b; Tatu et al., 2018).The ALE map derived from the analysis of the whole insula (obtained through Search 1) was thresholded at a voxel-level (FWE $p < 0.05$) (Eickhoff et al., 2017; Eickhoff et al., 2016), while the maps related to Search 2 were thresholded at a cluster-level (FWE $p < 0.01$).

In order to provide a further element to improve the interpretation of the co-alteration networks, we finally performed an ALE analysis on data derived from the

BrainMap functional repository in order to construct the meta-analytic co-activation pattern of each of the five bilateral parcels of the insula (Robinson et al., 2010). A third search was performed based on the following criteria:

Search 3:

[Experiments Context is Normal Mapping] AND [Experiment Activation is Activations Only] AND [Locations MNI image is *]

where the MNI images represent each of the bilateral parcels selected from the work of Kelly et al. (2012), as it was in Search 2. Search 3 was thus repeated 5 times.

According to ALE literature, brain areas exhibiting common activation patterns are considered to be connected.

Comparison between co-alteration and co-activation patterns

In order to inspect the similarities and divergences between the couples of co-alteration and co-activation patterns originating from a same bilateral parcel (i.e. results of Search 2 and Search 3), the following analyses were performed. First, we ran Pearson's correlation between each couple of maps. Second, we computed the extension of the co-alteration map being in overlap with the corresponding co-activation map. In this second analysis the insula was excluded from the maps.

Analysis of behavioral profile

To associate specific psychological functions with the areas forming the co-alteration patterns related to the five bilateral parcels, we performed on the VBM ALE maps only (data from Search 2) an analysis of behavioral profile using the behavioral analysis plug-in for the software Mango (Lancaster et al., 2012). This tool is based on the BrainMap functional database and provides a quantitative association between a user defined ROI (i.e., each of the ALE maps) and 51 behavioral sub-domains, organized in 5 classes: action, cognition, emotion, interoception, and perception. In accordance with Lancaster et al. (2012), only sub-domains with a z-score ≥ 3 were maintained. An average value was obtained for

each of the 5 classes, by computing the mean of the related sub-domains with above threshold z-score.

Construction of the morphometric co-alteration networks

In order to describe in detail the statistical relationship between the insula and the co-altered regions, we constructed the anatomical co-alteration networks of the bilateral insulae, applying a methodology recently developed by our group to the data obtained through Search 1. This kind of analysis can determine whether or not the alteration of the insula is statistically related to the alteration of other brain areas. In the output produced, nodes represent altered regions, whereas edges link couples of nodes which are more likely to be altered together rather than one independently from the other. This particular dependency was computed using the Patels' κ index (Patel et al., 2006) (for a more detailed description of this approach, see Cauda et al. (2018a) and Manuello et al. (2018b)). From this complete whole brain network we extracted one sub-network for each of the selected Kelly's unilateral parcels (a total of 4 sub-networks for the K2 solution, and 6 sub-networks for the K3 solution). This was achieved with a three-steps procedure. First, the nodes anatomically located inside the given parcel of interest were identified and considered as roots. Second, only the first neighbors of the root nodes (i.e., nodes directly linked with at least one node located in the parcel) were preserved. Third, all the edges between non-roots nodes were eliminated (See Figure 1 for a graphic summary of this procedure, as well as of the other analyses performed). For each of the obtained sub-networks, we calculated the total number of nodes and edges. In order to describe the spatial pattern of co-alteration of each parcel at macro-level, we distinguished the location of the non-root nodes in 7 groups: frontal lobe, parietal lobe, temporal lobe, occipital lobe, midbrain, subcortical areas and insula. Of note, non-root nodes located in the insulae were counted separately from the other lobes, in order to highlight the co-alteration between them. The repartition of the nodes was based on the Talairach Client tool (Lancaster et al., 2000) and refined by two expert researchers. To estimate the strength of co-alteration of each insula parcel with every lobe, for every sub-network the values of the edges connecting the root nodes with the nodes in a same lobe were summed, and then divided for the summed values of all the edges of the sub-network. Values were then expressed as percentages. We interpreted this measure as the strength of the co-alteration of each insula parcel with each lobe.

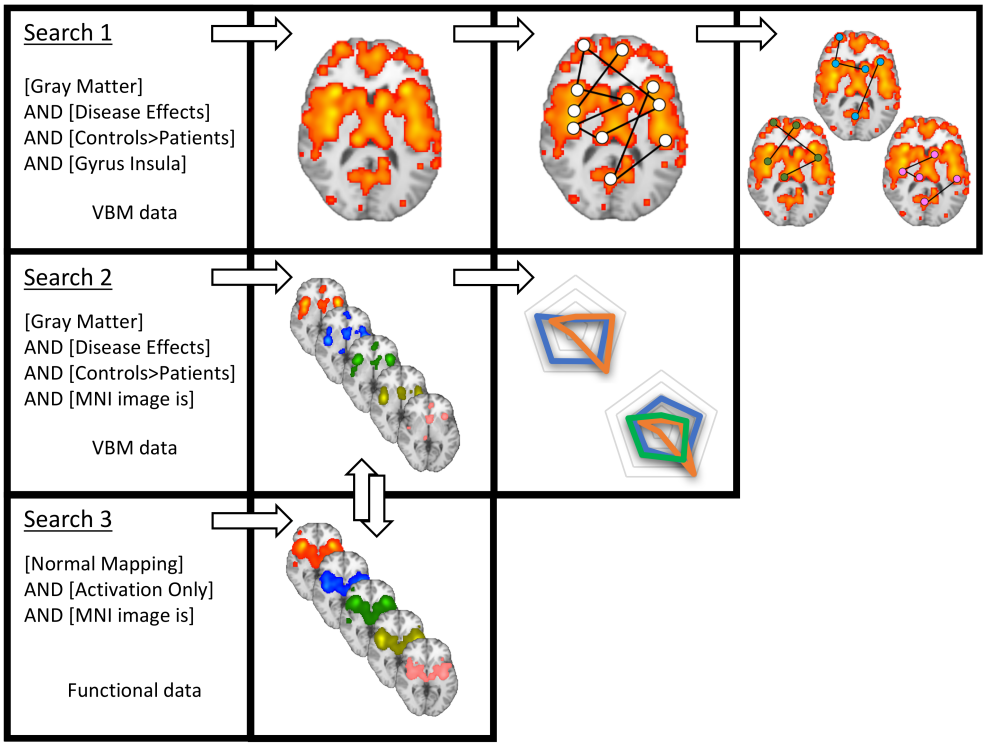

Figure 2: A graphic summary of the analyses performed. Top row: from Search 1 on VBM data, the co-alteration pattern was obtained. Based on this, we generated the whole brain co-alteration network, that was then broken up into one unilateral sub-network for each unilateral insula parcel (networks shown in this figure were built for visualization purpose only). Middle row: from Search 2 on VBM data we obtained five bilateral co-alteration patterns, one for each insula sub-parcel. On each co-alteration pattern the behavioral analysis was performed. Bottom row: from Search 3 on functional data we obtained five bilateral co-activation patterns, one for each insula sub-parcel. The corresponding co-alteration and co-activation patterns where then compared.

Data and code availability

Both VBM and functional meta-analytic data are freely available as part of the BrainMap database.

Kelly's insula ROIs can be freely downloaded from http://fcon_1000.projects.nitrc.org.

No specific tools where developed to perform the analyses described.

Results

Results from the queries

Our first search retrieved a total of 207 papers, 277 experiments, 4213 foci, for a total of 14916 subjects (7218 pathological subjects) (see also Figure S1 and Table S1). This means that the 8.8% of VBM experiments included in the BrainMap database report a decrease effect in the insula. Only five brain regions obtained a slightly higher value (see section 2 in the Supplementary methods and Tab S4 for a comparison with the rest of the brain). Experiments were distributed across 23 disorders, the most represented being schizophrenia (with 48 experiments). 51 experiments were classified as "Other" since they investigated more than one brain disorder, or because less than 3 experiments retrieved in the data set investigated that same neuropathology (see Tab. S2 for the complete breakdown, and section 5 of the Supplementary methods for the analysis of potential representation bias across disorders). Based on the spatial distribution of the foci, the alteration density of the insula was found to be almost three times greater than the rest of the brain.

The insula co-alteration pattern

K2 solution

Anterior bilateral cluster

The related search retrieved 122 experiments and 2080 foci. Along with the insula, alterations affect preferentially the superior and inferior frontal gyri, anterior cingulate gyrus, superior temporal gyrus, caudate, thalamus, and claustrum (Fig. 2).

Posterior bilateral cluster

The related search retrieved 80 experiments and 1330 foci. Along with the insula, alterations affect mainly the precentral and postcentral gyri, inferior frontal gyrus, anterior cingulate gyrus, left hippocampus, caudate, and thalamus (Fig. 2).

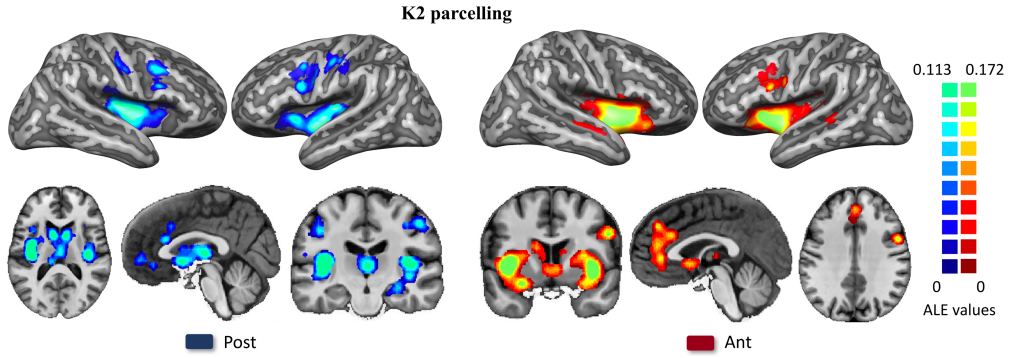

Figure 2: The co-alteration patterns of the anterior (red) and posterior (blue) bilateral parcels of the K2 solution. The color scale represents ALE values.

K3 solution

Anterior bilateral cluster

The related search retrieved 76 experiments and 1433 foci. Along with the insula, alterations are mainly located in the medial frontal gyrus, middle frontal gyrus, anterior cingulate gyrus, right precuneus, left hippocampus, claustrum, amygdala, thalamus, and caudate (Fig. 3).

Middle bilateral cluster

The related search retrieved 87 experiments and 1317 foci. Along with the insula, alteration are mainly located in the left middle and inferior frontal gyri, right hippocampus, right claustrum, left amygdala, thalamus, and caudate (Fig. 3).

Posterior bilateral cluster

The related search retrieved 40 experiments and 664 foci. Along with the insula, alterations are mainly located in the left inferior frontal gyrus, right middle frontal gyrus, left anterior cingulate cortex, thalamus, and caudate (Fig. 3).

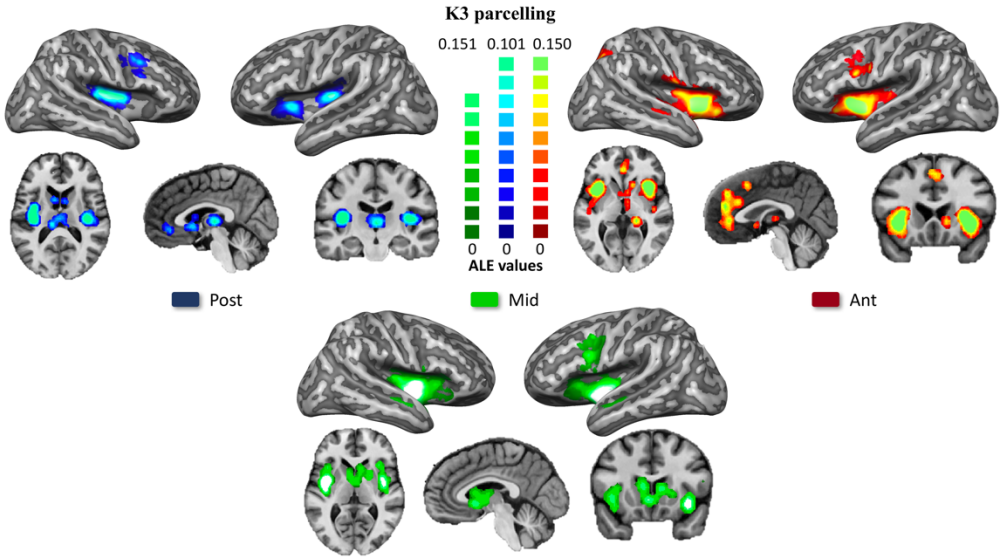

Figure 3: The co-alteration patterns of the anterior (red), mid (green), and posterior (blue) bilateral parcels of the K3 solution. The color scale represents ALE values.

Comparison between co-alteration and co-activation patterns of the insula

K2 solution

The degree of correlation between the co-alteration and the co-activation patterns of the anterior bilateral parcel of the insula was r = 0.56. The 54% of the co-alteration map was in overlap with the corresponding co-activation map. In the posterior bilateral cluster, the correlation between the 2 conditions was r = 0.61, and the 57% of the co-alteration map was in overlap with the corresponding co-activation map (Fig. 4 and Fig. S4) (See Tab.S3 for details of the fMRI paradigms included in the functional data behind the co-activation patterns).

K3 solution

The degree of correlation between the co-alteration and the co-activation patterns of the anterior bilateral parcel of the insula was r = 0.53. The 52% of the co-alteration map was in overlap with the corresponding co-activation map. In the middle bilateral cluster, the correlation between the 2 conditions was r = 0.62, and the 60% of the co-alteration map was in overlap with the corresponding co-activation map.

Finally, the degree of correlation between the co-alteration and the co-activation patterns of the posterior bilateral parcel of the insula was r = 0.56. The 60% of the co-alteration map was in overlap with the corresponding co-activation map. (Fig. 4 and Fig. S4) (See Tab.S3 for details of the fMRI paradigms included in the functional data behind the co-activation patterns).

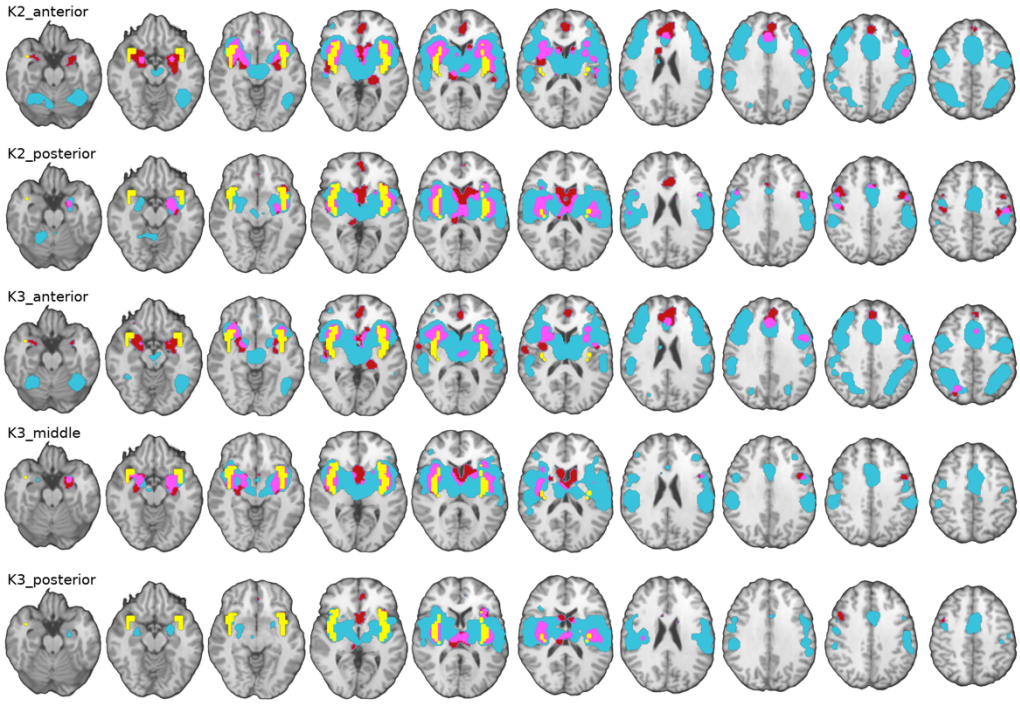

Figure 4: Comparison between the co-alteration (red) and co-activation (light blue) patterns for each bilateral parcel (both K2 and K3 solutions). The overlap between the two condition is in magenta, while the insula is in yellow.

Analysis of behavioral profile

K2 solution

The behavioral profile of the co-alteration pattern related to the anterior parcel had peak score for "Emotion (z=7.1), "Interoception" (z=7) and "Perception" (z=7). In turn, the co-alteration pattern related to the posterior parcel had peak score for "Emotion" (z=8) (Fig. 5).

K3 solution

The behavioral profile of the co-alteration pattern related to the anterior parcel had peak score for "Cognition" (z=6.5) and "Emotion" (z=6.4). Scores of the co-alteration pattern related to the middle parcel had the highest peak for "Emotion" (z=6.2). Lastly, the behavioral decoding of the co-alteration pattern related to the posterior parcel had the peak score for "Emotion" (z=7.7) (Fig. 5).

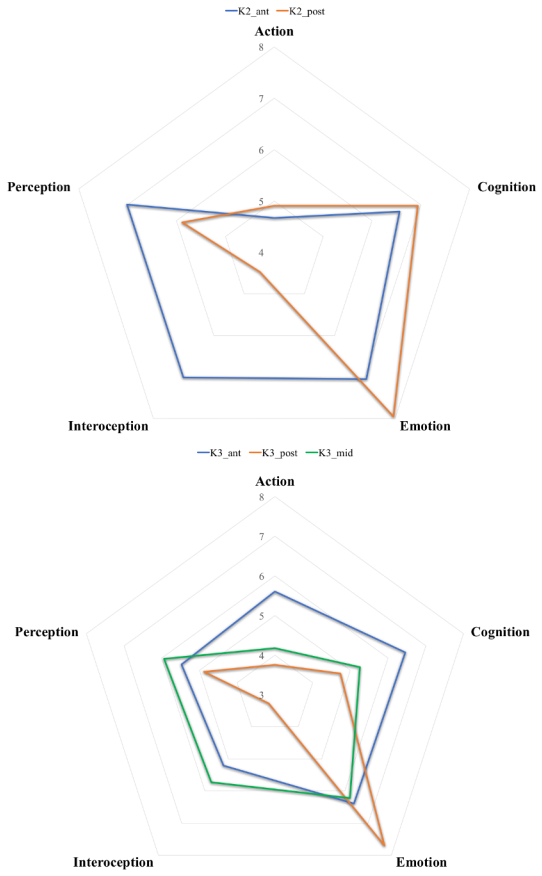

Figure 5: Results of the behavioral analysis computed on the co-alteration bilateral patterns for both the K2 (top), and the K3 (bottom) solutions. Blue = anterior; orange = posterior; green = middle.

The insula co-alteration network

The complete bilateral network counts 14 nodes in the right insula and 6 in the left insula. Of note, none of the nodes is localized in the middle parcel of left insula when using the tripartite subdivision (i.e. K3 solution). Therefore, it was not possible

to create the co-alteration network for the middle parcel of the left insula (K3_mid_L). Coherently, the co-alteration networks for the anterior and posterior parcel of the left insula in the bipartite subdivision (K2_ant_L and K2_post_L) are identical to the co-alteration networks for the anterior and posterior parcel of the left insula in the tripartite subdivision (K3_ant_L and K3_post_L) respectively. When moving from the bipartite partition to the tripartite one, all but one of the nodes becoming part of the right middle partition where previously in the posterior one (for the Talairach coordinates of the nodes as well as their membership to Kelly's parcels, please see Table 1). Details of the number of nodes and edges in each sub-network are provided in Table 2, while the distribution of the nodes across lobes is described in figures 6 and 7.

Node (Name)	*TAL coordinates*			*Kelly's parcels*	
	x	***y***	***z***	***K=2***	***K=3***
Insula_R	28	12	-20	K2_ant_R	K3_mid_R
Insula_R_1	40	2	-14	K2_ant_R	K3_mid_R
Insula_R_2	42	-6	-10	K2_ant_R	K3_mid_R
Insula_R_3	40	0	-10	K2_ant_R	K3_mid_R
Insula_R_4	48	14	-6	K2_ant_R	K3_ant_R
Insula_R_5	44	4	-4	K2_ant_R	K3_mid_R
Insula_R_6	44	14	-4	K2_ant_R	K3_ant_R
Insula_R_7	38	22	-2	K2_ant_R	K3_ant_R
Insula_R_8	38	12	2	K2_ant_R	K3_ant_R
Insula_R_9	40	14	2	K2_ant_R	K3_ant_R
Insula_R_10	42	14	2	K2_ant_R	K3_ant_R
Insula_R_11	44	-8	4	K2_post_R	K3_post_R
Insula_R_12	34	-24	10	K2_post_R	K3_post_R
Insula_R_13	42	-24	-2	K2_post_R	K3_mid_R
Insula_L	-36	16	-12	K2_ant_L	K3_ant_L
Insula_L_1	-34	16	-12	K2_ant_L	K3_ant_L
Insula_L_2	-46	-14	-10	K2_post_L	K3_post_L
Insula_L_3	-42	-14	-10	K2_post_L	K3_post_L
Insula_L_4	-32	-12	-10	K2_post_L	K3_post_L
Insula_L_5	-50	4	-4	K2_post_L	K3_post_L

Table 1: Talairach coordinates of the nodes and their membership to Kelly's parcels for both K2 and K3 solutions.

	Sub-network	n of root nodes	n of nodes	n of edges
K2 solution	left anterior	2	268	449
	left posterior	4	259	871
	right anterior	11	312	2084
	right posterior	3	218	437
K3 solution	right anterior	6	235	1041
	right middle	6	312	1184
	right posterior	2	177	296

Table 2: Details of the number of nodes and edges composing the co-alteration network of each insula parcel.

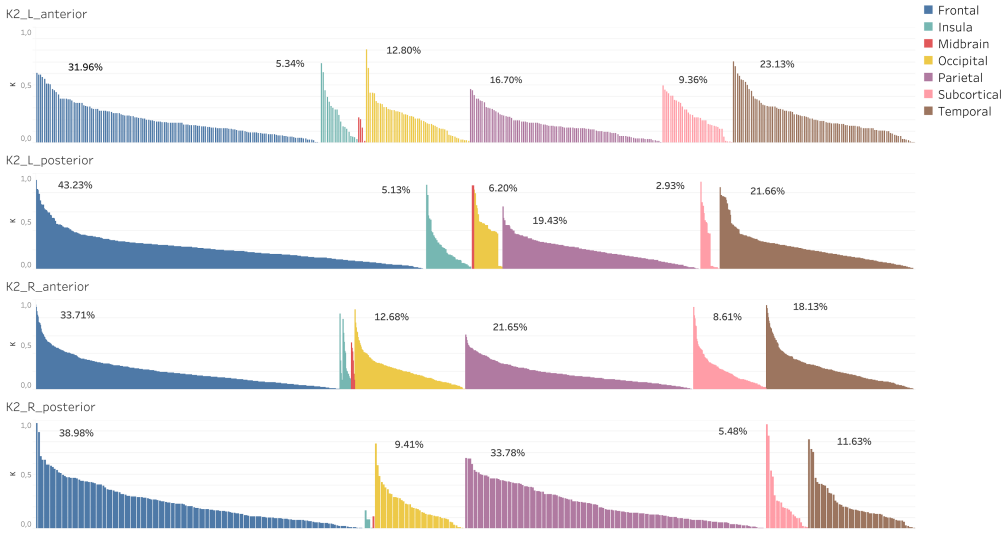

Figure 6: Distribution of the edges' values for each lobe/group, for the K2 solution. Only lobes/groups accounting at least for the 2% of the total Patel's κ were visualized. Blue = frontal lobe, green = insula (non-root), red = midbrain, yellow = occipital lobe, purple = parietal lobe, pink = subcortical regions, brown = temporal lobe.

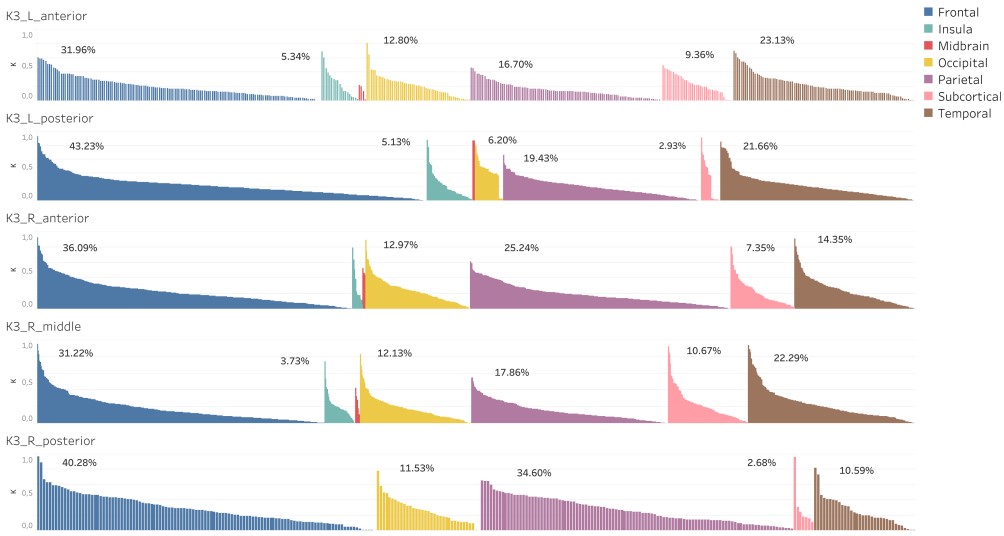

Figure 7: Distribution of the edges' values for each lobe/group, for the K3 solution. Only lobes/groups accounting at least for the 2% of the total Patel's κ were visualized. Blue = frontal lobe, green = insula (non-root), red = midbrain, yellow = occipital lobe, purple = parietal lobe, pink = subcortical regions, brown = temporal lobe.

Discussion

The insula co-alteration pattern

Our analysis confirms what previously evidenced in Cauda et al. (2020; 2019; 2014): the insular cortex is frequently and differently altered by a wide variety of brain disorders (Alcauter et al., 2015; Fathy et al., 2019; Igata et al., 2017; Seok and Cheong, 2020; Torres et al., 2016; Wang et al., 2019). Interestingly, the insula, together with some subcortical nuclei, appears to be one of the most altered areas of the brain (Cauda et al., 2019), as confirmed by the high fraction of BrainMap experiments reporting at least one focus of alteration in this brain region. Coherently, we found the insula to exhibit a density of alteration that is approximately three times the alteration of the whole brain. Moreover, the range of diseases that produce alterations in the insular cortex is highly diversified, including neurological and psychiatric conditions.

Each of the obtained co-alterations patterns of the insula comprises cortical and subcortical areas. In particular, frontal areas (especially the inferior frontal gyrus)

and subcortical regions (such as the thalamus and the caudate) are present in co-alteration patterns based on either bipartite or tripartite parceling. On the contrary, the amygdala and parietal sites show to be co-altered with the insula only in patterns based on the tripartite parceling, which might indicate more specificity compared with the bipartite parceling.

Overall, the results reflect the extensive anatomical connections of the insula with many brain sites (Cauda et al., 2012a; Cauda et al., 2011; Dosenbach et al., 2007; Mesulam and Mufson, 1982; Taylor et al., 2009; van den Heuvel et al., 2009). Parts of these pathways are long-range projections, as the insula has been found to be rich of Von Economo's neurons (VENs), large spindle-shaped cells that appear to be involved in processes capable of monitoring the state of the body, such as interoception and proprioception (Allman et al., 2005; Cauda et al., 2014; Cauda et al., 2013; Medford and Critchley, 2010; Seeley et al., 2007). In particular, the anterior cingulate cortex (ACC) appears to be frequently co-altered with the insula. It is well known that these two areas are central parts of the salience network (SN), a disruption of which could account for the symptoms of impairment of salience detection and self-monitoring that can be found transdiagnostically in a variety of neurological and psychiatric syndromes.

Analysis of edges distribution

It is interesting to observe that the edges connect the insula with regions tending to be not below the z coordinate of the insula node itself, with no co-alteration with the cerebellum and only few with the midbrain and subcortical regions. This observation suggests that the insula is co-altered by pathology only together with higher-order structures, especially with cortical areas. As the insula is associated with functions that integrate lower- and higher-order cognitive areas, evaluating sensory and limbic stimuli, monitoring the body and the environment to carry out error detection processes (Ahmed et al., 2016; Cauda et al., 2012a; Cauda et al., 2011; Cauda et al., 2012b; Douaud et al., 2014; Fjell et al., 2015; Jagust, 2013; Jones et al., 2016; Klein et al., 2013; Manuello et al., 2016; Nieuwenhuys, 2012; Vercelli et al., 2016; Voytek and Knight, 2015; Wylie and Tregellas, 2010), it should appear surprising that it is not greatly co-altered with limbic and subcortical regions. As the co-activation map shows that the insula can be functionally connected with many extracortical structures, for instance, the cerebellum (Figs. 4 and S4), the co-alteration patterns of each insular parcel seem to suggest that the insula has a bottom-up pathoconnectivity profile, in which it appears to be co-altered mostly with those cortical areas with which it is functionally connected so as to exert a bottom-up influence (e.g. error or

salience detection), rather than with those lower-order regions whose information is thought to be subjected by an insular integration.

Each cluster is widely connected with all the cortices, but their co-alteration edges are not equally distributed between the lobes (Figs. 6 and 7). The most strongly co-altered lobe with each insular cluster is the frontal one, confirming that the insula tends to be altered together with higher-order and philogenetically recent areas. This might also be due to the anatomical proximity between the frontal cortices and the insula. In turn, the occipital lobe, which is far away from the insula and has chiefly a sensory nature, is one of the less co-altered areas with the insula.

The lobar distribution of the edges is also different between clusters. For instance, the left posterior cluster is the one which is the most co-altered with the frontal lobe. Also in the right insula, the posterior cluster for the bipartite solution (K2_R_post) is slightly more strongly co-altered than the anterior (K2_R_ant), and the posterior cluster for the tripartite solution (K3_R_ant), even if it has overall less edges than other cluster, exhibits a 40% of the strength of its co-alteration directed to the frontal cortices. Surprisingly, posterior clusters are less associated to the occipital lobe than the anterior ones. These findings are unexpected, as Kelly and colleagues (2012) have found that the posterior clusters are preeminently associated with motor and perceptual functions, while the anterior ones are more related to cognition. It should be observed, however, that all the insular clusters have been associated to some extent with cognition, both in our analysis and in that by Kelly and colleagues (2012). Still, our results point out that the co-alteration network of the posterior insula might be more associated with cortices characterized by higher-order functions.

Another interesting observation is that the right insula presents much more nodes and edges of co-alterations than the left one. This suggests that the right insula may be more susceptible than the left one to pathology. Finally, the distributions of the strength of co-alteration of each cluster for every lobe are clearly heavy-tailed (Figs. 6 and 7), with few edges characterized by high κ values and many weak edges with low κ values.

Relationship between co-alteration and co-activation with the insula

With the exception of the subcortical structures (such as the cerebellum) that are co-activated but not co-altered with the insula, overall the insula co-alteration patterns correlate well with the corresponding co-activation ones, with the former widely being in overlap with the latter. This finding provides evidence that the brain areas

that are altered along with the insula are not randomly affected; rather, they tend to be altered in terms of their functional connectivity. This is also a significant result that confirms the strict relationship between anatomical and functional connectivity profiles (Abdelnour et al., 2014) and accords well with the line of research suggesting that brain connectivity might play a role in the development and distribution of neuronal alterations (Cauda et al., 2018b; Iturria-Medina and Evans, 2015; Raj et al., 2012; Zhou et al., 2012). In particular, distinct structural and functional connectivity patterns have been associated with the spatial distribution of brain disorders, for instance in amyotrophic lateral sclerosis, Alzheimer's disease and the behavioral variant of frontotemporal dementia (Buckner et al., 2009; Du et al., 2007; Ravits, 2014; Zhou et al., 2010). A relationship between dementia and intrinsic connectivity network has been strongly put forward (Seeley et al., 2009), and functional abnormal patterns related to deficits of semantic memory have been found in the default mode network (DMN) of patients with mild cognitive impairment (Gardini et al., 2015).

All these findings support the conjecture that large functional networks involved in synchronous neural activity may be selectively more vulnerable and, thereby, may enhance the development of alterations more quickly than region-specific functional systems. In addition, abnormalities in functional connectivity hubs and pathways might couple to neurophysiological, metabolic, and genetic aspects of brain cell biology to increase the impact and the distribution of the alteration process (Iturria-Medina and Evans, 2015; Saxena and Caroni, 2011). Both anatomical and functional connectivity seem therefore to be correlated not only in the normal and healthy brain (Cauda et al., 2011; Honey et al., 2009) but also in the brain that is pathologically affected (Crossley et al., 2016b; Gardini et al., 2015; Iturria-Medina and Evans, 2015; Iturria-Medina et al., 2014; Seeley et al., 2009).

Our results point out that, (at least) when the insula is altered, the co-alteration networks reflect the functional connectivity patterns, thus providing support for the nodal stress hypothesis in the development and distribution of alterations (Crossley et al., 2016a; Crossley et al., 2014). When impaired, the insular cortex might bring about hyperexcitability to its functionally connected areas, and thereby cause metabolic stress and disruption.

Overall, considering the bipartite parceling the peaks of overlap between co-alteration and co-activation patterns are mainly localized in frontal and subcortical areas. In the patterns based on the tripartite parceling instead, the peaks of overlap

are not only mainly localized in frontal and subcortical areas, but also in temporal and parietal sites. This may provide evidence for the more specificity of the solution based on the tripartite parcellation.

However, the uncoupling between co-alteration and co-activation for what concerns subcortical and lower cortical regions suggests that also other mechanisms might take place in the distribution of co-alterations other than the influence of normative connectivity. A shared vulnerability factor (Zhou et al., 2012) is usually expected to play a role in the development of pathological alterations, for instance in the form of a genetic influence (Cauda et al., 2018b). However, our results indicate that such uncoupling might derive also from other biological factors, as the "bottom-up" (from the insula to cortical areas) pathoconnectivity profile is unlikely to be related exclusively to functional aspects of brain organization.

The fact that the insula is more involved in co-alteration patterns with higher-order cortical regions rather than with lower-order areas (such as subcortical and hippocampal structures) deserves an explanation. If pathological alterations are guided by connectivity constraints, which in case of the insula co-alteration network are pre-eminently functional ones, why only the connections between the insula and higher-order areas are involved in patterns of co-alterations, and not those between the insula and lower-order regions? In fact, the insular cortex is strongly connected with both brain sites (cortical and subcortical). Are there biological factors (such as, for instance, cytological or genetic aspects) that make the insula more likely to be co-altered with the former areas rather than with the latter? The question is intriguing and requires further investigations.

Analysis of behavioral profile

The behavioral profiles of the co-alteration patterns show a prevalence of labels related to the emotional and cognitive spheres, which is consistent with the fact that emotional and cognitive processes are frequently disrupted in many neurological and psychiatric conditions. As we have seen, the insular cortex has important cognitive and interoceptive functions; in particular, it is mainly involved in the processing of salience, attention, emotions, and in the integration of sensory and interoceptive stimuli.

The insula is an essential part of the salience network (SN), along with the dorsal anterior cingulate cortex (dACC) and other subcorti¬cal and limbic structures (Seeley et al., 2007; Uddin, 2015). This important network has a pivotal role in processing the perception of behaviorally significant stimuli as well as in

coordinating the use of brain resources (Uddin et al., 2013; Uddin et al., 2011). In fact, being an essential hub of the SN, the insula (especially the right one) is involved in the dynamic coordination of two other important brain networks, the DMN and the central executive network (CEN) (Chen et al., 2013; Goulden et al., 2014; Sridharan et al., 2008; Supekar and Menon, 2012). The insular cortices seem therefore involved in a plurality of functions associated with subjective salience, independent of the nature of the stimuli, being those homeostatic, emotional or cognitive (Bartra et al., 2013; Craig, 2002). Also, it has been found that dysfunction of the SN can occur in many brain conditions, including dementia, schizophrenia, psychosis, bipolar disorder, addiction, anxiety, depression, obsessive-compulsive disorder, chronic pain, and autism spectrum disorder (Di Martino et al., 2009; Etkin et al., 2009; Goodkind et al., 2015; Hamilton et al., 2012; Kapur, 2003; Klin et al., 2003; Li et al., 2010; Palaniyappan and Liddle, 2012; Schroeter et al., 2008; Seeley et al., 2012; Simons et al., 2014). Furthermore, the insular cortex plays a fundamental role in the emotional evaluation of bodily states. Specifically, the coordinated activity of insula, amygdala and prefrontal cortex is pivotal for regulating emotions, both in normal and pathological conditions (Foland et al., 2008; Lee et al., 2012).

In sum, with regard to the solution based on two parcels, the anterior sub-network seems to be more oriented towards the processing of interoception and perception, whereas the posterior sub-network appears to be more associated with the processing of emotion. These two sub-networks show comparable scores for the functions of action and cognition. Instead, with regard to the solution based on three parcels, the anterior sub-network appears to be more oriented towards the processing of action and cognition, while the middle sub-network appears to be more oriented towards the processing of perception and interoception and the posterior sub-network towards the emotional processing.

Limitations and future directions

The principle limitation of our study is that we cannot say how differently brain disorders are supposed to impact on the insular cortex. We know that a great number of conditions affect this cortical area but we do not know which parts of the insula are the most affected and by which disorders. However, we decided to consider all brain disorders in the BrainMap database because the aim of this study was to achieve the most comprehensive investigation about the pathological processes affecting the insula. Indeed, the leave-one-pathology-out analysis suggested that none of the included disorder is guiding the results (Tab. S5). There was also the

methodological constraint of analyzing the most numerous sample of studies to achieve a better statistical outcome. As in any meta-analysis, the data selection procedure could be affected by biases. However, the implemented fail-safe analysis (Fig. S3) suggested a good robustness of the results at least to the drawer-effect. This approach was intended to provide useful insight for further examinations with more specific aims. Related to this, we could not use a more fine-grained parcellation, since this was not supported by a sufficient amount of data to achieve reliable results. The selection of any predetermined parcellation is per se a questionable step. However, in doing this we opted for a solution with high multimodal consensus, as explained above.

Future investigations need to explore the directionality, both spatial and temporal, followed by alterations across the different brain areas when a pivotal hub, like the insula, is initially affected. Although regions presenting high node degrees are thought to be pathoconnectivity hubs, we cannot infer from our data whether alterations first originate in the insula and then propagate to other areas or vice versa.

Conclusion

This study performed a pathoconnectivity network analysis of the insula, one of the most connected and important hubs of the both health and pathological brain. Our findings indicate that the insula is altered by a variety of brain disorders. This result is in line with recent research that found the insula to be among the most affected brain areas by a wide range of brain diseases (Cauda et al., 2019) as well as in six different important psychiatric conditions – i.e., schizophrenia, bipolar disorder, depression, addiction, obsessive-compulsive disorder, and anxiety (Goodkind et al., 2015). Our analysis not only confirms that finding, but provides further evidence that the insula is significantly affected by both neurological and psychiatric disorders. Its central and intense activity may account for the fact that this area appears to be so vulnerable to neuronal alterations.

The insula pathoconnectivity network analysis reveals 1) that the pattern of distribution of GM alterations associated with the insular cortex is composed of areas that are mainly located in cortical rather than in subcortical sites; 2) that the insula co-alteration patterns correlate, and overlap, well with the corresponding co-alteration patterns; and that 3) these co-alteration patterns may implicate the disruption of cognitive (i.e., salience) and emotional processes. The fact that higher-order areas appear to contribute more to the co-alteration network of the insula than lower-order regions suggests that, along with functional connectivity constraints,

other factors (perhaps biological ones, such as cytological and genetic mechanisms) may play a role in the development of patterns of co-alterations.

These findings provide evidence that the brain areas that are altered along with the insula are not randomly disrupted but tend to be altered on the basis of their functional connectivity. Finally, the significant coherence between the co-alteration and co-activation of the insula suggests that alterations caused by brain disorders can exhibit a distribution according to the logic of functional network architecture. This might be typical whenever brain hubs are involved in the alteration process. According to this view, brain hubs may lie at the center of networks composed of co-altered areas. If confirmed by future studies, this finding will help to better address the issue of how brain connectivity can predict regional alteration profiles and severity of symptoms in both neurological and psychiatric disorders.

Supplementary methods

Experiments search

1.1 Identification

We adopted the definition of meta-analysis accepted by the Cochrane Collaboration (Green et al., 2008) and the "PRISMA Statement" international guidelines in order to ensure a transparent and complete report of data selection (Liberati et al., 2009; Moher et al., 2009).

A systematic search strategy was used to identify relevant experiments, published until February 2018, across the voxel-based morphometry (VBM) database of BrainMap (Fox et al., 2005; Fox and Lancaster, 2002; Laird et al., 2005; Vanasse et al., 2018). BrainMap comprises a database of thousands of neuroimaging studies (functional and structural MRI data), from which data on regional effects can be retrieved (in our case, regions of altered gray matter density). At the moment of the search, the BrainMap VBM database contained 994 articles, for a total of 3151 neuroimaging experiments, 75727 subjects, and 21827 stereotaxic locations (x, y, z).

In order to assess the impact of brain disorders on the insular cortex we performed a systematic search using the software application Sleuth 2.4. (http://www.brainmap.org/sleuth/), capable of retrieving all the VBM experiments that matched the following query:

Search 1:

[Experiments Contrast is Gray Matter] AND [Experiment Context is Disease Effects] AND [Observed Changes is Controls>Patients] AND [TD Label is Gyrus Insula]

1.2 Screening

Our search retrieved 207 articles, for a total of 277 experiments, 14916 subjects and 4231 foci of alteration. Experiments were distributed as follows (see also Figures S1 and S3):

schizophrenia (48), multiple sclerosis (24), Alzheimer's disease (22), epilepsy (15), depression (12), frontotemporal dementia (9), bipolar disorder (9), Huntington's disease (9), supranuclear palsy (9), multiple system atrophy (8), migraine (8), psychosis (7), mild cognitive impairment (7), Parkinson's disease (7), post-traumatic stress disorder (7), autism spectrum disorder (4), frontotemporal lobe degeneration (3), obsessive-compulsive disorder (3), Lewy body dementia (3), olfactory disorders (3), panic/anxiety disorder (3), at-risk mental state (3), and amyotrophic lateral sclerosis (3). Other papers (51) were classified as "Others" if they investigated more than one brain disorder or if the study was the only one retrieved in the data set on a certain condition.

1.3 Eligibility

All the selected experiments were reviewed in order to ensure:

1) they were published in a peer reviewed English language journal;

2) that the experiments described cerebral structural changes visible with VBM;

3) both the presence of the healthy control group and the pathological sample;

4) that the results were reported by using the Talairach/Tournoux or Montreal Neurological Institute (MNI) coordinates.

The meta-analysis was carried out in the Talairach (TAL) brain space. Meta-data reported in MNI coordinates were converted into TAL using the icbm2tal algorithm designed by Lancaster et al. (2007).

1.4 Inclusion

For the overview of the selection strategy see Figure S1 [PRISMA flow chart]. For the distribution of the selected experiments see also Table S1.

Frequency of alteration analysis

In order to compare the reporting frequency of decrease results for the insula with the rest of the brain, Search 1 was repeated for each of the 52 TD labels available in the Sleuth tool. We then computed for each brain region the percentage of BrainMap VBM experiments reporting alteration in it.

The results of this analysis are reported in Table S4.

Alteration density analysis

As it was previously described in literature, the insula can be found structurally altered in a variety of brain disorders. This evidence suggests the role of pathological hub for this region in the development of co-alteration networks. However, we wanted to know whether or not the insula may be more densely altered than the rest of the brain.

To answer this question, the following search was performed:

Search 4:

[Experiments Contrast is Gray Matter] AND [Experiment Context is Disease Effects] AND [Observed Changes is Controls>Patients]

In this way, we retrieved all the foci (through the whole brain) in which a decrease was reported due to a disease effect. Based on this, the alteration density of the insula was computed as

$$\frac{number\ of\ foci\ in\ the\ insula}{number\ of\ voxels\ in\ the\ insula}$$

while the density of the rest of the brain was computed as

$$\frac{number\ of\ foci\ in\ the\ rest\ of\ the\ brain}{number\ of\ voxels\ in\ the\ rest\ of\ the\ brain}$$

where the insula was, of course, not included.

The alteration density of the insula was then expressed as percentage of the alteration density of the rest of the brain.

Of note, the alteration density should not be confused with GM density as measured by VBM. The former describes the amount of foci reporting a decrease effect in a given area (the insula, or the whole brain), while the latter describes changes in the structure of GM.

Fail-safe analysis

The "fail-safe" technique is a common tool to assess the robustness of results against potential publication bias in classical meta-analyses. Originally introduced by Rosenthal (1979), it was recently adapted to ALE meta-analyses by Acar et al. (2018). This method is based on the hypothesis that there are unpublished studies with contra-evidence results, and allows to estimates the amount of these studies that can be added to the original data set before results get invalidated. In other words, the procedure introduces into the sample increasing amount of noise (i.e. unreported experiments). In the present work, the "fail-safe" technique has been used to address the possibility that in BrainMap an amount of contra-evidence experiments has not been stored.

Our analysis was based on the code developed by Acar et al. (2018) (https://github.com/NeuroStat/GenerateNull). The procedure consists of two steps: 1) noise generation; 2) robustness estimation.

Step 1: noise generation

The first step generates the required amount of noise experiments. In doing this, the algorithm is constrained by the distributions of the number of foci and the number of subjects of the real meta-analytic sample, in order to lend the noise realistic features. The foci are then randomly localized within the same GM mask used in the ALE algorithm.

Step 2: robustness estimation

At this point the noise and original experiments are combined and fed into the ALE algorithm. Results were tested for statistical significance with 1000 permutations. In other words, the second step is a replication of the meta-analysis now taking into account potential experiments "remained in the drawer". This procedure was iterated several times adding an increasing amount of noise experiments (between k/2 and 3k, where k is the number of the original experiments). Finally, Pearson's correlation was computed between the original

map and the ALE map obtained at each level of noise, in order to estimate the possible bias effect.

Results show that adding increasing amount of noise Pearson's correlation between the maps linearly decreases (Fig. S3). Nonetheless, even in the most extreme case (i.e. 300% of noise added) we still obtained r=0.65.

Leave-one-pathology-out analysis

The cross-disorder approach followed in the present work has two main advantages. First, it allows to consider a wide variety of pathological processes intervening in the different clinical conditions, rather than describing a specific case. Second, it maximizes the statistical power, allowing a more substantial data set. However, computing ALE on a cross-disorder input makes difficult to estimate the specific weight of each pathology, and in particular to detect the possible predominant (and biasing) effect of the most represented ones. In order to address this issue, we implemented a leave-one-out strategy, called "leave one pathology out". In particular, we recursively removed from the original data set all the experiments from a same disorder, and repeated the ALE analysis considering the remaining elements. Each of the obtained map was then correlated (Pearson's r) with the original whole sample co-alteration pattern. A marked reduction of the r value in a given iteration means the removal of the respective pathology caused a considerable modification of the alteration pattern, revealing a predominant disorder.

As showed in Table S5, the correlation values are overall strong, and the impact of a disorder does not seem to be related with the number of experiments removed.

Despite schizophrenia and multiple sclerosis standing out, running the analysis on only one of them would have not been comparable to our cross-disorder approach. In fact, the correlation between the ALE map for schizophrenia only (48 experiments) and the original co-alteration pattern was r=0.41. Coherently, the correlation between the ALE map for multiple sclerosis only (24 experiments) and the original co-alteration pattern was r=-0.14.

Finally, we assessed the overall impact of those disorders with less than 7 experiments, to verify if they were introducing some kind of noise to the data set. This implied the removal of 76 experiments (including the 51 categorized as 'Other'). The Pearson's correlation between the resulting ALE map and the original co-alteration pattern was r=0.75.

In light of all these analyses, we think the cross-disorder approach originally adopted, that allows to maximize the statistical power, confirmed its validity. In fact, it is neither dominated by singular pathologies, nor biased by noise coming from the scarcely represented clinical conditions, which instead bring informative data.

Supplementary figures

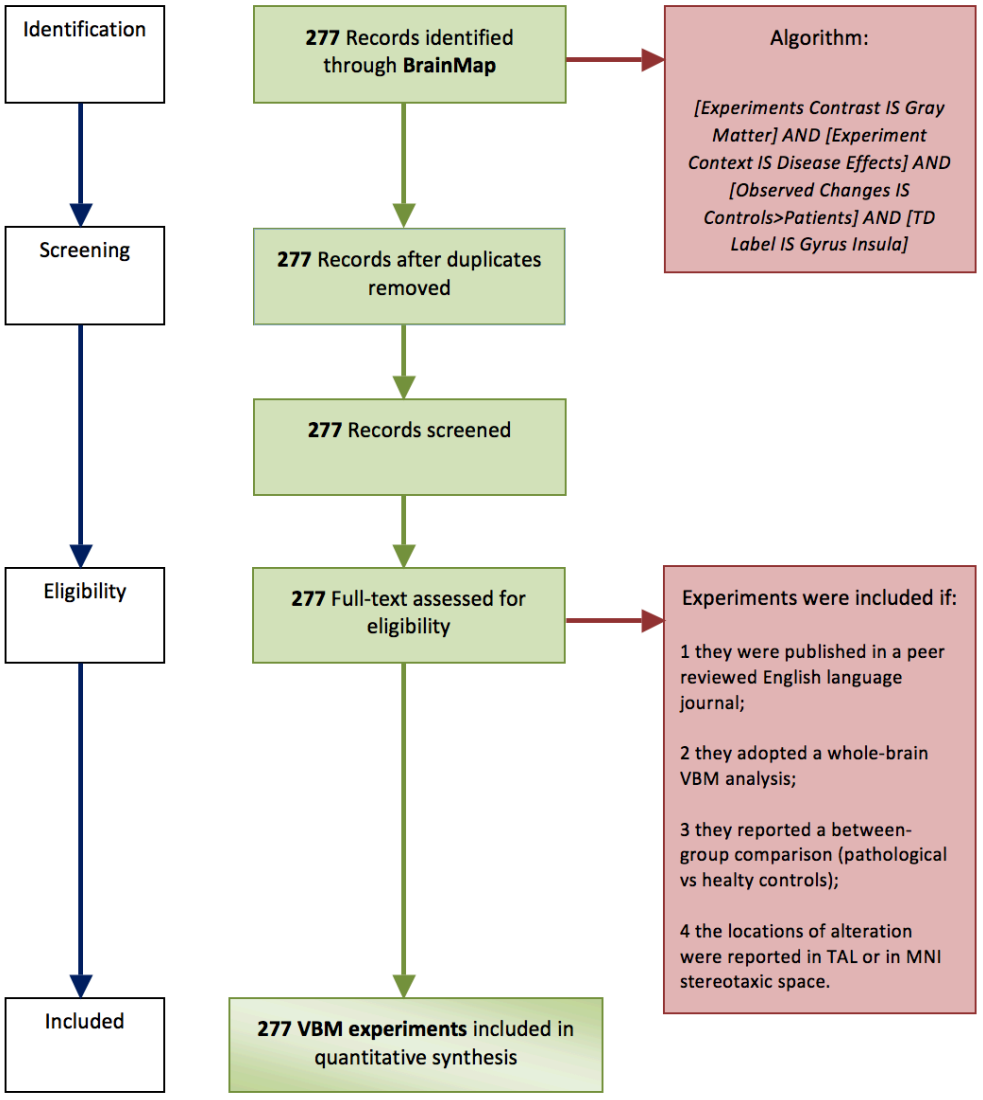

Figure S1: PRISMA flow diagram illustrating the selection of articles.

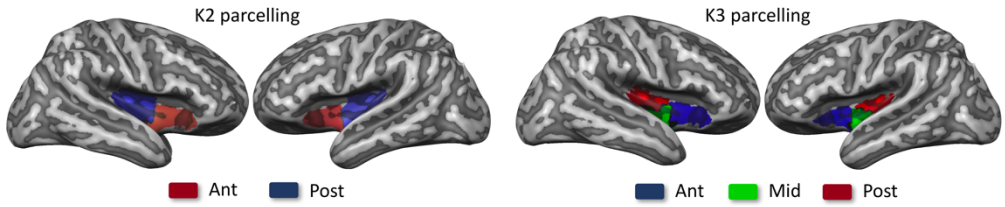

Figure S2: Visualization of the clustering solutions, as proposed by Kelly et al. (2012). K2: Red=anterior cluster (K2_ant); Blue=posterior cluster (K2_post). K3: Blue=anterior cluster (K3_ant); Green=middle cluster (K3_mid); Red=posterior cluster (K3_post).

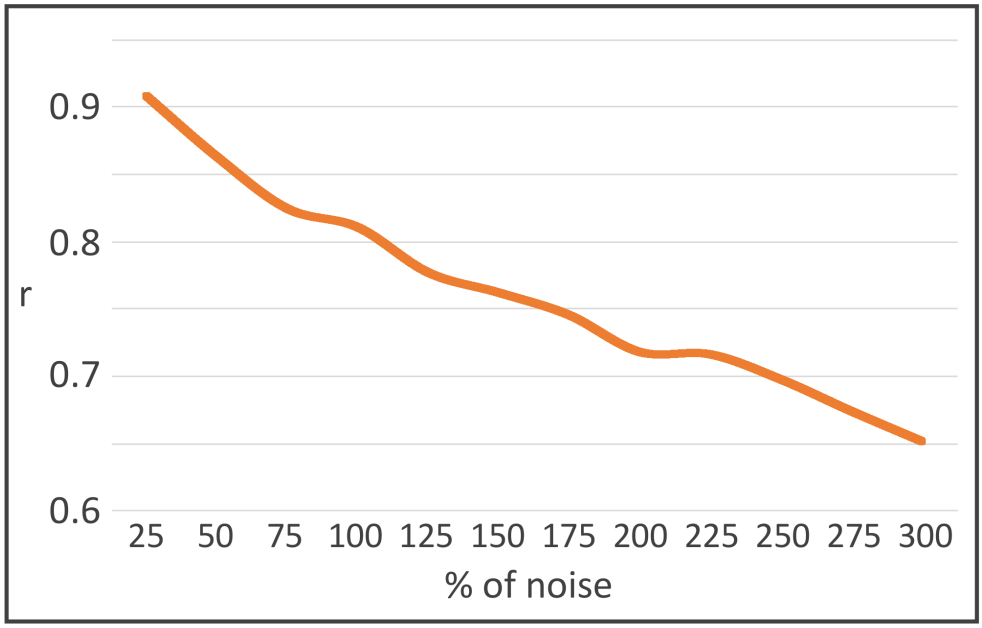

Figure S3: Fail-safe results. The addition of an increasing amount of contra-evidence experiments caused a linear reduction of Pearson's correlation between the original co-alteration pattern and those accounting for the "noise" injection.

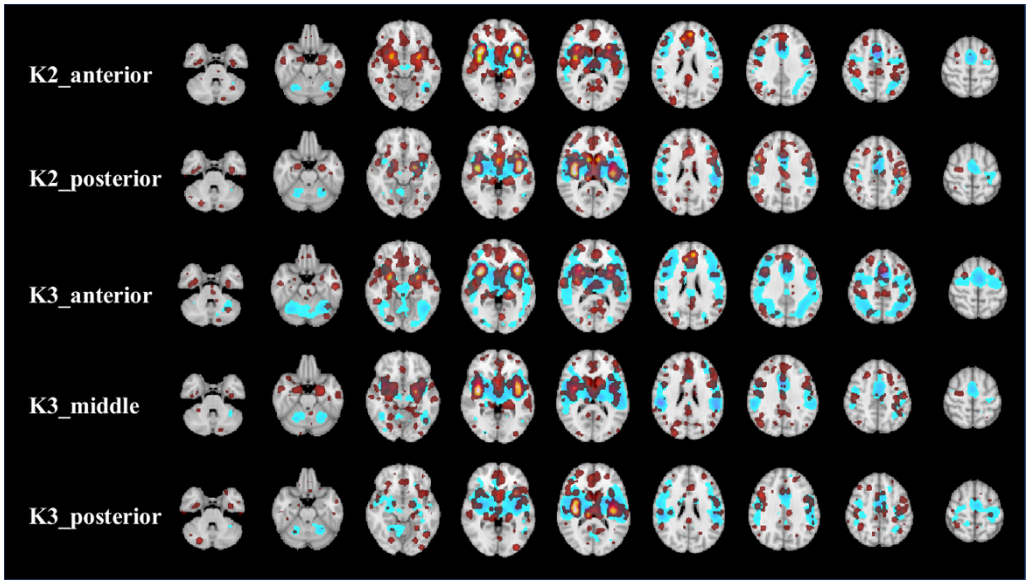

Figure S4: Overlap between co-atrophy (red) and functional MACM (blue).

Supplementary tables

ID	First Author	Year	Condition	Subj	Experiments
1	Adleman N E	2012	Bipolar disorder	55	1
2	Agosta F	2010	Supranuclear palsy	20	2
3	Agosta F	2011	Alzheimer's disease	15	1
4	Alcauter S	2011	Other	9	1
5	Antonova E	2005	Schizophrenia	40	1
6	Arnone D	2009	Depression	25	1
7	Asami T	2009	Panic/Anxiety disorder	9	1
8	Ash S	2011	Lewy body dementia	11	1
9	Ash S	2009	Other	13	2
10	Aubert-Broche B	2011	Multiple sclerosis	29	1
11	Audoin B	2007	Multiple sclerosis	38	1

12	Barbeau E	2008	Mild cognitive impairment	16	1
13	Baron J C	2001	Alzheimer's disease	32	4
14	Bassitt D P	2007	Schizophrenia	30	1
15	Baxter L C	2006	Alzheimer's disease	15	1
16	Bell-McGinty S	2005	Mild cognitive impairment	14	2
17	Bendfeldt K	2009	Multiple sclerosis	17	1
18	Bernasconi N	2004	Epilepsy	45	1
19	Bertsch K	2013	Other	25	2
20	Bitter T	2010	Olfactory disorders	41	2
21	Bitter T	2011	Olfactory disorders	22	1
22	Boccardi M	2005	Frontotemporal dementia	9	1
23	Boddaert N	2004	Other	5	1
24	Bodini B	2009	Multiple sclerosis	23	1
25	Boghi A	2011	Other	10	1
26	Bonavita S	2011	Multiple sclerosis	18	1
27	Bonilha L	2004	Epilepsy	22	1
28	Borgwardt S J	2007	At-risk mental state	22	1
29	Borgwardt S J	2010	Schizophrenia	9	1
30	Borgwardt S J	2007	At-risk mental state	12	1
31	Borroni B	2008	Other	20	1
32	Boxer A L	2006	Supranuclear palsy	15	1
33	Bozzali M	2006	Alzheimer's disease / Mild cognitive impairment	62	3
34	Brambati S M	2004	Other	10	1

35	Brambati S M	2009	Other	25	3
36	Brenneis C	2004	Supranuclear palsy	12	1
37	Brenneis C	2007	Multiple system atrophy	14	1
38	Brenneis C	2003	Other	9	1
39	Brenneis C	2006	Multiple system atrophy	22	2
40	Brenneis C	2003	Multiple system atrophy	12	1
41	Brenneis C	2004	Alzheimer's disease / Lewy body dementia	20	2
42	Brys M	2009	Alzheimer's disease	8	1
43	Burton E J	2002	Lewy body dementia	25	1
44	Burton E J	2004	Parkinson's disease	57	2
45	Cascella N	2010	Schizophrenia	38	2
46	Castro-Manglano P D	2011	Psychosis	38	2
47	Ceccarelli A	2009	Multiple sclerosis	17	1
48	Chang C C	2009	Multiple system atrophy	46	2
49	Chanraud S	2007	Other	28	1
50	Chen S	2006	Post-traumatic stress disorder	24	2
51	Chen S	2009	Post-traumatic stress disorder	12	1
52	Chua S E	2007	Psychosis	26	1
53	Cordato N J	2005	Supranuclear palsy	21	1
54	Critchley H D	2003	Other	15	1
55	de Araujo-Filho G M	2009	Epilepsy	16	1
56	de Oliveira-Souza R	2008	Other	15	1

57	Di Paola M	2007	Alzheimer's disease	18	1
58	Douaud G	2007	Schizophrenia	25	1
59	Farrow T F D	2007	Alzheimer's disease	14	2
60	Feldmann A	2008	Alzheimer's disease	6	1
61	Frisoni G B	2002	Alzheimer's disease	26	1
62	Fusar-Poli P	2011	At-risk mental state	15	1
63	Gale S D	2005	Other	18	2
64	Garcia-Marti G	2008	Schizophrenia	17	1
65	Garrido L	2009	Other	17	1
66	Gavazzi C	2007	Huntington's disease	9	1
67	Ghosh B C	2012	Supranuclear palsy	22	1
68	Giuliani N R	2005	Schizophrenia	34	1
69	Gobbi C	2014	Multiple sclerosis	336	5
70	Gong Q	2011	Depression	23	1
71	Gregory S	2012	Other	17	1
72	Grieve S M	2013	Depression	34	1
73	Guo X	2010	Alzheimer's disease	13	1
74	Ha T H	2010	Bipolar disorder	23	1
75	Ha T H	2004	Bipolar disorder	35	1
76	Han X	2017	Multiple sclerosis	20	1
77	Henley S M	2009	Huntington's disease	20	1
78	Herringa R	2012	Post-traumatic stress disorder	13	1
79	Hoeft F	2008	Other	18	1

80	Hoeft F	2007	Other	19	1
81	Honea R A	2008	Schizophrenia	169	1
82	Honea R A	2009	Alzheimer's disease	56	1
83	Horn H	2009	Schizophrenia	13	1
84	Huang W	2011	Epilepsy	31	1
85	Huey E D	2009	Other	14	1
86	Hulshoff Pol H E	2001	Schizophrenia	158	1
87	Hulshoff Pol H E	2004	Schizophrenia	158	1
88	Ille R	2011	Huntington's disease	18	1
89	Ivo R	2013	Other	14	1
90	Jang D P	2007	Other	20	1
91	Janssen J	2008	Psychosis	25	1
92	Jayakumar P N	2005	Schizophrenia	18	1
93	Kasai K	2008	Post-traumatic stress disorder	18	1
94	Kasparek T	2010	Schizophrenia	49	1
95	Kassubek J	2004	Huntington's disease	22	1
96	Kassubek J	2007	Amyotropic lateral sclerosis	12	1
97	Kaufmann C	2002	Other	12	1
98	Kawachi T	2006	Alzheimer's disease	30	1
99	Kawada R	2009	Schizophrenia	26	1
100	Kawasaki Y	2007	Schizophrenia	30	1
101	Kawasaki Y	2004	Schizophrenia	100	2
102	Kesler S R	2008	Other	30	4

103	Kim J H	2008	Migraine	20	1
104	Kim S	2011	Other	20	1
105	Kim S J	2009	Other	17	1
106	Koprivova J	2009	Obsessive-compulsive disorder	14	1
107	Kosaka H	2010	Other	32	1
108	Koutsouleris N	2008	Schizophrenia	230	4
109	Kubicki M	2002	Schizophrenia / Psychosis	32	2
110	Kuchinad A	2007	Other	10	1
111	Lai C H	2015	Panic/Anxiety disorder	53	1
112	Lee J E	2013	Mild cognitive impairment	30	2
113	Leung K K	2009	Depression	17	1
114	Libon D J	2009	Frontotemporal dementia	62	2
115	Lin C H	2013	Parkinson's disease	20	2
116	Lin K	2009	Epilepsy	60	2
117	Lochhead R A	2004	Bipolar disorder	4	1
118	Lui S	2009	Schizophrenia	20	2
119	Lyoo I K	2004	Bipolar disorder	39	1
120	Maneru C	2003	Other	13	1
121	Marcelis M	2003	Psychosis	58	2
122	Marti-Bonmati L	2007	Schizophrenia	10	1
123	Matsuda H	2002	Alzheimer's disease	15	1
124	McAlonan G M	2008	Autism spectrum disorder	33	2
125	McIntosh A M	2004	Bipolar disorder	19	1

126	Meda S A	2008	Schizophrenia	163	3
127	Meisenzahl E M	2008	Schizophrenia	306	4
128	Mesaros S	2008	Multiple sclerosis	21	1
129	Mezzapesa D M	2007	Amyotropic lateral sclerosis	9	1
130	Milham M P	2005	Panic/Anxiety disorder	17	1
131	Minnerop M	2007	Multiple system atrophy	16	1
132	Molina V	2011	Schizophrenia	30	1
133	Moorhead T W	2005	Schizophrenia	23	1
134	Morgen K	2006	Multiple sclerosis	19	1
135	Muhlau M	2007	Huntington's disease	46	1
136	Muhlau M	2013	Multiple sclerosis	49	1
137	Nardo D	2010	Post-traumatic stress disorder	10	2
138	Narita K	2011	Bipolar disorder	14	1
139	Neckelmann G	2006	Schizophrenia	12	1
140	Nestor P J	2003	Other	10	1
141	O'Daly O	2007	Schizophrenia	28	1
142	Obermann M	2013	Other	98	2
143	Padovani A	2006	Supranuclear palsy	14	1
144	Paillere-Martinot M L	2001	Schizophrenia	20	1
145	Peinemann A	2005	Huntington's disease	75	3
146	Pell G S	2008	Epilepsy	19	1
147	Peng J	2010	Depression	22	1
148	Pereira J B	2009	Parkinson's disease	20	1

149	Pereira J M	2009	Frontotemporal dementia / Other	27	5
150	Petrie E C	2014	Other	18	1
151	Preziosa P	2016	Multiple sclerosis	38	1
152	Price G	2010	Schizophrenia	47	1
153	Prinster A	2006	Multiple sclerosis	34	1
154	Prinster A	2010	Multiple sclerosis	35	1
155	Pujol J	2004	Obsessive-compulsive disorder	72	1
156	Quarantelli M	2006	Other	30	1
157	Rabinovici G D	2007	Other	18	1
158	Riccitelli G	2012	Multiple sclerosis	312	4
159	Riederer F	2008	Epilepsy	12	1
160	Riederer F	2012	Migraine	29	1
161	Riva D	2011	Autism spectrum disorder	21	1
162	Rocca M A	2006	Migraine	45	3
163	Rossi R	2006	Other	14	1
164	Rossi R	2012	Other	40	2
165	Rowan A	2007	Other	10	1
166	Salmond C H	2007	Autism spectrum disorder	9	1
167	Santana M	2010	Epilepsy	90	3
168	Saykin A J	2006	Mild cognitive impairment	40	1
169	Scheuerecker J	2010	Depression	13	1
170	Schiffer B	2013	Schizophrenia	73	3
171	Schmidt-Wilcke T	2010	Other	11	1

172	Schmidt-Wilcke T	2008	Migraine	31	1
173	Schmidt-Wilcke T	2005	Migraine	20	1
174	Schwartz D L	2010	Other	44	1
175	Seeley W W	2008	Frontotemporal lobar degeneration	45	3
176	Senda J	2011	Amyotropic lateral sclerosis	17	1
177	Serra-Blasco M	2013	Depression	44	2
178	Shad M U	2012	Depression	22	1
179	Shapleske J	2002	Schizophrenia	63	2
180	Shiino A	2006	Alzheimer's disease	40	1
181	Shin S	2012	Parkinson's disease	25	1
182	Sowell E R	2001	Other	7	1
183	Spano B	2010	Multiple sclerosis	10	1
184	Stratmann M	2014	Depression	229	2
185	Sydykova D	2007	Alzheimer's disease	13	1
186	Takahashi R	2011	Frontotemporal dementia / Supranuclear palsy	32	2
187	Tang L R	2014	Bipolar disorder	27	1
188	Tiihonen J	2008	Other	25	1
189	Tir M	2009	Parkinson's disease	14	1
190	Tregallas J R	2007	Schizophrenia	32	1
191	Tzarouchi L C	2010	Multiple system atrophy	11	1
192	Wang F	2011	Bipolar disorder	41	1
193	Wei W	2016	Epilepsy	30	1

194	Whitwell J L	2005	Frontotemporal dementia	9	1
195	Whitwell J L	2013	Supranuclear palsy	16	1
196	Wolf R C	2008	Schizophrenia	14	1
197	Wolf R C	2009	Huntington's disease	12	1
198	Xie S	2006	Alzheimer's disease	13	1
199	Xu L	2009	Schizophrenia	120	1
200	Yamada M	2007	Schizophrenia	20	1
201	Yang F C	2013	Migraine	23	1
202	Yasuda C L	2010	Epilepsy	44	2
203	Yasuda C L	2010	Epilepsy	40	1
204	Yoo S Y	2008	Obsessive-compulsive disorder	47	1
205	Zamboni G	2008	Frontotemporal dementia	14	1
206	Zhang T	2009	Depression	15	1
207	Zhang X	2016	Multiple sclerosis	29	1
			Total	**7218**	**277**

Table S1: Selected studies for the meta-analysis. The items shown in the table are the result of the entire selection process (Search 1) as shown in the PRISMA flow chart (Figure S1) and in the supplementary literature analysis. The starting point for the selection can be traced in the algorithms and in the additional considerations previously proposed. The number of subjects refers to the pathological samples only.

Condition	Experiments	% of exp.	Subjects	% of subj.
Schizophrenia	48	17.3	2094	29.1
Multiple sclerosis	24	8.6	1072	14.8

Alzheimer's disease	22	7.9	396	5.5
Epilepsy	15	5.4	409	5.7
Depression	12	4.3	444	6.1
Frontotemporal dementia	9	3.2	131	1.8
Bipolar disorder	9	3.2	257	3.6
Huntington's disease	9	3.2	202	2.8
Supranuclear palsy	9	3.2	136	1.9
Multiple system atrophy	8	2.9	95	1.3
Migraine	8	2.9	168	2.3
Psychosis	7	2.6	163	2.2
Mild cognitive impairment	7	2.6	122	1.7
Parkinson's disease	7	2.6	136	2
Post-traumatic stress disorder	7	2.6	77	1
Autism spectrum disorder	4	1.4	63	0.9
Frontotemporal lobe degeneration	3	1.1	45	0.6
Obsessive-compulsive disorder	3	1.1	133	1.8
Lewy body dementia	3	1.1	46	0.6
Olfactory disorders	3	1.1	63	0.9
Panic/Anxiety disorder	3	1.1	79	1.1
At-risk mental state	3	1.1	49	0.7
Amyotrophic lateral scerosis	3	1.1	38	0.5
Other	51	18.4	800	11.1
Total	**277**	**100**	**7218**	**100**

Table S2: Details of the repartition of experiments and pathological subjects across the disorders represented in the dataset. The percentages are based on the total number of experiments and subjects in the dataset respectively.

Paradigm Class	K2_ant	K2_post	K3_ant	K3_mid	K3_post
Acupuncture	5	6	5	5	3
Affective pictures	17	10	15	6	5

Affective words	2	1	2	0	1
Anti-saccades	1	0	1	0	0
Chewing/swallowing	12	4	7	8	3
Classical conditioning	13	4	10	3	4
Competition/cooperation	3	0	3	0	0
Counting/calculation	23	5	22	3	3
Cued explicit recognition/recall	25	13	21	9	8
Deception	3	1	2	1	1
Delay discounting	0	2	0	0	2
Delayed match to sample	27	5	26	5	2
Divided auditory attention	5	1	4	2	0
Drawing	1	2	1	0	2
Driving	1	1	1	1	0
Emotion induction	27	18	22	18	8
Emotional body language perception	3	0	3	0	0
Encoding	13	3	13	1	2
Episodic recall	5	4	5	3	1
Face monitoring/discrimination	37	26	24	27	12
Figurative language	0	1	0	1	0
Film viewing	36	16	26	24	5
Finger tapping/button press	107	48	96	39	24

Fixation	1	2	0	2	1
Flanker	4	1	4	1	0
Flexion/extension	10	11	5	8	8
Fluency induction	0	0	0	0	0
Free list word record	1	2	0	1	2
Gambling	18	5	15	4	4
Go/No go	41	18	40	12	11
Grasping	2	1	2	0	1
Hand-Eye coordination	0	2	0	1	1
Hypercapnia/air hunger	4	0	1	3	0
Imagined movement	8	1	7	3	0
Imagined objects/scenes	4	4	4	3	1
Induced panic	0	1	0	1	0
Isometric force	3	3	3	2	1
Lexical decision	2	1	2	1	0
Magnitude comparison (distance)	0	1	0	1	0
Magnitude comparison (luminance)	1	0	1	0	0
Magnitude comparison (symbolic)	2	0	2	0	0
Meditation	2	5	1	5	1
Mental rotation	1	1	1	0	1
Micturition	5	2	5	1	1

Motor learning	3	0	3	0	0
Multi tasking	1	0	1	0	0
Music comprehension	29	11	24	12	5
Music production	6	1	5	2	0
N-back	23	2	23	0	2
Naming (covert)	11	0	10	1	0
Naming (overt)	6	3	5	1	3
Oddball discrimination	8	2	8	2	1
Olfactory monitoring/discrimination	11	8	7	10	2
Orthographic discrimination	8	1	7	2	0
Pain monitor/discrimination	116	77	93	57	56
Paired associate recall	7	4	7	1	3
Passive listening	7	5	6	4	2
Passive viewing	42	26	28	25	13
Phonological discrimination	17	0	15	2	0
Pitch monitor/discrimination	8	4	7	3	2
Reading (covert)	7	2	6	1	2
Reading (overt)	13	4	13	0	4
Reasoning/problem solving	14	5	12	4	3
Recitation/repetition (covert)	3	0	2	1	0
Recitation/repetition (overt)	9	4	5	5	3

Rest	0	2	0	2	0
Reward	89	23	81	17	14
Saccades	5	2	4	2	1
Self-reflection	3	0	3	0	0
Semantic monitor/discrimination	45	11	37	12	8
Sequence recall/learning	6	1	5	1	0
Sexual arousal/gratification	22	14	16	14	6
Stroop - color	12	4	12	0	4
Stroop - emotional	0	1	0	0	1
Stroop - spatial	1	0	1	0	0
Syntactic discrimination	1	0	0	1	0
Tactile monitor/discrimination	11	16	7	10	10
Task switching	4	5	4	3	2
Taste	14	5	13	5	3
Theory of mind	6	7	5	4	5
Thirst induction	0	1	0	0	1
Tone monitor/discrimination	18	4	16	7	0
Tower of London	3	0	1	2	0
Transcranial magnetic stimulation	3	3	2	1	3
Trauma recall	1	0	0	1	0
Vestibular stimulation	1	2	1	0	2

Vibrotactile monitor/discrimination	0	1	0	0	1
Video games	1	1	1	1	0
Visual motion	3	0	3	1	0
Visual object identification	12	7	10	4	5
Visual pursuit/tracker	5	1	5	1	0
Visuospatial attention	30	7	25	11	2
Wisconsin card sorting test	4	0	4	0	0
Word generation (covert)	14	3	14	2	1
Word generation (overt)	10	4	10	0	4
Word stem completion (covert)	2	0	2	0	0
Word stem completion (overt)	1	0	1	0	0
Total	**1151**	**516**	**972**	**440**	**293**

Table S3: Details of the fMRI paradigms included in the functional data retrieved through Search 3.

Brain region	% of experiments
Middle frontal gyrus	10.1
Superior temporal gyrus	9.5
Parahippocampal gyrus	9.5
Medial frontal gyrus	9.0
Inferior frontal gyrus	8.9
Insula	8.8
Thalamus	8.1
Middle temporal gyrus	7.8
Precentral gyrus	7.7
Superior frontal gyrus	7.5

Cingulate gyrus	6.4
Caudate	6.3
Postcentral gyrus	5.4
Anterior cingulate	5.0
Precuneus	5.0
Inferior parietal lobule	4.9
Lentiform nucleus	4.4
Sub-gyral	4.3
Inferior temporal gyrus	3.8
Claustrum	3.6
Culmen	3.5
Fusiform Gyrus	3.4
Uncus	3.3
Cuneus	3.2
Middle occipital gyrus	3.0
Cerebellar tonsill	2.9
Posterior cingulate	2.5
Declive	2.4
Lingual gyrus	2.3
Superior parietal lobule	1.7
Paracentral lobule	1.5
Inferior semi-lunar lobule	1.3
Subcallosal gyrus	1.3
Supramarginal gyrus	1.1
Transverse temporal gyrus	1.1
Inferior occipital gyrus	1.0
Angular gyrus	1.0
Pyramis	0.9
Tuber	0.7
Rectal gyrus	0.7
Extra-nuclear	0.6
Uvula	0.6
Orbital gyrus	0.4
Superior occipital gyrus	0.4
Cerebellar lingual	0.2
Fastigium	0.1

Culmen of vermis	0.1
Nodule	0.1
Declive of vermis	0.0
Pyramis of vermis	0.0
Tuber of vermis	0.0
Uvula of vermis	0.0

Table S4: Results of the frequency of alteration analysis. Frequency of alteration for each brain region listed in the BrainMap database. The percent is computed with respect to the total number of VBM experiments included in BrainMap at the moment of the analysis.

Removed Disorder	**r**	**n Of Removed Experiments**
Schizophrenia	0.63	48
Multiple sclerosis	0.65	24
Other	0.80	51
Alzheimer's disease	0.81	22
Epilepsy	0.85	15
Huntington's disease	0.87	9
Frontotemporal lobar degeneration	0.88	3
Depression	0.89	12
Multiple system atrophy	0.89	8
Supranuclear palsy	0.89	9
Migraine	0.89	8
Parkinson's disease	0.90	7
Mild cognitive impairment	0.90	7
Bipolar disorder	0.91	9
Frontotemporal dementia	0.91	9
Post traumatic stress disorder	0.91	7
Lewy body dementia	0.91	3
Psychosis	0.91	7
Olfactory disorders	0.92	3
Obsessive compulsive disorder	0.92	3
Autism spectrum disorder	0.92	4
At risk mental state	0.92	3

Amyotropic lateral sclerosis	0.92	3
Panic/Anxiety disorder	0.93	3

Table S5: Results of the leave-one-pathology-out analysis. Pearson's correlation between the original co-alteration pattern and the co-alteration patterns obtained after the removal of all the experiments of a given disorder.

References

Abdelnour, F., Voss, H.U., Raj, A., 2014. Network diffusion accurately models the relationship between structural and functional brain connectivity networks. Neuroimage 90, 335-347.

Ahmed, R.M., Devenney, E.M., Irish, M., Ittner, A., Naismith, S., Ittner, L.M., Rohrer, J.D., Halliday, G.M., Eisen, A., Hodges, J.R., Kiernan, M.C., 2016. Neuronal network disintegration: common pathways linking neurodegenerative diseases. J Neurol Neurosurg Psychiatry.

Alcauter, S., Lin, W., Keith Smith, J., Gilmore, J.H., Gao, W., 2015. Consistent anterior-posterior segregation of the insula during the first 2 years of life. Cereb Cortex 25, 1176-1187.

Allman, J.M., Watson, K.K., Tetreault, N.A., Hakeem, A.Y., 2005. Intuition and autism: a possible role for Von Economo neurons. Trends Cogn Sci 9, 367-373.

Ashburner, J., Friston, K.J., 2001. Why voxel-based morphometry should be used. Neuroimage 14, 1238-1243.

Bartra, O., McGuire, J.T., Kable, J.W., 2013. The valuation system: a coordinate-based meta-analysis of BOLD fMRI experiments examining neural correlates of subjective value. Neuroimage 76, 412-427.

Behrens, T.E., Fox, P., Laird, A., Smith, S.M., 2013. What is the most interesting part of the brain? Trends Cogn Sci 17, 2-4.

Buckholtz, J.W., Meyer-Lindenberg, A., 2012. Psychopathology and the human connectome: toward a transdiagnostic model of risk for mental illness. Neuron 74, 990-1004.

Buckner, R.L., Sepulcre, J., Talukdar, T., Krienen, F.M., Liu, H., Hedden, T., Andrews-Hanna, J.R., Sperling, R.A., Johnson, K.A., 2009. Cortical hubs revealed by intrinsic functional connectivity: mapping, assessment of stability, and relation to Alzheimer's disease. J Neurosci 29, 1860-1873.

Burton, E.J., Karas, G., Paling, S.M., Barber, R., Williams, E.D., Ballard, C.G., McKeith, I.G., Scheltens, P., Barkhof, F., O'Brien, J.T., 2002. Patterns of cerebral atrophy in dementia with Lewy bodies using voxel-based morphometry. Neuroimage 17, 618-630.

Caspi, A., Houts, R.M., Belsky, D.W., Goldman-Mellor, S.J., Harrington, H., Israel, S., Meier, M.H., Ramrakha, S., Shalev, I., Poulton, R., Moffitt, T.E., 2014. The p Factor: One General Psychopathology Factor in the Structure of Psychiatric Disorders? Clin Psychol Sci 2, 119-137.

Cauda, F., Costa, T., Nani, A., Fava, L., Palermo, S., Bianco, F., Duca, S., Tatu, K., Keller, R., 2017. Are schizophrenia, autistic, and obsessive spectrum disorders dissociable on the basis of neuroimaging morphological findings?: A voxel-based meta-analysis. Autism Research, n/a-n/a.

Cauda, F., Costa, T., Torta, D.M., Sacco, K., D'Agata, F., Duca, S., Geminiani, G., Fox, P.T., Vercelli, A., 2012a. Meta-analytic clustering of the insular cortex: characterizing the meta-analytic connectivity of the insula when involved in active tasks. Neuroimage 62, 343-355.

Cauda, F., D'Agata, F., Sacco, K., Duca, S., Geminiani, G., Vercelli, A., 2011. Functional connectivity of the insula in the resting brain. Neuroimage 55, 8-23.

Cauda, F., Geminiani, G.C., Vercelli, A., 2014. Evolutionary appearance of von Economo's neurons in the mammalian cerebral cortex. Front Hum Neurosci 8, 104.

Cauda, F., Nani, A., Costa, T., Palermo, S., Tatu, K., Manuello, J., Duca, S., Fox, P.T., Keller, R., 2018a. The morphometric co-atrophy networking of schizophrenia, autistic and obsessive spectrum disorders. Hum Brain Mapp.

Cauda, F., Nani, A., Liloia, D., Manuello, J., Premi, E., Duca, S., Fox, P.T., Costa, T., 2020. Finding specificity in structural brain alterations through Bayesian reverse inference. Hum Brain Mapp n/a.

Cauda, F., Mancuso, L., Nani, A., Costa, T., 2019a. Heterogeneous neuroimaging findings, damage propagation and connectivity: an integrative view. Brain 142.

Cauda, F., Nani, A., Manuello, J., Liloia, D., Tatu, K., Vercelli, U., Duca, S., Fox, P.T., Costa, T., 2019b. The alteration landscape of the cerebral cortex. Neuroimage 184, 359-371.

Cauda, F., Nani, A., Manuello, J., Premi, E., Palermo, S., Tatu, K., Duca, S., Fox, P.T., Costa, T., 2018b. Brain structural alterations are distributed following functional, anatomic and genetic connectivity. Brain 141, 3211-3232.

Cauda, F., Palermo, S., Costa, T., Torta, R., Duca, S., Vercelli, U., Geminiani, G., Torta, D.M., 2014. Gray matter alterations in chronic pain: A network-oriented meta-analytic approach. Neuroimage Clin 4, 676-686.

Cauda, F., Torta, D.M., Sacco, K., D'Agata, F., Geda, E., Duca, S., Geminiani, G., Vercelli, A., 2013. Functional anatomy of cortical areas characterized by Von Economo neurons. Brain Struct Funct 218, 1-20.

Cauda, F., Torta, D.M., Sacco, K., Geda, E., D'Agata, F., Costa, T., Duca, S., Geminiani, G., Amanzio, M., 2012b. Shared "core" areas between the pain and other task-related networks. PLoS One 7, e41929.

Cauda, F., Vercelli, A., 2013. How many clusters in the insular cortex? Cereb Cortex 23, 2779-2780.

Chang, L.J., Yarkoni, T., Khaw, M.W., Sanfey, A.G., 2013. Decoding the role of the insula in human cognition: functional parcellation and large-scale reverse inference. Cereb Cortex 23, 739-749.

Chen, A.C., Oathes, D.J., Chang, C., Bradley, T., Zhou, Z.W., Williams, L.M., Glover, G.H., Deisseroth, K., Etkin, A., 2013. Causal interactions between fronto-parietal central executive and default-mode networks in humans. Proc Natl Acad Sci U S A 110, 19944-19949.

Cole, M.W., Repovs, G., Anticevic, A., 2014. The frontoparietal control system: a central role in mental health. Neuroscientist 20, 652-664.

Craig, A.D., 2002. How do you feel? Interoception: the sense of the physiological condition of the body. Nat Rev Neurosci 3, 655-666.

Craig, A.D., 2003. Interoception: the sense of the physiological condition of the body. Curr Opin Neurobiol 13, 500-505.

Crossley, N.A., Fox, P.T., Bullmore, E.T., 2016a. Meta-connectomics: human brain network and connectivity meta-analyses. Psychol Med 46, 897-907.

Crossley, N.A., Mechelli, A., Ginestet, C., Rubinov, M., Bullmore, E.T., McGuire, P., 2016b. Altered Hub Functioning and Compensatory Activations in the Connectome: A Meta-Analysis of Functional Neuroimaging Studies in Schizophrenia. Schizophr Bull 42, 434-442.

Crossley, N.A., Scott, J., Ellison-Wright, I., Mechelli, A., 2015. Neuroimaging distinction between neurological and psychiatric disorders. Br J Psychiatry 207, 429-434.

Crossley, N.A., Mechelli, A., Scott, J., Carletti, F., Fox, P.T., McGuire, P., Bullmore, E.T., 2014. The hubs of the human connectome are generally implicated in the anatomy of brain disorders. Brain 137, 2382-2395.

Di Martino, A., Ross, K., Uddin, L.Q., Sklar, A.B., Castellanos, F.X., Milham, M.P., 2009. Functional brain correlates of social and nonsocial processes in autism spectrum disorders: an activation likelihood estimation meta-analysis. Biol Psychiatry 65, 63-74.

Dosenbach, N.U., Fair, D.A., Miezin, F.M., Cohen, A.L., Wenger, K.K., Dosenbach, R.A., Fox, M.D., Snyder, A.Z., Vincent, J.L., Raichle, M.E., Schlaggar, B.L., Petersen, S.E., 2007. Distinct brain networks for adaptive and stable task control in humans. Proc Natl Acad Sci U S A 104, 11073-11078.

Douaud, G., Groves, A.R., Tamnes, C.K., Westlye, L.T., Duff, E.P., Engvig, A., Walhovd, K.B., James, A., Gass, A., Monsch, A.U., Matthews, P.M., Fjell, A.M., Smith, S.M., Johansen-Berg, H., 2014. A common brain network links development, aging, and vulnerability to disease. Proc Natl Acad Sci U S A 111, 17648-17653.

Du, A.T., Schuff, N., Kramer, J.H., Rosen, H.J., Gorno-Tempini, M.L., Rankin, K., Miller, B.L., Weiner, M.W., 2007. Different regional patterns of cortical thinning in Alzheimer's disease and frontotemporal dementia. Brain 130, 1159-1166.

Eickhoff, S.B., Bzdok, D., Laird, A.R., Kurth, F., Fox, P.T., 2012. Activation likelihood estimation meta-analysis revisited. Neuroimage 59, 2349-2361.

Eickhoff, S.B., Laird, A.R., Fox, P.M., Lancaster, J.L., Fox, P.T., 2017. Implementation errors in the GingerALE Software: Description and recommendations. Hum Brain Mapp 38, 7-11.

Eickhoff, S.B., Laird, A.R., Grefkes, C., Wang, L.E., Zilles, K., Fox, P.T., 2009. Coordinate-based activation likelihood estimation meta-analysis of neuroimaging data: a random-effects approach based on empirical estimates of spatial uncertainty. Hum Brain Mapp 30, 2907-2926.

Eickhoff, S.B., Nichols, T.E., Laird, A.R., Hoffstaedter, F., Amunts, K., Fox, P.T., Bzdok, D., Eickhoff, C.R., 2016. Behavior, sensitivity, and power of activation likelihood estimation characterized by massive empirical simulation. Neuroimage 137, 70-85.

Ellison-Wright, I., Bullmore, E., 2010. Anatomy of bipolar disorder and schizophrenia: a meta-analysis. Schizophr Res 117, 1-12.

Etkin, A., Prater, K.E., Schatzberg, A.F., Menon, V., Greicius, M.D., 2009. Disrupted amygdalar subregion functional connectivity and evidence of a compensatory network in generalized anxiety disorder. Arch Gen Psychiatry 66, 1361-1372.

Fathy, Y.Y., Hoogers, S.E., Berendse, H.W., van der Werf, Y.D., Visser, P.J., de Jong, F.J., van de Berg, W.D.J., 2019. Differential insular cortex sub-regional atrophy in neurodegenerative diseases: a systematic review and meta-analysis. Brain Imaging Behav.

Fjell, A.M., Amlien, I.K., Sneve, M.H., Grydeland, H., Tamnes, C.K., Chaplin, T.A., Rosa, M.G., Walhovd, K.B., 2015. The Roots of Alzheimer's Disease: Are High-Expanding Cortical Areas Preferentially Targeted?dagger. Cereb Cortex 25, 2556-2565.

Foland, L.C., Altshuler, L.L., Bookheimer, S.Y., Eisenberger, N., Townsend, J., Thompson, P.M., 2008. Evidence for deficient modulation of amygdala response by prefrontal cortex in bipolar mania. Psychiatry Res 162, 27-37.

Fornito, A., Zalesky, A., Breakspear, M., 2015. The connectomics of brain disorders. Nat Rev Neurosci 16, 159-172.

Fox, P.T., Laird, A.R., Fox, S.P., Fox, P.M., Uecker, A.M., Crank, M., Koenig, S.F., Lancaster, J.L., 2005. BrainMap taxonomy of experimental design: description and evaluation. Hum Brain Mapp 25, 185-198.

Fox, P.T., Lancaster, J.L., 2002. Opinion: Mapping context and content: the BrainMap model. Nat Rev Neurosci 3, 319-321.

Frisoni, G.B., Fox, N.C., Jack, C.R., Jr., Scheltens, P., Thompson, P.M., 2010. The clinical use of structural MRI in Alzheimer disease. Nat Rev Neurol 6, 67-77.

Gardini, S., Venneri, A., Sambataro, F., Cuetos, F., Fasano, F., Marchi, M., Crisi, G., Caffarra, P., 2015. Increased functional connectivity in the default mode network in mild cognitive impairment: a maladaptive compensatory mechanism associated with poor semantic memory performance. J Alzheimers Dis 45, 457-470.

Goodkind, M., Eickhoff, S.B., Oathes, D.J., Jiang, Y., Chang, A., Jones-Hagata, L.B., Ortega, B.N., Zaiko, Y.V., Roach, E.L., Korgaonkar, M.S., Grieve, S.M., Galatzer-Levy, I., Fox, P.T., Etkin, A., 2015. Identification of a common neurobiological substrate for mental illness. JAMA Psychiatry 72, 305-315.

Goulden, N., Khusnulina, A., Davis, N.J., Bracewell, R.M., Bokde, A.L., McNulty, J.P., Mullins, P.G., 2014. The salience network is responsible for switching between the default mode network and the central executive network: replication from DCM. Neuroimage 99, 180-190.

Hamilton, J.P., Etkin, A., Furman, D.J., Lemus, M.G., Johnson, R.F., Gotlib, I.H., 2012. Functional neuroimaging of major depressive disorder: a meta-analysis and new integration of base line activation and neural response data. Am J Psychiatry 169, 693-703.

Honey, C.J., Sporns, O., Cammoun, L., Gigandet, X., Thiran, J.P., Meuli, R., Hagmann, P., 2009. Predicting human resting-state functional connectivity from structural connectivity. Proc Natl Acad Sci U S A 106, 2035-2040.

Igata, N., Kakeda, S., Watanabe, K., Ide, S., Kishi, T., Abe, O., Igata, R., Katsuki, A., Iwata, N., Yoshimura, R., Korogi, Y., 2017. Voxel-based morphometric brain comparison between healthy subjects and major depressive disorder patients in Japanese with the s/s genotype of 5-HTTLPR. Sci Rep 7, 3931.

Iturria-Medina, Y., Evans, A.C., 2015. On the central role of brain connectivity in neurodegenerative disease progression. Front Aging Neurosci 7, 90.

Iturria-Medina, Y., Sotero, R.C., Toussaint, P.J., Evans, A.C., 2014. Epidemic spreading model to characterize misfolded proteins propagation in aging and associated neurodegenerative disorders. PLoS Comput Biol 10, e1003956.

Jagust, W., 2013. Vulnerable neural systems and the borderland of brain aging and neurodegeneration. Neuron 77, 219-234.

Jones, D.T., Knopman, D.S., Gunter, J.L., Graff-Radford, J., Vemuri, P., Boeve, B.F., Petersen, R.C., Weiner, M.W., Jack, C.R., Jr., 2016. Cascading network failure across the Alzheimer's disease spectrum. Brain 139, 547-562.

Kapur, S., 2003. Psychosis as a state of aberrant salience: a framework linking biology, phenomenology, and pharmacology in schizophrenia. Am J Psychiatry 160, 13-23.

Kelly, C., Toro, R., Di Martino, A., Cox, C.L., Bellec, P., Castellanos, F.X., Milham, M.P., 2012. A convergent functional architecture of the insula emerges across imaging modalities. Neuroimage 61, 1129-1142.

Klein, T.A., Ullsperger, M., Danielmeier, C., 2013. Error awareness and the insula: links to neurological and psychiatric diseases. Front Hum Neurosci 7, 14.

Klin, A., Jones, W., Schultz, R., Volkmar, F., 2003. The enactive mind, or from actions to cognition: lessons from autism. Philos Trans R Soc Lond B Biol Sci 358, 345-360.

Kuperberg, G.R., Broome, M.R., McGuire, P.K., David, A.S., Eddy, M., Ozawa, F., Goff, D., West, W.C., Williams, S.C.R., van der Kouwe, A.J.W., Salat, D.H., Dale, A.M., Fischl, B., 2003. Regionally Localized Thinning of the Cerebral Cortex in Schizophrenia. Arch Gen Psychiatry 60, 878-888.

Kurth, F., Zilles, K., Fox, P.T., Laird, A.R., Eickhoff, S.B., 2010. A link between the systems: functional differentiation and integration within the human insula revealed by meta-analysis. Brain Structure and Function 214, 519-534.

Laird, A.R., Fox, P.M., Price, C.J., Glahn, D.C., Uecker, A.M., Lancaster, J.L., Turkeltaub, P.E., Kochunov, P., Fox, P.T., 2005a. ALE meta-analysis: controlling the false discovery rate and performing statistical contrasts. Hum Brain Mapp 25, 155-164.

Laird, A.R., Lancaster, J.L., Fox, P.T., 2005b. BrainMap: the social evolution of a human brain mapping database. Neuroinformatics 3, 65-78.

Laird, A.R., Lancaster, J.L., Fox, P.T., 2009. Lost in localization? The focus is meta-analysis. Neuroimage 48, 18-20.

Lancaster, J.L., Laird, A.R., Eickhoff, S.B., Martinez, M.J., Fox, P.M., Fox, P.T., 2012. Automated regional behavioral analysis for human brain images. Front Neuroinform 6, 23.

Lancaster, J.L., Woldorff, M.G., Parsons, L.M., Liotti, M., Freitas, C.S., Rainey, L., Kochunov, P.V., Nickerson, D., Mikiten, S.A., Fox, P.T., 2000. Automated Talairach atlas labels for functional brain mapping. Hum Brain Mapp 10, 120-131.

Lee, H., Heller, A.S., van Reekum, C.M., Nelson, B., Davidson, R.J., 2012. Amygdala-prefrontal coupling underlies individual differences in emotion regulation. Neuroimage 62, 1575-1581.

Lee, S.-Y., Chen, M.-H., Chiang, P.-L., Chen, H.-L., Chou, K.-H., Chen, Y.-C., Yu, C.-C., Tsai, N.-W., Li, S.-H., Lu, C.-H., Lin, W.-C., 2018. Reduced gray matter volume and respiratory dysfunction in Parkinson's disease: a voxel-based morphometry study. BMC Neurology 18, 73.

Li, H., Chan, R.C., McAlonan, G.M., Gong, Q.Y., 2010. Facial emotion processing in schizophrenia: a meta-analysis of functional neuroimaging data. Schizophr Bull 36, 1029-1039.

Liloia, D., Cauda, F., Nani, A., Manuello, J., Duca, S., Fox, P.T., Costa, T., 2018. Low entropy maps as patterns of the pathological alteration specificity of brain regions: A meta-analysis dataset. Data Brief 21, 1483-1495.

Manuello, J., Nani, A., Cauda, F., 2018a. Attention, Salience, and self-awareness: The role of insula in meditation. In: Turgut, M., Yurttas, C., Shane Tubbs, R. (Eds.), Island of Reil (Insula) in the Human Brain. Springer Verlag, Berlin, pp. 213-221.

Manuello, J., Nani, A., Premi, E., Borroni, B., Costa, T., Tatu, K., Liloia, D., Duca, S., Cauda, F., 2018b. The Pathoconnectivity Profile of Alzheimer's Disease: A Morphometric Coalteration Network Analysis. Front Neurol 8.

Manuello, J., Vercelli, U., Nani, A., Costa, T., Cauda, F., 2016. Mindfulness meditation and consciousness: An integrative neuroscientific perspective. Conscious Cogn 40, 67-78.

Matsuda, H., 2013. Voxel-based Morphometry of Brain MRI in Normal Aging and Alzheimer's Disease. Aging Dis 4, 29-37.

McTeague, L.M., Huemer, J., Carreon, D.M., Jiang, Y., Eickhoff, S.B., Etkin, A., 2017. Identification of Common Neural Circuit Disruptions in Cognitive Control Across Psychiatric Disorders. American Journal of Psychiatry 174, 676-685.

McTeague, L.M., Goodkind, M.S., Etkin, A., 2016. Transdiagnostic impairment of cognitive control in mental illness. J Psychiatr Res 83, 37-46.

Medford, N., Critchley, H.D., 2010. Conjoint activity of anterior insular and anterior cingulate cortex: awareness and response. Brain Struct Funct 214, 535-549.

Menon, V., 2013. Developmental pathways to functional brain networks: emerging principles. Trends Cogn Sci 17, 627-640.

Menon, V., Uddin, L.Q., 2010. Saliency, switching, attention and control: a network model of insula function. Brain Struct Funct 214, 655-667.

Mesulam, M.M., Mufson, E.J., 1982. Insula of the old world monkey. III: Efferent cortical output and comments on function. J Comp Neurol 212, 38-52.

Mühlau, M., Wohlschläger, A.M., Gaser, C., Valet, M., Weindl, A., Nunnemann, S., Peinemann, A., Etgen, T., Ilg, R., 2009. Voxel-based morphometry in individual patients: a pilot study in early Huntington disease. AJNR Am J Neuroradiol 30, 539-543.

Muñoz-Ruiz, M., Hartikainen, P., Koikkalainen, J., Wolz, R., Julkunen, V., Niskanen, E., Herukka, S.K., Kivipelto, M., Vanninen, R., Rueckert, D., Liu, Y., Lötjönen, J., Soininen, H., 2012. Structural MRI in frontotemporal dementia: comparisons between hippocampal volumetry, tensor-based morphometry and voxel-based morphometry. PLoS One 7, e52531.

Namkung, H., Kim, S.-H., Sawa, A., 2017. The Insula: An Underestimated Brain Area in Clinical Neuroscience, Psychiatry, and Neurology. Trends Neurosci 40, 200-207.

Nieuwenhuys, R., 2012. The insular cortex: a review. Prog Brain Res 195, 123-163.

Niu, M., Wang, Y., Jia, Y., Wang, J., Zhong, S., Lin, J., Sun, Y., Zhao, L., Liu, X., Huang, L., Huang, R., 2017. Common and Specific Abnormalities in Cortical Thickness in Patients with Major Depressive and Bipolar Disorders. EBioMedicine 16, 162-171.

Palaniyappan, L., Liddle, P.F., 2012. Does the salience network play a cardinal role in psychosis? An emerging hypothesis of insular dysfunction. J Psychiatry Neurosci 37, 17-27.

Patel, R.S., Bowman, F.D., Rilling, J.K., 2006. A Bayesian approach to determining connectivity of the human brain. Hum Brain Mapp 27, 267-276.

Pereira, A.M., Campos, B.M., Coan, A.C., Pegoraro, L.F., de Rezende, T.J.R., Obeso, I., Dalgalarrondo, P., da Costa, J.C., Dreher, J.C., Cendes, F., 2018. Differences in Cortical Structure and Functional MRI Connectivity in High Functioning Autism. Front Neurol 9, 539.

Raj, A., Kuceyeski, A., Weiner, M., 2012. A network diffusion model of disease progression in dementia. Neuron 73, 1204-1215.

Ravits, J., 2014. Focality, stochasticity and neuroanatomic propagation in ALS pathogenesis. Exp Neurol 262 Pt B, 121-126.

Robinson, J.L., Laird, A.R., Glahn, D.C., Lovallo, W.R., Fox, P.T., 2010. Metaanalytic connectivity modeling: delineating the functional connectivity of the human amygdala. Hum Brain Mapp 31, 173-184.

Saxena, S., Caroni, P., 2011. Selective neuronal vulnerability in neurodegenerative diseases: from stressor thresholds to degeneration. Neuron 71, 35-48.

Schroeter, M.L., Raczka, K., Neumann, J., von Cramon, D.Y., 2008. Neural networks in frontotemporal dementia--a meta-analysis. Neurobiol Aging 29, 418-426.

Seeley, W.W., Crawford, R.K., Zhou, J., Miller, B.L., Greicius, M.D., 2009. Neurodegenerative diseases target large-scale human brain networks. Neuron 62, 42-52.

Seeley, W.W., Menon, V., Schatzberg, A.F., Keller, J., Glover, G.H., Kenna, H., Reiss, A.L., Greicius, M.D., 2007. Dissociable intrinsic connectivity networks for salience processing and executive control. J Neurosci 27, 2349-2356.

Seeley, W.W., Zhou, J., Kim, E.J., 2012. Frontotemporal dementia: what can the behavioral variant teach us about human brain organization? Neuroscientist 18, 373-385.

Seok, J.W., Cheong, C., 2020. Gray Matter Deficits and Dysfunction in the Insula Among Individuals With Intermittent Explosive Disorder. Front Psychiatry 11, 439.

Simons, L.E., Elman, I., Borsook, D., 2014. Psychological processing in chronic pain: a neural systems approach. Neurosci Biobehav Rev 39, 61-78.

Soloff, P., Nutche, J., Goradia, D., Diwadkar, V., 2008. Structural brain abnormalities in borderline personality disorder: A voxel-based morphometry study. Psychiatry Research: Neuroimaging 164, 223-236.

Sporns, O., Tononi, G., Kotter, R., 2005. The human connectome: A structural description of the human brain. PLoS Comput Biol 1, e42.

Sprooten, E., Rasgon, A., Goodman, M., Carlin, A., Leibu, E., Lee, W.H., Frangou, S., 2017. Addressing reverse inference in psychiatric neuroimaging: Meta-analyses of task-related brain activation in common mental disorders. Hum Brain Mapp 38, 1846-1864.

Sridharan, D., Levitin, D.J., Menon, V., 2008. A critical role for the right fronto-insular cortex in switching between central-executive and default-mode networks. Proc Natl Acad Sci U S A 105, 12569-12574.

Stephani, C., Fernandez-Baca Vaca, G., Maciunas, R., Koubeissi, M., Luders, H.O., 2011. Functional neuroanatomy of the insular lobe. Brain Struct Funct 216, 137-149.

Supekar, K., Menon, V., 2012. Developmental maturation of dynamic causal control signals in higher-order cognition: a neurocognitive network model. PLoS Comput Biol 8, e1002374.

Tatu, K., Costa, T., Nani, A., Diano, M., Quarta, D.G., Duca, S., Apkarian, A.V., Fox, P.T., Cauda, F., 2018. How do morphological alterations caused by chronic pain distribute across the brain? A meta-analytic co-alteration study. Neuroimage Clin 18, 15-30.

Taylor, K.S., Seminowicz, D.A., Davis, K.D., 2009. Two systems of resting state connectivity between the insula and cingulate cortex. Hum Brain Mapp 30, 2731-2745.

Tian, Y., Zalesky, A., 2018. Characterizing the functional connectivity diversity of the insula cortex: Subregions, diversity curves and behavior. Neuroimage 183, 716-733.

Torres, U.S., Duran, F.L., Schaufelberger, M.S., Crippa, J.A., Louzã, M.R., Sallet, P.C., Kanegusuku, C.Y., Elkis, H., Gattaz, W.F., Bassitt, D.P., Zuardi, A.W., Hallak, J.E., Leite, C.C., Castro, C.C., Santos, A.C., Murray, R.M., Busatto, G.F., 2016. Patterns of regional gray matter loss at different stages of schizophrenia: A multisite, cross-sectional VBM study in first-episode and chronic illness. Neuroimage Clin 12, 1-15.

Turkeltaub, P.E., Eden, G.F., Jones, K.M., Zeffiro, T.A., 2002. Meta-analysis of the functional neuroanatomy of single-word reading: method and validation. Neuroimage 16, 765-780.

Turkeltaub, P.E., Eickhoff, S.B., Laird, A.R., Fox, M., Wiener, M., Fox, P., 2012. Minimizing within-experiment and within-group effects in Activation Likelihood Estimation meta-analyses. Hum Brain Mapp 33, 1-13.

Uddin, L.Q., 2015. Salience processing and insular cortical function and dysfunction. Nat Rev Neurosci 16, 55-61.

Uddin, L.Q., Supekar, K., Lynch, C.J., Khouzam, A., Phillips, J., Feinstein, C., Ryali, S., Menon, V., 2013. Salience network-based classification and prediction of symptom severity in children with autism. JAMA Psychiatry 70, 869-879.

Uddin, L.Q., Supekar, K.S., Ryali, S., Menon, V., 2011. Dynamic reconfiguration of structural and functional connectivity across core neurocognitive brain networks with development. J Neurosci 31, 18578-18589.

van den Heuvel, M.P., Mandl, R.C., Kahn, R.S., Hulshoff Pol, H.E., 2009. Functionally linked resting-state networks reflect the underlying structural connectivity architecture of the human brain. Hum Brain Mapp 30, 3127-3141.

van den Heuvel, O.A., Remijnse, P.L., Mataix-Cols, D., Vrenken, H., Groenewegen, H.J., Uylings, H.B.M., van Balkom, A.J.L.M., Veltman, D.J., 2008. The major symptom dimensions of obsessive-compulsive disorder are mediated by partially distinct neural systems. Brain 132, 853-868.

van Haren, N.E.M., Schnack, H.G., Cahn, W., van den Heuvel, M.P., Lepage, C., Collins, L., Evans, A.C., Pol, H.E.H., Kahn, R.S., 2011. Changes in Cortical Thickness During the Course of Illness in Schizophrenia. Arch Gen Psychiatry 68, 871-880.

Vanasse, T.J., Fox, P.M., Barron, D.S., Robertson, M., Eickhoff, S.B., Lancaster, J.L., Fox, P.T., 2018. BrainMap VBM: An environment for structural meta-analysis. Hum Brain Mapp 39, 3308-3325.

Vercelli, U., Diano, M., Costa, T., Nani, A., Duca, S., Geminiani, G., Vercelli, A., Cauda, F., 2016. Node Detection Using High-Dimensional Fuzzy Parcellation Applied to the Insular Cortex. Neural Plast 2016, 1938292.

Voytek, B., Knight, R.T., 2015. Dynamic network communication as a unifying neural basis for cognition, development, aging, and disease. Biol Psychiatry 77, 1089-1097.

Wang, X., Luo, Q., Tian, F., Cheng, B., Qiu, L., Wang, S., He, M., Wang, H., Duan, M., Jia, Z., 2019. Brain grey-matter volume alteration in adult patients with bipolar disorder under different conditions: a voxel-based meta-analysis. J Psychiatry Neurosci 44, 89-101.

Wylie, K.P., Tregellas, J.R., 2010. The role of the insula in schizophrenia. Schizophr Res 123, 93-104.

Xue, F., Droutman, V., Barkley-Levenson, E.E., Smith, B.J., Xue, G., Miller, L.C., Bechara, A., Lu, Z.L., Read, S.J., 2018. The role of the dorsal anterior insula in sexual risk: Evidence from an erotic Go/NoGo task and real-world risk-taking. Hum Brain Mapp 39, 1555-1562.Yates, D., 2012. Neurodegenerative networking. Nat Rev Neurosci 13, 288.

Zhou, J., Gennatas, E.D., Kramer, J.H., Miller, B.L., Seeley, W.W., 2012. Predicting regional neurodegeneration from the healthy brain functional connectome. Neuron 73, 1216-1227.

Zhou, J., Greicius, M.D., Gennatas, E.D., Growdon, M.E., Jang, J.Y., Rabinovici, G.D., Kramer, J.H., Weiner, M., Miller, B.L., Seeley, W.W., 2010. Divergent network connectivity changes in behavioural variant frontotemporal dementia and Alzheimer's disease. Brain 133, 1352-1367.

2.4 Influence of gestational diabetes and Pre-gestational maternal BMI on the brain of six years old offspring

This study is in preparation for submission to International Journal of Obesity.

Abstract

Gestational diabetes (GD) and maternal excess weight are common pregnancy conditions which increase the risk of future complications for both the mother and her offspring. Their consequences on neurodevelopment are widely described in literature, but less is known concerning the potential transgenerational influence on the brain structure. We thus used a combination of support vectors machine and hierarchical clustering to investigate the potential presence of anatomical brain differences in a sample of 109 children aged 6 years, related to the diagnosis of GD during pregnancy and to the BMI of their mothers before pregnancy. Results showed that possible effects of GD are visible for the children of mothers with excess weight, and especially for mothers with overweight rather than those with obesity. On the contrary, no detectable differences emerged when considering mothers with normal weight. Relationships with maternal BMI were only found for the offspring of mothers with GD. Our study highlights the need for clinical attention of mothers with excess weight, in particular for those with overweight, diagnosed with GD, since this status was found to be associated with detectable transgenerational brain signs.

Introduction

Gestational diabetes (GD) is a serious pregnancy complication affecting 16.5% of pregnancies worldwide (Benhalima, et al., 2015; International Diabetes Federation, 2019), with long-term health consequences. The most relevant are Type 2 diabetes (T2DM) and cardiovascular diseases in both mother and offspring, macrosomia, future obesity and/or GD in the child (Benhalima, et al., 2015; Pintaudi, et al., 2018; Plows, et al., 2018). Pre-pregnancy excess weight has been also linked to several health consequences and long-term increased risk in the offspring, including child obesity, diabetes and cardiovascular diseases (Chu, et al., 2007; Reynolds, et al., 2013; Whitaker, 2004).

The effects of GD, as well as maternal excess weight, on the offspring neurodevelopment are widely investigated and well known (Adane, et al., 2016; Brinciotti, et al., 2011; Deardorff, et al., 2017; Sousa, et al., 2018; Torres-Espinola, et al., 2015; Yeung, et al., 2017). However, to the best of our knowledge, sparse researches addressed potential transgenerational effects on the brain function and

structure of those conditions (Li, et al., 2016; Ou, et al., 2015; Page, et al., 2019; Salzwedel, et al., 2018; Verdejo-Román, et al., 2019). Although clinical and sociological studies pointed out the relevance of environmental factors and domestics habits for the emergence of excess weight and even Type 2 diabetes (Bellou, et al., 2018; Solmi, et al., 2018) the identification of further associations between maternal health condition and brain structural characteristics in their offspring could help to consolidate a still developing research topic. To this aim, we investigated the potential presence of anatomical brain differences in a cohort of 6 years old children possibly related to the presence/absence of GD and to the BMI of their mothers before pregnancy (M_BMI).

To do so, we adopted a combined use of supervised and unsupervised learning methodologies. As pointed out by Koul et al. (2018), this twofold approach allows to address two different kinds of research questions. By means of supervised learning, and in the present case Support Vector Machine (SVM), it is possible to determine whether data have discriminatory information. In other words, SVM can answer to the question: are offspring's brains different enough to correctly assign each of them to the group it belongs to? (e.g.: child born to mother with GD or without GD). Unsupervised learning, and in the present case Hierarchical Clustering, allows to analyze the variability of the data (Koul, et al., 2018). This method can answer to the questions: can the subjects be organized into groups based on the characteristics of their brain? How many groups must be created? Who enters each of the groups?

In the present work, the variables of interest analyzed to answer to those range of questions are the structural properties of the 6 years old children's brains. Potential differences on these properties were not put into relationship with non-brain characteristics of the children themselves, but with the presence or absence of GD and to the pre-pregnancy maternal BMI. To evaluate whether results came from the whole brain characteristics or if they were due to specific tissues, analyses had been repeated on the whole brain, and using gray or white matters only.

Based in the previous research that found brain differences linked to both GD and prepregnancy excess weight, we hypothesized that SVM and HC methods will detect differences in the anatomical offspring characteristics based on maternal status.

Materials and methods

Selection of Subjects

The present study is based on the PREOBE (Berglund, et al., 2016) study, a prospective observational cohort study, designed to explore peri- and postnatal influence of maternal overweight, obesity and GD in the mothers and their offspring. Mothers were recruited between 2008 and 2012 in the Clinical University Hospital San Cecilio and the Mother-Infant University Hospital of Granada (Granada, Spain) and their peripheral health centers. Briefly, the database consists of medical and sociocultural information concerning 331 pregnant women aged between 18 and 45 years and their offspring. Full general inclusion and exclusion criteria can be found in Berglund, et al. (2016). In the present work we focused on the structural MRI images acquired up until October 2017 for 155 healthy children at the age of 6 years. 12 subjects were excluded because their mothers had been already diagnosed with diabetes before the beginning of pregnancy. The remaining 143 subjects were then divided into 6 groups, on the bases of their calculated maternal BMI (M_BMI) at the recruiting session (between week 12 to 20 of pregnancy) and the presence/absence of GD at 34 week of gestation. Cutoff points for M_BMI were taken as follows: 18.5<M_BMI<25 = normal weight group (NW); 25<M_BMI<30 = overweight group (OW); M_BMI>30 = obesity group (OB) (see Table 1 for groups details). The study was approved by the Human Research Ethics Committee of the Universidad de Granada and conducted in accordance with the Helsinki Declaration for human research studies. Written informed consent forms were obtained from all participants at the beginning of the study and before the magnetic resonance session.

MRI acquisition and preprocessing

Prior to the MRI session, the children participated in a practice session. They were familiarized with the MRI environment, and they were introduced in a mock scanner and listened to the real scanner's noise. Additionally, to reassure them and keep them from movement and falling asleep, the children watched a cartoon film during acquisition. Furthermore, a foam system was located around the participant's head.

T1 images were acquired for each participant, using a 3T Magnetom Trio scanner (Siemens Medical System, ERLANGEN, Germany), located at Mind, Brain and Behavior Research Centre (CIMCYC). A high resolution T1-weighted 3D magnetization-prepared rapid gradient-echo (MPRAGE) sequence was acquired with the following parameters: Repetition Time (TR)=2.3 ms, Echo Time (TE)=3.1 ms, flip angle=9º, Field of View (FOV)=256x256 mm, matrix size=320x320,

number of slices=208, resulting an isotropic resolution of 0.8x0.8x0.8 mm. Acquisition time was 6 min 35 sec. Of note, this scanner provides images on which field inhomogeneity correction has already been performed. These images were independently checked by two expert researchers, in order to detect artifacts due to motion of participants during acquisition or other causes. 34 subjects were excluded at this point, after convergent judgment (see Tab. S1 for details on the group subdivision).

T1 images were preprocessed and segmented into grey matter and white matter using DARTEL (Ashburner, 2007) as implemented in DBAPI 2.3 (Yan, et al., 2016). In order to obtain additional tissue segmentation maps with intensity values in it (instead of probability values as provided by DARTEL), the whole brain T1 of each subject was multiplied for either the binarized grey matter (GM) or binarized white matter (WM) DARTEL maps of the same subject.

	Non-gestational diabetes (N = 78)			Gestational Diabetes (N=31)		
	Normal weight (NW; n=44)	Overweight (OW; n=19)	Obesity (OB; n=15)	Normal weight (NWGD; n=12)	Overweight (OWGD; n=10)	Obesity (OBGD; n=9)
Maternal BMI (kg/m^2)	22.50 (1.65)	27.00 (1.25)	31.96 (1.28)	22.06 (2.01)	27.53 (1.15)	35.96 (4.86)
GWG (kg)	12.93 (5.73)	10.10 (6.67)	9.34 (6.52)	10.10 (7.63)	7.14 (4.25)	1.74 (10.15)
Birth weight (gr)	3246.36 (399.92)	3468.95 (574.30)	3382.67 (514.94)	3459.17 (514.94)	3056.00 (347.63)	3454.44 (418.81)
BMI at MRI (kg/m^2)	16.00 (1.50)	17.09 (2.29)	17.28 (2.51)	16.82 (2.60)	17.72 (2.85)	17.00 (2.30)

Table 1: Socio-demographic and anthropometric details of the sample analyzed.

Preliminary confounding interaction assessment

In order to exclude potential confounding effects, we performed linear regression between relevant couples of variables. These analyses were performed on GD groups and non-GD groups separately. In details, we contrasted: maternal BMI at the beginning of pregnancy (M_BMI) vs gestational weight gain (GWG); GWG vs BMI of the children at the moment of the evaluation; M_BMI vs birth weight of the

children; M_BMI vs BMI of the children at the moment of the evaluation. Moreover, we performed a one-way ANOVA on the BMI of the children at the moment of the evaluation.

Neuroimaging analyses

Support vector machine analyses

In order to investigate whether brain data contained discriminatory information, we performed classification task between the experimental groups, using PRONTO tool (Schrouff, et al., 2013). We used a binary support vector machine (SVM), with leave one subject out as Cross-Validation method, and no hyper-parameter optimization. SVM is one of the most widely used classification algorithm in the field of neuroimaging (Orrù, et al., 2012). In this class of algorithms, a hyperplane is searched so to optimally separate the items into two, or more, classes (Cortes and Vapnik, 1995). As a result of this, the best solution is based only on those items in the proximity of the hyperplane, rather than on the whole sample of items (Khosla, et al., 2019). Several comparisons were realized, in order to separately analyze the effect of GD and the effect of BMI (see Table 2 for an overview of the comparisons). The results were evaluated considering total accuracy (TA), balanced accuracy (BA) and area under curve (AUC). Chance level cutoffs for SVM accuracy were set in accordance with the work of Combrisson and Jerbi (2015) considering $p<0.05$ and two classes. This cut-off is dependent of the number of subjects included in each analysis, and critical cut-off for each one is specified in the results section. SVM was applied to the whole brain T1, and to GM and WM separately.

Hierarchical clustering analyses

In order to further verify the statistically significant SVM results, we performed hierarchical clustering analysis, using Orange 2.7 (Demsar, et al., 2013). Clustering algorithms are abundantly used in MRI research (Mirzaei and Adeli, 2019), and, generally speaking, they organize items into a set of nested partitions (Khosla, et al., 2019). Hierarchical clustering does not require the definition of a predetermined number of clusters, as it is instead necessary for the widely-used k-means clustering (Khosla, et al., 2019). In the present case, a NxM matrix was created, in which each row represented a different subject, and each column a same voxel through all the subjects. Non-brain voxels were excluded from the matrix by means of a group mask. Distances between rows (i.e. between subjects) were calculated using Euclidean metric, and Ward's linkage was used to build the dendrogram. Ward's linkage try to minimize the variability inside each cluster (Khosla, et al., 2019;

Ward, 1963). Hierarchical clustering was performed separately for GM and WM, due to computational constraints. Results were evaluated as a ratio between the majority class and the total number of items in each cluster. In other words, we observed if the majority of subjects in every given cluster belonged to the same study group.

Results

Confounding interaction analyses

Overall none of the linear regression analyses correlating variables related to the mothers with variables related to the offspring highlighted marked confounding effects (Fig. S1, Fig. S3, Fig. S4, Fig. S6-S9). The only relevant interaction was found between maternal BMI at the beginning of pregnancy (M_BMI) and GWG for the mothers with GD (R2=0.4) (Fig. S1 and Fig. S2). The higher the BMI was, the lesser the kg gained during the pregnancy. However, GWG does not seem to influence the BMI of the children at the moment of the evaluation (R2=0.07) (Fig. S3 and Fig. S4). The one-way ANOVA on the BMI of the subjects at the moment of the evaluation did not show statistically significant differences (see fig. S5).

Gestational diabetes effect

GD groups vs non-GD groups

SVM analyses

In order to assess the effect of GD, independently from maternal BMI, NW, OW and OB groups (N=78) and NWGD, OWGD and OBGD groups (N=31) were collapsed into two macro-groups. The SVM analysis at this macro-groups level (N=109), on whole brain data, showed TA=73.39%. However, due to the marked unbalance between the two classes, the BA=58.09% (critical cutoff of reference = 58%) must be considered a more reliable indicator (Fig. 1). The AUC was equal to 0.79. Our result could be interpreted as a moderate evidence of discriminability between the two groups (i.e.: mothers with GD vs. without GD). At the same time, it suggests the need of a set of more accurate analyses with a subtler subdivision of the groups. The SVM analysis of both WM and GM alone did not produce statistically significant results (see Tab. S2 and Tab. S3).

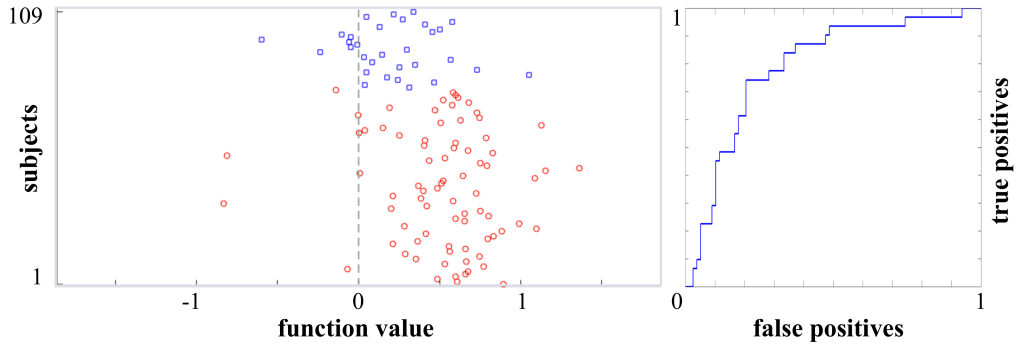

Figure 1: Results of the comparison between GD groups and non-GD groups. Left: details of subjects' discrimination based on whole brain images. Blue squares = GD subjects, red circles = non-GD subjects. Right: Area Under the Curve.

		Total N	Critical cutoff	Total accuracy	Balanced accuracy	AUC
GD effect	NW vs NWGD	56	60%	76.79%	48.86%	0.66
	OW vs OWGD	29	70%	**89.66%**	**87.37%**	0.88
	OB vs OBGD	24	70%	54.17%	47.78%	0.50
	EW vs EWGD	53	60%	**75.47%**	**70.43%**	0.76
	non-GD vs GD	109	58%	**73.39%**	**58.09%**	0.79
BMI effect (GD groups)	NWGD vs OWGD	22	70%	**72.73%**	**73.33%**	0.69
	OWGD vs OBGD	19	70%	63.16%	62.22%	0.78
	NWGD vs OBGD	21	70%	52.38%	47.22%	0.42
	NWGD vs EWGD	31	62.50%	64.52%	58.77%	0.64
BMI effect (non-GD groups)	NW vs OW	63	60%	68.25%	48.86%	0.30
	OW vs OB	34	62.50%	29.41%	26.32%	0.10
	NW vs OB	59	60%	74.58%	50%	0.35
	NW vs EW	78	58.70%	44.87%	41.11%	0.46

Table 2: Results of the SVM analyses based on whole brain images. Critical cutoff is based on Combrisson and Jerbi (2015), considering $p<0.05$ and two classes. Significant accuracy results are in bold..

Hierarchical clustering analyses

Coherently with the around-threshold SVM result, the dendrograms obtained on both GM and WM data did not showed a net separation between the GD groups and the non-GD groups.

In other words, the brain structural properties did not allow to clearly discriminate between children of mothers with GD and children of mothers without GD.

Excess-weight_GD groups vs Excess-weight_non-GD groups

SVM analyses

The around-threshold results obtained in previous analyses on the whole GD groups could have been at least in part due to the underlying effect of maternal BMI. To verify this hypothesis, we proceeded focusing on excess weight groups only. We hence collapsed OW and OB groups (EW group, N=34) and OWGD and OBGD groups (EWGD group, N=19), and let apart normal weight groups. The SVM analysis at this level (N=53), on whole brain data, showed TA=75.47%. Again, due to the marked unbalance between the two classes, the BA=70.43% (critical cutoff of reference = 60%) must be considered a more reliable indicator (Fig. 2). The AUC was equal to 0.76. Hence, our result can be interpreted as a quite strong evidence of discriminability between the two groups. The SVM analysis of both WM and GM alone produced statistically significant and comparable results as well (see Tab. S2 and Tab. S3).

Hierarchical clustering analyses

The dendrogram obtained on GM data shows the presence of two main clusters, one including 39 subjects, the second one including 14 subjects. 31 out 39 subjects (79.5%) in the first cluster belong to the excess-weight_non-GD group, while 11 out 14 subjects (78.6%) in the second cluster belong to the excess-weight_GD group (Fig. 2). Coherently with the SVM results, the clustering analysis showed a net separation between the two groups. On the contrary, the dendrogram obtained on WM data did not showed a net separation between the groups.

These results suggest that when focusing on mothers with excess-weight offspring only, the separation between children of mothers with GD and children of mothers without GD became clearer.

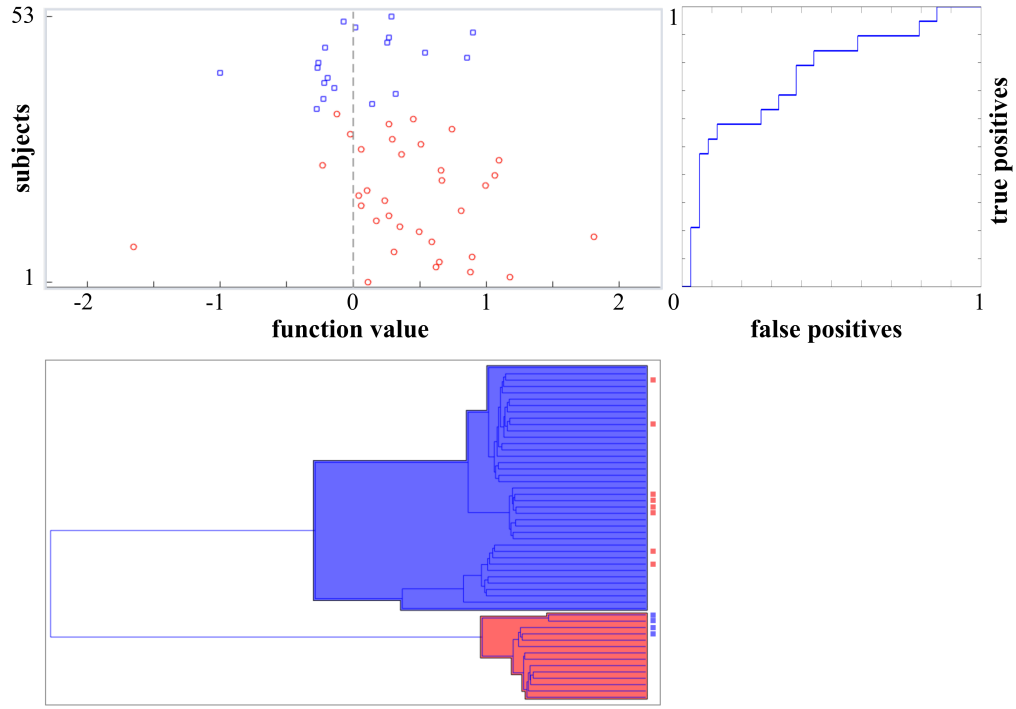

Figure 2: Results of the comparison between excess-weight_GD group excess-weight_non-GD group. Top left: details of subjects' discrimination based on whole brain images. Blue squares = GD subjects, red circles = non-GD subjects. Top right: Area Under the Curve. Bottom: hierarchical clustering results for GM. The blue cluster mainly includes excess-weight_non-GD subjects, while the red cluster mainly includes excess-weight_GD subjects. The squares on the right side of the dendrogram mark subjects not belonging to the majority group in that cluster.

Group by group comparisons

SVM analyses

In order to further refine the focus of the analyses, we then moved to the comparison between couples of groups with same BMI. The only condition to produce statistically significant results was OW group (N=19) vs OWGD group (N=10). The SVM analysis at this level (N=29), on whole brain data, showed TA=89.66% and BA=87.37% (critical cutoff of reference = 70%) (Fig. 3). The AUC was equal to

0.88. Our results can be interpreted as a marked evidence of discriminability between the two groups. The SVM analysis of both WM and GM alone produced statistically significant and comparable results as well (see Tab. S2 and Tab. S3).

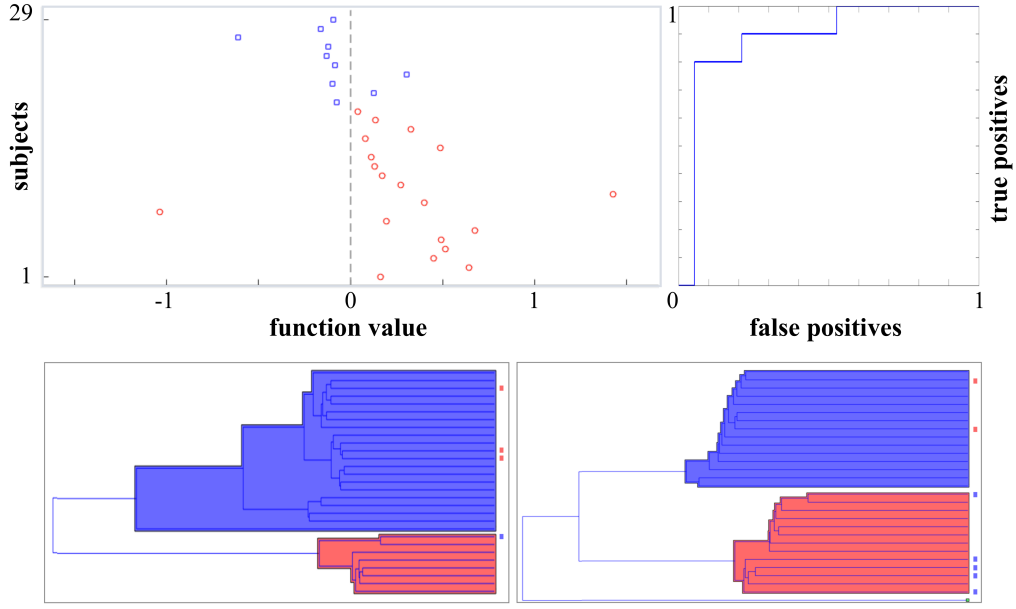

Figure 3: Results of the comparison between overweight_GD group and overweight_non-GD group. Top left: details of subjects' discrimination based on whole brain images. Blue squares = GD subjects, red circles = non-GD subjects. Top right: Area Under the Curve. Bottom left: hierarchical clustering results for GM. The blue cluster mainly includes excess-weight_non-GD subjects, while the red cluster mainly includes excess-weight_GD subjects. The squares on the right side of the dendrogram mark subjects not belonging to the majority group in that cluster. Bottom right: hierarchical clustering results for WM. Color scheme was used as described for GM.

Of note, the SVM comparison for NW vs NWGD did not produce significant results (TA=76.79%, BA=48.86%, AUC=0.66). This suggests that the barely significant results obtained when comparing all the groups without GD against all the groups with GD could be masked by the similarity among normal weight groups. After removing them, limiting the groups to excess weight condition, results became significant. However, while the comparison between overweight groups (OW vs

OWGD) resulted into statistically significant results, the comparison for OB vs OBGD did not produced significant results (TA=54.17%, BA=47.78%, AUC=0.50). Therefore, it probably was the discriminability between overweight groups to drive the results for excess weight groups.

Hierarchical clustering analyses

The dendrogram obtained on GM data for the OW vs OWGD comparison shows the presence of two main clusters, one including 21 subjects, the second one including 8 subjects. 18 out 21 subjects (85.7%) in the first cluster belong to the OW group, while 7 out 8 subjects (87.5%) in the second cluster belong to the OWGD group. The dendrogram obtained on WM data shows the presence of two main clusters, one including 15 subjects, the second one including 13 subjects. One subject from the OW group remained outside from the two clusters, appearing as an outlier. 13 out 15 subjects (86.7%) in the first cluster belong to the OW group, while 8 out 13 subjects (61.5%) in the second cluster belong to the OWGD group. Coherently with the SVM results, the clustering analysis showed a net separation between these two groups.

Maternal BMI effect

SVM analyses

To explore the effect of maternal BMI the same approach used for GD was followed, but in this case BMI groups without GD and BMI groups with GD were tested separately. In this context, the only comparison which produced statistically significant results was the one testing NWGD group (N=12) vs OWGD group (N=10). The SVM analysis at this level (N=22), on whole brain data, showed TA=72.73% and BA=73.33% (critical cutoff of reference = 70%) (Fig. 4). The AUC was equal to 0.69. Our result could be interpreted as a moderate evidence of discriminability between the two groups. The SVM analysis of both WM and GM alone produced statistically significant and comparable results as well (see Tab. S2 and Tab. S3).

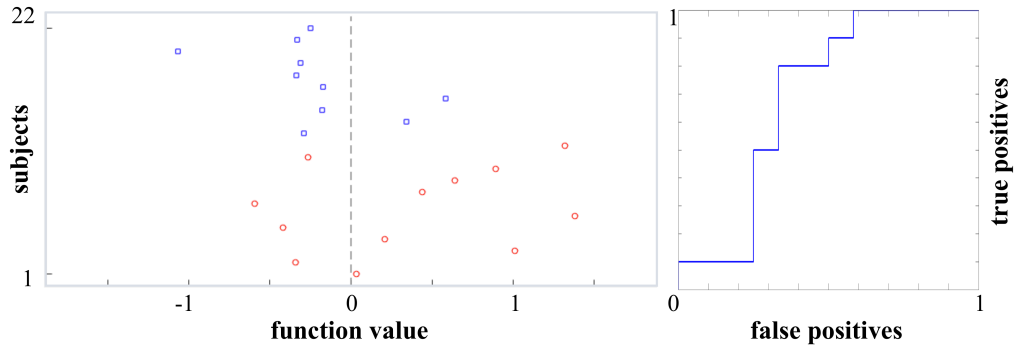

Figure 4: Results of the comparison between normal weight GD group and overweight GD group. Left: details of subjects' discrimination based on whole brain images. Black crosses = overweight subjects, red circles = normal weight subjects. Right: Area Under the Curve.

All the other comparisons focused on maternal BMI effect did not produce statistically significant results (see Tab. 2 and Tab. S2 for an overview).

Hierarchical clustering analyses

Despite the statistically significant SVM result, the dendrograms obtained on both GM and WM data did not showed a net separation neither between BMI groups with GD nor between BMI groups without GD.

Additional SVM comparisons focused on OWGD, evaluating the interaction between BMI and GD, are described in the supplementary material (see also Tab. S4).

Discussion

Gestational diabetes (GD) and maternal excess weight are common pregnancy conditions which can have a negative impact for both the mother and her offspring. In the present study, we tried to understand if these clinical variables can be put into relationship with the structural properties of the offspring's brains, using a combination of supervised and unsupervised learning methods. We found overall moderate evidence of differences on the brain of children born from mothers with and without GD. More in details, this effect is stronger when focusing on mothers with excess weight before pregnancy, especially overweight, but it was not found in children born from mothers with normal weight.

Based on the results, the effect of GD at increasing maternal BMI seems to follow a bell-shaped distribution. In fact, GD seems to play a relevant role especially in the case of children of mothers with overweight. On the contrary, there was no evidence of significant differences between the offspring of mothers with normal weight without GD and those of mothers with normal weight with GD. Similarly, no significant differences were detected between the offspring of mother with obesity without GD and those of mother with obesity mothers with GD.

To the best of our knowledge there is only one previous study that explored the additive association of GD and maternal prepregnancy BMI on children brains (Page, et al., 2019). The results showed a linear relation between maternal BMI and hypothalamic dysfunction, but the statistical significance of this effect disappeared when adjusting for GD exposition. Authors suggest that GD mediates the association between maternal BMI and brain function. These results could appear as conflicting with ours. However, some elements should be noted. First, the authors investigated a functional dysregulation limited to the hypothalamus, while the present study focused on whole brain structural properties. Second, the PREOBE children were scanned at the age of six years, while the sample analyzed in Page et al. (2019) ranged between 7 and 11 years. Lastly, our findings suggest a non-linear interaction, while Page and colleagues only tested a linear relationship. Other previous studies that found significant relationships between GD and offspring's neurodevelopment (Linder, et al., 2015; Torres-Espinola, et al., 2015) did not explore the additive impact of excessive maternal weight before pregnancy.

Our findings are in consonance with a previous study conducted on this same cohort that reported an additive effect of GD and maternal BMI on latencies of visual evoked potentials at 18 months of age (Torres-Espínola, et al., 2018). A similar bell-shaped relation was in fact found between maternal BMI and latencies for the GD group. Authors claimed that poorer myelination process of the auditory system may explain that results. However, previous analyses (Ou, et al., 2015), including one conducted on the PREOBE cohort (Verdejo-Román, et al., 2019) failed to find a significant association of WM with maternal BMI at 6 years old. Coherently, in the present study hierarchical clustering results gave better separation when applied to GM rather than WM, possibly suggesting that GD and maternal BMI could influence mainly GM at this stage. Nevertheless, the SVM analyses suggested that GM and WM are substantially equally informative to discriminate between groups. Further research at different development phases will help to elucidate the possible different role of these tissues.

Off note, the offspring of mothers with overweight and GD were not only found to differ from those of mothers with comparable BMI but no GD. They were also different from the offspring of mothers with normal weight, with or without GD, as well as from the offspring of mothers with obesity without GD. Hence, the co-occurrence of overweight and GD resulted in being the more effective condition. This aspect deserves further clinical consideration in light of the documentes increased risk of GD with increasing BMI (Kim, et al., 2012) On the contrary, the maternal BMI alone was not found to be associated with differences in offspring of mothers without GD.

The observed bell-shaped effect could also be influenced by different maternal conduct depending on group membership. If, on the one hand, prepregnancy normal weight could act as a protecting factor, on the other hand mothers with obesity could be more aware of the risks related to their BMI. In virtue of this, they could adopt special preventive measures. Conversely, mothers with overweight are still on the way to potentially enter obesity. As a consequence, they could still have those negative habits which were already abandoned (or at least mitigated) by mothers with obesity. Moreover, if the latter are likely to be followed by a specialist, the former could even not be aware of the risks they are exposed to. This hypothesis is supported by a qualitative survey realized on a sample of Latinas women, showing that mothers with overweight rarely gave importance to body weight, and underestimated the role of diet, compared to both healthy weight women and those with obesity (Wang, et al., 2015). More generally, Shub, et al. (2013) found that the majority of the interviewed mothers with prepregnancy excess weight had limited knowledge of the risk associated with maternal obesity. In light of this, it is not possible to exclude that mothers enrolled in PREOBE could have adopted more responsible behaviours for the fact of being part of a research project (a kind of Hawthorne effect). This could be reflected in the negative linear relation between prepregnancy BMI and gestational weight gain, especially marked for mothers with GD. Consequently, the influence between GD/BMI and offspring's brain structural properties in the real population could be more evident.

Finally, it is fundamental to note that at the moment of the evaluation there were no statistically significant differences for the BMI of the children. Coherently, no relationship was found between the maternal BMI during pregnancy and the BMI of their children at the age of 6. Therefore, the results are unlikely attributable to differences in build or development of the subjects.

Limitations and future directions

One potential limitation of the present work is the sample composition. Although quite consistent as a whole size, the decomposition into 6 sub-groups, and the data quality assessment, generated reduced cardinalities. Moreover, some of the comparisons involved unbalanced groups. However, this aspect, that reflects at least in part the rate of incidence of GD (Mack and Tomich, 2017; Rojo-Martínez, et al., 2020), was taken into consideration when evaluating the results. Head movement is a second relevant problematic, common to all the MRI research field, and particularly marked when working with children. In order to try to limit the influence on data, specific procedures were followed, as explained in the methods section. In addition to this precaution, data were subjected to manual screening and discarded when corrupted. Although many variables were collected and considered as controls, it is not possible to exclude confounding effects due to uninvestigated parameters. Lastly, hierarchical clustering had been performed for GM and WM separately, but it was not possible to jointly analyze the two for computational constraints. Of note, future studies could benefit from the addition of information concerning the fathers. Although the present study suggests the existence of structural brain differences, the analysis of cortical parameters, such as cortical thickness and gyrification, could help to clarify the contribution of specific regions. At the same time, the investigation of the functional counterpart would be meaningful. Finally, a longitudinal approach would allow to follow the temporal evolution of the transgenerational influences.

Conclusions

In the present paper we analyzed the potential transgenerational signs of maternal GD and excess-weight before pregnancy detectable on the offspring's brains at the age of 6 years. Results showed that the relationship with GD is visible for the children of mothers with excess-weight, and in particular those with overweight. On the contrary, no detectable differences emerged when considering mothers with normal weight. Relationship with BMI were only found for GD positive groups, suggesting that maternal BMI alone is not associated with transgenerational signs. From the clinical point of view, our study highlights the need for specific care of mothers with excess weight diagnosed with GD, since the combination of these two factors seems to have the capability to induce transgenerational brain signs.

Supplementary results

Additional SVM analyses on OWGD group

Seeing as how the OWGD group showed discriminability from OW group and from NWGD group, additional SVM comparisons were designed to investigate possible differences with the remaining groups, although these could be due to the interaction between BMI and GD. The comparison between OWGD group (N=10) and NW group (N=44) (TOT N= 54), on whole brain data, showed TA=85.19% and BA=67.73% (critical cutoff of reference = 62.5%). The AUC was equal to 0.90. Our results can be interpreted as a marked evidence of discriminability between the two groups. However, the SVM analysis of both WM and GM alone did not produce statistically significant results (see Tab. X). The comparison between OWGD group (N=10) and OB group (N=15) (TOT N= 25), on whole brain data, showed TA=80% and BA=80% (critical cutoff of reference = 70%) (Fig. SX). The AUC was equal to 0.90. Our results can be interpreted as a quite strong evidence of discriminability between the two groups. The SVM analysis of both WM and GM alone produced statistically significant and comparable results (see Tab. S3).

Supplementary tables

	Non-gestational diabetes (N = 78)			Gestational Diabetes (N=31)		
	NW; n=44	OW; n=19	OB; n=15	NWGD; n=12	OWGD; n=10	OBGD; n=9
Maternal age (years)	31.48 (3.75)	32.63 (4.34)	29.00 (4.14)	33.50 (5.20)	33.80 (2.97)	34.44 (4.72)
Child sex (M/F)	24 / 20	8 / 11	7 / 8	8 / 4	4 / 6	5 / 4
Gestational Age (Weeks)	39.57 (1.13)	39.56 (1.89)	39.60 (1.64)	39.58 (1.44)	39.10 (1.52)	39.44 (1.51)
Age at MRI (days)	2386.59 (116.10)	2373.84 (115.51)	2293.40 (105.90)	2317.83 (101.15)	2256.10 (75.69)	2256.44 (45.72)
Subjects removed	17	3	3	4	5	2

Table S1: Socio-demographic and anthropometric details of the sample.

		Total N	Critical cutoff	Total accuracy	Balanced accuracy	AUC
GD effect	NW vs NWGD	56	60%	78.57%	50%	0.08
	OW vs OWGD	29	70%	**89.66%**	**87.37%**	0.88
	OB vs OBGD	24	70%	50%	40%	0.49
	EW vs EWGD	53	60%	**77.36%**	**71.90%**	0.77
	non-GD vs GD	109	58%	68.81%	49.05%	0.67
BMI effect (GD groups)	NWGD vs OWGD	22	70%	**72.73%**	**73.33%**	0.71
	OWGD vs OBGD	19	70%	63.16%	62.22%	0.74
	NWGD vs OBGD	21	70%	42.86%	37.50%	0.15
	NWGD vs EWGD	31	62.50%	67.74%	61.40%	0.62
BMI effect (non-GD groups)	NW vs OW	63	60%	69.84%	50%	0.27
	OW vs OB	34	62.50%	38.24%	34.21%	0.07
	NW vs OB	59	60%	74.58%	50%	0.30
	NW vs EW	78	58.70%	48.72%	43.52	0.42

Table S2: Results of the SVM analyses based on gray matter only. Critical cutoff is based on Combrisson and Jerbi (2015), considering $p<0.05$ and two classes. Significant accuracy results are in bold.

		Total N	Critical cutoff	Total accuracy	Balanced accuracy	AUC
GD effect	NW vs NWGD	56	60%	78.57%	50%	0.41
	OW vs OWGD	29	70%	**89.66%**	**87.37%**	0.87
	OB vs OBGD	24	70%	54.17%	45.56%	0.53
	EW vs EWGD	53	60%	**75.47%**	**70.43%**	0.78
	non-GD vs GD	109	58%	69.72%	50.66%	0.70
BMI effect (GD groups)	NWGD vs OWGD	22	70%	**72.73%**	**73.33%**	0.74
	OWGD vs OBGD	19	70%	63.16%	62.22%	0.76
	NWGD vs OBGD	21	70%	42.86%	37.50%	0.36
	NWGD vs EWGD	31	62.50%	70.97%	65.57%	0.66
BMI effect (non-GD groups)	NW vs OW	63	60%	69.84%	50%	0.19
	OW vs OB	34	62.50%	32.35%	28.95%	0.05
	NW vs OB	59	60%	74.58%	50%	0.27
	NW vs EW	78	58.70%	46.15%	41.24%	0.31

Table S3: Results of the SVM analyses based on white matter only. Critical cutoff is based on Combrisson and Jerbi (2015), considering $p<0.05$ and two classes. Significant accuracy results are in bold.

		Total N	Critical cutoff	Total accuracy	Balanced accuracy	AUC
Whole brain	NW vs OWGD	54	62.50%	**85.19%**	**67.73%**	0.90
	OB vs OWGD	25	70%	**80%**	**80%**	0.90
Gray matter	NW vs OWGD	54	62.50%	79.63%	52.73%	0.85
	OB vs OWGD	25	70%	**80%**	**80%**	0.91
White matter	NW vs OWGD	54	62.50%	81.48%	57.73%	0.85
	OB vs OWGD	25	70%	**80%**	**80%**	0.93

Table S4: Results of the SVM analyses for OWGD group. Critical cutoff is based on Combrisson and Jerbi (2015), considering $p<0.05$ and two classes. Significant accuracy results are in bold.

Supplementary figures

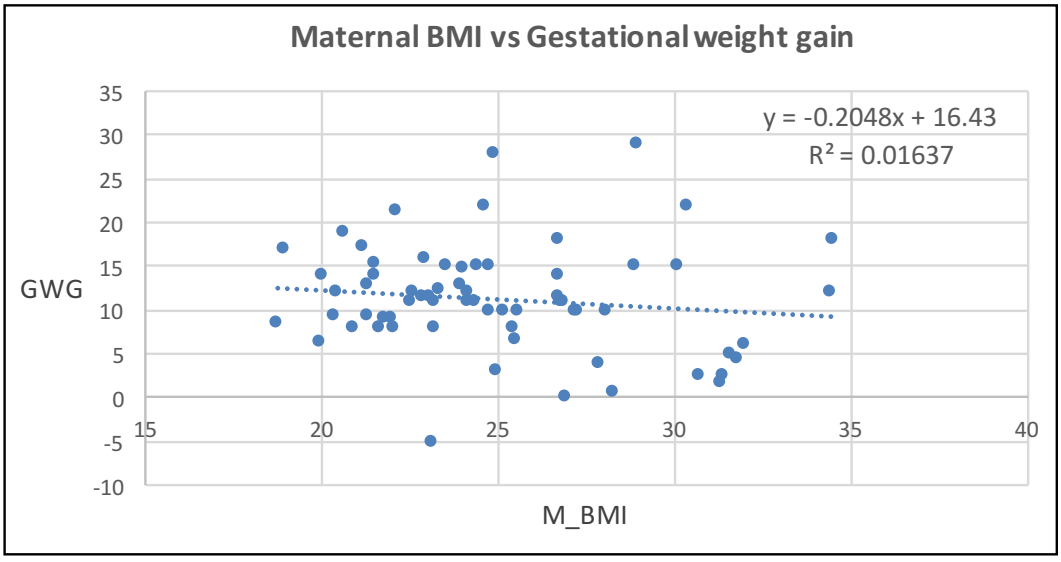

Figure S1: Linear regression between maternal BMI and gestational weight gain (measured in Kg) in non-GD groups.

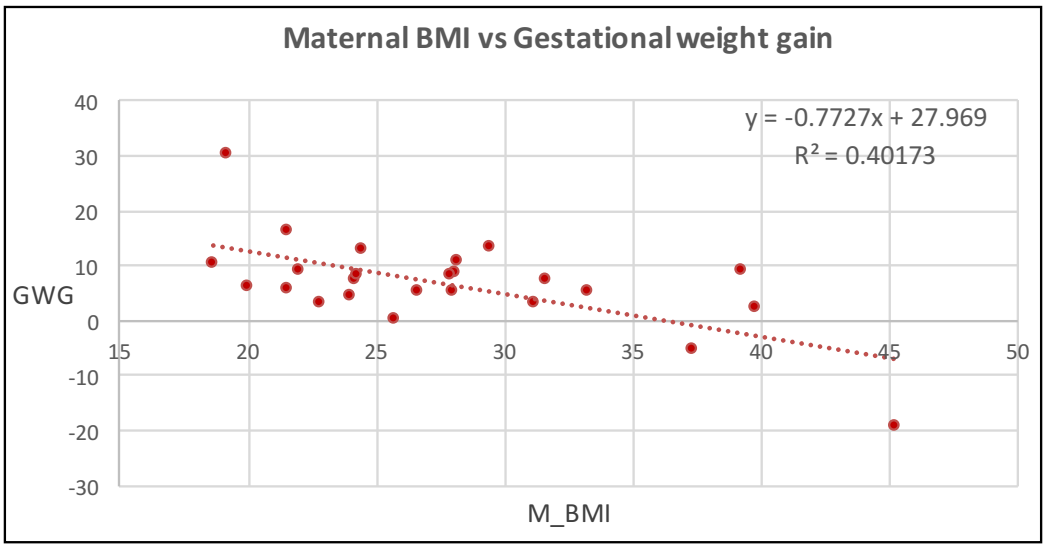

Figure S2: Linear regression between maternal BMI and gestational weight gain (measured in Kg) in GD groups.

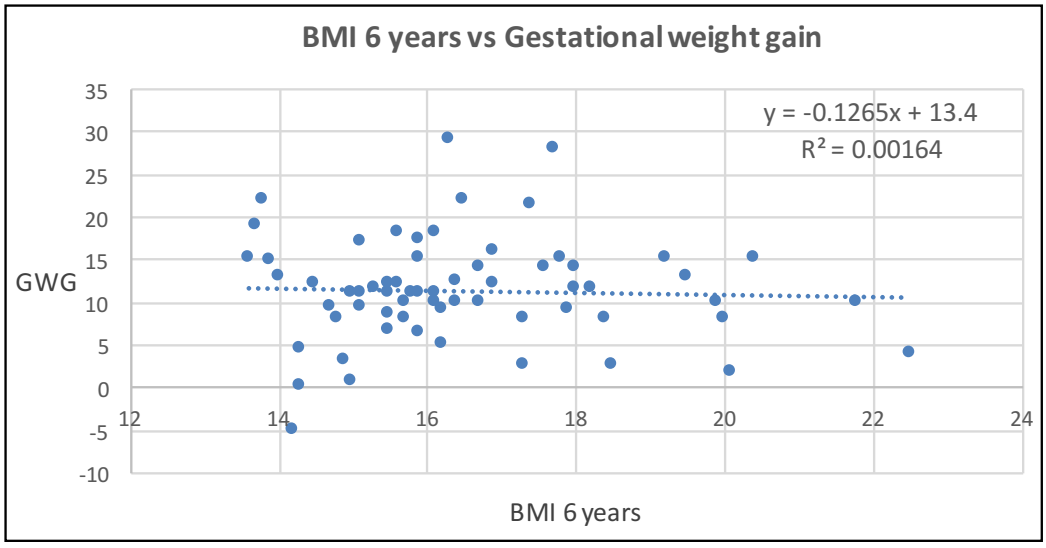

Figure S3: Linear regression between children's BMI at 6 years and gestational weight gain (measured in Kg) in non-GD groups.

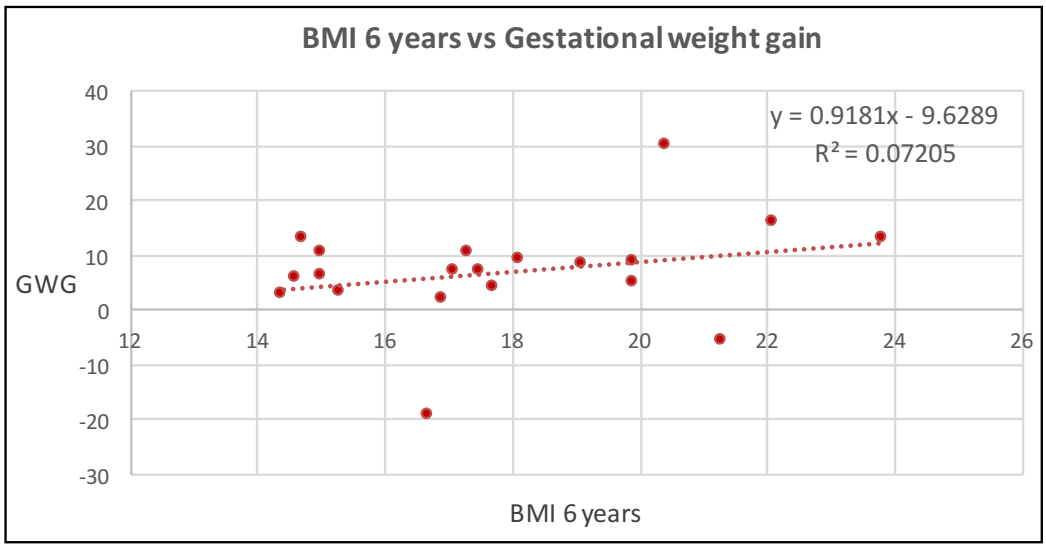

Figure S4: Linear regression between children's BMI at 6 years and gestational weight gain (measured in Kg) in GD groups.

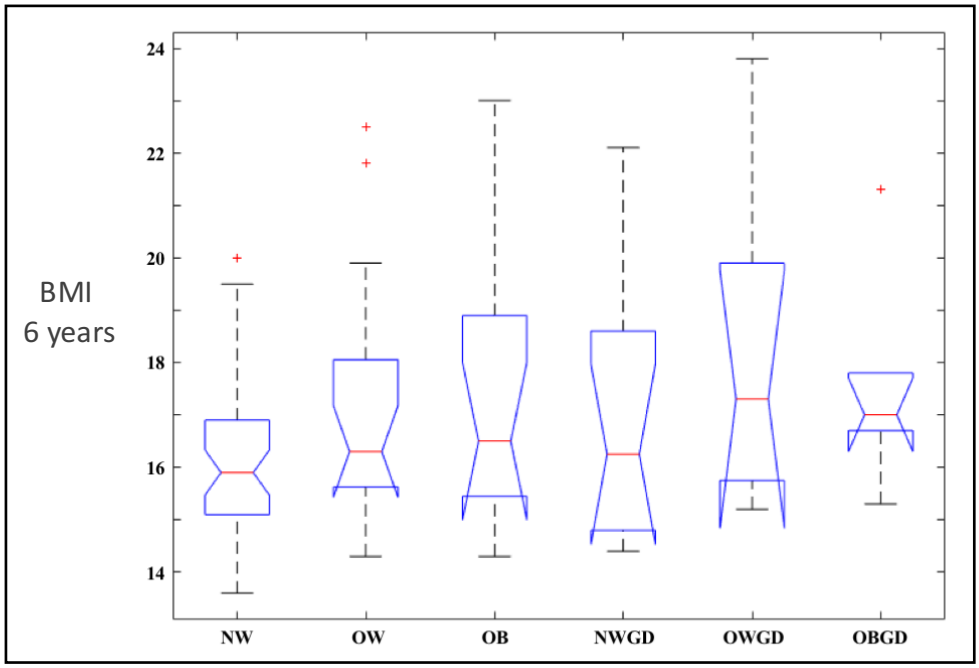

Figure S5: ANOVA results for BMI for the BMI of the subjects at the moment of the evaluation (6 years old).

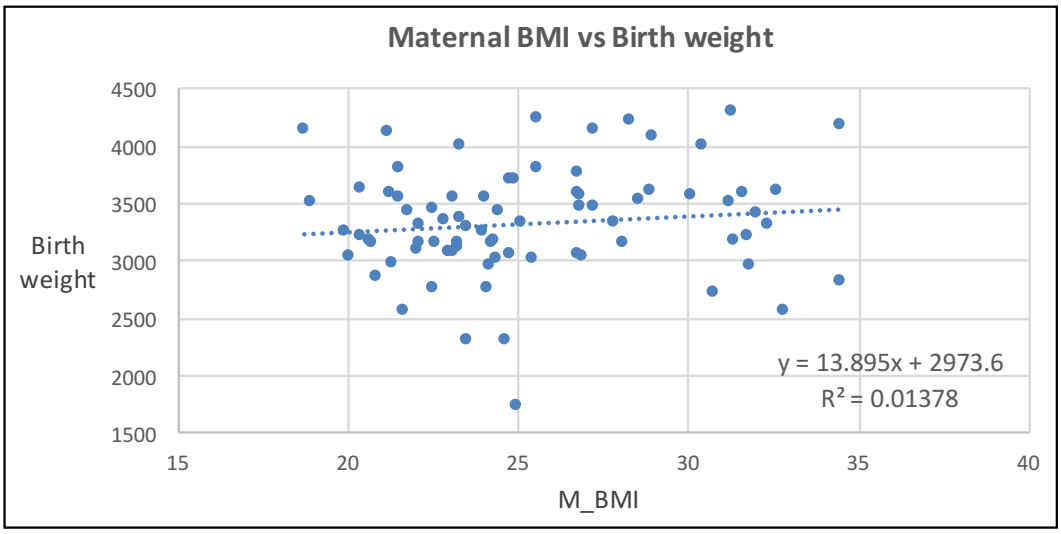

Figure S6: Linear regression between maternal BMI and birth weight of the children (measured in g) in non-GD groups.

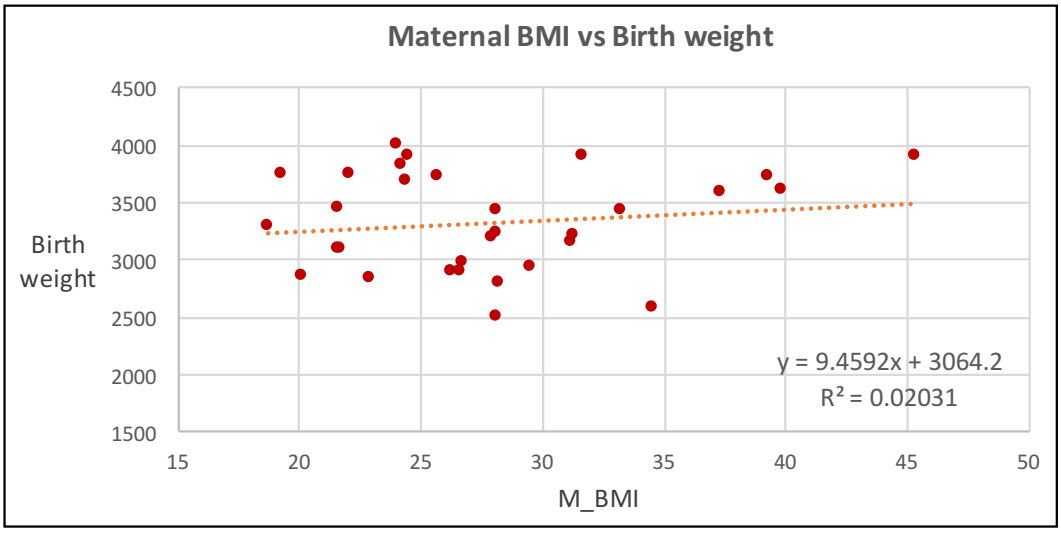

Figure S7: Linear regression between maternal BMI and birth weight of the children (measured in g) in GD groups.

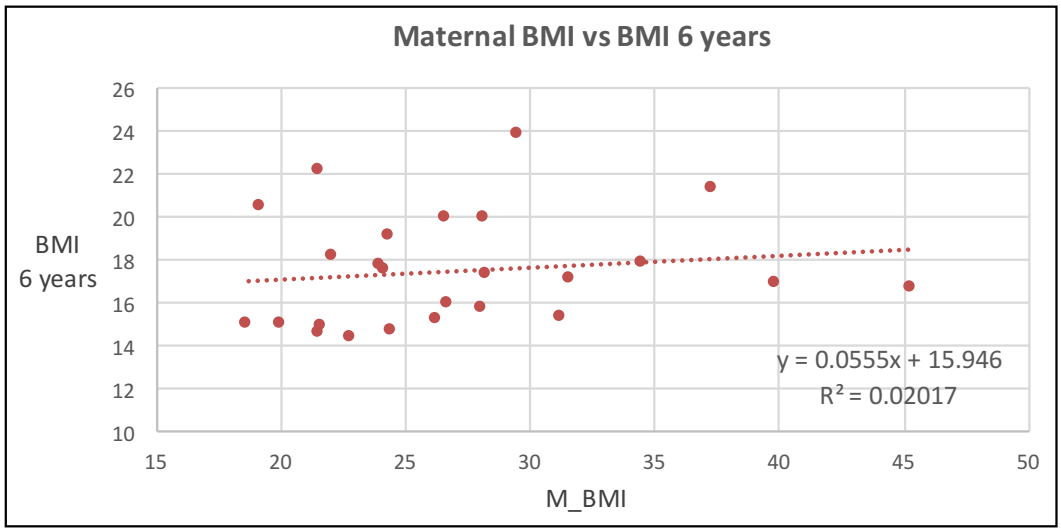

Figure S8: Linear regression between maternal BMI and children's BMI at 6 years in non-GD groups.

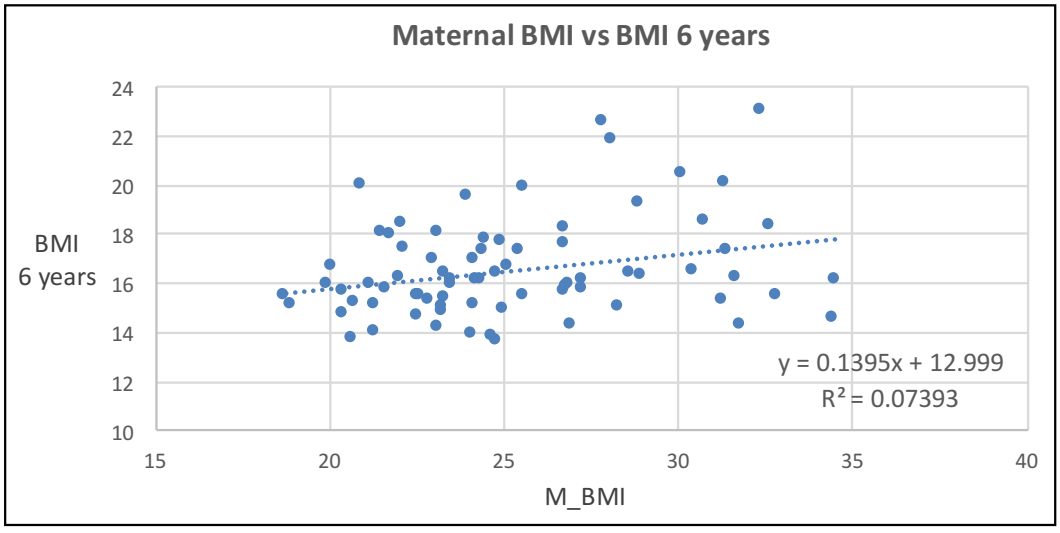

Figure S9: Linear regression between maternal BMI and children's BMI at 6 years in GD groups.

References

Adane, A.A., Mishra, G.D., Tooth, L.R. (2016) Maternal pre-pregnancy obesity and childhood physical and cognitive development of children: a systematic review. International journal of obesity (2005), 40:1608-1618.

Ashburner, J. (2007) A fast diffeomorphic image registration algorithm. NeuroImage, 38:95-113.

Bellou, V., Belbasis, L., Tzoulaki, I., Evangelou, E. (2018) Risk factors for type 2 diabetes mellitus: An exposure-wide umbrella review of meta-analyses. PloS one, 13:e0194127.

Benhalima, K., Devlieger, R., Van Assche, A. (2015) Screening and management of gestational diabetes. Best practice & research. Clinical obstetrics & gynaecology, 29:339-49.

Berglund, S.K., García-Valdés, L., Torres-Espinola, F.J., Segura, M.T., Martínez-Zaldívar, C., Aguilar, M.J., Agil, A., Lorente, J.A., Florido, J., Padilla, C., Altmäe, S., Marcos, A., López-Sabater, M.C., Campoy, C. (2016) Maternal, fetal and perinatal alterations associated with obesity, overweight and gestational diabetes: an observational cohort study (PREOBE). BMC public health, 16:207.

Brinciotti, M., Napoli, A., Mittica, A., Bitterman, O., Matricardi, M. (2011) Cortical evoked potentials in children of diabetic mothers. Experimental diabetes research, 2011:640535.

Chu, S.Y., Callaghan, W.M., Kim, S.Y., Schmid, C.H., Lau, J., England, L.J., Dietz, P.M. (2007) Maternal obesity and risk of gestational diabetes mellitus. Diabetes care, 30:2070-6.

Combrisson, E., Jerbi, K. (2015) Exceeding chance level by chance: The caveat of theoretical chance levels in brain signal classification and statistical assessment of decoding accuracy. Journal of neuroscience methods, 250:126-36.

Cortes, C., Vapnik, V. (1995) Support-vector networks. Machine Learning, 20:273-297.

Deardorff, J., Smith, L.H., Petito, L., Kim, H., Abrams, B.F. (2017) Maternal Prepregnancy Weight and Children's Behavioral and Emotional Outcomes. American journal of preventive medicine, 53:432-440.

Demsar, J., Curk, T., Erjavec, A., Gorup, C., Hocevar, T., Milutinovic, M., Mozina, M., Polajnar, M., Toplak, M., Staric, A., Stajdohar, M., Umek, L., Zagar, L., Zbontar, J., Zitnik, M., Zupan, B. (2013) Orange: Data Mining Toolbox in Python. Journal of Machine Learning Research

International Diabetes Federation. (2019) IDF Diabetes Atlas 9th edn. Brussels, Belgium. International Diabetes Federation.

Khosla, M., Jamison, K., Ngo, G.H., Kuceyeski, A., Sabuncu, M.R. (2019) Machine learning in resting-state fMRI analysis. Magnetic resonance imaging, 64:101-121.

Kim, S.Y., England, L., Sappenfield, W., Wilson, H.G., Bish, C.L., Salihu, H.M., Sharma, A.J. (2012) Racial/ethnic differences in the percentage of gestational diabetes mellitus cases attributable to overweight and obesity, Florida, 2004-2007. Preventing chronic disease, 9:E88.

Koul, A., Becchio, C., Cavallo, A. (2018) PredPsych: A toolbox for predictive machine learning-based approach in experimental psychology research. Behavior research methods, 50:1657-1672.

Li, X., Andres, A., Shankar, K., Pivik, R.T., Glasier, C.M., Ramakrishnaiah, R.H., Zhang, Y., Badger, T.M., Ou, X. (2016) Differences in brain functional connectivity at resting state in neonates born to healthy obese or normal-weight mothers. International journal of obesity (2005), 40:1931-1934.

Linder, K., Schleger, F., Kiefer-Schmidt, I., Fritsche, L., Kümmel, S., Böcker, M., Heni, M., Weiss, M., Häring, H.U., Preissl, H., Fritsche, A. (2015) Gestational Diabetes Impairs Human Fetal Postprandial Brain Activity. The Journal of clinical endocrinology and metabolism, 100:4029-36.

Mack, L.R., Tomich, P.G. (2017) Gestational Diabetes: Diagnosis, Classification, and Clinical Care. Obstetrics and gynecology clinics of North America, 44:207-217.

Mirzaei, G., Adeli, H. (2019) Segmentation and clustering in brain MRI imaging. Reviews in the neurosciences, 30:31.

Orrù, G., Pettersson-Yeo, W., Marquand, A.F., Sartori, G., Mechelli, A. (2012) Using Support Vector Machine to identify imaging biomarkers of neurological and psychiatric disease: a critical review. Neuroscience and biobehavioral reviews, 36:1140-52.

Ou, X., Thakali, K.M., Shankar, K., Andres, A., Badger, T.M. (2015) Maternal adiposity negatively influences infant brain white matter development. Obesity (Silver Spring, Md.), 23:1047-54.

Page, K.A., Luo, S., Wang, X., Chow, T., Alves, J., Buchanan, T.A., Xiang, A.H. (2019) Children Exposed to Maternal Obesity or Gestational Diabetes Mellitus During Early Fetal Development Have Hypothalamic Alterations That Predict Future Weight Gain. Diabetes care, 42:1473-1480.

Pintaudi, B., Fresa, R., Dalfrà, M., Dodesini, A.R., Vitacolonna, E., Tumminia, A., Sciacca, L., Lencioni, C., Marcone, T., Lucisano, G., Nicolucci, A., Bonomo, M., Napoli, A. (2018) The risk stratification of adverse neonatal outcomes in women with gestational diabetes (STRONG) study. Acta diabetologica, 55:1261-1273.

Plows, J.F., Stanley, J.L., Baker, P.N., Reynolds, C.M., Vickers, M.H. (2018) The Pathophysiology of Gestational Diabetes Mellitus. International journal of molecular sciences, 19.

Reynolds, R.M., Allan, K.M., Raja, E.A., Bhattacharya, S., McNeill, G., Hannaford, P.C., Sarwar, N., Lee, A.J., Bhattacharya, S., Norman, J.E. (2013) Maternal obesity during pregnancy and premature mortality from cardiovascular event in adult offspring: follow-up of 1 323 275 person years. Bmj, 347:f4539.

Rojo-Martínez, G., Valdés, S., Soriguer, F., Vendrell, J., Urrutia, I., Pérez, V., Ortega, E., Ocón, P., Montanya, E., Menéndez, E., Lago-Sampedro, A., González-Frutos, T., Gomis, R., Goday, A., García-Serrano, S., García-Escobar, E., Galán-García, J.L., Castell, C., Badía-Guillén, R., Aguilera-Venegas, G., Girbés, J., Gaztambide, S., Franch-Nadal, J., Delgado, E., Chaves, F.J., Castaño, L., Calle-Pascual, A. (2020) Incidence of diabetes mellitus in Spain as results of the nation-wide cohort di@bet.es study. Scientific reports, 10:2765.

Salzwedel, A.P., Gao, W., Andres, A., Badger, T.M., Glasier, C.M., Ramakrishnaiah, R.H., Rowell, A.C., Ou, X. (2018) Maternal Adiposity Influences Neonatal Brain Functional Connectivity. Frontiers in human neuroscience, 12:514.

Schrouff, J., Rosa, M.J., Rondina, J.M., Marquand, A.F., Chu, C., Ashburner, J., Phillips, C., Richiardi, J., Mourão-Miranda, J. (2013) PRoNTo: pattern recognition for neuroimaging toolbox. Neuroinformatics, 11:319-37.

Shub, A., Huning, E.Y., Campbell, K.J., McCarthy, E.A. (2013) Pregnant women's knowledge of weight, weight gain, complications of obesity and weight management strategies in pregnancy. BMC research notes, 6:278.

Solmi, M., Köhler, C.A., Stubbs, B., Koyanagi, A., Bortolato, B., Monaco, F., Vancampfort, D., Machado, M.O., Maes, M., Tzoulaki, I., Firth, J., Ioannidis, J.P.A., Carvalho, A.F. (2018) Environmental risk factors and nonpharmacological and nonsurgical interventions for obesity: An umbrella review of meta-analyses of cohort studies and randomized controlled trials. European journal of clinical investigation, 48:e12982.

Sousa, R.A.L., Torres, Y.S., Figueiredo, C.P., Passos, G.F., Clarke, J.R. (2018) Consequences of gestational diabetes to the brain and behavior of the offspring. Anais da Academia Brasileira de Ciencias, 90:2279-2291.

Torres-Espínola, F.J., Berglund, S.K., García, S., Pérez-García, M., Catena, A., Rueda, R., Sáez, J.A., Campoy, C. (2018) Visual evoked potentials in offspring born to mothers with overweight, obesity and gestational diabetes. PloS one, 13:e0203754.

Torres-Espinola, F.J., Berglund, S.K., García-Valdés, L.M., Segura, M.T., Jerez, A., Campos, D., Moreno-Torres, R., Rueda, R., Catena, A., Pérez-García, M., Campoy, C. (2015) Maternal Obesity, Overweight and Gestational Diabetes Affect the Offspring Neurodevelopment at 6 and 18 Months of Age--A Follow Up from the PREOBE Cohort. PloS one, 10:e0133010.

Verdejo-Román, J., Björnholm, L., Muetzel, R.L., Torres-Espínola, F.J., Lieslehto, J., Jaddoe, V., Campos, D., Veijola, J., White, T., Catena, A., Nikkinen, J., Kiviniemi, V., Järvelin, M.R., Tiemeier, H., Campoy, C., Sebert, S., El Marroun, H. (2019) Maternal prepregnancy body mass index and offspring white matter microstructure: results from three birth cohorts. International journal of obesity (2005), 43:1995-2006.

Wang, M.L., Arroyo, J., Druker, S., Sankey, H.Z., Rosal, M.C. (2015) Knowledge, Attitudes and Provider Advice by Pre-Pregnancy Weight Status: A Qualitative Study of Pregnant Latinas With Excessive Gestational Weight Gain. Women & health, 55:805-28.

Ward, J.H. (1963) Hierarchical Grouping to Optimize an Objective Function. Journal of the American Statistical Association, 58:236-244.

Whitaker, R.C. (2004) Predicting preschooler obesity at birth: the role of maternal obesity in early pregnancy. Pediatrics, 114:e29-36.

Yan, C.G., Wang, X.D., Zuo, X.N., Zang, Y.F. (2016) DPABI: Data Processing & Analysis for (Resting-State) Brain Imaging. Neuroinformatics, 14:339-51.

Yeung, E.H., Sundaram, R., Ghassabian, A., Xie, Y., Buck Louis, G. (2017) Parental Obesity and Early Childhood Development. Pediatrics, 139.

3 – **Discussion and conclusions**

The included studies provided an overview of different ways to investigate properties of GM networks. The first three ones, in particular, highlighted how the framework of pathoconnectomics can add new levels of interpretation to understand specific brain disorders, the pathological mechanisms behind them, and even the detailed involvement of a given brain region. As pointed out, all these different scales can be investigated with the same methodology, simply changing a few parameters during data selection. Interestingly, the evidence obtained adopting a transdiagnostic approach can provide a contribution to the still open debate concerning disorders taxonomy and diagnostic process in clinical practice, at least in the Western world. Notably, in their seminal paper in the field of pathoconnectomics Rubinov and Bullmore (2013) specified as one of the main challenges of this paradigm the "brain-network-based delineation of psychiatric disorders". The same can be extended to neurodegenerative diseases (Deco & Kringelbach, 2014). For many years, the predominant approach has been principally based on the identification of a disorder through the recognition of a collection of symptoms (Lilienfeld & Treadway, 2016). This guided the definition of both the ICDs system and the DSMs, so that each disease, either psychiatric or neurological, ended up to be considered as a clearly defined entity. Consequently, a relevant proliferation of diagnostic labels took place. However, clinicians often interpret particular combinations of symptoms as cases of comorbidity (Krueger & Markon, 2006). On the other hand, only a reduced set of clinical symptoms can be really considered pathognomonic, in virtue of their high specificity and sensitivity for a defined disease. In many cases symptoms appear instead in a cross-disorder way, and this is the conceptual base for the differential diagnosis in the clinical reasoning. In recent years, medical conditions usually thought as independent (or clinically distant one to each other) have shown to be not as far as initially considered. In some cases, this even motivated the inclusion in a common spectrum. A relevant evidence in this sense is the identification of a shared biological background. This was the case of frontotemporal dementia and amyotrophic lateral sclerosis, showing complex overlap from a neuropathological, clinical and genetic point of view (Ravits, 2014; Ravits et al., 2013). Shared elements were also described among multiple sclerosis, Baló's concentric sclerosis and tumefactive demyelination (T. A. Hardy, Tobin, & Lucchinetti, 2016), or between frontotemporal dementia and Alzheimer's disease (Padovani et al., 2013). Further commonalities between disorders are emerging thanks to the advances in genetics are (Anttila et al., 2018; Gershon & Grennan, 2015; Yokoyama et al., 2017) (Anttila et al. 2018; Gershon

and Grennan 2015; Yokoyama et al. 2017). For example, genetic correlation has been proposed for amyotrophic lateral sclerosis and schizophrenia (McLaughlin et al., 2017). This growing body of evidence matches with different initiatives, as the RDoC framework (Insel, 2014; Insel et al., 2010) or the HiTOP (Kotov, Krueger, & Watson, 2018), that started in last years a process of reconsideration of the approach to disorders taxonomy and diagnostic procedure.

The one-to-one mapping between symptoms and pathologies is challenged by latest findings and advances in the field of neuroimaging too. If taken as valid, in fact, the matching of each disorder with a distinct pattern of brain alteration should be expected. However, based on growing evidence, this seems to be the exception rather than the rule. This aspect was specifically investigated by our team in a recent study (not included in extenso in the present thesis because not based on the co-alteration network method) (Franco Cauda et al., 2019). Briefly, an index named "alteration entropy" was developed, to measure the amount of different disorders associated with structural alteration in each voxel of the brain. The results showed that the majority of the brain regions can be disrupted by a wide range of both psychiatric and neurodegenerative pathologies. In light of this, given a detected pattern of cerebral alteration is hardly possible to assign it to a single pathology. This could be due, at least in part, to the clinical stage captured by the experiments analyzed. In fact, clinical and research data collected from affected subjects often represent a symptomatic stage of the disease. Indeed, at this late phase the progression of the alteration could have reached a vast portion of the whole brain, although probably started from a circumscribed region (or set of regions). This aspect seems to be confirmed by a further work recently published by our group (not included in extenso) showing that, at least in Alzheimer's disease, the brain regions expressing higher specificity for this disorder are also among the first to be altered (Franco Cauda et al., 2020). As proposed in the introduction, the analysis of the co-alteration networks in place of simple patterns could help to disentangle this complex landscape. In fact, at least in theory, in case of two conditions showing similar ALE maps the obtained co-alteration networks could highlight different relationships between the same brain regions. This issue had been preliminarily addressed in abstract presented by our group during OHBM 2018, comparing the co-alteration networks of Alzheimer's disease and frontotemporal dementia (Nani et al., 2018). Results showed the overlap of altered nodes localized in superior temporal gyrus, amygdala, and hippocampus between the two conditions, but a well differentiated structure of their co-alteration networks. Moreover, although the co-alteration network of frontotemporal dementia consisted of more edges,

Alzheimer's disease presented a co-atrophy network with a greater number of highly co-altered nodes. This aspect, that would have not been identified through the analyses of the sole ALE patterns, possibly suggested a more intense process of co-alteration, yet needing further investigation to be confirmed.

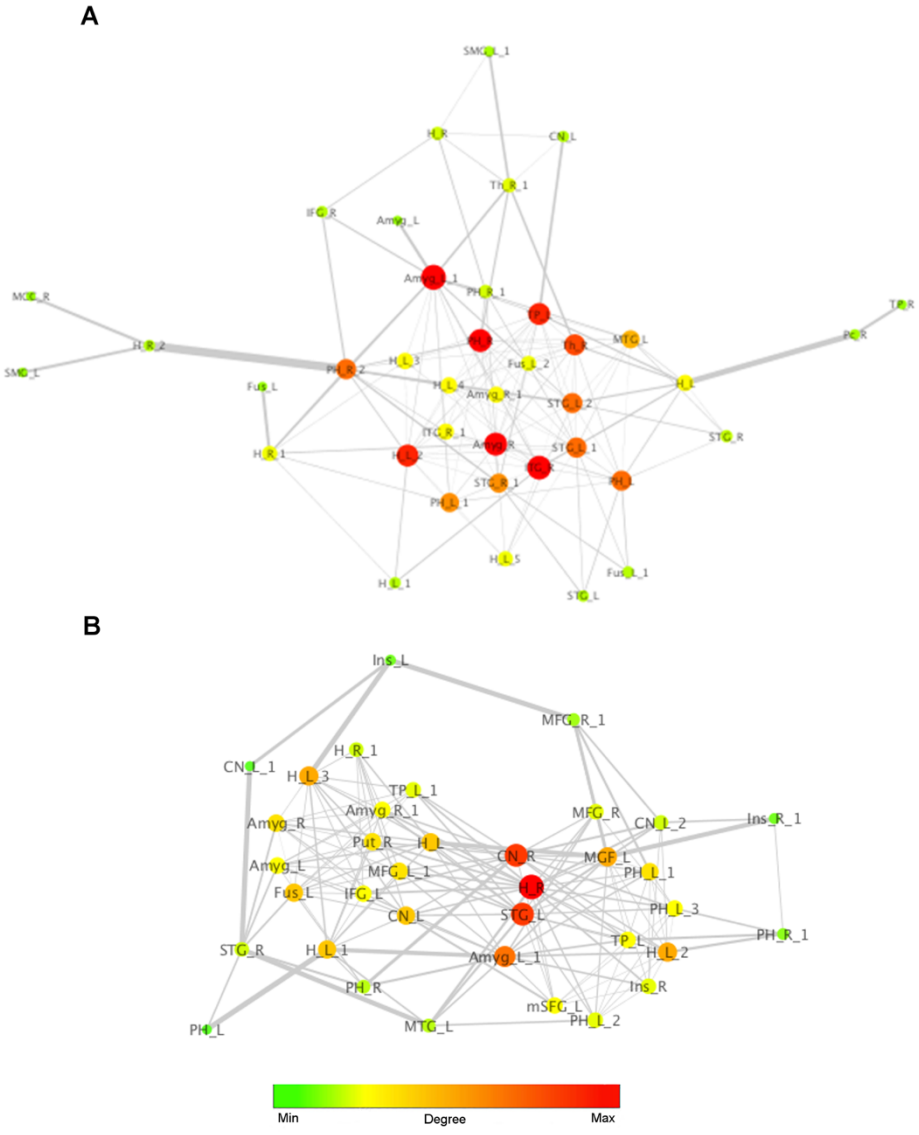

Figure 4: The co-alteration network of Alzheimer's disease (A) and frontotemporal dementia (B). Nodes' size and color represent degree, while edges' thickness represent edge betweenness.

A further possible approach to tackle the issue of distinction between disorders relies on the clustering of the nodes based on their profile of co-alteration. If applied to multiple co-alteration networks built using a same set of nodes, this procedure could highlight a different role of a brain region between two (or more) disorders, observing how it tends to be clustered with respect to the rest of the co-alteration network.

A second meaningful point that can be addressed by means of the co-alteration networks detection, and at the same time one of the ultimate goals of this approach, is the comprehension of how the alteration spreads across the brain. This aspect would help to follow the temporal evolution of a disease, since its early potentially asymptomatic stages. A key element to this aim, as mentioned in the selected studies, is the transition from undirected to directed co-alteration networks. Although already computationally possible, the soundness of using Patel's tau on this kind of data still needs further support. Providing this has high priority for the future development of our methodology. Nonetheless, it would be possible to argue that starting from structural meta-analytic data it is not possible to infer a pattern of propagation, requiring instead longitudinal data. In fact, VBM experiments provide a static picture of a state, while the concept of propagation implies a causal event characterized by a precise temporal directionality. However, it is possible to demonstrate that a description of the propagation pattern can be obtained modelling a diffusion process (Kondor & Lafferty, 2002) on the basis of the co-alteration matrix built using Patel's k (Abdelnour, Voss, & Raj, 2014). In fact, the co-alteration matrix (of size n x n, where n is the number of nodes in the network) is tantamount to an adjacency matrix, from which a degree matrix can be obtained, allowing to describe the transition between two states of a system (F. Cauda et al., 2018). The last element needed to fully model the spread trajectory is the starting point of the propagation, but, unfortunately, this information can't be extracted from meta-analytic data. However, even in absence of this, the existing theoretical support allows to reasonably state that a diffusion process occurs along the edges of a co-alteration network.

In addition to the introduction of directionality, a major goal for the future will be the comparison of the co-alteration network with further kind of data. In particular, relevant knowledge could come from the analysis of vascularization maps. First, the vascular system has a network-like nature, a favourable feature to be entered in a network-based framework. Notably, the available imaging techniques allow its in vivo detection to a very good level of detail, and relying much

less on probabilistic estimation than tractography. Moreover, the circulation allows to build a directed network without resorting to statistical strategies, unlike effective connectivity or Patel's tau. The information coming from the blood flow could also interact in a meaningful way with functional connectivity networks, being in turn based on BOLD effect. From a clinical point of view, data about vascularization could allow to think in terms of pathoconnectomics about cardiovascular disorders affecting the brain, while these are currently difficult to be included in transdiagnostic studies together with psychiatric and neurodegenerative pathologies due to their different nature. Finally, these data could support a hypothesized failure in the production of trophic factors behind the deterioration of neural wiring and, in turn, the propagation of alteration, known as trophic failure (Zhou et al., 2012). At the present stage, the main issue to be solved to turn this speculation into facts is the integration of vascular data, usually collected at subject level, and the ALE maps, by definition on a meta-analytic level. During the last years some attempts have been done to adapt our methodology to subject-level data. The individual spatially standardized GM maps obtained as intermediate product of the VBM pipeline could be technically suitable. However, in absence of normative intensity values to discriminate between T1 images of healthy and pathological subjects, the main issue remains the identification of focal structural alteration and the consequent creation of the nodes.

The advantages of working on subject-level data, especially in terms of design flexibility and chance to detect subtle effects, emerged from the fourth and fifth study included. In fact, the peculiarity of the PREOBE cohort allowed to investigate transgenerational effects, modelling two different clinical features at the same time. The research carried out in Oxford, instead, benefited from the significant sample size of UK Biobank, that made possible to characterize the association with variables explaining even a very small fraction of variance, but in a strongly significant way. Despite the different methodologies used in these two studies, the opposed way of inference ("from features to network" the former, "from network to features" the latter), and the different subjects' age, it is interesting to note that both converged in finding a role of diabetes and, to a less extent, body size measurements. This evidence, together with the effect for cholesterol and blood pressure in the Oxford study, could suggest a more general relationship between GM structural properties and cardiovascular state (Boots et al., 2019; Gonzales et al., 2017). Both these last studies potentially offer the prospect of follow-up researches. The children in the PREOBE cohort had been recently re-scanned at the age of 8 years, allowing an interesting prospective evaluation of the evolution of the effects described at 6

years old. As for UK Biobank, the sample size is intended to more than double while the goal of scanning 100,000 participants is reached.

Besides the incorporation of subject-level data, a future planned development of the co-alteration network methodology would allow to model further variables and meta-data associated with the single experiments. Although the classic meta-analytic level does not allow to access details for each subject included in the various samples, unless adopting something similar to a mega-analysis approach (Boedhoe et al., 2018), additional information about the sample analyzed is often available. This includes, at least, average age ad male/female ratio, but in some cases duration of illness, disorder sub-type, or score to specific clinical tests are also reported. These could be regressed on the MA maps as nuisance variables, propagating their effects to the ALE map, or modelled during the edges computation. One possible option could be to leverage the information on the contribution of the foci to each blob in the ALE map, already provided by the ALE implementation in the GingerALE tool. As described before, our methodology marks the local maxima of the ALE map with nodes, so that a correspondence exists between a node and a blob of the ALE map. It is also known which of the foci contribute to a blob (i.e. a node), as well as which experiment each of those foci belongs to. Therefore, when the aforementioned kinds of information are available for an experiment, these can be used to characterize the foci reported for that experiment. In turn, the features can be extended to the blob these foci contribute to, and hence to the corresponding node. In this way, the nodes in the co-alteration network could be enhanced with clinical/biological information. However, further development is needed to turn this hypothetical approach into a concrete methodology. At the moment, for example, the information concerning duration of illness or disorder sub-type is used to split the available study into sub-groups (e.g. at risk for schizophrenia, early diagnosed, chronic patients) that are independently analyzed, with results being compared at a later stage. In other cases, this process leads to the identification of a small class that is removed from the pool. Alternatively, one general dataset could be preserved, improving the statistical power, and providing additional information not obtained with the current approach. A somewhat similar solution was developed to complement SDM methodology (Radua et al., 2012; Radua, van den Heuvel, Surguladze, & Mataix-Cols, 2010).

As described, the co-alteration network approach had been conceived and developed in the framework of CBMA. Nonetheless, the methodology could be shifted to IBMA without requiring serious modifications. In fact, the essential

elements of the described approach are the maps representing results of each experiment in the dataset, and a final higher-level (meta-analytic) map. In CBMA the former are the MA maps, while the latter is the ALE map. In actual fact, the MA maps are a reconstruction of the original results maps made from the foci. Therefore, in the IBMA original maps would be already available. The strategy described to define the nodes of a co-alteration network is equally suitable for any kind of spatial maps, including the results of a IBMA. Finally, Patels' k could be used to compute the likelihood of co-alteration of each couple of nodes across the maps related with each of the experiments. If compared with the CBMA scenario, the IBMA version could allow the identification of a higher number of nodes in the co-alteration network. In fact, a MA map heavily depends on the amount of foci reported, and this can vary from just one to several tens. The degree to which this reflects the real spatial extent of the original map is tied to the level of detail (and care) adopted by the authors of each experiment. On the other hand, the ALE algorithm considers the sample size of each experiment, giving a greater weight to bigger samples. In the IBMA version, the use of the original maps without some kind of correction would not allow to control for this possible bias. In light of the technical feasibility, a direct comparison between IBMA and CBMA on a same dataset (as in Salimi-Khorshidi et al., 2009) could help to evaluate the actual pros and cons of each scenario.

Although the scientific domain this research project belongs to is far from a direct clinical application, it is anyway possible and potentially useful to speculate on it. Especially because, in a hopefully not too far future, our approach could contribute to tackle brain disorders characterized by neurodegeneration. When co-alteration networks will have become directional, allowing to reliably estimate the propagation process, it could be possible to identify those focal brain regions that once compromised open the way to a fast and widespread propagation of the structural damage. Those hubs could thus be the target of future medicines or other therapeutic strategies to prevent the beginning of degenerative cascades still at a presymptomatic stage of the disease.

To conclude, the present thesis discussed different approaches to the analysis of GM networks in both healthy and pathological brain. When working on subject-level data, two different designs were adopted to investigate the relationship between GM structural properties and non-brain factors, having the chance to analyze peculiar healthy cohorts. On the pathological side, the development and application of a new method to enhance CBMA combining it with network analysis was described. At the end of this fascinating project I hope that the developed

technique and the results obtained will contribute to the progress of the pathoconnectomics field.

Acknowledgments

When I started this PhD course, I had clear in my mind this would have meant four years of hard work. It has been so indeed. But what I hadn't prefigured were the amazing experiences I had in front of me. This part of my career allowed me travelling a lot, living abroad in two different countries, meeting wonderful people, having a friendly meal with some of the greatest scientists active in my research field. I'm profoundly grateful to each of these people for what they left in my life.

Heartfelt thanks to my supervisor Prof. Franco Cauda for had allowed all this to happen. He has always been there to offer me his wise guidance, but letting me free to take decisions in the end.

I'm grateful to Prof. Tommaso Costa especially for having provided me the roots of my coding skills, that really saved me while I was dealing with the most complex stage of my project.

My wholehearted thanks to Dr. Sergio Duca for the chance he gave me to balance the computational side of my training with medical and clinical experience.

Thanks to all my current and past mates at FocusLab. We did a lot together, and we did it smiling most of the time. This should never be taken for granted.

Muchisimas gracias to Dr. Juan Verdejo-Román and Prof. Miguel Pérez-García for having welcomed me in the PNinsula group, and to all the amazing people of the lab. They turned the months spent in Granada into a life-changing experience, and I carry each of them in my heart.

Thanks from the bottom of my heart to Prof. Gwenaëlle Douaud for the incredible chance she gave me to work with her and to learn from her, in the iconic FMRIB at University of Oxford. That was nothing but a dream at the beginning of my PhD training.

I'm grateful to Prof. Emiliano Ricciardi and Prof. Michael Lombardo for the time spent to revise the present thesis, providing me with meaningful comments and suggestions.

Finally, the most profound thanks to my wife Caterina and my son Carlos, who was not on this Earth yet when this PhD career started. I'm sadly aware that some of the

hours I spent in front of my laptop should have been dedicated to you two instead. It had been hard at some point, but we came out from that holding each other hands tightly.

References

Abdelnour, F., Voss, H. U., & Raj, A. (2014). Network diffusion accurately models the relationship between structural and functional brain connectivity networks. *Neuroimage, 90*, 335-347. doi:10.1016/j.neuroimage.2013.12.039

Acar, F., Seurinck, R., Eickhoff, S. B., & Moerkerke, B. (2018). Assessing robustness against potential publication bias in Activation Likelihood Estimation (ALE) meta-analyses for fMRI. *PLoS One, 13*(11), e0208177. doi:10.1371/journal.pone.0208177

Aggarwal, R., & Ranganathan, P. (2016). Common pitfalls in statistical analysis: The use of correlation techniques. *Perspect Clin Res, 7*(4), 187-190. doi:10.4103/2229-3485.192046

Aguzzi, A., Nuvolone, M., & Zhu, C. (2013). The immunobiology of prion diseases. *Nat Rev Immunol, 13*(12), 888-902. doi:10.1038/nri3553

Alvarez-Hamelin, I., Dall'asta, L., Barrat, A., & Vespignani, A. (2005). k-core decomposition: a tool for the visualization of large scale networks. *ar.XiV; cs.NI/0504107*.

Anttila, V., Bulik-Sullivan, B., Finucane, H. K., Walters, R. K., Bras, J., Duncan, L., . . . Murray, R. (2018). Analysis of shared heritability in common disorders of the brain. *Science, 360*(6395). doi:10.1126/science.aap8757

Ashburner, J., & Friston, K. J. (2000). Voxel-based morphometry--the methods. *Neuroimage, 11*(6 Pt 1), 805-821. doi:10.1006/nimg.2000.0582

Ashburner, J., & Friston, K. J. (2001). Why voxel-based morphometry should be used. *Neuroimage, 14*(6), 1238-1243. doi:10.1006/nimg.2001.0961

Bader, G. D., & Hogue, C. W. (2003). An automated method for finding molecular complexes in large protein interaction networks. *BMC Bioinformatics, 4*, 2.

Barabási, D. L., & Barabási, A. L. (2020). A Genetic Model of the Connectome. *Neuron, 105*(3), 435-445.e435. doi:10.1016/j.neuron.2019.10.031

Bedia, C. (2018). Chapter Two - Experimental Approaches in Omic Sciences. In J. Jaumot, C. Bedia, & R. Tauler (Eds.), *Comprehensive Analytical Chemistry* (Vol. 82, pp. 13-36): Elsevier.

Behrens, T. E., & Sporns, O. (2012). Human connectomics. *Curr Opin Neurobiol, 22*(1), 144-153. doi:10.1016/j.conb.2011.08.005

Berglund, S. K., García-Valdés, L., Torres-Espinola, F. J., Segura, M. T., Martínez-Zaldívar, C., Aguilar, M. J., . . . Campoy, C. (2016). Maternal, fetal and perinatal alterations associated with obesity, overweight and gestational diabetes: an observational cohort study (PREOBE). *BMC Public Health, 16*, 207. doi:10.1186/s12889-016-2809-3

Binvignat, O., & Olloquequi, J. (2020). Excitotoxicity as a Target Against Neurodegenerative Processes. *Curr Pharm Des, 26*(12), 1251-1262. doi:10.2174/1381612826666200113162641

Boedhoe, P. S. W., Heymans, M. W., Schmaal, L., Abe, Y., Alonso, P., Ameis, S. H., . . . Twisk, J. W. R. (2018). An Empirical Comparison of Meta- and Mega-Analysis With Data From the ENIGMA Obsessive-Compulsive Disorder Working Group. *Front Neuroinform, 12*, 102. doi:10.3389/fninf.2018.00102

Boots, E. A., Zhan, L., Dion, C., Karstens, A. J., Peven, J. C., Ajilore, O., & Lamar, M. (2019). Cardiovascular disease risk factors, tract-based structural connectomics, and cognition in older adults. *Neuroimage, 196*, 152-160. doi:10.1016/j.neuroimage.2019.04.024

Bourdenx, M., Koulakiotis, N. S., Sanoudou, D., Bezard, E., Dehay, B., & Tsarbopoulos, A. (2017). Protein aggregation and neurodegeneration in prototypical neurodegenerative diseases: Examples of amyloidopathies, tauopathies and synucleinopathies. *Prog Neurobiol, 155*, 171-193. doi:10.1016/j.pneurobio.2015.07.003

Bullmore, E., & Sporns, O. (2009). Complex brain networks: graph theoretical analysis of structural and functional systems. *Nat Rev Neurosci, 10*(3), 186-198. doi:10.1038/nrn2575

Caspers, J., Zilles, K., Beierle, C., Rottschy, C., & Eickhoff, S. B. (2014). A novel meta-analytic approach: mining frequent co-activation patterns in neuroimaging databases. *Neuroimage, 90*, 390-402. doi:10.1016/j.neuroimage.2013.12.024

Caspers, J., Zilles, K., Eickhoff, S. B., & Beierle, C. (2012, 20-22 June 2012). *PaMiNI: A comprehensive system for mining frequent neuronal patterns of the human brain.* Paper presented at the 2012 25th IEEE International Symposium on Computer-Based Medical Systems (CBMS).

Catani, M., Thiebaut de Schotten, M., Slater, D., & Dell'Acqua, F. (2013). Connectomic approaches before the connectome. *Neuroimage, 80*, 2-13. doi:10.1016/j.neuroimage.2013.05.109

Cauda, F., Nani, A., Costa, T., Palermo, S., Tatu, K., Manuello, J., . . . Keller, R. (2018). The morphometric co-atrophy networking of schizophrenia, autistic and obsessive spectrum disorders. *Hum Brain Mapp*. doi:10.1002/hbm.23952

Cauda, F., Nani, A., Liloia, D., Manuello, J., Premi, E., Duca, S., . . . Costa, T. (2020). Finding specificity in structural brain alterations through Bayesian reverse inference. *Hum Brain Mapp, n/a*(n/a). doi:10.1002/hbm.25105

Cauda, F., Nani, A., Manuello, J., Liloia, D., Tatu, K., Vercelli, U., . . . Costa, T. (2019). The alteration landscape of the cerebral cortex. *Neuroimage, 184*, 359-371. doi:https://doi.org/10.1016/j.neuroimage.2018.09.036

Chevalier-Larsen, E., & Holzbaur, E. L. (2006). Axonal transport and neurodegenerative disease. *Biochim Biophys Acta, 1762*(11-12), 1094-1108. doi:10.1016/j.bbadis.2006.04.002

Cioli, C., Abdi, H., Beaton, D., Burnod, Y., & Mesmoudi, S. (2014). Differences in human cortical gene expression match the temporal properties of large-scale functional networks. *PLoS One, 9*(12), e115913. doi:10.1371/journal.pone.0115913

Clarke, E., & Dewhurst, K. (1996). *An illustrated history of brain function*. San Francisco: Norman Publishing.

Clavaguera, F., Bolmont, T., Crowther, R. A., Abramowski, D., Frank, S., Probst, A., . . . Tolnay, M. (2009). Transmission and spreading of tauopathy in transgenic mouse brain. *Nat Cell Biol, 11*(7), 909-913. doi:10.1038/ncb1901

Clavaguera, F., Grueninger, F., & Tolnay, M. (2014). Intercellular transfer of tau aggregates and spreading of tau pathology: Implications for therapeutic strategies. *Neuropharmacology, 76 Pt A*, 9-15. doi:10.1016/j.neuropharm.2013.08.037

Clavaguera, F., Lavenir, I., Falcon, B., Frank, S., Goedert, M., & Tolnay, M. (2013). "Prion-like" templated misfolding in tauopathies. *Brain Pathol, 23*(3), 342-349. doi:10.1111/bpa.12044

Congdon, E., Poldrack, R. A., & Freimer, N. B. (2010). Neurocognitive phenotypes and genetic dissection of disorders of brain and behavior. *Neuron, 68*(2), 218-230. doi:10.1016/j.neuron.2010.10.007

Costafreda, S. G., David, A. S., & Brammer, M. J. (2009). A parametric approach to voxel-based meta-analysis. *Neuroimage, 46*(1), 115-122. doi:10.1016/j.neuroimage.2009.01.031

Crossley, N. A., Mechelli, A., Scott, J., Carletti, F., Fox, P. T., McGuire, P., & Bullmore, E. T. (2014). The hubs of the human connectome are generally implicated in the anatomy of brain disorders. *Brain, 137*(Pt 8), 2382-2395. doi:10.1093/brain/awu132

Deco, G., & Kringelbach, M. L. (2014). Great expectations: using whole-brain computational connectomics for understanding neuropsychiatric disorders. *Neuron, 84*(5), 892-905. doi:10.1016/j.neuron.2014.08.034

Douaud, G., Groves, A. R., Tamnes, C. K., Westlye, L. T., Duff, E. P., Engvig, A., . . . Johansen-Berg, H. (2014). A common brain network links development, aging, and vulnerability to disease. *Proc Natl Acad Sci U S A, 111*(49), 17648-17653. doi:10.1073/pnas.1410378111

Du, M. Y., Wu, Q. Z., Yue, Q., Li, J., Liao, Y., Kuang, W. H., . . . Gong, Q. Y. (2012). Voxelwise meta-analysis of gray matter reduction in major depressive disorder. *Prog Neuropsychopharmacol Biol Psychiatry, 36*(1), 11-16. doi:10.1016/j.pnpbp.2011.09.014

Eickhoff, S. B., Laird, A. R., Grefkes, C., Wang, L. E., Zilles, K., & Fox, P. T. (2009). Coordinate-based activation likelihood estimation meta-analysis of neuroimaging data: a random-effects approach based on empirical estimates of spatial uncertainty. *Hum Brain Mapp, 30*(9), 2907-2926. doi:10.1002/hbm.20718

Eickhoff, S. B., Nichols, T. E., Laird, A. R., Hoffstaedter, F., Amunts, K., Fox, P. T., . . . Eickhoff, C. R. (2016). Behavior, sensitivity, and power of activation likelihood estimation characterized by massive empirical simulation. *Neuroimage, 137*, 70-85. doi:10.1016/j.neuroimage.2016.04.072

Fornito, A., Yücel, M., Patti, J., Wood, S. J., & Pantelis, C. (2009). Mapping grey matter reductions in schizophrenia: an anatomical likelihood estimation analysis of voxel-based morphometry studies. *Schizophr Res, 108*(1-3), 104-113. doi:10.1016/j.schres.2008.12.011

Fox, P. T., Laird, A. R., Fox, S. P., Fox, P. M., Uecker, A. M., Crank, M., . . . Lancaster, J. L. (2005). BrainMap taxonomy of experimental design: description and evaluation. *Hum Brain Mapp, 25*(1), 185-198. doi:10.1002/hbm.20141

Fox, P. T., & Lancaster, J. (1994). Neuroscience on the net. *Science, 266*(5187), 994-996. doi:10.1126/science.7973682

Fox, P. T., & Lancaster, J. L. (2002). Opinion: Mapping context and content: the BrainMap model. *Nat Rev Neurosci, 3*(4), 319-321. doi:10.1038/nrn789

Fox, P. T., Parsons, L. M., & Lancaster, J. L. (1998). Beyond the single study: function/location metanalysis in cognitive neuroimaging. *Curr Opin Neurobiol, 8*(2), 178-187. doi:10.1016/s0959-4388(98)80138-4

French, L., & Pavlidis, P. (2011). Relationships between gene expression and brain wiring in the adult rodent brain. *PLoS Comput Biol, 7*(1), e1001049. doi:10.1371/journal.pcbi.1001049

French, L., Tan, P. P., & Pavlidis, P. (2011). Large-Scale Analysis of Gene Expression and Connectivity in the Rodent Brain: Insights through Data Integration. *Front Neuroinform, 5*, 12. doi:10.3389/fninf.2011.00012

Frisoni, G. B., Fox, N. C., Jack, C. R., Jr., Scheltens, P., & Thompson, P. M. (2010). The clinical use of structural MRI in Alzheimer disease. *Nat Rev Neurol, 6*(2), 67-77. doi:10.1038/nrneurol.2009.215

Friston, K. J. (2011). Functional and effective connectivity: a review. *Brain Connect, 1*(1), 13-36. doi:10.1089/brain.2011.0008

Gershon, E. S., & Grennan, K. S. (2015). Genetic and genomic analyses as a basis for new diagnostic nosologies. *Dialogues Clin Neurosci, 17*(1), 69-78.

Girvan, M., & Newman, M. E. (2002). Community structure in social and biological networks. *Proc Natl Acad Sci U S A, 99*(12), 7821-7826. doi:10.1073/pnas.122653799

Goedert, M., Clavaguera, F., & Tolnay, M. (2010). The propagation of prion-like protein inclusions in neurodegenerative diseases. *Trends Neurosci, 33*(7), 317-325. doi:10.1016/j.tins.2010.04.003

Goedert, M., Masuda-Suzukake, M., & Falcon, B. (2017). Like prions: the propagation of aggregated tau and alpha-synuclein in neurodegeneration. *Brain, 140*(2), 266-278. doi:10.1093/brain/aww230

Gonzales, M. M., Ajilore, O., Charlton, R. C., Cohen, J., Yang, S., Sieg, E., . . . Lamar, M. (2017). Divergent Influences of Cardiovascular Disease Risk Factor Domains on Cognition and Gray and White Matter Morphology. *Psychosom Med, 79*(5), 541-548. doi:10.1097/psy.0000000000000448

Good, C. D., Johnsrude, I. S., Ashburner, J., Henson, R. N., Friston, K. J., & Frackowiak, R. S. (2001). A voxel-based morphometric study of ageing in 465 normal adult human brains. *Neuroimage, 14*(1 Pt 1), 21-36. doi:10.1006/nimg.2001.0786

Hallahan, B., Newell, J., Soares, J. C., Brambilla, P., Strakowski, S. M., Fleck, D. E., . . . McDonald, C. (2011). Structural magnetic resonance imaging in bipolar disorder: an international collaborative mega-analysis of individual adult patient data. *Biol Psychiatry, 69*(4), 326-335. doi:10.1016/j.biopsych.2010.08.029

Hardy, J., & Revesz, T. (2012). The Spread of Neurodegenerative Disease. *New England Journal of Medicine, 366*(22), 2126-2128. doi:10.1056/NEJMcibr1202401

Hardy, T. A., Tobin, W. O., & Lucchinetti, C. F. (2016). Exploring the overlap between multiple sclerosis, tumefactive demyelination and Balo's concentric sclerosis. *Mult Scler, 22*(8), 986-992. doi:10.1177/1352458516641776

Havlicek, M., Roebroeck, A., Friston, K. J., Gardumi, A., Ivanov, D., & Uludag, K. (2017). On the importance of modeling fMRI transients when estimating effective connectivity: A dynamic causal modeling study using ASL data. *Neuroimage, 155*, 217-233. doi:10.1016/j.neuroimage.2017.03.017

Honey, C. J., Sporns, O., Cammoun, L., Gigandet, X., Thiran, J. P., Meuli, R., & Hagmann, P. (2009). Predicting human resting-state functional connectivity from structural connectivity. *Proc Natl Acad Sci U S A, 106*(6), 2035-2040. doi:10.1073/pnas.0811168106

Huang, H., & Ding, M. (2016). Linking Functional Connectivity and Structural Connectivity Quantitatively: A Comparison of Methods. *Brain Connect, 6*(2), 99-108. doi:10.1089/brain.2015.0382

Insel, T. (2014). The NIMH Research Domain Criteria (RDoC) Project: precision medicine for psychiatry. *Am J Psychiatry, 171*(4), 395-397. doi:10.1176/appi.ajp.2014.14020138

Insel, T., Cuthbert, B., Garvey, M., Heinssen, R., Pine, D. S., Quinn, K., . . . Wang, P. (2010). Research domain criteria (RDoC): toward a new classification framework for research on mental disorders. *Am J Psychiatry, 167*(7), 748-751. doi:10.1176/appi.ajp.2010.09091379

Jucker, M., & Walker, L. C. (2011). Pathogenic protein seeding in Alzheimer disease and other neurodegenerative disorders. *Ann Neurol, 70*(4), 532-540. doi:10.1002/ana.22615

Jucker, M., & Walker, L. C. (2013). Self-propagation of pathogenic protein aggregates in neurodegenerative diseases. *Nature, 501*(7465), 45-51. doi:10.1038/nature12481

Kondor, R. I., & Lafferty, J. (2002). Diffusion kernels on graphs and other discrete input spaces *ICML* (Vol. 2, pp. 315-322).

Korth, C. (2012). Aggregated proteins in schizophrenia and other chronic mental diseases: DISC1opathies. *Prion, 6*(2), 134-141. doi:10.4161/pri.18989

Kotov, R., Krueger, R. F., & Watson, D. (2018). A paradigm shift in psychiatric classification: the Hierarchical Taxonomy Of Psychopathology (HiTOP). *World Psychiatry, 17*(1), 24-25. doi:10.1002/wps.20478

Kraus, A., Groveman, B. R., & Caughey, B. (2013). Prions and the potential transmissibility of protein misfolding diseases. *Annu Rev Microbiol, 67*, 543-564. doi:10.1146/annurev-micro-092412-155735

Krueger, R. F., & Markon, K. E. (2006). Reinterpreting comorbidity: a model-based approach to understanding and classifying psychopathology. *Annu Rev Clin Psychol, 2*, 111-133. doi:10.1146/annurev.clinpsy.2.022305.095213

Laird, A. R., Lancaster, J. L., & Fox, P. T. (2005). BrainMap: the social evolution of a human brain mapping database. *Neuroinformatics, 3*(1), 65-78.

Lederberg, J., & McCray, A. T. (2001). 'Ome Sweet 'Omics-- A Genealogical Treasury of Words *The Scientist*.

Lee, S.-Y., Chen, M.-H., Chiang, P.-L., Chen, H.-L., Chou, K.-H., Chen, Y.-C., . . . Lin, W.-C. (2018). Reduced gray matter volume and respiratory dysfunction in Parkinson's disease: a voxel-based morphometry study. *BMC Neurology, 18*(1), 73. doi:10.1186/s12883-018-1074-8

Lichtman, J. W., & Sanes, J. R. (2008). Ome sweet ome: what can the genome tell us about the connectome? *Curr Opin Neurobiol, 18*(3), 346-353. doi:10.1016/j.conb.2008.08.010

Lilienfeld, S. O., & Treadway, M. T. (2016). Clashing Diagnostic Approaches: DSM-ICD Versus RDoC. *Annu Rev Clin Psychol, 12*(1), 435-463. doi:10.1146/annurev-clinpsy-021815-093122

Lin, C., Lee, S. H., & Weng, H. H. (2016). Gray Matter Atrophy within the Default Mode Network of Fibromyalgia: A Meta-Analysis of Voxel-Based Morphometry Studies. *Biomed Res Int, 2016*, 7296125. doi:10.1155/2016/7296125

Liu, M., Song, C., Liang, Y., Knöpfel, T., & Zhou, C. (2019). Assessing spatiotemporal variability of brain spontaneous activity by multiscale entropy and functional connectivity. *Neuroimage, 198*, 198-220. doi:10.1016/j.neuroimage.2019.05.022

Logothetis, N. K., & Wandell, B. A. (2004). Interpreting the BOLD signal. *Annu Rev Physiol, 66*, 735-769. doi:10.1146/annurev.physiol.66.082602.092845

Mancuso, L., Fornito, A., Costa, T., Ficco, L., Liloia, D., Manuello, J., . . . Cauda, F. (2020). A meta-analytic approach to mapping co-occurrent grey matter volume increases and decreases in psychiatric disorders. *Neuroimage, 222*, 117220. doi:https://doi.org/10.1016/j.neuroimage.2020.117220

Matsuda, H. (2016). MRI morphometry in Alzheimer's disease. *Ageing Res Rev, 30*, 17-24. doi:10.1016/j.arr.2016.01.003

McLaughlin, R. L., Schijven, D., van Rheenen, W., van Eijk, K. R., O'Brien, M., Kahn, R. S., . . . Veldink, J. H. (2017). Genetic correlation between amyotrophic lateral sclerosis and schizophrenia. *Nat Commun, 8*, 14774. doi:10.1038/ncomms14774

Mendonça, C. F., Kuras, M., Nogueira, F. C. S., Plá, I., Hortobágyi, T., Csiba, L., . . . Rezeli, M. (2019). Proteomic signatures of brain regions affected by tau pathology in early and late stages of Alzheimer's disease. *Neurobiol Dis, 130*, 104509. doi:10.1016/j.nbd.2019.104509

Mohan, A., Roberto, A. J., Mohan, A., Lorenzo, A., Jones, K., Carney, M. J., . . . Lapidus, K. A. (2016). The Significance of the Default Mode Network (DMN) in Neurological and Neuropsychiatric Disorders: A Review. *Yale J Biol Med, 89*(1), 49-57.

Moseley, M. E., Cohen, Y., Kucharczyk, J., Mintorovitch, J., Asgari, H. S., Wendland, M. F., . . . Norman, D. (1990). Diffusion-weighted MR imaging of anisotropic water diffusion in cat central nervous system. *Radiology, 176*(2), 439-445. doi:10.1148/radiology.176.2.2367658

Müller, V. I., Cieslik, E. C., Laird, A. R., Fox, P. T., Radua, J., Mataix-Cols, D., . . . Eickhoff, S. B. (2018). Ten simple rules for neuroimaging meta-analysis. *Neurosci Biobehav Rev, 84*, 151-161. doi:10.1016/j.neubiorev.2017.11.012

Muñoz-Ruiz, M., Hartikainen, P., Koikkalainen, J., Wolz, R., Julkunen, V., Niskanen, E., . . . Soininen, H. (2012). Structural MRI in frontotemporal dementia: comparisons between hippocampal volumetry, tensor-based morphometry and voxel-based morphometry. *PLoS One, 7*(12), e52531. doi:10.1371/journal.pone.0052531

Niu, M., Wang, Y., Jia, Y., Wang, J., Zhong, S., Lin, J., . . . Huang, R. (2017). Common and Specific Abnormalities in Cortical Thickness in Patients with Major Depressive and Bipolar Disorders. *EBioMedicine, 16*, 162-171. doi:10.1016/j.ebiom.2017.01.010

Ogawa, S., Menon, R. S., Tank, D. W., Kim, S. G., Merkle, H., Ellermann, J. M., & Ugurbil, K. (1993). Functional brain mapping by blood oxygenation level-dependent contrast magnetic resonance imaging. A comparison of signal characteristics with a biophysical model. *Biophys J, 64*(3), 803-812. doi:10.1016/s0006-3495(93)81441-3

Olloquequi, J., Cornejo-Córdova, E., Verdaguer, E., Soriano, F. X., Binvignat, O., Auladell, C., & Camins, A. (2018). Excitotoxicity in the pathogenesis of neurological and psychiatric disorders: Therapeutic implications. *J Psychopharmacol, 32*(3), 265-275. doi:10.1177/0269881118754680

Padovani, A., Premi, E., Pilotto, A., Gazzina, S., Cosseddu, M., Archetti, S., . . . Borroni, B. (2013). Overlap between frontotemporal dementia and Alzheimer's disease: cerebrospinal fluid pattern and neuroimaging study. *J Alzheimers Dis, 36*(1), 49-55. doi:10.3233/jad-121969

Patel, R. S., Bowman, F. D., & Rilling, J. K. (2006). A Bayesian approach to determining connectivity of the human brain. *Hum Brain Mapp, 27*(3), 267-276. doi:10.1002/hbm.20182

Pereira, A. M., Campos, B. M., Coan, A. C., Pegoraro, L. F., de Rezende, T. J. R., Obeso, I., . . . Cendes, F. (2018). Differences in Cortical Structure and Functional MRI Connectivity in High Functioning Autism. *Front Neurol, 9*, 539. doi:10.3389/fneur.2018.00539

Radua, J., & Mataix-Cols, D. (2009). Voxel-wise meta-analysis of grey matter changes in obsessive-compulsive disorder. *Br J Psychiatry, 195*(5), 393-402. doi:10.1192/bjp.bp.108.055046

Radua, J., Mataix-Cols, D., Phillips, M. L., El-Hage, W., Kronhaus, D. M., Cardoner, N., & Surguladze, S. (2012). A new meta-analytic method for neuroimaging studies that combines reported peak coordinates and statistical parametric maps. *Eur Psychiatry, 27*(8), 605-611. doi:10.1016/j.eurpsy.2011.04.001

Radua, J., van den Heuvel, O. A., Surguladze, S., & Mataix-Cols, D. (2010). Meta-analytical comparison of voxel-based morphometry studies in obsessive-compulsive disorder vs other anxiety disorders. *Arch Gen Psychiatry, 67*(7), 701-711. doi:10.1001/archgenpsychiatry.2010.70

Raj, A., Kuceyeski, A., & Weiner, M. (2012). A network diffusion model of disease progression in dementia. *Neuron, 73*(6), 1204-1215. doi:10.1016/j.neuron.2011.12.040

Ravits, J. (2014). Focality, stochasticity and neuroanatomic propagation in ALS pathogenesis. *Exp Neurol, 262 Pt B*, 121-126. doi:10.1016/j.expneurol.2014.07.021

Ravits, J., Appel, S., Baloh, R. H., Barohn, R., Brooks, B. R., Elman, L., . . . Ringel, S. (2013). Deciphering amyotrophic lateral sclerosis: what phenotype, neuropathology and genetics are telling us about pathogenesis. *Amyotroph Lateral Scler Frontotemporal Degener, 14 Suppl 1*, 5-18. doi:10.3109/21678421.2013.778548

Robinson, J. L., Laird, A. R., Glahn, D. C., Lovallo, W. R., & Fox, P. T. (2010). Metaanalytic connectivity modeling: delineating the functional connectivity of the human amygdala. *Hum Brain Mapp, 31*(2), 173-184. doi:10.1002/hbm.20854

Rocha, E., Achaval, M., Santos, P., & Rodnight, R. (1998). Lithium treatment causes gliosis and modifies the morphology of hippocampal astrocytes in rats. *Neuroreport, 9*(17), 3971-3974. doi:10.1097/00001756-199812010-00037

Romme, I. A., de Reus, M. A., Ophoff, R. A., Kahn, R. S., & van den Heuvel, M. P. (2017). Connectome Disconnectivity and Cortical Gene Expression in Patients With Schizophrenia. *Biol Psychiatry, 81*(6), 495-502. doi:10.1016/j.biopsych.2016.07.012

Rubinov, M., & Bullmore, E. (2013). Fledgling pathoconnectomics of psychiatric disorders. *Trends Cogn Sci, 17*(12), 641-647. doi:10.1016/j.tics.2013.10.007

Rubinov, M., & Sporns, O. (2010). Complex network measures of brain connectivity: uses and interpretations. *Neuroimage, 52*(3), 1059-1069. doi:10.1016/j.neuroimage.2009.10.003

Salimi-Khorshidi, G., Nichols, T. E., Smith, S. M., & Woolrich, M. W. (2011). Using Gaussian-process regression for meta-analytic neuroimaging inference based on sparse observations. *IEEE Trans Med Imaging, 30*(7), 1401-1416. doi:10.1109/tmi.2011.2122341

Salimi-Khorshidi, G., Smith, S. M., Keltner, J. R., Wager, T. D., & Nichols, T. E. (2009). Meta-analysis of neuroimaging data: a comparison of image-based and coordinate-based pooling of studies. *Neuroimage, 45*(3), 810-823. doi:10.1016/j.neuroimage.2008.12.039

Sarrazin, S., Poupon, C., Teillac, A., Mangin, J. F., Polosan, M., Favre, P., . . . Houenou, J. (2019). Higher in vivo Cortical Intracellular Volume Fraction Associated with Lithium Therapy in Bipolar Disorder: A Multicenter NODDI Study. *Psychother Psychosom, 88*(3), 171-176. doi:10.1159/000498854

Schiefer, J., Niederbühl, A., Pernice, V., Lennartz, C., Hennig, J., LeVan, P., & Rotter, S. (2018). From correlation to causation: Estimating effective connectivity from zero-lag covariances of brain signals. *PLoS Comput Biol, 14*(3), e1006056. doi:10.1371/journal.pcbi.1006056

Schröter, M., Paulsen, O., & Bullmore, E. T. (2017). Micro-connectomics: probing the organization of neuronal networks at the cellular scale. *Nat Rev Neurosci, 18*(3), 131-146. doi:10.1038/nrn.2016.182

Sebert, S., Lowry, E., Aumüller, N., Bermúdez, M. G., Bjerregaard, L. G., de Rooij, S. R., . . . Järvelin, M. R. (2019). Cohort Profile: The DynaHEALTH consortium - a European consortium for a life-course bio-psychosocial model of healthy ageing of glucose homeostasis. *Int J Epidemiol, 48*(4), 1051-1051k. doi:10.1093/ije/dyz056

Seung, S. (2013). *Connectome: How the Brain's Wiring Makes Us Who We Are*: Mariner Books.

Shannon, P., Markiel, A., Ozier, O., Baliga, N. S., Wang, J. T., Ramage, D., . . . Ideker, T. (2003). Cytoscape: a software environment for integrated models of biomolecular interaction networks. *Genome Res, 13*(11), 2498-2504. doi:10.1101/gr.1239303

Skudlarski, P., Jagannathan, K., Calhoun, V. D., Hampson, M., Skudlarska, B. A., & Pearlson, G. (2008). Measuring brain connectivity: diffusion tensor imaging validates resting state temporal correlations. *Neuroimage, 43*(3), 554-561. doi:10.1016/j.neuroimage.2008.07.063

Smith, J. F., Pillai, A., Chen, K., & Horwitz, B. (2010). Identification and validation of effective connectivity networks in functional magnetic resonance imaging using switching linear dynamic systems. *Neuroimage, 52*(3), 1027-1040. doi:10.1016/j.neuroimage.2009.11.081

Smith, S. M., Miller, K. L., Salimi-Khorshidi, G., Webster, M., Beckmann, C. F., Nichols, T. E., . . . Woolrich, M. W. (2011). Network modelling methods for FMRI. *Neuroimage, 54*(2), 875-891. doi:10.1016/j.neuroimage.2010.08.063

Song, G., Tin, C., & Poon, C. S. (2015). Multiscale fingerprinting of neuronal functional connectivity. *Brain Struct Funct, 220*(5), 2967-2982. doi:10.1007/s00429-014-0838-1

Soto, C., & Estrada, L. D. (2008). Protein misfolding and neurodegeneration. *Arch Neurol, 65*(2), 184-189. doi:10.1001/archneurol.2007.56

Sporns, O. (2016). Connectome Networks: From Cells to Systems. In H. Kennedy, D. C. Van Essen, & Y. Christen (Eds.), *Micro-, Meso- and Macro-Connectomics of the Brain*. Cham (CH): Springer

Copyright 2016, The Editor(s) (if applicable) and the Author(s) This book is published open access.

Sporns, O., Tononi, G., & Kötter, R. (2005). The Human Connectome: A Structural Description of the Human Brain. *PLoS Comput Biol, 1*(4), e42. doi:10.1371/journal.pcbi.0010042

Stoodley, C. J. (2014). Distinct regions of the cerebellum show gray matter decreases in autism, ADHD, and developmental dyslexia. *Front Syst Neurosci, 8*, 92. doi:10.3389/fnsys.2014.00092

Swanson, L. W., & Lichtman, J. W. (2016). From Cajal to Connectome and Beyond. *Annu Rev Neurosci, 39*(1), 197-216. doi:10.1146/annurev-neuro-071714-033954

Tahmasian, M., Sepehry, A. A., Samea, F., Khodadadifar, T., Soltaninejad, Z., Javaheripour, N., . . . Eickhoff, C. R. (2019). Practical recommendations to conduct a neuroimaging meta-analysis for neuropsychiatric disorders. *Hum Brain Mapp, 40*(17), 5142-5154. doi:10.1002/hbm.24746

Thompson, P. M., Hibar, D. P., Stein, J. L., Prasad, G., & Jahanshad, N. (2016). Genetics of the Connectome and the ENIGMA Project. In H. Kennedy, D. C. Van Essen, & Y. Christen (Eds.), *Micro-, Meso- and Macro-Connectomics of the Brain* (pp. 147-164). Cham (CH): Springer

Copyright 2016, The Author(s).

Ting, C., Seghouane, A., Salleh, S., & Noor, A. M. (2015). Estimating Effective Connectivity from fMRI Data Using Factor-based Subspace Autoregressive Models. *IEEE Signal Processing Letters, 22*(6), 757-761. doi:10.1109/LSP.2014.2365634

Toro, R., Fox, P. T., & Paus, T. (2008). Functional coactivation map of the human brain. *Cereb Cortex, 18*(11), 2553-2559. doi:10.1093/cercor/bhn014

Torres, U. S., Portela-Oliveira, E., Borgwardt, S., & Busatto, G. F. (2013). Structural brain changes associated with antipsychotic treatment in schizophrenia as revealed by

voxel-based morphometric MRI: an activation likelihood estimation meta-analysis. *BMC Psychiatry, 13*, 342. doi:10.1186/1471-244x-13-342

Tuch, D. S., Reese, T. G., Wiegell, M. R., & Wedeen, V. J. (2003). Diffusion MRI of complex neural architecture. *Neuron, 40*(5), 885-895. doi:10.1016/s0896-6273(03)00758-x

Turkeltaub, P. E., Eden, G. F., Jones, K. M., & Zeffiro, T. A. (2002). Meta-analysis of the functional neuroanatomy of single-word reading: method and validation. *Neuroimage, 16*(3 Pt 1), 765-780.

van den Heuvel, M. P., & Fornito, A. (2014). Brain networks in schizophrenia. *Neuropsychol Rev, 24*(1), 32-48. doi:10.1007/s11065-014-9248-7

van den Heuvel, M. P., & Hulshoff Pol, H. E. (2010). Exploring the brain network: a review on resting-state fMRI functional connectivity. *Eur Neuropsychopharmacol, 20*(8), 519-534. doi:10.1016/j.euroneuro.2010.03.008

van Haren, N. E. M., Schnack, H. G., Cahn, W., van den Heuvel, M. P., Lepage, C., Collins, L., . . . Kahn, R. S. (2011). Changes in Cortical Thickness During the Course of Illness in Schizophrenia. *Arch Gen Psychiatry, 68*(9), 871-880. doi:10.1001/archgenpsychiatry.2011.88

Vanasse, T. J., Fox, P. M., Barron, D. S., Robertson, M., Eickhoff, S. B., Lancaster, J. L., & Fox, P. T. (2018). BrainMap VBM: An environment for structural meta-analysis. *Hum Brain Mapp*. doi:10.1002/hbm.24078

Wager, T. D., Lindquist, M., & Kaplan, L. (2007). Meta-analysis of functional neuroimaging data: current and future directions. *Soc Cogn Affect Neurosci, 2*(2), 150-158. doi:10.1093/scan/nsm015

Wager, T. D., Lindquist, M. A., Nichols, T. E., Kober, H., & Van Snellenberg, J. X. (2009). Evaluating the consistency and specificity of neuroimaging data using meta-analysis. *Neuroimage, 45*(1 Suppl), S210-221. doi:10.1016/j.neuroimage.2008.10.061

Walker, L. C., Diamond, M. I., Duff, K. E., & Hyman, B. T. (2013). Mechanisms of protein seeding in neurodegenerative diseases. *JAMA Neurol, 70*(3), 304-310. doi:10.1001/jamaneurol.2013.1453

Wang, Y., David, O., Hu, X., & Deshpande, G. (2017). Can Patel's tau accurately estimate directionality of connections in brain networks from fMRI? *Magn Reson Med*. doi:10.1002/mrm.26583

White, J. G., Southgate, E., Thomson, J. N., & Brenner, S. (1986). The structure of the nervous system of the nematode Caenorhabditis elegans. *Philos Trans R Soc Lond B Biol Sci, 314*(1165), 1-340. doi:10.1098/rstb.1986.0056

Xia, M., Wang, J., & He, Y. (2013). BrainNet Viewer: A Network Visualization Tool for Human Brain Connectomics. *PLoS One, 8*(7), e68910. doi:10.1371/journal.pone.0068910

Yadav, S. P. (2007). The wholeness in suffix -omics, -omes, and the word om. *J Biomol Tech, 18*(5), 277.

Yates, D. (2012). Neurodegenerative networking. *Nat Rev Neurosci, 13*(5), 288. doi:10.1038/nrn3248

Yokoyama, J. S., Karch, C. M., Fan, C. C., Bonham, L. W., Kouri, N., Ross, O. A., . . . Desikan, R. S. (2017). Shared genetic risk between corticobasal degeneration, progressive

supranuclear palsy, and frontotemporal dementia. *Acta Neuropathol, 133*(5), 825-837. doi:10.1007/s00401-017-1693-y

Zhou, J., Gennatas, E. D., Kramer, J. H., Miller, B. L., & Seeley, W. W. (2012). Predicting regional neurodegeneration from the healthy brain functional connectome. *Neuron, 73*(6), 1216-1227. doi:10.1016/j.neuron.2012.03.004